PERFORMANCE OF THE DIATOM PHAEODACTYLUM TRICORNUTUM (BOHLIN) IN SYNTHETIC POLLUTED WATER AND ITS USE IN THE SYNTHESIS OF SILVER NANOPARTICLES

Antonio José Galán Galán

A thesis submitted to McGill University in partial fulfillment of the requirement of the degree of

Doctor of Philosophy

June 2017

Department of Bioresource Engineering

McGill University, Montreal

© Antonio José Galán Galán, 2017. All Rights Reserved

Dedicated to

My Beloved Wife

ABSTRACT

A strain of Phaeodactylum tricornutum (CPCC 162) was cultured to determine its performance and ability to withstand pollution with heavy metals (i.e. Ag, Mo, V). Treatments to simulate heavy metal pollution in water were performed at four levels each based on predicted maximum concentrations of 1 × 10⁻⁴ M for silver (1.079 x 10⁻⁵ g Ag·L⁻ ¹), 1.5×10^{-4} M for vanadium (7.64 x 10^{-6} g Ag·L⁻¹), and 1.0×10^{-4} M for molybdenum (9.594) x 10⁻⁶ g Mo·L⁻¹) from a preliminary experiment and new levels for silver (i.e. 0, 3.75 x 10⁻⁵, 9.24×10^{-5} , 1.47×10^{-4} , 1.85×10^{-4} g Ag·L⁻¹), vanadium (i.e. 0, 5.97 x 10^{-5} , 1.47×10^{-4} , 2.35 $\times 10^{-4}$, 2.95 x 10^{-4} g V·L⁻¹), and molybdenum (i.e. 0, 3.43 x 10^{-5} , 8.45 x 10^{-5} , 1.35 x 10^{-4} , 1.69 x 10⁻⁴ g Mo·L⁻¹) were assigned. Inductively coupled plasma mass spectrometry (ICP-MS) analysis showed a positive relation between cell growth and ionic concentrations, suggesting that P. tricornutum cells were responsible for 70 to 90 % reduction in silver and vanadium levels in the surrounding medium and that *P. tricornutum* can be used as a bioremediation alternative to treat relatively high concentrations of these two elements in water. Difficulties with the standards limited the possibility for calculations on molybdenum, and it was only possible to establish that the presence of molybdenum in medium-high concentrations (i.e. 1.35 x 10⁻⁴ g Mo·L⁻¹) aided in the consistency of ionic assimilation by the algae. Additionally, some of the cultures of P. tricornutum under silver stress showed an interesting trait by producing particles of nanoscopic size of what was determined to be only elemental silver (Ag⁰) and not silver salts (i.e. AgCl, AgNO₃). A life cycle analysis (LCA) of the use of P. tricornutum as a vector to produce silver nanoparticles showed an overall lower impact on the environment when compared to a traditional industrially used redox method. Except for the use of land, all categories and perspectives from the analysis using ReCiPe (1.11) and TRACI (2.1) were considerably lower in the impacts for the biogenic method (less than 50% of the impacts caused by the redox methodology) and, in general, close to 75% of the impact in all categories can be avoided using the algae alternative. Further analysis with different algal species and alternative methods for industrial production might provide better insights to the potential of algae as a vector for the industrial manufacturing of metal nanoparticles.

RÉSUMÉ

Une souche de *Phaeodactylum tricornutum* (CPCC 162) a été cultivée pour déterminer dans quelle mesure elle pourrait résister à la pollution par les métaux lourds (Ag, Mo, V). Des traitements pour simuler la pollution des métaux lourds dans l'eau ont été effectuées (Ag, Mo, V) à quatre niveaux, chacun étant basé sur les concentrations maximales prévues de 1 × 10⁻⁴ M pour l'argent (1,079 x 10⁻⁵ g Ag·L⁻¹), 1,5 × 10⁻⁴ M pour le vanadium (7,64 x 10⁻⁶ g Ag·L⁻¹), et de 1,0 × 10⁻⁴ M pour le molybdène (9,594 x 10⁻⁶ g·L⁻¹) à partir d'une expérience préliminaire. De ce fait, les niveaux ont été ajustés pour l'argent (0, 3,75 x 9,24 x 10⁻⁵, 10⁻⁵, 10⁻⁴, 1,85 x 1,47 x 10⁻⁴), le vanadium (0, 5,97 x 1,47 x 10⁻⁵, 10⁻⁴, 10⁻⁴, 2,35 x 2,95 x 10⁻⁴) et le molybdène (0, 3,43 x 8,45 x 10⁻⁵, 10⁻⁵, 10⁻⁵, 10⁻⁴, 1,69 x 1,35 x 10⁻⁴). L'analyse ICP a montré une relation positive qui suggère que les cellules de *P. tricornutum* étaient responsables de 70 à 90 % de réduction en argent en vanadium dans le milieu environnant ce qui suggère que *P. tricornutum* offre un potentiel de biorestauration pour traiter des concentrations relativement élevées de ces deux éléments dans l'eau.

Certaines des cultures de P. tricornutum avait une réaction supplémentaire produisant des particules de taille microscopique de ce qui a été déterminé être seulement de l'argent élémentaire et non pas des sels d'argent. Ceci a ouvert de nouvelles perspectives dans l'utilisation de P. tricornutum comme un vecteur biogènes pour produire des nanoparticules d'argent avec un faible impact sur l'environnement et, pour confirmer ce fait, une étude comparative de l'évaluation du cycle de vie d'une méthode traditionnelle utilisée industriellement pour produire l'oxydo-réduction des nanoparticules d'argent (AGP) et une alternative à l'aide de la méthode d'origine biogénique (P. tricornutum) ont montré que les performances environnementales de l'alternative étaient biogéniques et moins intrusives sur les effets éventuellement produits sur l'environnement. Sauf pour l'utilisation des terres, toutes les catégories analysées en utilisant le module ReCiPe 1.11 et TRACI version 2.1 ont eu un impact nettement plus faible par la méthode biogénique (moins de 50 % de l'impact causé par la méthodologie de l'hydroquinone). En general, près de 75 % des impacts dans toutes les catégories (sauf l'utilisation des terres) peuvent être évités lors de l'utilisation de l'alternative biogéniques. Une analyse avec différentes espèces d'algues et d'autres méthodes pour la production industrielle pourrait fournir une

meilleure compréhension du potentiel des algues, comme vecteur pour la fabrication industrielle de nanoparticules métalliques.

ACKNOWLEDGMENTS

I would like to express my sincere thanks to my supervisors Dr. Mark G. Lefsrud, and Dr. Vijaya Raghavan whose kindness, guidance, help, and encouragement made it possible for me to finish this study.

I would also like to express my deepest thanks to Dr. Darwin Lyew for his friendship and support when times of hardship rocked this boat, his microbiology knowledge and his invaluable help on the design of the experiment involving the unicellular algae. Additionally, I would like to thank Mr. Yvan Gariépy for his technical support and patience with the set-up of all things mechanical used in this study.

A special mention and thanks to Dr. Robert Williams for his encouragement and constant questioning of my statements, either in or out of this study. Special mention to Dr. Patrick Cortbaoui for his support and friendship during all this madness. Additionally, thanks to Dr. Michael Ngadi for opening the doors to such a magnificent institution; Dr. Valerie Orsat for being supportive when the start of this work came to a difficult trial, and for allowing me to use her safety hood when the culture required total axenic care; Dr. Timothy Schwinghamer for his valuable orientation and help for the statistical analysis of this document; Mr. John Gavita, Olympus Canada for allowing me access to his ADX microscope; Dr. Raynald Gauvin, Dr. Florence Paray, and Mr. Nicolas Brodusch for allowing the use of the Hitachi SEM that made the final stitches of this work possible; and special thanks to Ms. Hélèn Lalande for her invaluable contribution and patience while using the ICP-MS equipment.

Special words of appreciation to Ms. Susan Gregus, Ms. Patricia Singleton, and Ms. Abida Subhan for their support and help with all administrative matters related to this study and my time at McGill. And finally, but not less important, thank you to all laboratory partners, office neighbors, those who came and those who stayed, and those involved in the development of this study, a long list but not less important so alphabetically to be fair, Ademola, Adetunji, Adeyemi, Amarachi, Andrew, Anil, Anne Sophie, Antoine, Arturo, Blake, Bo-Sen, Camilo, Chanez, Chelsea, Christine, Claire-Mélodie, Debora, Ebenezer, Edris, Elizabeth, Emmet, George, Hernan, Hsin-Hui, Hui, Jamshid, Jasmeen, Julie, Lizzette,

Lucas, Malek, Marcos, Mark, Nafiseh, Nicolas, Ogan, Patricia, Peter, Philip, Polina, Rajvinder, Richa, Ryan, Sadman, Samuel, Satyanarayan, Shrikalaa, Srinivasa, Stephanus, Stephen, Viviane, Yasmin, Yves, and probably a lot more of you that escape my mind at this moment, thank you for bringing challenges and happy moments to my days.

This research was funded by a Natural Sciences and Engineering Research Council of Canada (NSERC) Discovery grant (RGPIN 355743-13), and McGill University, QC, Canada.

CONTRIBUTIONS OF THE AUTHORS

In accordance to McGill guidelines for theses, the contributions made by the candidate and the co-authors to the completion of this dissertation are described below.

All the contents presented in this dissertation were written by Mr. Antonio José Galán and reviewed by Dr. Mark Lefsrud, and Dr. Vijaya Raghavan, Department of Bioresource Engineering, McGill University. Mr. Galán was responsible for the development of protocols, the design of experiments, the conduction of research, testing, statistical analysis, and record of documentation. Dr. Lefsrud and Dr. Raghavan guided technically, financially, and morally, proofread the document, and provided the required criticisms and suggestions towards the research.

Dr. Raynald Gauvin, from the Department of Mining and Materials Engineering, supported the final outcomes with the technical description and use of the SEM-EDS analysis microscope and probes, used to determine the fate of silver ions within the culture. Graphs were produced automatically by the equipment and the selection of spots for analysis was solely the responsibility of the Ph. D. student Mr. Galán.

No portion of this thesis has been submitted for presentation in annual conferences or meetings.

TABLE OF CONTENTS

	•••••••••••••••••••••••••••••••••••••••	
RÉSUMÉ	•••••	3
ACKNOWLEDG	GMENTS	5
CONTRIBUTIO	NS OF THE AUTHORS	7
	NTENTS	
	ES	
	RES	
	OLS AND ABBREVIATIONS	
CHAPTER I	INTRODUCTION	
1.1	RATIONALE AND PROBLEM STATEMENT	
1.2	HYPOTHESIS	
1.3	OBJECTIVES	
1.3.1	General objective	
1.3.2	Specific objectives	
CHAPTER II	LITERATURE REVIEW	
2.1	DIATOMS	
2.1.1	Origins	
2.1.2	General considerations	
2.1.3	Current uses for live diatoms	
2.1.4	Current uses for diatom frustules	
2.1.5	Phaeodactylum tricornutum (Bohlin)	
2.2	HEAVY METAL REMEDIATION USING ALGAE	
2.3	BIOMINERALIZATION	
2.3.1	Definition of biomineral	
2.3.2	Evolution of biominerals	
2.3.3	Biomineralization in microorganisms	
2.4	ORGANISMS IN NANOTECHNOLOGY	
2.4.1	Synthesis of nanoparticles	
2.4.2	Biogenic and transition to green alternatives for AgNP synthesis	
2.5	LIFE CYCLE ASSESSMENT	
2.6	FINAL CONSIDERATIONS	
CHAPTER III	MATERIALS AND METHODS	
3.1	ALGAE CULTURES	66
3.1.1	Culture medium	66
3.1.2	Cell count	69
3.1.3	Treatments	72
3.2	SAMPLING	73
3.2.1	Medium (supernatant)	
3.2.2	Frustules (pellets)	
3.3	Monitoring	76
3.3.1	Nitrogen monitoring	
3.3.2	Temperature	
3.3.3	Irradiance	
3.3.4	pH	
3.4	OPTICAL MICROSCOPY	
3.5	SCANNING ELECTRON MICROSCOPY	
3.5.1	Sample preparation	7 <u>9</u>

3.5.2	Tabletop SEM preliminary exploration	79			
3.5.3	SEM-EDS	79			
3.6	ICP-MS ANALYSIS OF THE LIQUID PHASE	80			
3.7	LIFE CYCLE ASSESSMENT (LCA)	81			
3.7.1	Goal and scope of study	81			
3.7.2	System description and boundaries	83			
3.7.3	Inventory data collection	90			
3.7.4	Life cycle impact assessment	92			
3.8					
3.8.1	M-EDS				
3.9	ADDITIONAL CONSIDERATIONS				
CHAPTER IV	RESULTS AND DISCUSSION	99			
4.1	GENERAL MONITORING	99			
4.2	CELL CULTURE AND BIOMASS DETERMINATION	100			
4.2.1	Ion removal from the water column	107			
4.2.2					
4.2.3	· · · ·				
4.3	•				
4.3.1	Comparison of characterized results between both production methods	126			
4.3.2	Ecosystem Categories	126			
4.3.3	Climate change	130			
4.3.4	Ecotoxicity	131			
4.3.5	Freshwater eutrophication	133			
4.3.6	Acidification potential	133			
4.3.7	Resource depletion categories	134			
4.3.8					
4.3.9	Process contribution analysis	136			
CHAPTER V	CONCLUSIONS	137			
CHAPTER VI	CONTRIBUTIONS TO KNOWLEDGE, FUTURE RESEARCH				
	·	140			
6.1	·				
6.2					
6.3					
ALLEINDICES		тоэ			

LIST OF TABLES

Table 2.1. Mechanical properties of a typical diatom frustule	32
Table 2.4. Biomineralization in biological organisms	
Table 2.5. Synthesis of nanoparticles by microorganisms	
Table 3.1. Ionic concentration of the CML ₁ +Si medium	
Table 3.2. Impact categories available per impact analysis method	
Table 3.3. Comparison of impact categories TRACI 2.1 vs. ReCiPe 1.11	
Table 4.1. Classification and composition of structures	
Table 4.2. Impact values from the TRACI 2.1 LCIA method	
Table 4.3. Normalized midpoint results and ratio of difference	

LIST OF FIGURES

Figure 2.1. Schematic diagram diatom structures	23
Figure 2.2. Sexual reproduction of diatoms	25
Figure 2.3. Example of a diatom frustule	26
Figure 2.4. Typical centric diatom	27
Figure 2.5. Representation of diatom frustules	29
Figure 2.6. Diatom frustule pores	30
Figure 2.7. Frustule manufacture process.	31
Figure 2.8. Diatom cellular division in cross section	32
Figure 2.9. Metallic ionic uptake and detox processes inside a living cell	44
Figure 2.10. Elements of a life cycle analysis	
Figure 3.1. Culture vessel	74
Figure 3.2. Experimental sample distribution	76
Figure 3.3. Production boundaries HQ-AgNP process	84
Figure 3.4. Production boundaries biogenic-AgNP process	84
Figure 3.5. Schematic representation of the reduction process	85
Figure 3.6. Schematics of an integrated microalgae biorefinery	86
Figure 3.7. Simplified diagram of an integrated microalgae biorefinery	
Figure 3.8. Experimental levels	96
Figure 4.1. Temperature by irradiance.	
Figure 4.2. Nitrogen concentration curves	
Figure 4.3. Cell density graphs	
Figure 4.4. Growth performances under silver stress at different levels	103
Figure 4.5. Surface plots for cell density	
Figure 4.6. Scree and variance plots principal component analysis	106
Figure 4.7. Silver and vanadium removal ratios agglomerated by molybdenum level	
Figure 4.8. P. tricornutum under optical microscope	
Figure 4.9. Typical <i>P. tricornutum</i> frustule damage after heavy metal treatment	
Figure 4.10. Typical extracellular particles under silver stress in <i>P. tricornutum</i>	
Figure 4.11. Surface frustule secretion on <i>P. tricornutum</i> under heavy metal treatment	
Figure 4.12. Abnormal surface growth in <i>P. tricornutum</i> under heavy metal treatment	
Figure 4.13. Abnormal apical formations in <i>P. tricornutum</i> under heavy metal treatments	
Figure 4.14. Substrate analysis and imaging	120
Figure 4.15. TRACI 2.1 impact categories	
Figure 4.16. ReCiPe 1.11 egalitarian relative endpoint comparison	
Figure 4.17. ReCiPe 1.11 hierarchist relative endpoint comparison	
Figure 4.18. ReCiPe 1.11 individualist relative endpoint comparison	
Appendix Figure 1. Hemocytometer	
Appendix Figure 2. Single beam spectrophotometer	
Appendix Figure 3. Overall contributions of hydroquinone-AgNP production TRACI 2	
Appendix Figure 4. Overall contributions of biogenic-AgNP production TRACI 2.1	197

LIST OF SYMBOLS AND ABBREVIATIONS

 ΔE^0 Change in electropositive reduction potential

2-CEPA 2-carboxyethyl-phosphonic acid

a-Si Amorphous silica

AEAPTMS N- (2-aminoethyl)-3aminopropyl) trimethoxysilane

AFM Atomic force microscope

AgNP Silver nanoparticle

APTES 3-aminopropyltriethoxysilane

ASTM American Society for Testing and Materials

AuNP Gold nanoparticle

BET Brunauer – Emmet – Teller surface analysis

c-Si Crystalline silica

Caltech California Institute of Technology

CAS Chemical Abstracts Service a division of the American Chemical Society

Electropositive reduction potential

EC number European Commission Number

EG Ethylene glycol

EIA Environmental impact assessment

EPA Environmental Protection Agency

FEM Field emission microscope

FIM Field ion microscope

GPTMS (3-Glycidyloxypropyl) trimethoxysilane

HIV Human immunodeficiency virus

HQ Hydroquinone

IBM International Business Machines

ICP-MS Inductively coupled plasma mass spectrometry

ISO International Organization for Standardization

ISO/TS ISO technical standard

LCPA Long-chain polyamines

LED Light emitting diode

MAR Minimum angle of resolution. Minute of arc equivalent to 1/60 degree

mPEG m-polyethylene glycol

MSDS Material safety data sheet

N/A Not applicable or not available

NLM National Library of Medicine

NIH United States National Institutes of Health

NCBI National Center for Biotechnology Information component of the NLM, and

part of the NIH

Nd-YAG Neodymium-doped yttrium aluminum garnet

nm Nanometer

NMR Nuclear magnetic resonance

NNI National Nanotechnology Initiative

NP Nano particle

OTS n-octadecyltrichlorosilane

PAR Photosynthetically active radiation

PDMAEMA Poly (2-dimethylaminoethyl methacrylate)

PDMS Polydimethylsiloxane

pH Potential of hydrogen

PHA Polyhydroxyalkanoate

PSDS Product safety data sheet

PtNP Platinum nanoparticle

PubChem Public Chemical Database maintained by the BCBI

PVP Polyvinylpyrrolidone

sc Single crystal

SDBS Sodium dodecyl benzene sulfonate

SDS Safety data sheet

SDV Silicon deposition vesicle

SEM Scanning electron microscope

SEM-EDS Scanning electron microscopy with energy dispersive x-ray spectroscopy

SI International System of Units (Système International d'Unités)

SiTs Silicon transporters

STM Scanning tunneling microscope

STV Silicon transport vesicle

TBA Tetrabutylammonium salt

TGA Thermogravimetric analysis

tw Twinned particle

UV Ultraviolet

UV-Vis Ultraviolet to visible spectrum 320 – 700 nm wavelengths

UVA Ultraviolet A radiation 315 – 400 nm

wt% Percentage by weight

XRPD X-Ray powder diffraction analysis

μm Micrometer

CHAPTER I

Nanotechnology is defined as the "application of scientific knowledge to manipulate and control matter at the nanoscale to make use of size- and structure- dependent properties and phenomena, as distinct from those associated with individual atoms or molecules or with bulk materials" (ISO, 2010). The size of "nano" is known to be in a factor of 10⁻⁹ times that of the measure standard unit, as defined by the International System of Units (Système International d'Unités, SI), i.e. one nanometer is a billionth of a meter. In perspective, one nanometer would equal in proportion to that of an average human wide step (roughly one meter) in a length 2.6 times the distance between the Earth and the Moon (one billion meters). No wonder nanomaterials have unique properties that can be customized to different and novel applications, as the size of the particles in question gets smaller the applications and interest in these particles grow. For example, virus encapsulation of influenza and HIV are in the range from 100-120 nm (Briggs et al., 2003; Bovier & Pelase, 2008). Having particles at the nanoscale for different materials, their physical and chemical properties are quite different than those of bulk sized counterparts (Hornyak et al., 2008). At the nanoscale, the properties of the particles are influenced by what is known as "quantum effects" related directly with size. For instance, the surface area that can be obtained with nanoscopic arrangements, when compared to microscopic equivalent, increases inversely proportional to the reduction in size and thus a 1 cm³ particle will have a 6 cm² surface area while the same volume completely divided in 1 mm³ and 1 nm³ particles will have a 60 cm² and 6 x 10⁷ cm² surface areas respectively (National Nanotechnology Initiative, 2017).

The production of nano-scaled particles of metals, and more specifically those of noble metals (silver nanoparticle – AgNP, gold – AuNP, and platinum – PtNP) grows in interest due to their potential applications in fields such as spectroscopy (Mulvaney, 1996), drug delivery (Pacioti et al., 2004), tissue and tumor imaging (Jain et al., 2006), cancer therapy (Peng et al., 2009), bacterial control (Aziz et al., 2012), and other applications, because nobel metals are resistant to chemical action, corrosion and attack by acids. The drawback from this seemingly impressive array of applications derives from the methods

required to produce the particles themselves as harsh and highly polluting chemicals (e.g. sodium borohydride, dimethylformamide, carbon monoxide, hydrazine, hydroxylamine hydrochloride, hydrogen peroxide) all considered hazardous in nature, and contributing to both eco- and human toxicity and other negative environmental impacts (Daniel, 2004; Durnán et al., 2009; Croteau et al., 2011) and the potential toxic effects produced by excess of nanoparticles in the environment (Miao et al., 2010; Croteau et al., 2011; Castro-Bugallo et al., 2014). Other methods, used to produce polymeric nanoparticles use highly toxic compounds (i.e. dichloromethane, ethyl acetate, benzyl alcohol, cyclohexane, acetonitrile, acetone). Even though these methods produce nanoparticles in an efficient manner, downstream, midpoint, and endpoint eco-toxicity calls for an expensive separation of hazardous compounds from the result, as even trace amounts of these solvents render the nanoparticles unsuitable for some applications (e.g. biomedical, drug, cancer treatment).

Algae, otherwise considered by many as pond-scum, waste, and an environmental pressure agent, can be one of the unsung heroes in this battle to produce better and more environmentally friendly nanoparticles. It is known now that some bacterial species can manufacture nanoparticles (Mandal et al., 2006; Narayanan & Sakthivel, 2010) of different elements as a toxicity defense mechanisms, and in recent studies algae (Scaiano et al., 2009; Schröfel et al., 2011; Sinha et al. 2015), and more interestingly microalgae, have been proven to be capable of the same feature. Microalgae are unicellular photosynthetic organisms with relatively simple nutritional requirements and are thus easy to culture. Their vast numbers and variety make them one of the most promising organisms for biotechnology applications (Bozarth et al., 2009). Amongst the different groups of microalgae, diatoms are one of the most widespread taxonomic groups consisting of approximately 100,000 species belonging to over 250 genera (Norton et al., 1996; van den Hoek et al., 1995). Diatoms contribute nearly 25% of global photosynthetic productivity (Scalas & Bowler, 2001; Falciatore & Bowler, 2002; Falkowski & Raven, 2007) and play an influential role in the biochemical cycles of primary elements, i.e., carbon, nitrogen, phosphorus, and silicon (Armbrust, 2009). These highly successful organisms are

present in salt and freshwater, as well as soil and moisture rich non-aquatic environments (Armbrust, 2009).

One of the most interesting features of diatoms is their unique pillbox-like silica-based framework (frustule) of their cell wall (Losic et al., 2006a; Martin-Jézéquel & López, 2003; McConville et al., 1999). This frustule structure is incorporated into an organic envelope typically composed of proteins and polysaccharides (Hecky et al., 1973). Among the characteristics that make this structural feature different are the unique optical properties (Ingalls et al., 2010; Hsu et al., 2012), their reported exceptional strength (Hamm et al., 2003), and the intricate architecture of the frustule (Perry, 2003; López et al., 2005). The diatoms frustule has been highly studied with possible applications of the silicification process for industrial applications (Perry, 2003; López et al., 2005).

Depending on the species and growth conditions (Csögör et al., 1999), diatom frustules display a broad range of morphologies allowing for bio-designed frustules with properties suitable for the nanotechnology industry (Parkinson & Gordon, 1999). As an example, four different morphotypes of P. tricornutum, depend on the amount of nutrients in the surrounding environment (Perales-Vela et al., 2006; Masmoudi et al., 2013) controlled via a cascade of enzymatic events (Cobbett & Goldsbrough, 2002) regulated by a complex set of proteomic triggers (Cumming & Gregory, 1990; Conner & Schimid, 2003; Bowler et al., 2010). Nonetheless, the ability of humans to control the environmental conditions (i.e. culture conditions) during targeted production of diatoms can result in highly repeatable outcomes compared to those found in nature (Vrieling et al., 1999a; Vrieling et al., 2007), reducing the need for further purification. Diatom production can be further controlled for cell size and structural properties, as silica formation is a uniform process at the nanoscale (Vrieling et al., 2007). However, further research is necessary as the homogeneity of the final product is dependent on pH (Parkinson & Gordon, 1999; Vrieling et al., 1999b), chemical interactions (Vrieling et al., 2007), concentration of silicon, and the stage of the cell cycle (Martin-Jézéquel & López, 2003). Scarcity of nutrients, osmotic pressure and the presence of waste products from the culture conditions are other causes of frustule malformation in laboratory cultures (Estes & Dute, 1994; Falasco et al., 2009).

Besides their interesting structural characteristics, diatoms share most of the properties observed in other groups of algae. Current biotechnological uses for diatoms include: the production of eicosapentaenoic acid (EPA) and other polyunsaturated fatty acids (PUFA) for pharmaceutical applications, amino acids for cosmetics and nutraceuticals, lipids for biodiesel, antiproliferative (i.e. antibacterial) agents, and biogenic materials such as semiconductors and other nanotechnology products (Bozarth, et al., 2009). Water treatment for phosphorus, nitrogen, and heavy metal bioremediation are in the initial stages of diatom research and their competitiveness for these processes is still not well defined given the lack of life cycle assessment studies that are currently available.

An additional promising area of research for diatom-based biotechnological applications derives from the known resistance of several species of the group (e.g., Cylindrotheca fusiformis, P. tricornutum, Skeletonema costatum, and Thalassiosira pseudonana) to relatively high concentrations of heavy metals (Braek at al., 1980; Pistocchi et al., 2000; Schmitta et al., 2001). Diatoms can uptake heavy metals and accumulate them inside the cell or the cell wall either as particles mixed with the organic envelope or embedded in the silicon structure (Torres et al., 1998; Perales-Vela et al., 2006; Li et al., 2010). This property makes them suitable as a potential bioremediative agent (Craggs et al., 1995; Craggs et al., 1997; Sivakumar et al., 2012). Research has been carried out where these diatoms can regulate the environmental presence of heavy metal pollutants (Vrieling et al., 1999a; Vrieling, 2007), which dwells in their capacity to take metal-originated ionic species and either accumulating them on the cell wall or inside the cell as particles combined with the organic envelope or fixed in the silicon assembly (Torres et al., 1998; Perales-Vela et al., 2006; Li et al., 2010) or push them out as non-reactive complex molecules (Mandal et al., 2006; Saravanamuthu, 2010). Although not fully understood, this characteristic offers the possibility to design an industrial process for the manufacture of highly repeatable silicon metal structures, which would be a new and promising area of research for diatom-based biotechnological applications.

Among the type of particles generated by these microorganisms, nanoparticles of different types (e.g. gold, silver, magnetite, selenium, tellurium, cobalt oxide, cadmium sulfide) are of interest because of their potential in current trends in manufacturing.

Different studies reported some species of bacteria (Kasama et al., 2006; Luef et al., 2013; Iwahori et al., 2014), fungi (Durán et al., 2005; Durán et al., 2009), and algae (Schröfel et al., 2011; Castro et al., 2013; Aziz et al., 2015) capable of producing nanoparticles by synthesis.

Nano particles, can be categorized as ultrafine (1-100 nm), fine (100-2,500 nm), and coarse (2,500 – 10,000 nm) (EPA, 2016; ASTM, 2012). The growing interest in the use of nanoparticles is derived from the differences in the properties of a material when its size approaches the nanoscale (Hubler & Osuagwu, 2010; Taylor et al., 2013; Hewakuruppu et al., 2013). Among the methods for the manufacture of nanoparticles, gas condensation, attrition, chemical precipitation, pyrolysis, and hydrothermal synthesis are currently available and readily selected by industrial manufacturers (Charistides et al., 2014). Unfortunately, traditional manufacturing of nanoparticles, based on any form generates environmental impacts which vary in category, vector (i.e. directionality and strength), magnitude, time frame, and geolocation which makes it difficult to standardize values for all the industrial manufacturing methodologies (Taghavi et al., 2013; Sajid et al., 2015; Reid & Reed, 2016).

Current requirements and standards for sustainability challenge the identification of impacts to minimize those which can be reduced, mitigate those that can be exchanged by means of transformation of the technology, and remediate those that cannot be avoided (Ray et al., 2010). Green chemistry and biogenic methods are now regarded as some of the most promising alternatives to generalized industrial manufacturing methodologies (e.g. gas condensation, attrition, chemical precipitation) because of their lower impact on the environment (Durán et al., 2009; Iwahori et al., 2014; Kathiraven et al., 2015).

Using the knowledge of organisms that create nanoparticles and combining this with the pillbox-like cell wall of diatoms would open a range of options in biotechnology. A better understanding of the complex array of biochemical processes required to produce nanoparticles, together with the diatoms ability to regulate environmental conditions are required. However, given that diatoms are a promising organism for applications in biotechnology contingent upon a better understanding of their biology and biochemical

pathways (Parkinson & Gordon, 1999) which is the point of entry for any approaches where diatom biotechnology is to be understood for their resistance to the elemental treatments in producing the desired materials or structures.

1.1 Rationale and problem statement

Based on the previous statements, it was determined that, to identify and develop cleaner and environmentally friendly methodologies for new materials, the following basic problems needed a structured and systematic solution:

- 1. To develop cleaner and more environment friendly (i.e. green) methods to produce novel materials (i.e. nanoparticles) that can be used in sensitive applications (e.g. biomedical applications, drug delivery, antibacterial materials) requires species (i.e. organism) capable of surviving the introduction of treatments (i.e. stress) in their culture environment, and at least generate a considerably lower impact on the environment when compared to other processes that are currently available.
- The proposed organism must be responsible for the production of the material and not be an unrelated and aleatory outcome of other processes within the production settings.
- The culture conditions must be standardized to guarantee replicability of the material and improve the quality of the final product, thereby generating better monitoring and control mechanisms for culturing of the organism.

1.2 Hypothesis

P. tricornutum can sustain external pressure from a heavy metal stressor (i.e. silver, vanadium, and molybdenum) or a combination of stressors. *P. tricornutum* will react to the condition in a manner that will produce useful materials. It is possible to integrate the biochemical machinery of Bacillariophyceae (i.e. diatoms) with the production of highly pure and valuable nanoparticles.

1.3 Objectives

1.3.1 General objective

The primary objective of this research is to assess the potential use of an organism from the group of Bacillariophyceae algae known as diatoms (i.e. *P. tricornutum*) in the remediation of heavy metal pollution.

1.3.2 Specific objectives

- Assess the resistance of *P. tricornutum* to high concentrations of ionic silver in the surrounding medium;
- II Determine the potential use of *P. tricornutum* in the bioremediation of silver contamination in water streams;
- III Determine the resistance and potential use of *P. tricornutum* in bioremediation of vanadium and molybdenum contamination in waters;
- IV Synthesize silver nanoparticles via regulated culture of diatoms (Bacillariophyceae), establishing the most adequate protocol for the synthesis of these particles using a regulated culture of *P. tricornutum*;
- V Determine the potential environmental impacts of an alternative biogenic manufacturing process (i.e. culture of *P. tricornutum*) of silver nanoparticles; and
- VI Compare the results with the impact of a current methodology (i.e. redox) used to produce particles with similar size and shape.

CHAPTER II LITERATURE REVIEW

Understanding the underlying theory and previous research on the subjects contained on this document is necessary to better lay out the foundations for the work required to reach the objectives. The literature review focused on the organisms (diatoms) with a grasp of the origins and current knowledge about the group in human applications. Next, it addressed the remediation of heavy metal pollution in water bodies using algae and the underlying process that makes this possible (i.e. biomineralization). Third, the review considered the role of organisms in nanotechnology, and finally the structure and overarching principles of a life cycle assessment.

2.1 Diatoms

Diatoms have gradually attained more interest from the scientific community. Previous work was focused only on the variety of particularly shaped frustules (von Stosch, 1950; 1951; 1956; and 1958; Csögör et al., 1999; Theriot, 2001); a bio-deposited hydrated amorphous silica shell distinctive of these organisms. Over one hundred thousand (100,000) estimated diatom species (Round et al., 1990) have exclusive shells with a set of unique structures and patterns. One of the most remarkable characteristics of diatom cells is the silicon-based cell wall known as frustule. Initially believed to be a mere physical barrier to protect the inner cell it is now known multiple functions (Gordon et al., 2005). One example of the additional functionality of diatom frustules is their close relationship with light manipulation (Fuhrmann et al., 2004; Gordon et al., 2009; Toster et al., 2013a). The degree of success of these organisms is such that they exist in practically any aquatic environment known to man and handle approximately 25% of the total net primary photosynthetic production (Seckbach, 2011). Mostly autotrophic with some obligate heterotrophic exceptions, they are one of the most important carbon sinks on the planet (Fields et al., 2014).

From a strictly outer geometric perspective, diatoms have a symmetrical structure determined by the shell geometry (Round et al., 1990). This differentiated disposition allowed early taxonomical trials to divide the group between centric (radial symmetry) and pennate (bilateral symmetry) (De Stefano & De Stefano, 2005; Medlin, 2009;

Seckbach, 2011) as seen in Figure 2.1. Diatom frustules with a few exceptions have a two-valve array like a petri dish (i.e., hypovalve and epivalve), which overlap as shown in Figure 2.1 A and C (Round et al., 1990).

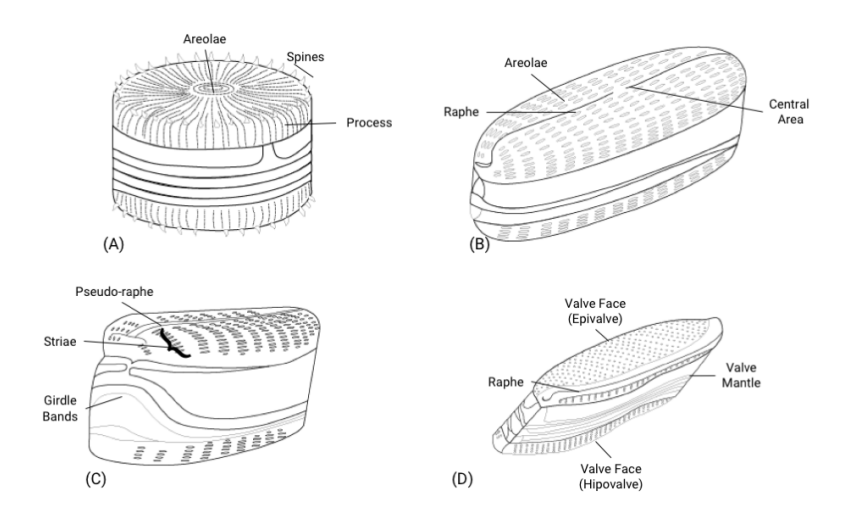


Figure 2.1. Schematic diagram diatom structures. Different structures of the two main groups of diatoms (A) Centric, (B, C and D) pennate diatoms. Image adapted and drawn based on Jones, 2007.

From fossil to current diatoms, frustules are the recognized means for identification. Diatoms belong to the heterokont algae group and differ from common heterokonts because the adult vegetative forms lack the two flagella found in other members of the group (von Stosch, 1958; van den Hoek, C. et al., 1995). These flagella are limited, with a few differences, to the spermatozoid form found in sexual reproduction processes of central diatoms (von Stosch, 1950 and 1951).

2.1.1 Origins

Diatoms exist in about every habitat with moisture content (Seckbach, 2011). They fix over one-quarter of the carbon dioxide in the world (Armbrust, 2004; Zimmermann et al., 2011). They appear to have originated in the boundary of the Permian-Triassic period and radiated at different taxonomic levels (Mock & Medlin, 2012). There is a hypothesis that an endosymbiotic event gave origin to the heterokonts from, a heterotrophic host that engulfed a red alga (Mock & Medlin, 2012). The original organism seemed to have lost the advantage of the photosynthetic functionality of their new symbiotic organelle

yielding the modern divergence of the group (Medlin et al., 1993). It appears as if the organism exchanged an original green plastid for the red algae one (Teich et al., 2007; Baurain et al., 2010). These series of changes allowed for a thesis around the presence of both green and red plastids after the secondary endosymbiosis contributed to the origin of heterokonts (Medlin et al., 1993).

2.1.2 General considerations

As mentioned before, diatoms thrive in hydrated ecosystems and handle over one-quarter of the primary productivity in the ocean (Gordon et al., 2005). On average, it can be estimated that there are around 2×10⁸ diatom cells in a cubic meter of sea water (Nelson et al., 1995).

2.1.2.1 Ecology

Given their abundance, diatoms are one of the major components of plankton in aquatic environments. However, their habitat is not limited to free-range water bodies, as these organisms have the capacity to attach to substrates (e.g., root systems of floating plants, turtles, and whales) and inhabit shallow benthic ecosystems (e.g., shallow rocky streams and river beds) under the right conditions. They can also thrive in relatively non-aquatic environments (e.g., soil and moss) if the humidity conditions are acceptable as well as in iron-depleted settings. Open-ocean centric species (e.g., species of the genus Thalassiosira) seem to have modified their photosynthetic biochemistry and require less iron (Armbrust, 2009).

This uncanny ability to survive makes them quite important within the primary producers in food webs. They are also responsible for silicon mineralization and influence global climate, atmospheric carbon dioxide concentration and the general function of varied ecosystems (Wassmann et al., 2006; Armbrust, 2009).

2.1.2.2 Diatom reproduction

Reproduction in diatoms is achieved vegetatively via mitotic cell division (Seckbach, 2011; Chepurnov et al., 2012). The frustule is reproduced intracellularly as opposite-sided valves that will replace one of the parental halves, and thus one maternal and one daughter half cover each daughter cell (Tiffany, 2005; Cao et al., 2013). This process is

repeated generation after generation reducing the size of the cells. Ultimately, the cell must cope with this reduction and increases the girdle size creating auxospores that will combine to increase the volume back to the species average during sexual reproduction (Figure 2.2). Martin-Jézéquel et al. (2000), Round et al. (1990), van den Hoek et al. (1995), and Kröger & Poulsen (2008a) describe in more detail the metabolism of the diatom frustule formation, since this process keeps repeating in time, the outcome is an excessive reduction in cell size. This decrease in turn would eliminate all likelihood of life on the final cells in most species, with few exceptions, such as *Gomphonema parvulum* (Rose & Cox, 2013). Sexual reproduction takes place to circumvent this singularity. During this stage, cells within a certain size range will produce an increased number of gametes within the maternal cells via meiosis (Round et al., 1990). Figure 2.2 shows a diagram representing the process.

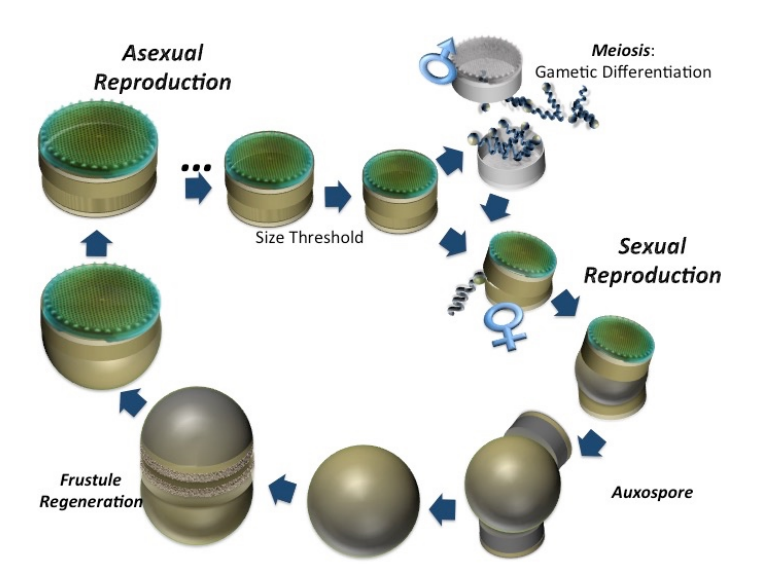


Figure 2.2. Sexual reproduction of diatoms. Image based on Round et al., (1990) accessed online from (Mann, 2007)

Sexual reproduction is not always possible as only the appropriate conditions (e.g., light, temperature, nutrient availability, and the presence of well-suited mates) can trigger the mechanism. After two gametes meet, a larger than average structural formation (auxospore) regulates the protection of the gametal conjugation and allows the growth of a new full-sized diatom cell (von Stosch, 1950, 1951, and 1956; Tiffany, 2005; Mather et al., 2014).

2.1.2.3 Shapes and properties

All diatoms typically have a perforated silica wall (frustule), usually bipartite with some exceptions, such as *P. tricornutum* and endosymbiotic species (Cox, 2012). Figure 2.3 shows SEM images with some of the most representative structures on the diatom frustule. The diatom frustule provides structural pathways for the exchange of nutrients, gasses and cellular product secretions (e.g., polysaccharides); and a protective physical barrier to the protoplast. Some structural features can be concomitant with specific functions, such as raphe slits linked to motility, fultoportulae with the excretion of chitin fibers, ocelli, pseudocelli and apical pore fields associated with mucilage secretion for attachment, and spines for linkage to produce filaments (Cox, 1999).

Diatoms contain all the inner structures of typical photosynthetic cells, such as nucleus, chloroplasts, mitochondria, endoplasmic reticulum, Golgi complex lipid vacuoles, and chromatophore (Yang et al., 2011). An additional layer between the plasmalemma and the frustule (diatotepum) can exist in some diatoms species (Seckbach, 2011). Figure 2.4 shows a diagram representing the outer and inner workings of a diatom cell.

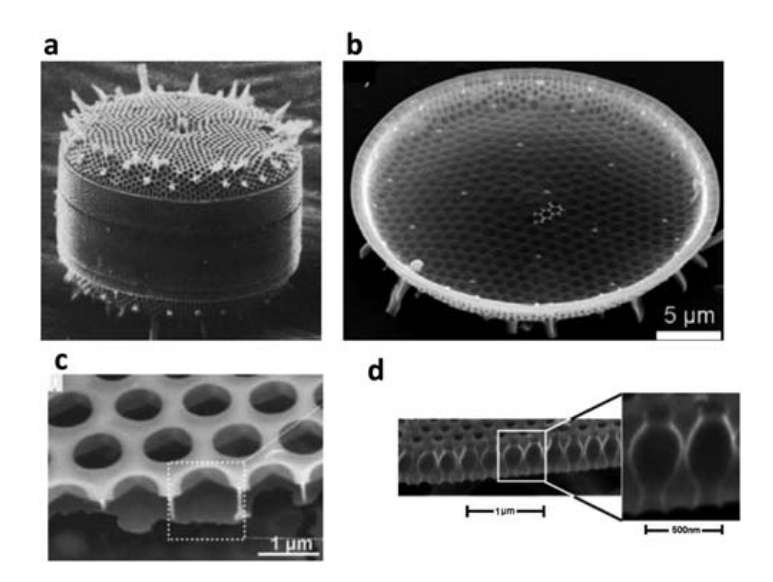


Figure 2.3. Example of a diatom frustule. An example of a diatom frustule a, b and c: *Thalassiosira* spp. frustule, d: *Coscinodiscus* spp. pore structure of the girdle band (Yang et al., 2011).

2.1.2.4 Light harvesting

When observed under different types of light, diatom frustules yield diffraction and interference effects. Being made entirely from amorphous silica (glass), reflections from the multilayered surface modulate the incident light amplifying or attenuating it, depending on the angle of incidence or the frequency. The presence of pores that act as slits smaller than the wavelength of visible light often yield quantum-like effects (Gordon et al., 2009), an impressive property with optical and nanotechnological applications.

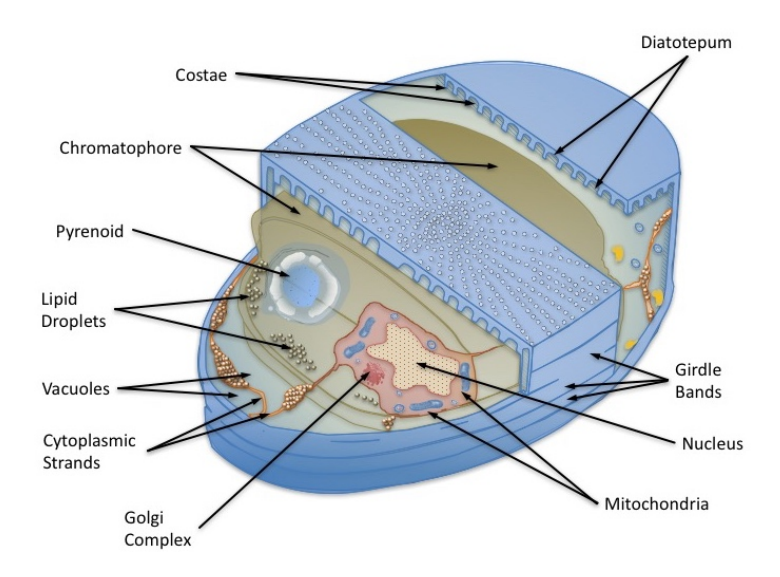


Figure 2.4. Typical centric diatom. Schematic representation of a typical centric diatom image based on Yang et al. (2011).

The diatom frustule shows a good transmittance throughout the light spectrum from ultraviolet to red light allowing the incidence of approximately 90% of visible light available for photosynthesis (Zhang et al., 2012). Therefore, frustules are believed to be an important and essential element in the successful adaptation of diatoms in the world. One of the most incredible consequences of the high porosity of the frustules is the ability to harvest light in a whole different way. When a ray of light enters the pore structure, it is scattered, and thus the probability of photon absorption increases (De Stefano et al., 2007; De Tommasi et al., 2010; Mazumder et al., 2014). In other cases, the porosity of the frustule can have a light concentration effect (microlensing) as is usually seen when a red light is beamed onto the cells (De Stefano et al., 2007; De Tommasi et al., 2010). Because of these highly-specialized abilities diatom frustules are natural photonic

structures (Fuhrmann et al., 2004; Kröger & Poulsen, 2008b; Parker, 2012).

2.1.2.5 Diatom frustules

As mentioned, the most interesting feature of diatoms is the frustule, shown by the diversity of species in the stramenopiles. These structures (pores) are highly complex and show micro and nanoscopic features (Rosengarten, 2009). Figure 2.5 shows a general schematic of diatom frustule shape and components.

It is possible to see in Figure 2.5 (A1 and B1) how the two halves of the frustule come together by the conjunction of the girdle bands (Figure 2.5. A1-g). The largest of both halves is the epivalve or epitheca (e) and correspondingly, the smallest half is known as hypotheca or hypovalve (h). Both the valve surface (vs_1 and vs_2) and mantle (vm_1 and vm_2) of the epitheca and hypotheca possess pore structures of varying diameters. The connecting bands on the girdle band are adorned with pore structures (Cupp, 1943; Losic et al., 2006a).

The pores of the valve surface usually consist of a three-layered pore superposition comprised of a cribellum (external pores), a cribrum (intermediate pores) and an internal porous layer as shown in Figure 2.6 (Gordon et al., 2009).

2.1.2.5.1 Biosilicification and frustule formation

Biominerals are minerals produced by a living organism made of a combination of both organic and inorganic compounds and formed under controlled conditions (Weiner & Dove, 2003; Skinner & Ehrlich, 2014). Diatoms and sponges are the main groups of organisms responsible for biosilicification on the planet (Martin-Jézéquel et al., 2000; Wang et al., 2012; Wang & Nilsen-Hamilton, 2013), with a few other organisms able to mineralize silicon such as radiolarians and higher plants (Schröder et al., 2008). In diatoms, the process is highly regulated by a group of biomolecules (e.g. SiTs, silaffins, polyamines), responsible for introducing and directing the movement of silicon ions within the cell (Thamatrakoln & Hildebrand, 2008; Durkin et al., 2016).

Before frustule formation, a strong silicon uptake takes place inside the silicon deposition vacuole SDV. When the valves are completed the cell divides as represented in Figure 2.7 (Kröger & Poulsen, 2008a).

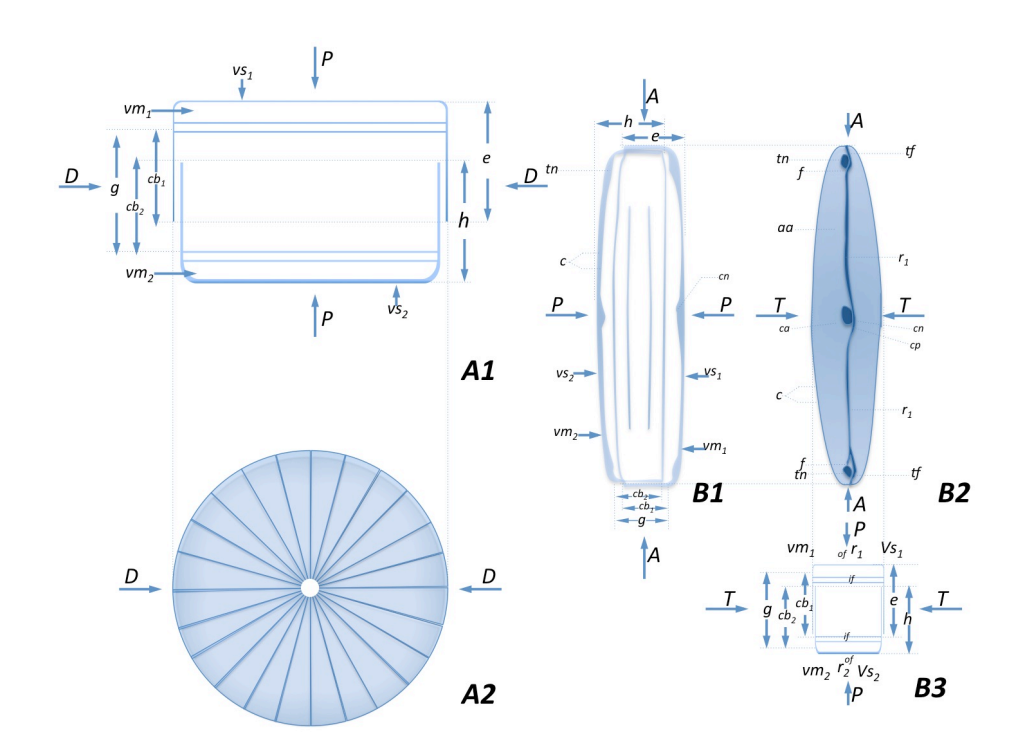


Figure 2.5. Diagrammatic representation of diatom frustules. Early representation of diatom frustules with general schematics and components. (A1) girdle view and (A2) valve view of a centric diatom. (B1) Broad girdle view; (B2) valve view; (B3) transverse section (narrow girdle view) of a pennate type diatom. P: pervalvar axis; D: diameter; A: pervalvar axis (pennate); T: trans apical axis (pennate); e: epivalve; h: hypovalve; cb₁: connecting band of epivalve; cb₂: connecting band of hypovalve; g: girdle; vs₁: valve surface of epivalve; vs₂: valve surface of hypovalve; vm₁: valve mantle of epivalve; vm₂: valve mantle of hypovalve; tn: terminal nodule (pennate); cn: central nodule (pennate); cp: central pore (pennate); r₁: raphe of epivalve (pennate); r₂: raphe of hypovalve (pennate); tf: terminal fissure or polar cleft (pennate); f: funnel- shaped body (pennate); aa: axial or longitudinal area (pennate); ca: central area (pennate); c: costae (pennate); of: outer fissure of raphe (pennate); if: inner fissure of raphe (pennate). Modified from: Cupp (1943).

The preliminary silicon surge required for the successful genesis of the frustule is guided and regulated by the feedback between internal and external conditions by the action of SiTs (Martin-Jézéquel et al., 2000; Curnow et al., 2012 Durkin et al., 2016). When silicon is available in appropriate concentrations, the inner machinery of the cell channels the

material to the SDVs (Silicon Deposition Vesicles), which contain silaffins-polyamide complexes responsible for the final frustule genesis (Vrieling et al., 1999a). Valve and band genesis is taxon-specific (Cox, 2011). In an oversimplified description of the genesis of the frustule, the process starts as a silicified annulus (Pickett-Heaps & Wetherbee, 1988; Cox, 2011; Sato et al., 2013) or a pi-shaped structure (Vartanian et al., 2009) from where the ribs expand to form the porous structures. Figures 2.7 and 2.8 show a general representation on how diatom cells produce their frustule (Cox 2011).

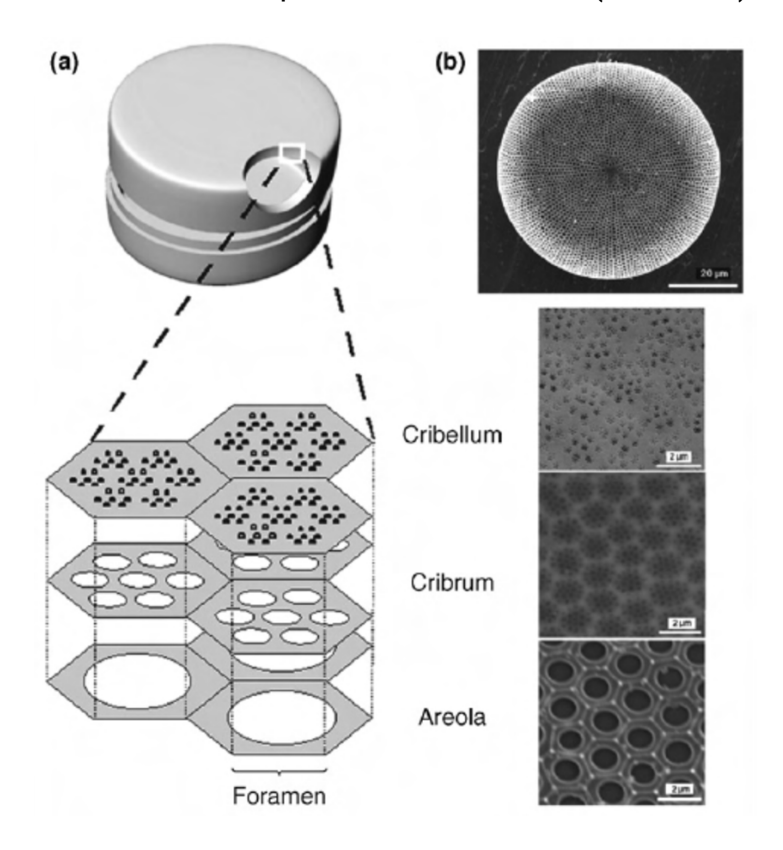


Figure 2.6. Diatom structure. (a) Schematic of a centric diatom frustule with cross-sectional three-dimensional (3D) profile of the silica wall based on SEM data. The inner layer contains honeycomb-like vertical chambers called areolae. The large hole in the floor of an areola is known as a foramen. The roof of the areolae is called the cribrum, which contains a regular pattern of pores. The layer over the cribrum is a thin siliceous membrane known as the cribellum, which consists of small pores. (b) SEM image of a *Coscinodiscus* sp. with corresponding layers (Gordon et al., 2009).

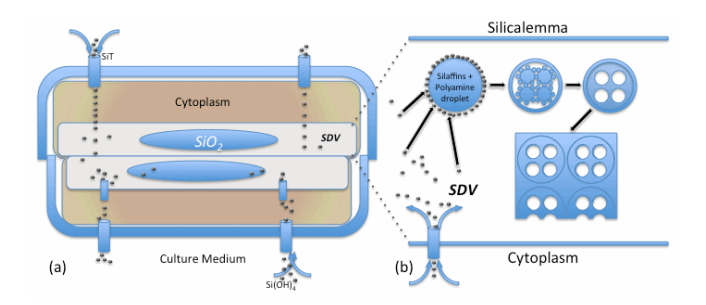


Figure 2.7. Frustule manufacturing process. Schematic diagram of the frustule manufacturing process in a diatom cell. Si(OH)₄ flows via active transport into the cytoplasm and the SDV by silicon-transport proteins (SiT). Silaffins and a polyamine system (a) catalyzes the reaction that allows soluble silicon to turn into insoluble species forming the patterned frustule (b). Based on Jeffryes (2009) and Jeffryes et al. (2013).

2.1.2.5.2 Material properties of diatom frustules

Physically and chemically like quartz (Patwardhan et al., 2005) a diatom frustule has an approximate density that ranges from 2.1 to 2.3 kg/m³ (Zhang et al., 2012) depending on the species and level of silicification. Using atomic force microscopy (AFM), Losic et al. (2007b) determined that average hardness and the elastic modulus for the cribellum, differed from those values for the cribrum, the internal, the girdle bands, the porous silicon film, and the porous silicon membrane (Table 2.1). During the same study, they managed to determine that the overall mechanical properties of *Coscinodiscus* sp. frustule silica were comparable to those of porous silicon (Tomozawa, 2001; Vinegoni et al., 2001).

Hamm et al. (2003) determined the compressive strength of four types of diatoms (*Thalassiosira punctigera*, *Coscinodiscus granii* and *Fragilariopsis kerguelensis*). Their studies found values of up to 680 MPa on the valve and 330 MPa on the girdle band. They also found a value for the Young's modulus E of up to 22.4 GPa comparable to cortical bone which stands at 20 GPa (Ashman et al., 1984; Hamm et al., 2003) or dental composites (Willems et al., 1992; Hamm et al., 2003).

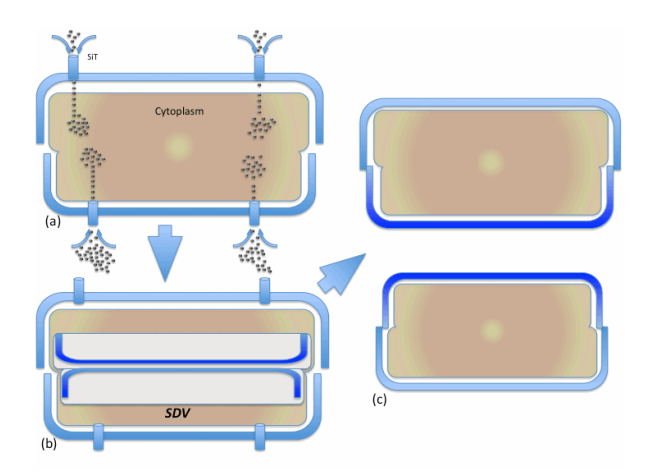


Figure 2.8. Diatom cellular division in cross section. Before separation, a mother cell harvests enough $Si(OH)_4$ (a) to produce two daughter valves (hypo and epivalve) inside the SDV (b). Later, the cell divides (c) into two daughter diatom cells with composite frustule made by the combination of one mother valve and one daughter valve from the SDV. Diagram based on Jeffryes (2009).

Diatom frustules are highly resistant to temperature (Umemura et al., 2009), which is consistent with the properties of porous silica. This resistance is one of the most attractive features of diatoms, as they manufacture the shell under low temperatures and reduced pressure conditions.

Table 2.1. Mechanical Properties of a typical diatom frustule. Mechanical Properties of Different layers of the diatom frustule of *Coscinodiscus sp.* Determined from AFM-Based nanoindentation experiments (Losic et al., 2007b).

	Porosity	Thickness (mm)	Pore Size (nm)	Hardness (GPa)	Elastic modulus (GPa)	n
Cribellum	7.5 ± 1.2	~ 0.050	45 ± 9	0.076 ± 0.034	3.4 ± 1.35	100
Cribrum	25 ± 2.5	~ 0.200	192 ± 35	0.13 ± 0.11	1.7 ± 0.84	370
Internal plate	35 ± 3.0	~ 1.000	1150 ± 130	0.53 ± 0.13	15.61 ± 5.13	300
Girdle bands	32 ± 5.0	~ 0.500	120 ± 15	0.059 ± 0.043	4.00 ± 1.9	50
Porous film	70 – 80	~ 3.000	35 ± 20	0.043 ± 0.016	8.11 ± 2.54	100
Porous membrane	60 – 65	~ 100	60 ± 20	0.62 ± 0.15	22.33 ± 3.78	50

The reader can envision the frustule as a Petri dish-like structure and has two distinctive perceptive views. One from the side (girdle) and the other one from the top (valve) with a lot more perceived variations in morphology (i.e. patterns, pores, and raphe) for the later one. In general terms, the variety of forms and symmetries can account for the vast array

of shapes and designs both from the ultrastructure and microarray of pores of the diatoms.

2.1.3 Current uses for live diatoms

Both living and dead (frustules), diatoms have found plenty of applications for humans (Gordon et al., 2005). From animal feed uses in aquaculture to medicine delivery using diatom frustules, the range of applications will be described in the following paragraphs.

2.1.3.1 Feed for other organisms

One of the most important uses of diatoms from an economic perspective, is the use of diatoms in aquaculture (Dunstan et al., 1996; van Dam et al., 2002; Kesarcodi-Watson et al., 2008). Several zooplanktonic species require diatoms and other algae species as nutritional sources. These organisms are highly regarded by producers in larval rearing facilities (Lavens & Sorgeloos, 1996) as they constitute the primary levels of the trophic web (McGinnis et al., 1997; Patil et al., 2007; Caramujo et al., 2008). Some diatoms are being researched as a possible source of non-antibiotic bactericide treatments for fish rearing facilities (Desbois & Mearns-Spragg, 2009; Li & Tsai, 2009).

2.1.3.2 Biofuel stock

Several diatom species are a target for biofuel production, as some of them produce high lipid contents under the right conditions. Ever since the late 1930s, when scientist from Germany started to explore the possibility of oil production from diatoms and proposed the use of said organisms for flue gas management in the industrial district of Ruhr, diatoms have attracted the attention of biofuel researchers (Huntley & Redalje, 2006). Some geologists believe that big petroleum deposits originated from diatom extinctions based on biostratigraphy studies (Holba et al., 1998; Theriot, 2001). Several species produce enhanced lipid bodies under nutrient (silicon, nitrogen) limitations (Tabatabaei et al., 2011; Fields et al., 2014) and under environmental stressing factors (Sharma et al., 2012; Fields et al., 2014). The lipid and fatty acid profiles of diatoms were found to be of interest to produce biofuels, and thus these organisms are a feedstock for second-generation biofuels (Ramachandra et al., 2009; Leonardi et al., 2011). It comes as no

surprise that 60% of the species recommended for further study by the Algae Species Program were diatoms (Sheehan et al., 1998; Dahiya, 2012).

2.1.3.3 EIA indicators

One of the early uses of diatom research involved work associated with water quality and eutrophication, both in marine and freshwater ecosystems (Dixit et al., 1992; Rabalais et al., 1996; Smith, 2003). Given the high success rate of several diatom species and the variation in diatom diversity found in different studies, these algae are still used as indicators of eutrophication and water quality (Dixit & Smol, 1994; Pan et al., 1996). Diatom diversity is affected by nutrient availability. When high concentrations of nutrients are available in waters, the predominant species most probably belong to the pennate group of diatoms with little to no appearance of centric diatom species (Pan et al., 1996). In contrast, a high diversity and abundance of centric diatoms occurs when water quality is better (Dixit et al., 1992; Niemi & McDonald, 2004).

2.1.3.4 Water treatment

Like other microalgal organisms, diatom communities have been used and researched for different water treatment approaches (Patel et al., 2012), the most frequent being nutrient and CO₂ regulation in aquatic bodies (Congestri & Albertano, 2011). Some diatom cells accumulate heavy metals, apparently during the silicon uptake process when the latter is scarce in the surrounding environment (Pokrovsky et al., 2005; Nam et al., 2014; Sbihi et al., 2014). One additional benefit offered by diatoms is the bioaccumulation of the heavy metals is physically constrained in the frustule structure (Olguín & Sánchez-Galván, 2012; Richards & B.J. Mullins, 2013; Sbihi et al., 2014).

2.1.4 Current uses for diatom frustules

After diatoms death, and further bacterial decay consumes the organic biomass within the shell, the frustule remains somewhat intact. Some frustules even remain unaltered after undergoing digestion from grazers (Liu & Wu, 2016). Their density and lack of buoyancy without the help of diatom oil vesicles or motility structures, force them to the bottom of the ocean where further bacterial action thoroughly cleans the shells. The accumulation of these shells creates diatomaceous earth. When diatomaceous earth is

accumulated over thousands of years, they can generate geological structures of considerable size (Antonides, 1998; Armbrust, 2009). Diatomaceous earth for human use is predominantly diatomite; a mined mineral constituted mostly by frustules of several different diatom species accumulated over thousands of years in marine or freshwater bottoms. Diatomite although readily available and cheap to mine comes with some disadvantages. The lack of uniformity in the shapes and sizes of the particles, and the presence of some pollutant species precipitated are examples of concern (Antonides, 1998; Armbrust, 2009; Liu & Wu, 2016).

Diatomaceous earth works well as absorbent agent, abrasive powder, pest control product, thermal protection and isolation coating, anticaking agent and even as a health supplement for humans and pets. Nevertheless, current developments in algae culture, and research on the intricate mechanisms of frustule formation and silicification in diatoms, open a door for newer and more elaborate applications (Gordon et al., 2005; Gordon et al., 2009).

Diatomite, kieselgur, and kieselguhr is frequently found in ancient river, lake and ocean basins around the world. Allegedly discovered in the 1830s by Peter Kasten it became a material of regular use within a short period. Alfred Nobel used it to stabilize nitroglycerin in what is now known as dynamite. Later it was used as the primary material for filtering devices by Wilhelm Berkefeld, which proved useful during the cholera epidemic in Hamburg in the early 1890s (Antonides, 1998; Group, 2014).

Presently, algal cultures offer another and somehow more reliable source of diatom shells. Mono-specific cultures can produce high yields in terms of biomass and cell counts in relatively short periods of time, given the appropriate growth conditions and protection to predatorial pressure from grazers (Andersen, 2005; Falkowski & Raven, 2007; Barlow et al., 2016), the characteristics of mono-algal-cultures allow to control the general outcome of the shells, and thus size, shape and general surface composition of the frustules can be predicted. The potential biomass yield from diatom cultures aiming to produce biofuel feedstock can in turn drive the production of frustules as a by product (Norton et al., 1996; Andersen, 2005).

2.1.4.1 Potential enhancement of culture reared diatomaceous earth

Diatom frustules produced under highly controlled environments can be easily modified to produce an enhanced final product via different approaches (Parkinson & Gordon, 1999; Gordon et al., 2009; Barlow et al., 2016).

2.1.4.2 Structurally modified diatom frustules

Diatom frustules are particles that can be as big as 500 μ m or as small as 2 μ m (Round et al., 1990). To keep things in perspective, the average size of a typical bacterium ranges between 1 and 10 μ m, the average diameter of human hair is 100 μ m, and the thickness of a conventional credit card is 760 μ m. These size ranges imply that the porous structures found in diatoms are of the order of magnitude of 40 nm, which is 10 nm smaller than the smallest airborne virus, one-third the size of HIV and approximately a fifth of the common rabies virus. From this point of view, the properties that can be added to materials transformed from diatom frustules in controlled environments are quite interesting. One example of frustule manipulation is the deposition of surface substances to reduce pore size (Losic et al., 2006d; Aw et al., 2012). Using atomic layer deposition, it is possible to coat onto the frustule surface a wide arrange of chemicals, such as Al₂O₃, ZrO₂, SnO₂, V₂O₅, ZnO, and tin (Losic et al., 2006a; Aw et al., 2012; André et al., 2013).

Another approach takes advantage of the biogenesis of the frustule. As mentioned before, from water soluble silicon compounds (Si(OH)₄), the mineral is introduced to the protoplasm machinery by SiTs and then directed to the silicon deposition vacuole (SDV) via silicon transport vacuoles (STVs). Inside the SDV, the silanol groups are hydrolyzed to Si-O-Si (Wiens et al., 2009; Wang et al., 2013; Durkin et al., 2016). At this point, the silaffins and long-chain polyamines (LCPA) catalyze the hydrolysis that directs the shape and disposition of the silicon within the structure of the frustule (Xu et al., 2006; Townley, 2011; Zane et al., 2014). Given this sequence of events, the contents of the SDV can be modified and additional elements can be added, e.g., Ti (Sewell & Wright, 2006; Lang et al., 2013; Chauton et al., 2015), Ge (Jeffryes et al., 2008a; Sewell et al., 2008; Chauton et al., 2015), Sn and Zr (Basharina et al., 2012), Cd (Gutu et al., 2009; Heredia et al., 2012), Zn (Croteau et al., 2011; Dybowska et al., 2011), Ni (Townley et al., 2007). Other

modifications to medium composition can even alter the shape of the daughter frustules after extended periods of time (Zhang et al., 2012).

Alternatively, using the biological size reduction typical for some species can generate modified structures. When carefully regulated, cultures can be synchronized to have a greater percentage of cells in the same stages of reproduction (Pollock & Pickett-Heaps, 2005; Huysman et al., 2014) and thus reducing cell frustule and pore sizes.

The highly hierarchical 3D shapes of the diatom frustules allow for their use as templates for structures made from modified materials (Pouget et al., 2007; He et al., 2013; Fattakhova-Rohlfing et al., 2014). Because hydrofluoric acid (HF) and strong alkalis dissolve the silica frustule, it is possible to partially or completely reduce the presence of silicon in the structure, increase pore size and reduce thickness (Zhang et al., 2012). Using diatoms as templates is perhaps the widest use of the shell as a manufacturing material (Sandhage et al., 2002; Gordon et al., 2009; Davis et al., 2013; Kieu et al., 2014) and frustule decoration with additional materials of interest follows closely in second place (Losic et al., 2007a; Martin et al., 2008; Elkhooly, 2014; Green et al., 2014).

Diatom silica (amorphous silica – a-Si) can be directly used in semiconductor applications albeit its lower electronic performance when compared to crystalline silica (c-Si). The highly repeatable shape and organization of the diatom frustule biogenesis is an attractive pathway for alternative bottom-up production of highly complex semiconducting nanomaterials. To date, there are different approaches looking to tap into this wide array of amazing micro and nanostructures. One approach is to use the silica-based frustules of dead diatoms and via chemical deposition of semiconducting materials (metal oxides) copy the structure under high pressure and temperatures. This process is known as bioclastic ("turning living into mineral") frustule replication (Jeffryes, 2009). Some downfalls to this method are low-throughput, high temperatures and pressures, and the fact that toxic materials must be used (Sandhage et al., 2002). Another approach is to make duplications that mimic the shape of the diatom frustule with other substances. The recurring method coats a layer of metallic titanium (Unocic et al., 2004; Van Eynde et al., 2013; Mao et al., 2014), silver (Ren et al., 2013; Toster et al., 2013b), gold (Losic et al., 2006b; Losic et al., 2007a) or another metallic element (Losic et al., 2007b;

Toster et al., 2014), directly onto the frustule. Subsequently, either the silicon is dissolved to leave the coated layer with the general shape of the frustule (Unocic et al., 2004; Losic et al., 2005; Mao et al., 2014) or the coated frustule is used as the final product (Huang et al., 2011; Toster et al., 2013b; Toster et al., 2014). Similarly, molding with sucrose can be used to produce a substrate for later use co-polymers or sol-gel silica to form the structure that is intended (Weatherspoon et al., 2005; Gautier et al., 2006; Van Eynde et al., 2013). Analogously, soft lithography with a soft polymer (PDMS) can generate a mold to cure a UV-curable polymer to generate a positive impression of a diatom frustule (Hlúbiková et al., 2012).

Alternatively, biogenic mechanisms that take advantage of the diatom natural 'disposition' to introduce impurities into the frustule have been noted as a direct bottom-up method to produce precursor materials for semiconductor manufacture (Jeffryes et al., 2008b; Lee et al., 2008; Townley et al., 2008). There are two main approaches for this purpose. The first is to recruit the cell machinery to introduce dopants such as germanium, titanium, or gallium directly into the frustule structure (Jeffryes, 2009; Gale et al., 2011; Jeffryes et al., 2011). The second is to use silaffins and long-chain polyamines directly to reproduce the bio-deposition of silica in vitro without the organism (Annenkov et al., 2006; Wieneke et al., 2011; André et al., 2013).

2.1.4.3 Semiconducting materials from diatoms

Lewin (1966) first thought about using germanium in diatoms, albeit for an entirely different purpose. Unexpectedly, Lewin discovered a correlation between the amount of silica and the effect of germanium on diatom growth, and the role of both in the silica deposition and biochemistry within the cells. Lewin also found different responses from different species to similar concentrations of germanium in the culture medium and concluded that it was a growth inhibitor. However, the concentrations used by Lewin ranged from 1 to 10 mg of GeO₂/L and were applied initially in low-silicon conditions (starvation). Further trials showed that it was possible to mitigate the effect of germanium oxide on the growth by increasing the concentration of silicon dioxide in the medium. Additionally, these series of experiments shed some light on the required conditions for a successful diatom growth inhibition using germanium (Lewin, 1966).

For the first methodology, it is important to consider the dopant concentrations and the metabolism of each species used as recipient of dopants. Given that the chemical similarity of the dopants to silicon tricks the algae into using such elements upon starvation, it is possible to create highly intricate designs with periodically inserted dopants on a silica matrix and, in theory, a frustule with a well-tuned silica-dopant ratio (Lutz et al., 2005; Jeffryes, 2009). Consequently, there are different possibilities for achieving insertion and different ratios, rates, and supplementation periods could in turn yield different structural results, even with the same species of algae.

2.1.4.4 Nanodevices and nanomaterials

Diatoms are used as reference for the fabrication of nanodevices and recently for the synthesis of nanomaterials, as their remarkable growth mechanism has inspired the production of ceramic, metal and polymer products (Norris, 2007; Schröfel, et al., 2011; Todd et al., 2014). As an emerging technology, bioinspired manufacturing can close the gap between the nanoscopic and the manufacturing world of modern industry. The use of the biological machinery available from diatoms has yielded an impressive set of results. André et al. (2012; 2013) coated glass with a polyamine-based substance and produced self-cleaning tin oxide substrates. Similarly, synthetic silaffin peptides had been used for the precipitation of silica (Wieneke et al., 2011), and a synthetic counterpart (PDMAEMA) to precipitate biological titanium (Yang et al., 2008; Yang et al., 2009; Tong et al., 2014), CdSe (Kim et al., 2012) and the production of polystyrene-graphene oxide microspheres (Kim et al., 2014). Schröfel et al. (2011) synthesized gold nanoparticles using diatoms. Similarly, Mandal et al. (2006) and Saravanamuthu (2010) synthesized cadmium sulfide nanoparticles using P. tricornutum. Although not a lot of development in the understanding of the mechanisms that aid the biogenic production of nanomaterials, the field is developing rapidly and the prospectives for the future are promising.

2.1.4.5 Biomedical and pharmacological applications

Biogenic silica (e.g. sponge spicules and diatom frustules) have shown to have unusual properties for bone regeneration working as scaffolding-materials (Pietak et al., 2004;

Toskas et al., 2013; Rentsch et al., 2014). These substances have been shown to be osteoconductive, osteoproductive and osteoinductive also aiding on the proliferation of osteoblast-like cells (Arcos & Vallet-Regí, 2010; Wiens et al., 2010; Wiens et al., 2014). Frustules have been used as vector capsules for drug delivery (Arcos et al., 2001; Arcos et al., 2003). The highly porous structure of the shell allows for relatively large molecules to enter the frustule and remain encapsulated for a while. The porosity provides a slow delivery mechanism and protection from the acidic environment of the human digestive tract, allowing acid-sensitive compounds to survive the initial steps of the gastrointestinal tract (Arcos et al., 2009; Aw et al., 2013; Bariana et al., 2013).

Interesting research found that magnetite-modified silica shells were capable of being redirected towards a tumor growth within an organism via magnetic field manipulation (Todd et al., 2014). The use of diatom shells can improve the administration of drugs. The high porosity of diatom shells combined with their prolonged liquid retention can increase the interval between doses and residence time of the drug. This dose reduction decreases the concentration requirement of the medication limiting adverse effects on human physiology (Juzenas et al., 2008). Additionally, the use of magnetized diatom shells can minimize the interaction of drugs with healthy tissues. Current pharmacological trials using diatom frustules as carriers for medication have shown the effectiveness of the pharmacological compound, the surface functional process and loading procedure as well as the maximum loading capacity, along with the method used for the analysis and the results.

2.1.4.6 Water treatment

Naturally occurring diatom frustules found an early application as water filtration materials, in a type of filter known as Berkefeld filters (Group, 2014). As mentioned before, the porosity of the shells can keep refined materials (< 40 nm) from water bodies, and that is the reason diatomaceous earth filters have found their way into beverage and pharmaceutical industries.

Magnetite-modified shells can be used to attract some metallic elements and compounds and in turn acquire magnetic properties (Müller, 2011). Additionally,

magnetite and other iron-oxide nanoscopic structures have been suggested for wastewater treatment given their ability to remove Cr(VI) from aqueous solutions (Korbekandi et al., 2009; Rai, 2009; Bhushan et al., 2014). Additionally, the use of embedded silver and gold to enhance polymer composites used for water treatment (Goho, 2004; Bhushan et al., 2014) to take advantage of their antimicrobial activity, which can be an interesting application for modified diatom frustules. When combined with chitosan and gelatin blends, they can produce an incredible hydrogel with useful capabilities, including wastewater treatment and antibacterial applications and preparations (Venugopal, 2016). Finally, in combination with live cultures of microalgae or photosynthetic bacteria, it is possible to treat biological environments (Richmond, 2004). The possibilities are so broad that it is not practical to cover them all here.

2.1.4.7 Photovoltaic applications

Among the most interesting uses thought for diatom frustules is the potential enhancement and production of low-cost, high performance photovoltaic solar cells. Solar cells require the presence of semiconducting materials to convert photonic energy into electricity. From primitive to recent materials used for solar cells, silicon stands as one of the most interesting option. Currently in use, a mix of silicon-based solar cells and dyes, sensitized via polymeric inclusion of organic elements, can produce low-cost and high-efficiency photovoltaic devices (Parker & Townley, 2007; Jeffryes et al., 2011; Lee, 2014). For silicon solar cells, it is typical to find dopants such as phosphorous and boron (Evans-Freeman & Peaker, 2001; Nishikawa, 2001). Doping alternatives include phosphorous because its electronic differences with silicon, as five valence electrons in phosphorous compared to the four regularly found in silicon, would generate a negative charge on the surface of the material (Smestad, 1998; Adachi, 2009). Boron yields a positive junction as the electron difference works towards the four provided by silicon, and hence this kind of inclusion will produce a p-type area (Adachi, 2009). When a semiconductor material contains dopants in such a way as to establish both n-type and p-type areas, a p-n junction is created (Adachi, 2009; Bhushan et al., 2014).

In 1961, solar cell efficiencies were believed to have a limit of nearly 30%, known as the Shockley-Queisser limit (Shockley & Queisser, 1961). At present, the highest value

reported for solar cell efficiency is set at 40% achieved by multi-junction solar cells in 2014. Commercial counterparts have not been able to surpass the Shockley-Queisser limit due to cost-related constraints. To date, 25.6% is the maximum effectiveness for regular silicon-based cells. The efficiency is even lower for thin-film cells that cannot reach values above 15%. Additionally, these efficiencies drop with prolonged use (Nat Nano editorial, 2014). One way to circumvent this issue is via advanced material architecture and non-conventional approaches to the manufacture of materials (Lockwood & Pavesi, 2004; Nat Nano editorial, 2014).

2.1.4.8 Light harvesting in solar cells with frustule-based materials

Amorphous silica solar cells do not have the highest efficiencies reported to date, the potential reduction in production cost of diatom-based materials and their higher efficiency as light-harvesting structures has brought them more attention (Fuhrmann et al., 2004; Toster et al., 2013a; Wu & Wang, 2014). Using ordered structures within organized silicon materials might have the same effect in low-cost photovoltaic materials as those found in regular frustules. Further advances in diatom frustule modification technologies and methodologies provides a promising future for this line of research and development.

2.1.4.9 Photocatalytic applications

As mentioned before, the possibility to dope and enhance diatom frustules with silver, gold, titanium and other elements allows for photocatalytic applications, such as water treatment and pollutant remediation (Losic et al., 2006b; Liu & Antonietti, 2013; Liu et al., 2014). Additionally, hydrogen production via water splitting can be achieved via the photocatalytic activity of materials derived from diatom-frustule modification (Reece et al., 2011; Mohan & Pandey, 2013; Mao et al., 2014). In fact, the possibility to create Si – Ge nanocomposites opens a door for future research into more advanced nanocrystalline electronic junctions from simple biomineralized materials (Liu, 2005).

2.1.5 Phaeodactylum tricornutum (Bohlin)

P. tricornutum described for the first time by Bohlin (1897) is an ideal pennate model diatom (Lewin, 1958) because it is an organism with a fully sequenced genome (Martin-

Jézéquel & López, 2003; Bowler et al., 2008; Montsant et al., 2005). Most cultures of P. tricornutum reproduce asexually (Bowler et al., 2010) allowing for better control and specialization of the cultures for analyses focused on growth conditions and nutritional assays (Yang et al., 2011). P. tricornutum does not require silicon to grow under laboratory conditions (Brzezinski et al., 1990). However, with the addition of silicon to the culture medium it grows a silicon-dense shell (i.e. frustule), like all diatoms (Borowitzka & Volcani, 1978; Lewin et al., 1958; De Martino et al., 2011). This selectivity use of silicon for the manufacture of the frustule has been known for guite a while and results in the occurrence of four different morphotypes (i.e. oval, fusiform, triradiate and tetraradiate) because different silicification levels will produce different structural configurations on the frustule and it was suggested by McConville et al. (1999) that some silicified portions of the cell wall and the level of silicification could be a response to the abundant presence of organic or inorganic components. Using atomic force microscopy, Francius et al. (2008) found that the silicified valves of oval cells provide higher mechanical resistance than valves of the fusiform, triradiate and tetraradiate morphotypes. The degree of adaptability in cell wall composition in response to environmental conditions stands as an interesting property that may allow adaptation for highly controlled silicon-based nanofabrication of materials.

2.2 Heavy metal remediation using algae

Metals are naturally occurring either as essential components (e.g. copper and zinc) or toxic elements (e.g. lead and mercury) in ecosystems (Allan, 1995). Environmental pollution by metals has become widespread as mining and industrial activities have expanded (Kennish, 1996). These industries systematically release pollutants that progressively alter aquatic ecosystems (McFarlane & Burchett, 2000) and, in areas with a high concentration of heavy industry, heavy metal pollution is one of the most difficult and serious environmental concern (Wikfors & Ukeles, 1982; Cotté-Krief et al., 2002; Esser & Volpe, 2002).

In an aquatic environment, metallic elements are present either in the sediment or in the solution, in an assortment of species (i.e. chemical forms). In the sediment as insoluble inorganic complexes, suspended particles, or organic colloid-metal associations. In

solution, metals appear as ions and organic or inorganic complexes (Kaplan, 2013). Toxic metal ions (e.g., copper, cadmium, lead, mercury) crossing membranes is the main process for heavy metal accumulation in organisms and in the case of this work, unicellular algae (Perales-Vela et al., 2006; Singh et al., 2011). The first mechanism of cation defense is complexation via functional groups (e.g. amide, amino, carbonyl, carboxyl, phosphate, sulfonate) located along the surface or the porous structures of the organism (Fourest & Volesky, 1997). Once the metal enters the cytoplasmic space (Conner & Schimid, 2006), different mechanisms can be present to protect or at least mitigate the effects on the overall bioprocesses within the organism (Cobbett & Goldsbrough, 2002). Algal species can be used to remediate heavy metal pollution in water bodies, depending directly on the resistance to the toxic treatments of the algae strain, the level of toxicity of the metal (i.e., the reactivity of the chemical species), and the time of exposure (Muse et al., 1999; Yu et al., 2010).

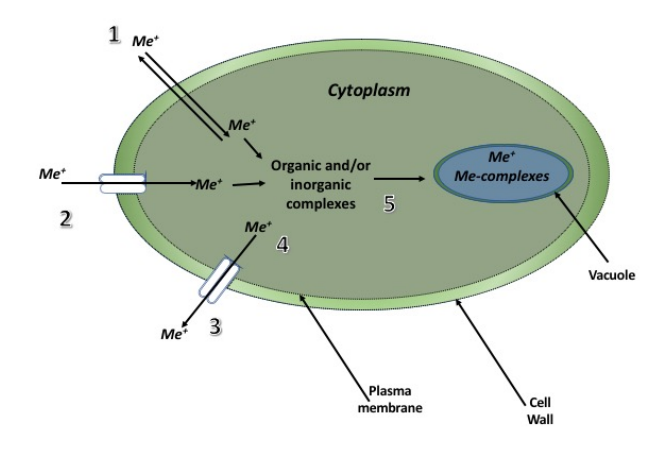


Figure 2.9. Metallic ionic uptake and detox processes inside a living cell. Schematic diagram of the five processes involved in the ionic uptake and detoxification of metallic species inside a living cell. Diffusion (1); active uptake via ion transporters (2); active efflux of free ionic metals (3); complexation of ionic species with organic/inorganic compounds and (4); vacuole transport and storage (5). Image based on Kaplan (2013).

Some bacillariophyceae replace chemicals with analogous properties along multivalent ion carriers binding sites (e.g. Ca²⁺ channels) or bind undesirable molecules that enter the cell using protein-ion complexes (Weaver et al., 2003). Later these molecules will be placed in the frustule structure or isolated in vacuoles. In diatoms, the presence of

metabolical silicon constitutes an additional advantage as this element is an efficient sorbent of metallic ions (Tsiourvasa et al., 2013). Other mechanisms used to reduce the detrimental effects of metal ions inside the cell are the use of specialized proteins and antioxidants (Cobbett & Goldsbrough, 2002) that act as metal-chelators (Cumming & Gregory, 1990; Cardozo et al., 2002; Conner & Schmid, 2003). These molecules are highly regulated and closely depend on the individual tolerance and "self-cleaning" mechanisms of the organism (Cumming & Gregory, 1990; Rosen, 1996).

Biosorption (i.e. the property of biomass to bind and concentrate heavy metals from aqueous solutions) is perhaps one of the most attractive applications for algae cultures in present times (Simkiss & Wilbur, 1989). A biphasic process comprised of adsorption followed by absorption with accumulation. The first by means of extracellular materials (e.g. polysaccharides and mucilage) and cell wall components (e.g. carboxyl and hydroxyl groups) in a non-metabolic process which is a fast response to high levels of stressors in the environment (Naja & Volesky, 2011; Kaplan, 2013). The second phase takes place in the cytoplasm. A slow enzyme-led process involving active transport through the cell membrane and binding proteins as intracellular counterparts to the ionic presence of metallic species (Wilde & Beneman, 1993; Naja & Volesky, 2011; Kaplan, 2013).

Since the early 1990s, the number of publications related to biological processes for metal removal increased and showed a growing interest in the potential of microalgae to be used as biosorption routes (Perales-Vela et al., 2006; Kaplan 2013).

2.3 Biomineralization

Biomineralization is the process used by biological organisms to form minerals in a controlled fashion instead of abiotic forces interacting with chemical species (Perkins, 2002). The interest in understanding processes that regulate the mineralization under organic control has increased with the improved knowledge of biochemical systems (Weiner & Dove, 2003).

Fossil evidence suggests that these interactions started approximately 3.8 billion years ago with metamorphic rocks found in Isua, Greenland, that showed the carbon within was deposited by bacterial species (Crick, 1989) and over several geologic periods, both

prokaryotic and eukaryotic organisms developed the capacity to shape minerals (Weiner & Dove, 2003). As an example, it is now hypothesized that autotrophic bacteria may have been responsible for the pyrite sediments of the Archaean period (Crick, 1989).

Biomineralization and archaic biomineralizing organisms contributed to the development of more sophisticated organisms and adaptations. For instance, the action of sulfur autotrophic bacteria led to a more stable and milder environment for evolutionary success as sulfate was reduced to produce oxygen under conditions presently found close to volcanic vents in the ocean, typical of ancient environments (Crick, 1989; Dahl & Friedrich, 2008). This newly acquired source of oxygen decreased the discharge of methane and carbon dioxide from ferrous iron cycling and subsequently, lowered the concentration of atmospheric greenhouse gases and helped reduce atmospheric temperatures (Crick, 1989) and apparently, this ability of bacteria to reduce sulfate was a prerequisite for an oxygen-rich atmosphere and the evolution of eukaryotes and metazoan organisms (Garrels, 1989). The evolution of biomineralization mechanisms, benefited the prehistoric ocean as the buildup of calcium deposits was paramount on the advent of multicellular life through biocalcification (Kempe et al., 1989). Most minerals identified to date appear to be the result of abilities that evolved over 500 million years ago in a variety of taxonomical groups (Knoll, 2003).

2.3.1 Definition of biomineral

A biomineral is a mineral produced by a living organism, via combination of both organic and inorganic constituents under controlled conditions (Weiner & Dove, 2003; Skinner & Ehrlich, 2014). Biochemical control allows the production of materials with enhanced properties (e.g. shape, size, elemental composition, crystalline structure) that would be unlikely displayed in geologically or inorganically formed equivalents (Crick, 1989; Chen et al., 2004; Skinner & Ehrlich, 2014). A wide variety of elements can be found in biominerals with calcium as the most abundant ion present in biominerals (González-Muñoz et al., 1996; Naka, 2007; Wei et al., 2007) and one of the most important ions associated with metabolism (Wilbur & Simkiss, 1979; Simkis, 1984; Simkiss & Taylor, 2001). Other minerals include silicon, employed by different taxonomical groups both for structure and defense (Scröder et al., 2008; Tesson & Hildebrand, 2013; Skinner & Ehrlich,

2014), iron (magnetite and others), phosphorous (phosphates), and sulfur (sulfates).

Two key aspects of biomineralization are specificity (ions and conditions) and replicability (Bäuerlein, 2003; Sumper et al., 2005; Skinner & Ehrlich, 2014). Research is aiming to understand the biochemical regulation of these processes. For example, it is known that approximately 60% of all biogenic materials including all known silicon-based biominerals, contain water or hydroxyl groups (Weiner & Dove, 2003). There is compiling evidence of a considerable number of carbonate biominerals undergoing a preliminary hydrated phase (Beniash et al., 1997; Treves et al., 2003; Metzler et al., 2008), which is consistent with a reduction in energetic barriers in aqueous solutions. This phenomenon is a possible explanation for the high degree of intricacy achieved by biominerals when compared to inorganically formed counterparts. At the nano and microscopic level, these structures and levels of complexity, visible throughout micro and macroscopic organisms, would require extensive research and development to replicate using human-made approaches. Another key characteristic is the presence of organic materials (e.g. collagen, chitin) bridging the compound mineral crystals clusters (Beniash et al., 1999; Treves et al., 2003; Metzler et al., 2008).

2.3.2 Evolution of biominerals

Evolution aided in the development of locations and mechanisms within organisms to enable the biomineralization process, guaranteeing the availability of minerals in sufficient quantities for cytoplasmic machinery to collect these minerals into matrixes (Wilbur & Simkiss, 1979; Kröger & Poulsen, 2008a; Annenkov et al., 2013) with ions flowing by passive diffusion or active pumping, facilitated by diverse mechanisms, such as the action of membrane or transport proteins, osmotic differentials, and pH regulation (Vrieling et al., 2005; Matsunaga et al., 2007; Durkin et al., 2016).

Biomaterials can be generated either by biologically induced or controlled mineralization (Hübler, 2010). When biological activity results in mineral precipitation, biomineralization is a secondary outcome usually which involves cell surfaces producing the nucleation of mineral growth (Weiner & Dove, 2003). These processes often occur without metabolic control and are the result of responses to regulate environmental conditions (e.g. pH, ion

concentration, temperature) and the presence of specific substances (Wang & Müller, 2009; Li et al., 2013; Moisescu et al., 2014). Some organisms can use a complex system involving morphology features and intracellular processes to mineralize (Li et al., 2013; Livingston et al., 2006; Bäuerlein, 2003); the outcome is controlled not by environmental conditions, but biochemically and is usually constrained to an isolated structure (Li et al., 2013; Wang et al., 2009; Ehrlich, 2010). Consequently, the degree of complexity and replicability in these processes are remarkable, and these organisms and the mechanisms regulating this type of mineralization are increasingly becoming a research target. These processes can occur extracellularly, internally or intracellular.

In extracellular mineralization, a cell produces a three-dimensional extracellular matrix (e.g. polysaccharide or glycoprotein) and transfers materials into this array either via ionic pumps in the membrane (Wilbur & Simkiss, 1979; Simkiss, 1984; Simkiss & Wilbur, 1989) or vesicle-release into the adjacent structure (Anderson et al., 1970; Cassella et al., 1996; Beniash et al., 1999), in either case, the cell is actively supplying ions to the matrix. This type of mineralization is characteristic in foraminifera, mollusca, bryozoa, and metazoa (Wilt, 2005; Griesshaber et al., 2007; Skinner & Ehrlich, 2014).

Intracellular mineralization typically occurs in colony-forming or community-living unicellular organisms, often confused with extracellular mineralization, because the structure lies on the outskirts of the cellular protoplasm. However, the outer membrane of the organism functions as the isolating site for the mineralization process to advance, while the organism regulates the shape of the mineral (Borowitzka & Larkum, 1974; Borowitzka, 1982).

Finally, when mineralization occurs within a specialized structure of the cell protoplasm, the process is said to be intracellular, a common strategy among several taxonomical groups. The cell has high control over all conditions regulating the process (e.g., concentration of ions, pH, salinity, proteins, trace metals) and generates quite intricate structures, such as shells of diatoms and radiolarians, exoskeleton of echinoderms (Wilt, 2002; Finkel & Kortc, 2010; Not et al., 2012). The cell walls (frustules) of diatoms are an excellent example of the intricacy and replicability of controlled intracellular mineralization. Nonetheless, not all structures with an intracellular origin protrude outside

the protoplasm. For some organisms, this mechanism produces vital structures within the cell membrane, e.g. magnetotactic bacteria (Kirschvink et al., 1996; Matsunaga et al., 2007; Kolinko et al., 2016).

2.3.3 Biomineralization in microorganisms

All major taxa have organisms with the capacity to produce biomineralized materials or structures. Table 2.2 provides a general summary of research work on each taxon (i.e. group), the element or material that is produced, and the structures responsible for the process. Additionally, it provides a list of references for further reading.

Table 2.2. Biomineralization in biological organisms.

Group	Chemical compounds	Structures	Sources
Bacteria	Metal carbonates, silicates, magnetite, selenium, cadmium, silver, gold, platinum, zinc, mercury, cobalt	Mineral deposits	Lowenstam, 1981; Skinner & Ehrlich, 2014
Foraminiferida	Aragonite, calcite (CaCO ₃)	Shells	Ellis, 1940; Skinner & Ehrlich, 2014
Calcareous Algae	CaCO ₃	Carbonate deposits, endodermal cell deposits for coral reefs	Borowitzka & Larkum, 1976; Skinner & Ehrlich, 2014
Coccolithophores	CaCO ₃	Coccoliths	Sawada & Shiraiwa, 2004; Skinner & Ehrlich, 2014
Stremenopiles (i. diatoms)	e. SiO ₂ ·nH ₂ O	Frustules	Falciatore & Bowler, 2002; Kröger, 2007; Skinner & Ehrlich, 2014
Radiolaria	SiO ₂ ·nH ₂ O, CaSO ₄ ·2H ₂ O	Outer shell/skeleton	Skinner & Jahren, 2007; Suzuki & Aita, 2011; Skinner & Ehrlich, 2014

2.3.3.1 Bacterial

Bacteria are one of the earliest organisms on Earth (Dobrestov et al., 2008). Several groups of bacteria are responsible for paleontological mineral deposits and a wide range of mineralization processes (Lowenstam, 1981) including those involving metal carbonates (Chen et al., 2009; Kim et al., 2011; Liang et al., 2013), silicates (Likhoshway et al., 2008; Jaroch et al., 2011; Ni et al., 2008) and other elements such as magnetite particles (Prozorov et al., 2013; Lang & Schüler, 2008; Iwahori et al., 2014), selenium (Lloyd et al., 2008; Butler, 2012; Lenz et al., 2011), cadmium (Okuda et al., 2010), silver (Naik et al., 2002; Malhotra et al., 2013), gold (Bäuerlein , 2003; Malhotra et al., 2013; Fairbrother et al., 2013), platinum (Bäuerlein, 2003), zinc (Naik et al., 2002; Yan et al.,

2009), mercury (Tazaki, 2013), and cobalt (Prozorov et al., 2013; Shim et al., 2011; Wolff et al., 2012).

Bacteria can act upon mineral species in mild and harsh conditions (Li et al., 2013; Furey & Liess, 2013). Cyanobacteria is an example which can inhabit even the harshest of environments (e.g. thermal springs) and has generated great interest for research (Benning et al., 2004; Amores et al., 2009; Skinner & Ehrlich, 2014). Cyanobacteria can produce extracellular amorphous deposits of silicon in polysaccharide casings (Weiner & Dove, 2003; Benning et al., 2004) although they lack the specific differentiation and control seen in diatoms and porifera.

2.3.3.2 Foraminiferida

Analysis of foraminifera residues yields copious chronological and environmental information in biostratigraphy (Skinner & Ehlrich, 2014). There are over 4,000 extant (mostly benthic) and around 30,000 extinct known species of foraminifera (Ellis, 1940). The material attached to the shell defines the divisions of foraminifera (Ellis, 1940; Skinner & Jahren, 2007; Skinner & Elrich, 2014). Some species (e.g. organisms from the Allogromia) insert environmental materials into a membranous shell, with some material-specific species, others attach any minerals found in the medium (acidic cementation on a protein matrix) using pseudopodia (Roberts & Murray, 1995; Skinner & Elrich, 2014) and others use highly complex mineralized shells (tests) made of aragonite- or calcite-based minerals (De Nooijer et al., 2014). Finally, some coexist symbiotically with photosynthetic organisms, e.g. dinoflagellates and chlorophytes (Martin, 1996), while the symbionts handle most of the mineralization process (Brummer et al., 1987; Doo et al., 2014).

2.3.3.3 Calcareous algae (green, coralline, red algae), and dinoflagellates

Some species of algae produce intercellular sheaths (e.g., *Halimeda* sp. – Borowitzka & Larkum, 1976; *Udotea* sp. – Nakatsu et al., 1981; Kleypas & Yates, 2009), filament or blade-like calcified structures (e.g. *Penicillus* sp., *Rhipocephalus* sp., some *Udotea* sp. – Kleypas & Yates, 2009), all triggered by photosynthesis induced pH changes at the calcification site (Borowitzka, 1981; Borowitzka 1982).

Dinoflagellates are calcifying organisms with approximately 2,000 mostly free-living heterotrophic and some parasitic species (Godhe et al., 2008). The former are important primary producers in coastal environments (Koumandou et al., 2004; Valiadi et al., 2012; Marcinko et al., 2013), and most species from the latter are symbionts with corals (e.g., Symbiodinium sp. in endodermal cells of corals) having little or no direct contact with the surrounding environment (Farrant et al., 1987; McGinty et al., 2012; Weber & Medina, 2012).

2.3.3.4 Coccolithophores

Organisms of the algae phylum Haptophyta (approximately 500 marine species) handle approximately 50% of CaCO₃ deposition on Earth. The term coccolithophore derives from the calcite scales (coccoliths) that cover the cell. *Emilliania huxleyi*, their best-known representative, is highly abundant and a critical component of the ocean equilibrium because it fixes environmental carbon via mineralization and photosynthesis (Sawada & Shiraiwa, 2004; Vasconcelos et al., 2004; Not et al., 2012). Coccolithophorid blooms influence local climate because the optical properties of the organisms can reflect sunlight and block the entrance of heat into the water column (Hovland et al., 2014). In some cases, the rate at which inorganic carbon is fixed (CaCO₃) can be comparable to that of photosynthetic carbon (Moheimani et al., 2011; Moheimani et al., 2012).

2.3.3.5 Stramenopiles (diatoms)

Silicon biomineralization is perhaps one of the most exciting processes studied to date. Diatoms (Bacillariophyta) are the major component of phytoplanktonic communities. Around 100,000 species (marine, freshwater, and terrestrial) handle over 40% of the total marine primary productivity (Drum & Gordon, 2003; Not et al., 2012; Fon Sing et al., 2013), and are the dominant group regulating oceanic silicon cycles (Ragueneau et al., 2006; Likhoshway et al., 2008; Fields et al., 2014). The interest in silicon mineralization in diatoms comes from the intricate structure and high reproducibility of the frustule, the latter being the source of taxonomic differentiation and a source of an incredible amount of shapes and functionality with potential industrial applications. The frustule manufacturing process involves several steps. The first step is the accumulation of

silicon by active transportation by membrane proteins known as Silicon Transporters or SiTs (Falciatore & Bowler, 2002; Brunner et al., 2009; Durkin et al., 2016). As the silicon content increases within the protoplasm, transport vesicles (STVs) feed the deposition of silicon in the deposition vacuole (SDV) where the new frustules will form (Hazelaar et al., 2005; Kröger & Pulsen, 2008b; Annenkov et al., 2013). A group of proteins known as silaffins combined with polyamines regulates this deposition (Poulsen & Kröger, 2004; Armbrust, 2009; Poulsen et al., 2013). A more detailed explanation of the process of frustule formation will be presented in detail later.

2.3.3.6 Radiolaria

Radiolaria (Rhizaria) manufacture an intricate outer shell made of silicon (Spumellaria and Nassellaria) or other materials, e.g. strontium sulfate in Acantharea (Suzuki & Aita, 2011). Their structures help distinguishing between taxonomic entities within the group and identify organisms (Ben Fadhel et al., 2014). These organisms take monomeric silicic acid and by dehydration and polymerization processes produce an opal-based shell with different hardness levels (Skinner & Jahren, 2007; Skinner & Ehrlich, 2014). It is common to study the uptake rates and levels of polymerization and dehydration in organisms by substituting silicon with germanium, i.e. Si(OH)₄ with Ge(OH)₄ (Skinner & Ehrlich, 2014).

2.4 Organisms in nanotechnology

From Greek, "nano" means dwarf and the SI defines one nanometer as one billionth of a meter (1 nm = 1×10^{-9} m). As mentioned before, nanotechnology deals in sizes of a thousandth of a micron or a millionth of a millimeter so to be clear, only objects of 6 to 29 µm can be seen by good eyes at a focal distance of roughly 100 mm with an average maximal acuity of 0.4 to 1 MAR (i.e. Minimum angle of resolution defined by Kalloniatis & Luu, 2007). Although modern interest in nanotechnology circa the 1960s after a lecture by Richard Feynman entitled "There's Plenty of Room at the Bottom" (Feynman, 1959), the use of nanotechnology is not new and can be traced to ancient civilizations (Daniel & Astruc, 2004; Paul & Chugh, 2011; Krishnaswamy, 2015).

The advent of nanotechnology has its origins in 400 BC, when Leucippus and Democritus proposed the atom as a discrete, indestructible, and fundamental particle composing

matter (Fitzpatrick, 2006; Malpas, 2012; Redmond, 2014). Two millennia after that depiction (1803), John Dalton took the concept once more and built a theory around it (Dalton, 1808) that was dominant for nearly a century until in 1897, when J. J. Thomson discovered the charged particles that constitute the atom (Thomson, 1904). Nearly three decades later (1926), Schrödinger formulated the wave equation, a series of differential equations that described the properties of electrons assuming these particles exist as waves, this opened the new train of thinking about atoms as mathematical equations instead of concrete structures (Schrödinger, 1926). One year later, Heisenberg derived the Uncertainty Principle which has significant implications for small particles as to the more precise the determination of the position, the less precise the knowledge of the momentum and vice versa. Within one year (1927), the Solvay Physics Conference, held in Brussels, Belgium brought forward the contributions of Schrödinger, Heisenberg, Planck, de Broglie, Einstein, Bohr, Oppenheimer, and Dirac to the field of quantum mechanics (Bohr, 1961; Bacciagaluppi & Valentini, 2009).

At this point in time it was more accepted that matter has different properties at the microscopic and macroscopic levels and laws of physics and chemistry that applied to large masses were not equivalent for small particles such as electrons. Four years later Knoll and Ruska (1931) invented the first electron microscope (Freundlich, 1963; Ruska, 1979; Ruska, 1987), and five after that Müller (1936), invented the field emission microscope (FEM). Almost two decades later Müller (1951) invents the field ion microscope (FIM) which allowed them to first experimentally observe atoms in 1957. As mentioned before, in December 1959 Feynman delivers the classic talk "There's Plenty of Room at the Bottom" opening the doors to the new field of physics, at the annual meeting of the American Physical Society at Caltech (Feynman, 1959). In his talk, Feynman suggested the manipulation of individual atoms and molecules to manufacture novel materials and structures, and challenged the audience to print a book page on an area of 1/25,000 smaller in linear scale to the original, and manufacture a rotating electric motor that could be controlled from the outside with a size of an 1/64-inch cube.

In 1960, McLellan collected the check from Feynman's challenge by building a motor that met the conditions (Lyshevski, 2005). Five years later, Moore (1965) predicted that the

number of circuits on a silicon chip would double every year and modified the prediction in 1975 to every 18-24 months, on what is now known as "Moore's Law," just one year after Taniguchi (1974) coined the term "Nanotechnology." Six years later, Binning and Rohrer (1983, 1984, 1986, 1987) invented the scanning tunneling microscope (STM) based on the properties of electrons and has the potential to pick and move individual atoms and molecules to construct nanoscale objects (Binning & Rohrer, 1987). The same year Drexler (1981) publishes the first scientific paper on molecular nanotechnology. Four years later, and 25 years after the challenge was put forth, Newman reduced the size of the first page of "A Tale of Two Cities" by Charles Dickens to 1/25,000 of its size using a focused electron beam to carve the letters on the substrate (Gribbin & Gribbin, 1997). In the same year, an allotrope of carbon (i.e. buckminsterfullerene) was discovered by Smalley, Curl, and Kroto. This allotrope was the basis for the construction of carbon structures known as nanotubes (Kroto, et al., 1985).

The next year, Binning, Quate, and Gerber invented the atomic force microscope (AFM), a modification of the STM where a tip meets the surface under analysis (Binning et al., 1986), and the Nobel prize was divided among Ruska for the invention of the first electron microscope, and Binning and Rohrer for the invention of the STM (Nobel Media, 2017). Three years later, Eigler became the first person to move and control individual atoms spelling "IBM" with xenon atoms on the surface of nickel, and 35 individual xenon atoms were used to spell the name of the company using STM with an unprecedented precision (Eigler & Schweizer, 1990). One year after this feat, the first global peer-reviewed journal in nanoscale science and engineering (i.e. "Nanotechnology") was launched in the UK. In 1991, the EPA coined the term "Green Chemistry" which later was complemented by the postulation of the 12 principles of Green Chemistry (Anastas & Warner, 2000; Abraham & Nguyen, 2003; Anastas & Zimmerman, 2003). In the same year (1990) lijima discovered the presence of carbon nanotubes in soot after vaporization of carbon in an electric arc (Ijima, 1991). In 1995, Choi and Eastman proposed that nanoparticles have the potential to enhance thermal conductivity in some fluids and opened the door for the research of nanofluids (Choi & Eastman, 1995). One year later, Curl, Kroto, and Smalley shared a Nobel prize in chemistry for their work on fullerenes (Nobel Media, 2017), and IBM's

James Gimzewski and his team created the first "atomic" abacus (Cuberes et al., 1996). Four years later, the National Nanotechnology Initiative (NNI, 2016) was launched by the U. S. Government and several universities and research institutes made plans and created nanoscience and nanotechnology centers (e.g. MINATEC, Grenoble, France; National Center for Nanoscience and Technology, Beijing, China; National Applied Research Labs, Hsinchu, Taiwan; National Institute for Nanotechnology, Alberta, Canada). From that date forward, the number of publications and articles related to the subject of silver nanoparticles has reached over 12,000 in Web of Science, 37,000 in Scopus and 970,000 in Google Scholar, with over 2,500; 11,000; and 400,000 devoted to the synthesis of nanoparticles for Web of Science, Scopus and Google Scholar respectively, and 1, 7, and 325 publications directly referencing the term "silver nanoparticle" and the algae *P. tricornutum*, for the mentioned publications, although not closely related with synthesis but biotoxicity of the material on the algae and three of them reviews (Web Of Science, 2017; Scopus, 2017; Google Scholar, 2017). A list of some terminology related to nanotechnology, taken from the ASTM E 2456-06 standards, can be seen in Appendix I.

Nevertheless, the use of silver nanoparticles in different industries and applications is not new. According to Nowack, et al. (2011) humans have used silver nanoparticles for more than 120 years, and scientific work targeted them as objects of interese since long before the term "nano" started to appear in the nomenclature of articles in recent years. Metallic nanoparticles have been the center of attention in contemporary researches due to their size-, shape-, and crystal structure-specific physical, chemical, electronical, and optical properties, which differ substantially from those of their bulk sized counterparts (Sau & Rogach, 2012; Krisnaswamy, 2015). Among the choices of metallic elements, iron (Fe), copper (Cu), zinc (Zn), palladium (Pd), silver (Ag), cadmium (Cd), platinum (Pt), and gold (Au), are some of the most commonly synthesized metallic nanoparticles (Rodríguez & Fernández-García, 2007; White et al., 2009; Makarov et al., 2014). A range of microorganisms, including diatoms, have been reported to synthesize nanoparticles of different types, such as gold, silver, magnetite, selenium, tellurium, cobalt oxide, cadmium sulfide (Table 2.3).

Table 2.3. Synthesis of nanoparticles by microorganisms (Mandal et al., 2006; Narayanan & Sakthivel, 2010; Hulkoti & Taranath, 2014).

Cadmium sulfide and selenide Bacteria: Clostridium thermoaceticum, Gluconoacetobacter xylinus, Klebsiella aerogenes, Rhodopseudomonas Escherichia coli, Klebsiella pneumoniae Actinomycetes, yeast, and fungi: Candida glubrata, Schizosaccharomyces pombe, Coriolus versicolor, oxysporum (both) Virus (viral capsid template): M13 bacteriophage, Tobacco mosaic virus (TMV) Cyanobacteria and algae: Phaeodactylum tricornutum Gold and gold-silver alloy Bacteria: Escherichia coli, Klebsiella pneumoniae, Bacillus megatherium, Geobacillus sp., Marinobacter Plectonema boryanum, Rhodobacter capsulatus, Rhodopseudomonas capsulate, Thermomonospora sp., Slalgae, Bacillus subtilis, Pseudomonas fluorescens, Lactobacillus sp. (both), Pseudomonas aeruginosa Actinomycetes, yeast, and fungi: Aspergillus oryzare, Colletotrichum sp., Pichia jadinii, Rhodococ Thermomonospora sp., Trichothecium sp., Verticilum luteoalbum, Yarrowia lipolytica, Schizosaccharomyces of Volvariella volvácea (both), Fusarium oxysporum (both), Verticillium sp. Virus (viral capsid template): M13 bacteriophage, Tobacco mosaic virus (TMV) Cyanobacteria and algae: Anabaena sp., Calothrix sp., Chlorella sp., Chlorella vulgaris, Coelastrella sp., Diadesm Gracilaria corticata, Leptolyngbya sp., Lyngbya majuscule, Microcoleus chthonoplastes, Navicula atomus Navicula minima, Padina gymnospora, Phormidium valderianum, Phormidium willei, Plectonema b Rhizoclonium fontinale, Rhizoclonium hieroglyphum, Rhizoclonium riparium, Sargassum wightii, Spirulina Spirulina subsalsa, Steochespermum marginatum, Tetraselmis kochinensis, Tetraselmis suecica, Turbinaria	Fusarium Pelagius, hewanella
Actinomycetes, yeast, and fungi: Candida glubrata, Schizosaccharomyces pombe, Coriolus versicolor, oxysporum (both) Virus (viral capsid template): M13 bacteriophage, Tobacco mosaic virus (TMV) Cyanobacteria and algae: Phaeodactylum tricornutum Gold and gold-silver alloy Bacteria: Escherichia coli, Klebsiella pneumoniae, Bacillus megatherium, Geobacillus sp., Marinobacter Plectonema boryanum, Rhodobacter capsulatus, Rhodopseudomonas capsulate, Thermomonospora sp., Sl algae, Bacillus subtilis, Pseudomonas fluorescens, Lactobacillus sp. (both), Pseudomonas aeruginosa Actinomycetes, yeast, and fungi: Aspergillus oryzare, Colletotrichum sp., Pichia jadinii, Rhodocod Thermomonospora sp., Trichothecium sp., Verticilum luteoalbum, Yarrowia lipolytica, Schizosaccharomyces of Volvariella volvácea (both), Fusarium oxysporum (both), Verticillium sp. Virus (viral capsid template): M13 bacteriophage, Tobacco mosaic virus (TMV) Cyanobacteria and algae: Anabaena sp., Calothrix sp., Chlorella sp., Chlorella vulgaris, Coelastrella sp., Diadesm Gracilaria corticata, Leptolyngbya sp., Lyngbya majuscule, Microcoleus chthonoplastes, Navicula atomus Navicula minima, Padina gymnospora, Phormidium valderianum, Phormidium willei, Plectonema backeria in the programment of	Pelagius, hewanella ccus sp.,
Virus (viral capsid template): M13 bacteriophage, Tobacco mosaic virus (TMV) Cyanobacteria and algae: Phaeodactylum tricornutum Gold and gold- silver alloy Bacteria: Escherichia coli, Klebsiella pneumoniae, Bacillus megatherium, Geobacillus sp., Marinobacter Plectonema boryanum, Rhodobacter capsulatus, Rhodopseudomonas capsulate, Thermomonospora sp., Sł algae, Bacillus subtilis, Pseudomonas fluorescens, Lactobacillus sp. (both), Pseudomonas aeruginosa Actinomycetes, yeast, and fungi: Aspergillus oryzare, Colletotrichum sp., Pichia jadinii, Rhodocor Thermomonospora sp., Trichothecium sp., Verticilum luteoalbum, Yarrowia lipolytica, Schizosaccharomyces of Volvariella volvácea (both), Fusarium oxysporum (both), Verticillium sp. Virus (viral capsid template): M13 bacteriophage, Tobacco mosaic virus (TMV) Cyanobacteria and algae: Anabaena sp., Calothrix sp., Chlorella sp., Chlorella vulgaris, Coelastrella sp., Diadesm Gracilaria corticata, Leptolyngbya sp., Lyngbya majuscule, Microcoleus chthonoplastes, Navicula atomus Navicula minima, Padina gymnospora, Phormidium valderianum, Phormidium willei, Plectonema b Rhizoclonium fontinale, Rhizoclonium hieroglyphum, Rhizoclonium riparium, Sargassum wightii, Spirulina	hewanella ccus sp.,
Gold and gold-silver alloy Bacteria: Escherichia coli, Klebsiella pneumoniae, Bacillus megatherium, Geobacillus sp., Marinobacter Plectonema boryanum, Rhodobacter capsulatus, Rhodopseudomonas capsulate, Thermomonospora sp., Sl algae, Bacillus subtilis, Pseudomonas fluorescens, Lactobacillus sp. (both), Pseudomonas aeruginosa Actinomycetes, yeast, and fungi: Aspergillus oryzare, Colletotrichum sp., Pichia jadinii, Rhodocod Thermomonospora sp., Trichothecium sp., Verticilum luteoalbum, Yarrowia lipolytica, Schizosaccharomyces of Volvariella volvácea (both), Fusarium oxysporum (both), Verticillium sp. Virus (viral capsid template): M13 bacteriophage, Tobacco mosaic virus (TMV) Cyanobacteria and algae: Anabaena sp., Calothrix sp., Chlorella sp., Chlorella vulgaris, Coelastrella sp., Diadesm Gracilaria corticata, Leptolyngbya sp., Lyngbya majuscule, Microcoleus chthonoplastes, Navicula atomus Navicula minima, Padina gymnospora, Phormidium valderianum, Phormidium willei, Plectonema backeria Rhizoclonium fontinale, Rhizoclonium hieroglyphum, Rhizoclonium riparium, Sargassum wightii, Spirulina	hewanella ccus sp.,
algae, Bacillus subtilis, Pseudomonas fluorescens, Lactobacillus sp. (both), Pseudomonas aeruginosa Actinomycetes, yeast, and fungi: Aspergillus oryzare, Colletotrichum sp., Pichia jadinii, Rhodococ Thermomonospora sp., Trichothecium sp., Verticilum luteoalbum, Yarrowia lipolytica, Schizosaccharomyces c Volvariella volvácea (both), Fusarium oxysporum (both), Verticillium sp. Virus (viral capsid template): M13 bacteriophage, Tobacco mosaic virus (TMV) Cyanobacteria and algae: Anabaena sp., Calothrix sp., Chlorella sp., Chlorella vulgaris, Coelastrella sp., Diadesm Gracilaria corticata, Leptolyngbya sp., Lyngbya majuscule, Microcoleus chthonoplastes, Navicula atomus Navicula minima, Padina gymnospora, Phormidium valderianum, Phormidium willei, Plectonema b Rhizoclonium fontinale, Rhizoclonium hieroglyphum, Rhizoclonium riparium, Sargassum wightii, Spirulina	ccus sp.,
Navicula minima, Padina gymnospora, Phormidium valderianum, Phormidium willei, Plectonema b Rhizoclonium fontinale, Rhizoclonium hieroglyphum, Rhizoclonium riparium, Sargassum wightii, Spirulina	nis gallica,
Ulva intestinalis, Chondrus crispus, Spyrogira insignis	platensi,
Lead sulfide Bacteria: Rhodobacter sphaeroides Actinomycetes, yeast, and fungi: Torulopsis sp.	
Virus (viral capsid template): Tobacco mosaic virus (TMV) Magnetite Bacteria: Actinobacter sp., Aquaspirillum magnetotacticum, Geobacter metallireducens, Magneto	ospirillum
Magnetospirillum magnetotacticum, Magnetospirillum gryphiswaldense, Thermoanaerobacter ethanolicus Actinomycetes, yeast, and fungi: Fusarium oxysporum, Verticillium sp. Virus (viral capsid template): Tobacco mosaic virus (TMV)	,opiimarii,
Others Bacteria: Brevibacterium casei (cobalt oxide)	
Actinomyvetes, yeast, and fungi: Fusarium oxysporum (zirconia, strontium carbonate, bismuth	າ oxide),
Schizosaccharomyces cerevisiae (antimony oxide) Palladium Bacteria: Desulfovibrio desulfuricans, Shewanella oneidensis	
Platinum Bacteria: Shewanella algae, Pseudomonas boryanum Actinomycetes, yeast, and fungi: Fusarium oxysporum	_
Selenium Bacteria: Pseudomonas aeruginosa, Bacillus selenitireducens, Sulfospirillum barnesii, Selenihalanaerobacter s Actinomycetes, yeast, and fungi:	shriftii
Silicon and silicon oxide Actionomycetes, yeast, and fungi: Fusarium oxysporum Virus (viral capsid templeate): Tobacco mosaic virus (TMV) Cyanobacteria and algae: Stauroneis sp	
Silver and silver sulfide Bacteria: Escherichia coli, Klebsiella pneumoniae, Bacillus subtilis, Pseudomonas fluorescens, Lactobacter sulfide Pseudomonas aeruginosa, Acetobacter xylinum, Aeromonas sp., Arthrobacter gangotriensis, Arthrobacter kerg Bacillus sp., Bacillus cereus, Bacillus indicus	guelensis,
Bacillus licheniformis, Bacillus stearothermophilus, Corynebacterium sp., Enterobacter cloacae, Morga Pseudomonas Antarctica, Pseudomonas meridian, Pseudomonas proteolítica, Salmonella typhirium, Staphy aureus, Pseudomonas stutzeri, Pseudomonas stutzeri (sulfide)	ylococcus
Actinomycetes, yeast, and Fungi: Coriolus versicolor, Volvariella volvacea, Fusarium oxysporum, Vertici Alternaria alternate, Aspergillus flavus, Aspergillus fumigatus, Aspergillus niger, Cladosporium clados Fusarium acuminatum, Fusarium semitectum, Fusarium solani, MKY3 (Yeast strain), Penicillium brevicor Penicillium fellutanum, Phanaerochaete chrysosporium, Phoma glomerata, Phoma sp., Rhizopus nigricans, Tricasperellum, Trichoderma viride	porioides, mpactum,
Cyanobacteria and algae: P. Tricornutum, Chondrus crispus, Spyrogira insignis, Stauroneis sp., Aphanoc Aphanothece sp., Caulerpa racemose, Colpmenia sinusa, Gleocapsa sp., Jania rubins, Lyngbya sp., Microc Ocillatoria sp., Phormidium sp., Pithophora oedogonia, Pterocladia capillacae, Spirulina sp., Spyrogira Synechococcus sp., Ulva fasciata	oleus sp.,
Tellurium Bacteria: Bacillus selenitireducens, Sulfospirillum barnesii	
Titanium and Bacteria: Lactobacillus sp. barium titanate Actinomycetes, yeast, and fungi: Fusarium oxysporum (both)	
Uranium oxide Bacteria: Shewanella oneidensis, Desulfosporosinus sp.	
Zinc sulfide and Bacteria: Desulfobacteriaceae, Rhodobacter sphaeroides	
zinc oxide Actinomycetes, yeast, and fungi: Aspergillus terreus Virus (viral capsid template): M13 bacteriophage Cyanobacteria and algae: Sargassum muticum (oxide)	

Combining the pillbox-like cell wall of diatoms with the capacity of production of nanoparticles would open a range of options in biotechnology. A better understanding of the complex array of biochemical processes required to produce nanoparticles, together with the diatoms ability to regulate environmental conditions are required (Parkinson & Gordon, 1999).

There are two ways of approaching the manufacture of nanomaterials and nanostructured materials: the top-down and the bottom-up approaches. The first based on the reduction of bulk sized materials to nanosize, that would be equivalent to obtaining a brick from the destruction of a fully built wall, while the second would manufacture the brick out of clay, sand, water and heat (Pacioni et al., 2015). In the case of AgNPs, elemental silver, either metallic or ionic, would be used to produce the final particle cluster of either silver oxide or metallic silver. For the production using a bottom-up approach, different pathways can be followed, either via gaseous, liquid, solid phase manipulations, or biological methods (Pacioni et al., 2015).

2.4.1 Synthesis of nanoparticles

Nanoparticles can be synthesized via physicochemical methods, or a biogenic alternative. The first set includes those methods that take advantage of the chemical and physical properties of the element or compound that is targeted for manufacturing. In the case of the biogenic alternatives, these reactions can be optimized by the action of organisms either because of the manufacture of assistant compounds or via direct enzymatic action.

2.4.1.1 Chemical reduction

The reduction of the corresponding cation is a straightforward method to obtain a specific metal nanoparticle. The reaction is generally carried in solution and the final product has colloidal characteristics. This process is known as co-precipitation and involves the concurrence of different phenomena; reduction, nucleation, growth, coarsening, and agglomeration (Cushing et al., 2004). The large electropositive reduction potential of silver (E^0 = + 7.99 V, Vanysek, 2004) allows for the use of several reducing

agents (e.g. hydrazine, sodium citrate, sodium borohydride, hydroquinone) as the ΔE^0 is higher than zero in each case ($\Delta E^0 > 0$).

2.4.1.2 Hydroquinone

Oxidation with hydroquinone (HQ) involves an electron transfer ($2e^-$) and a protonic loss ($2H^+$) (Hudnall, 2000) and can reduce Ag^+ to obtain AgNP. The higher concentration of HQ produces smaller sizes (10-30 nm) and diluted concentrations of HQ produce larger and more polydisperse AgNP of up to 200 nm. These observations are valid for AgNO₃ as precursor in a completely solvated Ag+ solution as compared to a complexed Ag^+ (e.g. $[Ag(NH_3)_2]^+$ in the presence of counter ions (e.g. CI^-) and monodispersity of particles (~ 14 nm) is achieved (Pérez et al., 2008). The process follows a three-stage mechanism that starts with the exothermic nucleation (reduction) of the Ag+ to produce silver clusters (~ 2.6 nm) process followed by an endothermic growth (~ 4.1 nm) and a final exothermic aggregation stage after further addition of HQ to reach the final size of 11 nm (Patakfalvi & Dekany, 2005). Gallic acid can be used as its oxidation produces a quinone form with a $E^0 = 0.5$ V (Yoosaf et al., 2007).

2.4.1.3 Sodium borohydride

Polte et al. (2012) developed a four-step mechanism for the growth of AgNP by reduction with NaBH₄. The first step involves reduction (<200 ms) of Ag⁺ to Ag⁰, forming dimers, trimers and other atom-based clusters. The second stage, coalescence of these clusters (\sim 5 s), generates small particles (2-3 nm). The third stage, constant-sized stage (5 – 10 min), generates particles that cluster in similar sizes (i.e. metastable state). Finally, a second coalescence stage (30 – 60 s) renders the last AgNP (5 – 8 nm). If colloidal stability is achieved during the intermediate metastable stage it is possible to stop further growth due to particle aggregation, and as the borohydride hydrolyzes it is added in excess to prevent losses or reduction in the stoichiometry values. The silver nanoparticles can undergo partial oxidation producing oxides and thus decrease the electrostatic stabilization of the AgNP causing aggregation. Enough BH₄⁻ can reverse the oxidation (Wuithschick et al., 2013). In some cases, plyvinylpyrrolidone (PVP) is used to decrease the polydispersity between 15 to 20% (Polte et al., 2012).

2.4.1.4 Citrate anion

Using sodium citrate, Turkevich et al. (1951) produced gold nanoparticles at boiling temperatures by the reduction of AuCl₄, developing what is now known as the Turkevich's method. It is now known that citrate reduce the metal cation and stabilizes the resulting nanoparticle. The citrate anions act at early stages complexing Ag2⁺ dimers and modulate the particle growth and the slow rate of the reduction method contributes to the formation of larger AgNP (50 - 100 nm), and after the first particle seeds are formed the anions complex to the surface of the metal decreasing the amount of available citrate and the amount of Ag⁺ that can be reduced diminishes, and fewer seeds are formed and the initial particles start to grow via Ostwald ripening and the larger particles grow at the expense of the smaller ones, and a longer time is required to reduce the total concentration of Ag⁺ in the solution when this method is applied (Pillai & Kamat, 2004). To control the size (30 nm), glycerol (40% V/V) can be added to reduce medium polydispersity without affecting the spherical shape, however, reduction rates are known to be slower (Steinigeweg & Schlücker, 2012). In the presence of NaOH, crystalline silver nanowires are made instead of silver nanoparticles, probably a consequence of the interference of the hydroxide ion with the association of citrate and silver (Caswell, et al., 2003)

2.4.1.5 Organic solvents

Synthesis of metal nanoparticles using organic solvents have advantages (e.g. high yield, narrow size distribution) and in some cases, the solvent itself can act as a reducing agent (Pastoriza-Santos & Liz-Marzán, 1999; Sun, 2013). It is possible to control the size, shape, and structure of the particles via the use of higher temperatures and different stabilizing agents (Pastoriza-Santos & Liz-Marzán, 1999; Pastoriza-Santos & Liz-Marzán, 2002; Rodríguez-Gattorno et al., 2002).

2.4.1.5.1 Polyol method: shape-controlled synthesis

The polyol method for synthesis of nanoparticles begins by reducing a metal salt known as a precursor using a polyol (e.g. ethylene glycol – EG), which acts as a reduction agent and solvent (Wiley et al., 2004). The reaction occurs at higher temperatures (~160°C for

EG) and a capping agent is added to prevent agglomeration, e.g. PVP (Wiley et al., 2004). The polyol oxidizes to an aldehyde species resulting in a change of the oxidation potential and the reduction power becomes highly dependent on temperature, providing an ability to control nucleation and growth by choosing the reaction temperatures (Wiley et al., 2005). Different temperatures of the reaction will result in the synthesis of different shaped particles (e.g. nanocubes, nanowires, and nanospheres). It was suggested that temperature changes can alternate the morphology between a kinetically stable single crystal (sc) and a thermodynamically stable twinned (tw) particle during the early stages of the growth (Wiley at al., 2004, Wiley et al., 2005). The combination of different conditions at different stages of growth of the particle can produce different shapes, e.g. a high concentration of AgNO₃ (0.125 – 0.25 M) with low PVP to Ag⁺ ratio (~1.5) can promote the formation of nanocubes given that the possibility of obtaining tw is reduced and sc particles are the predominant shape thus producing cubic structures (Wiley et al., 2005). The formation of nanowires or nanorods occurs when the concentration of AgNO₃ is reduced to 0.085 M and the PVP:Ag+ ratio remains constant (~1.5) with a reaction temperature above 110°C. An increase in the PVP:Ag+ ratio by a factor of three (3) overcomes the growth in a specific direction and the particle surface is covered by PVP ending mostly in spherical shapes, as seeds follow an isotropic growth pattern (Wiley et al., 2005).

2.4.1.6 Light-based, electrochemical, and sono-electrochemistry methods

Light selectively affects metal salts and has been used to produce modified materials with high spatial resolution and close to no modification to the surrounding media. Light approaches can be categorized both as top-down, i.e. photo-physical methods, and bottom-up, i.e. photochemical methods (Rycenga et al., 2011; Sakamoto et al., 2009; Stamplecoskie & Scaiano, 2012).

Photo-physical methods such as laser ablation using Nd-YAG lasers at 532 nm and anionic surfactants (e.g. $C_nH_{2n+1}SO_4Na - n=8$, 10, 12, 16 –, NaCl, silicon) are commonly used in the preparation of AgNP with size particles that ranges between 11 nm or higher (Mafuné et al., 2000; Bae et al., 2002; Tsuji et al., 2008). Photochemical approaches differ in that they target the reduction of the metal cation M^+ to M^0 by direct or indirect

(photosensitized) photolysis (Pacioni et al., 2015), usually by the direct excitation of a metal salt using high energy light sources (e.g. UV-light 254 nm) as the wavelength energy would transfer electrons from a solvent molecule to an electronically excited state of the metal form M⁺ to form a reduced M⁰ producing a highly stable mNP (Hada et al., 1976; Xu et al., 2008; Scaiano et al., 2009). In either case, the general mechanism of NP formation using photoreduction of a metal cation requires the use of solvent-assisted disproportionation processes dependent on the metal used as a precursor and the use of UV excitation, as most metal salts/cations only absorb wavelengths in this region, making the manufacture of mNPs cost prohibitive as UV-light sources are more expensive and not readily available (Pacioni et al., 2015). Photosensitized molecules (e.g. aromatic ketones, polyatomic anions, organic dyes) capable of absorbing UVA-visible light (320 – 700 nm) act as intermediate factories (e.g. anions, solvated electrons, free radicals) that will trigger the reduction of the M⁺ to the M⁰ form of the metal (Sakamoto et al., 2009). Nonetheless, even when these primers can reduce the cost of raw materials for the synthesis of nanoparticles, they are highly toxic and extremely reactive when poured to the surrounding environment.

Another method for producing AgNP is the use of electrochemical reduction to generate metallic particles via a platinum cathode and a silver anode in a tetrabutylammonium salt solution (TBA bromide or TBA acetate) in an inert solvent (acetonitrile). A second option is the use a platinum sheet as counter electrode for the electroreduction of AgNO₃ in aqueous solutions with rotating platinum cathodes and PVP to stabilize the reaction and agglomeration of the particles, and the addition of a surfactant (i.e. sodium dodecyl benzene sulfonate – SDBS). Another electrochemical method associated with sonication at 45°C in a media containing ultra-pure water, cyclohexane, acetone, tetraoctylammonium bromide, and hexadecyltrimethylammonium bromide was demonstrated by Jiang et al. (2004).

As mentioned before, the use of sonication combined with electrochemistry has become increasingly important as an alternative, simple, and cost effective method to obtain AgNP, and it is believed that the creation of microbubbles within the electrolyte is the main driver in the optimization of the electrochemical synthesis when sonication pre-

treatment is used (Reisse et al., 1994; Compton et al., 1997; Sáez & Mason, 2009), and requires the use of stabilizers and electrolytes (Zhu et al., 2000; Pacioni et al., 2015).

2.4.2 Biogenic and transition to green alternatives for AgNP synthesis

With the advent of biotechnology, several research efforts have focused on the use of organisms for the development of nanomaterials. Bionanotechnology, understood as the intersection of nanotechnology and biology, has developed over the last two decades to study biochemical pathways leading to the production of materials in the nanoscale (Gazit & Mitraki, 2013).

According to a definition by Anastas and Warner (2000), Green Chemistry involves the design and application of manufacturing processes aiming to reduce or eliminate the consumption and creation of harmful and hazardous substances during the generation of a chemical product. Accordingly, the definition carried the enunciation of twelve principles to work as guidelines for the development and implementation of green chemistry designs. The first principle enunciates that prevention of waste generation is preferable to cleaning up after waste is created. The second principle builds on the concept of atom economy by maximizing the incorporation of all materials used in the process into the final product, or set of usable and readily isolated by products. The third principle calls for the use of less hazardous chemical syntheses whenever practicable, as to reduce the generation of substances that pose little to no toxic threats to human health and the environment. The fourth principle calls for the design of safer chemicals to minimize toxicity while being able to affect their intended function. The fifth principle promotes the use of safer auxiliary substances (e.g. solvents, separation agents) advocating to the avoidance of use when unnecessary or the possibility to make them innocuous when used. The sixth principle champions the efficiency in the use of energy trying to minimize the process overall expenditure and environmental and economic impact, and when possible the use of ambient temperature and pressure for the synthesis of the materials. The seventh principle advocates for the use of renewable feedstocks whenever the possibility can avoid the use of depleting natural resources and is both technically and economically feasible. The reduction of derivatives is the core concept of the eighth principle, as intermediate or temporary modifications require additional reagents and potentially generates waste. The ninth principle enunciates that the use of catalytic reagents with high selectivity is preferable to stoichiometric reagents. The tenth principle calls for the design with degradation in mind, i.e. end-of-life mentality where at the end of the function the product degrades or breaks down into innocuous products that will not be persistent in the environment. The eleventh principle calls for the analysis for pollution prevention to be made in real-time via the use of analytical methodologies that can monitor and control prior the formation of hazardous substances. Finally, the twelfth principle calls for the improvement of accident prevention by the development of safer chemical substances that would minimize the potential for chemical accidents (e.g. releases, explosions, fire).

Simultaneously, based on the twelve principles of green chemistry, scientists devoted to the advocacy of green engineering developed a series of associated principles during the Conference "Green Engineering: Defining the Principles" (Sandestin, Florida, May 2003), known as "The Sandestin Declaration" (Abraham & Nguyen, 2003). The nine principles dictate that engineers should integrate environmental impact assessment tools to processes and products developed holistically using system analysis. Additionally, the focus of new green engineering practices would be to conserve and improve natural ecosystems, minimize the depletion of natural resources, while at the same time protecting the human health and well-being, and incorporate the use of life-cycle thinking in all engineering activities, to ensure that both material and energy inputs and outputs are as safe and benign as possible, striving to prevent waste. In an additional goal, engineering solutions should try to acknowledge the aspirations and cultures of the locals, as well as recognize the differences in the local geography, actively engaging stakeholders and communities in the development of the engineering solutions, which need to be tailor-made to specific circumstances with a clear objective to achieve sustainability by improving current or inventing new technologies.

2.5 Life cycle assessment

A Life Cycle Analysis or Assessment is a tool used to evaluate energy and raw material consumption, emissions, and other wastes related to a product or system's entire life cycle. It characterizes and quantifies the inputs, outputs, and environmental impacts of a

specific product or system at each life-cycle stage (ISO, 2006). The general procedure for conducting a life-cycle analysis is defined by the International Organization for Standards (ISO) 14000 series. The main phases of an LCA according to ISO guidelines, as shown in Figure 2.10, are goal, scope, and boundary definition; life-cycle inventory (LCI) analysis; life-cycle impact assessment; and interpretation (Guinee, 2002; ISO, 2006).

The methodology defined by the ISO 14040 is generally accepted as valid for the analysis of environmental performance of products and a key decision-making tool for managers and authorities providing a guide for the improvement of the production process (Hojer et al., 2008). A LCA study allows for the comparison of two or more products or services only if the functional unit remains the same.

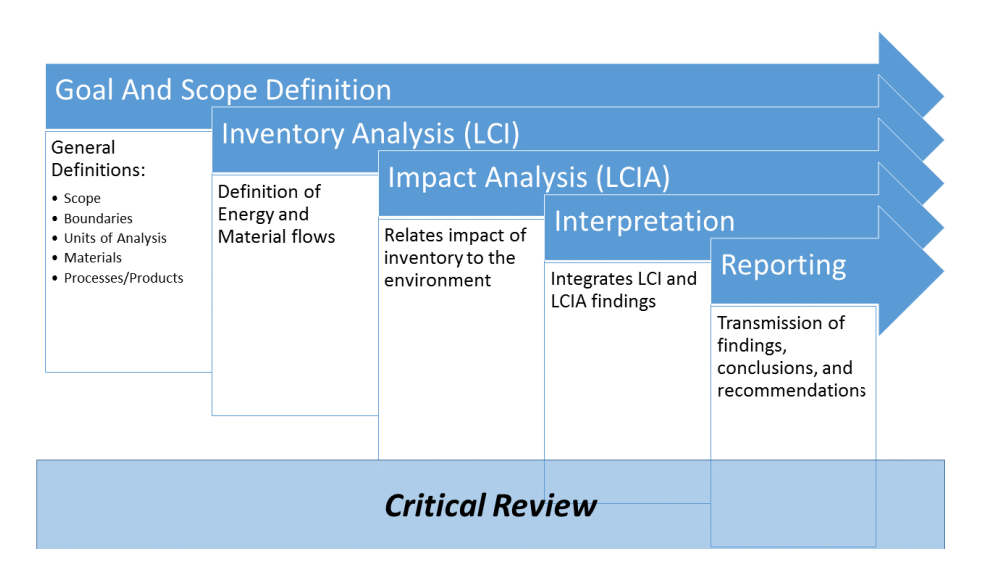


Figure 2.10. Elements of a life cycle analysis (ISO, 2006).

2.6 Final considerations

Given the diversity of potential applications for diatoms in human activities and industries, it was possible to envision an application of a simple procedure for the algal culture that would build on top of the biochemical performance of the organism. This new approach sought results both in the remediation of heavy metal contamination in a water body, and more specifically contamination of silver, vanadium, and molybdenum, using a model diatom (i.e. Phaeodactylum tricornutum) as the vector for the process. For that purpose, an experimental design was envisioned and a series of steps needed to be

established. The following chapter references the materials and methods used for this purpose. It starts by defining the proper culturing methodology specific for the algae in question and the method used (i.e. cell counting) to guarantee that the culture was advancing positively. The following subsection presents the description of the modifications required to address the simulation of a polluted environment (i.e. modifications of the culture medium) to introduce the treatments (i.e. stressors or pollutants). The following section presents the preferred methods for sampling and monitoring. The subsequent subsections describe the analysis methods used during the research, i.e. microscopy (optical and electron) and spectral (inductively coupled plasma mass spectrometry and energy-dispersed x-ray spectroscopy) analytical methods. The next portion of the materials and methods accounts for the methodology required to successfully implement a life cycle assessment for the comparison between a traditional chemical redox nanoparticle manufacturing process and the proposed biogenic alternative. Finally, the section presents the overarching experimental design and the methods for statistical analysis used to determine how well founded the conclusions could be drawn from the results of the study.

CHAPTER III MATERIALS AND METHODS

3.1 Algae cultures

A pure strain of *P. tricornutum* (CPCC 162) was obtained from the Canadian Phycological Culture Centre (Waterloo, ON, Canada). A primary culture was used as the source of inoculum and kept with strict culture conditions at $18-21^{\circ}$ C under constant mixing by shaking with 75-100 µmol $m^{-2} \cdot s^{-1}$ light applied from above, using fluorescent light tubes (Osram Biolux, Osram GmbH, Munich, Germany) with a 14-hour light: 10-hour dark photoperiod. The stock medium used throughout the series of the experiments was a modified L_1 medium (CML₁) prepared with artificial seawater to reduce variability derived from natural seawater. Concentrations of silicon and nitrogen were increased (25 and 20% respectively) while concentrations of other major nutrients and trace metals were kept constant based on the recipe by Guillard and Hargraves (1993). Some chemical species were modified and others were added (i.e. boron, sulfate, potassium) based on the recipe of Kilham et al. (1998).

A series of daughter cultures were used to perform the experiments in glass Erlenmeyer flasks (125 mL) under the same light and temperature conditions as the primary culture and constant aeration mixing. The culture medium for these daughter cultures was initially the same as the mother culture and later treatments were applied to achieve the desired final solution, following the procedures described in section 3.1.3 of this document.

3.1.1 Culture medium

The stock medium used throughout the series of experiments (henceforth referred to as ML_1) was a modified L_1 medium prepared with artificial seawater with enhanced concentration of silicon (25 %), phosphorus (0.15 %) and nitrogen (13.4 %) and concentrations of other major nutrients were kept constant based on the recipe by Guillard and Hargraves (1993) with some chemical species modifications and additions (i.e. boron, potassium) based on the recipe of Kilham et al. (1998). Trace metals were kept constant according to the original recipe from Guillard and Hargraves (1993).

Cultures were reared in a modified L_1+Si artificial seawater medium based on the recipe by Guillard and Hargraves (1993) with modifications based on the recipe of Kilham et al. (1998) to improve some concentrations and reduce limiting factors by depletion at the time of the experiment. Final concentrations were: NaNO₃ (9.01 x 10^{-2} g·L⁻¹), Ca₂Cl₂·2H₂O (3.68 x 10^{-2} g·L⁻¹), MgSO₄·7H₂O (3.97 x 10^{-2} g·L⁻¹), K₂HPO₄·H₂O (8.71 x 10^{-3} g·L⁻¹), NaHCO₃ (1.26 x 10^{-2} g·L⁻¹), Na₂SiO₃·9H₂O (2.77 x 10^{-2} g·L⁻¹), H₃BO₃ (2,4 x 10^{-2} g·L⁻¹), KCl (7.45 x 10^{-3} g·L⁻¹), Na₂-EDTA (4.36 x 10^{-5} g·L⁻¹), FeCl₃·6H₂O (1.17 x 10^{-5} g·L⁻¹), MnCl₂·H₂O (1.8 x 10^{-6} g·L⁻¹), CuSO₄·5H₂O (1.00 x 10^{-8} g·L⁻¹), ZnSO₄·7H₂O (2.2 x 10^{-7} g·L⁻¹), CoCl₂·6H₂O (1.00 x 10^{-8} g·L⁻¹), Na₂MoO₄·H₂O (2.22 x 10^{-7} g·L⁻¹), Na₂SeO₃ (2.00 x 10^{-8} g·L⁻¹), and Na₃VO₄ (2.00 x 10^{-8} g·L⁻¹). A list of chemicals with their corresponding SDS references is available in Appendix II.

Each stock solution was prepared in 14.6 % (1.011 ± 0.0005 sg) artificial seawater (Instant Ocean Aquarium Sea Salt Mixture, Instant Ocean, Blacksburg, VA) prepared by adding 17.8 g of stock sea salt mixture to 1 L of distilled water. To keep the seawater contribution equal for all treatments, a batch of stock seawater (20 ± 0.1 L) was prepared before all treatments by mixing 356 ± 0.01 g of Sea Salt Mixture in 5 ± 0.025 L of distilled water with mixing via magnetic vortex until all the crystals were completely dissolved. To prevent losses, the weighted mass of salt mixture was added using a funnel to 1 ± 0.005 L of distilled water in a five-liter Erlenmeyer flask until the salt crystals did not dissolve (~42 ± 0.01 g). One additional liter of distilled water was added to the Erlenmeyer flask and salt crystals were added until salt crystals did not dissolve (~90 ± 0.01g). The process was repeated three more times until the complete mass of salt was added and the solution was completed (at masses measured of ~170 ± 0.01 g, ~320 ± 0.01g, and 356 ± 0.01 g respectively). The five-liter solution was transferred to a clean plastic container with a previously measured 5 ± 0.025 L of distilled water and the final volume was reached (20 L) using 10 additional transfers of distilled water measured in a graded volumetric cylinder (1,000 ± 5 mL).

Stock solutions with nutrient addition were prepared in distilled water by adding an initial measured mass of each chemical reagent (based on concentration targets) to a volume of $1 \pm 0.005 \, \text{L}$ in a volumetric flask. Initially a small volume of water (~200 mL) was placed

in the flask and the weighted biomass was added with a clean funnel mixing thoroughly via gentle swirl until the salt crystals dissolved completely. Distilled water was then added to complete the volume to the labeled graded mark carefully so no excess water was added. Similarly, the stock solutions for the treatments were prepared on $1\pm0.005\,L$ of artificial seawater by adding the initial mass of each salt to $100\pm0.05\,mL$ and filling to the graded mark on the stem in a 100-mL volumetric flask. Stock solutions for the treatments were prepared on $1\pm0.005\,L$ of artificial seawater by adding the initial mass of each salt to $100\pm0.05\,mL$ and completing to the graded mark on the stem in a 100-mL volumetric flask. All prepared stock solutions were stored in dark at $4\,^{\circ}\text{C}$ until needed for medium preparation.

To prepare the different culture vessels, 1 mL of each stock solution was added to a volumetric flask and seawater was completed to 1 L. The prepared medium solution was divided equally into 50-mL Erlenmeyer flasks and sterilized to guarantee that the cultures were axenic, and to reduce the effects due to contaminants or the interactions of other organisms that gain access to the cultures. In a similar manner, all initial water was filtered and autoclaved prior to inoculation of starter biomass or addition to the culture systems. When water or medium was added to the growing cultures it was cooled to 18°C ± 1.5 °C measured by non-contact IR thermometer (BENETECH®, Shenzhen, PRC) before the addition to the culture. The autoclaving method was 15 minutes at 121-124 °C at 200 kPa (WHO, 2016) for sterilization, accounting for volume and size of the material to be sterilized. Sterilization success was confirmed by blank culture (i.e. flasks without inoculum) twice during the duration of the experiments.

After sterilization, the flasks with medium were stored at room temperature to allow for cooling and subsequently were randomly assigned to one unit and inoculated inside a clean bench chamber with axenic technique. Table 3.1 shows the final values for individual ions in the medium.

All inputs to the culture system (i.e. liquid or gas) were either sterilized or filtered prior to their use in the experiments. For the gas mixture used for bubble mixing, a two-step filtering process was used; a preliminary distilled water humidification mechanism was used to circulate water through a water column to later transport to tubbing-based

filtering systems using a 0.2 μm micropore syringe filter (NalgeneTM, Thermo Scientific, Waltham, MA) attached to an air inlet attached to the culture vessel. Similarly, liquid medium with treatments was filtered using the same micropore syringe filter (NalgeneTM, Thermo Scientific, Waltham, MA) attached to a sterile disposable syringe for each treatment and each unit to prevent cross contamination and errors in the introduction of treatments. Each syringe was used only on one specific level of each treatment and then discarded.

Table 3.1. Ionic concentration of the CML₁+Si medium.

Compound	Molecular Weight	Final concentration	
		[g·L ⁻¹]	[M]
CaCl ₂ ·2H ₂ O	147.01	3.68 x 10 ⁻²	2.50 x 10 ⁻⁴
MgSO ₄ · 7 H ₂ O	246.50	3.70 x 10 ⁻²	1.50 x 10 ⁻⁴
K ₂ HPO ₄	174.18	6.31 x 10 ⁻³	3.62 x 10 ⁻⁵
NaNO ₃	85.00	9.01 x 10 ⁻²	1.06 x 10 ⁻³
NaHCO ₃	84.01	1.26 x 10 ⁻²	1.50 x 10 ⁻⁴
Na ₂ SiO ₃ · 9 H ₂ O	284.20	3.77 x 10 ⁻²	1.33 x 10 ⁻⁴
H ₃ BO ₃	61.83	2.40 x 10 ⁻²	3.88 x 10 ⁻⁴
KCI	74.55	7.45 x 10 ⁻³	9.99 x 10 ⁻⁵
C ₁₀ H ₁₄ N ₂ Na ₂ O ₈ · 2 H ₂ O	372.24	4.36 x 10 ⁻⁶	1.17 x 10 ⁻⁸
FeCl ₃ · 6 H ₂ O	270.30	1.00 x 10 ⁻⁶	3.70 x 10 ⁻⁹
MnCl ₂ · 4 H ₂ O	197.91	1.80 x 10 ^{-/}	9.10 x 10 ⁻⁷
CuSO ₄ ·5 H ₂ O	249.68	1.00 x 10 ⁻⁹	4.01 x 10 ⁻⁹
ZnSO ₄ · 7 H ₂ O	287.50	2.20 x 10 ⁻⁸	7.65 x 10 ⁻⁸
CoCl ₂ ·6 H ₂ O	237.90	1.00 x 10 ⁻⁸	4.20 x 10 ⁻⁸
Na ₂ MoO ₄ · 2 H ₂ O	241.90	2.20 x 10 ⁻⁸	9.09 x 10 ⁻⁸
Na ₂ SeO ₃	172.90	1.60 x 10 ⁻⁹	9.25 x 10 ⁻⁹
Na ₃ VO ₄	183.90	1.80 x 10 ⁻⁹	9.79 x 10 ⁻⁹

3.1.2 Cell count

Initial cell concentration was determined via direct count with a Z1 Particle Counter (Beckman Coulter, Inc., Brea, California, USA), calibrated for 5 μ m and 10 μ m particles. Particles above 10 μ m were not measured as the goal was to determine the number of cells with an average less than 10 μ m in size. Samples were diluted in 10 mL of ISOTON

solution to guarantee average cell counts between 1 and 9×10^6 cells·mL⁻¹. Each one of the recorded measurements after dilution was done in triplicate.

During the second set of experiments, after the maximum values for ionic concentrations were determined, and due to time, sample availability, and measurement efficiency constraints, a second automated method used spectrophotometry to calculate cell density. Optical density of smaller samples (250 µL) were measured using a PowerWave Spectrophotometer (BioTek, Winooski, VT) with readings at 470; 517; 535; 562; 653; and 666 nm, and a regression equation was established by comparing spectrophotometric data to known concentrations obtained via manual cell count (Neubauer chamber, Hausser Scientific, Horsham, PA, USA).

3.1.2.1 Hemocytometer cell counts

Confirmation of the cell concentration values was done via hemocytometer counts following the procedure described in the literature review (Andersen, 2005). One sample (1 mL) of each culture units was taken at each interval and diluted (250 µL of sample and 750 µL of distilled water) to reduce the excess concentration of cells in the counting chamber and a 1:1 sample: 0.4% v/v solution of trypan blue (Gibco, Life Technologies, Carlsbad, CA) as stain before introducing the cells into the counting chamber. This stain is used to determine live and dead cells in the culture. Two methods of counting were selected and compared: area-based count and cell-standard count. The first consisted of a random predetermined path across the grid of the counting chamber to account for exactly 0.72 mm² of surface on the grid (13 squares of 0.04 mm² and 4 squares of 0.05 mm² – See image I in Appendix III). The second method consisted of counting 150 cells throughout the grid and then recording the area required for that count and calculating the volume, e.g. if the 150 cells required 13 squares of 0.04 mm² and 4 squares of 0.05 mm^2 , the volume for this area would be 72 nL (area x depth = 0.72 mm^2 x 0.1 mm = 0.0072 mm³ = 72 nL). Regression curves for both methods were prepared to account for differences and to determine if any correlations existed among the methods. Again, similarly to the previous method, correlations of these counts with the measurements calculated on the cytometric and spectrophotometry measurements were performed.

3.1.2.2 Automatic cytometer cell count

The initial cell concentration was determined via direct count using a Z1 Particle Counter (Beckman Coulter, Inc., Brea, CA). A previous calibration for particle sizes of 5 μ m and 10 μ m was done using Standard, L5, Nominal 5 μ m, Latex Particles (Beckman Coulter, Mississauga, ON). Particles above 10 μ m were not measured as the goal was to determine the number of cells with an average less than 10 μ m in size. Samples were diluted in 10 mL of ISOTON (Beckman Coulter Canada LP, Mississauga, ON) solution to guarantee average cell counts in the range between 1,000,000 and 9,000,000 cells·mL⁻¹, placed on Accuvette cups (Beckman Coulter Canada LP, Mississauga, ON) and measured using a ZSeries Aperture Tube 70 μ m for a range of 1.4 – 42 μ m (Beckman Coulter, Inc., Brea, CA). Each one of the recorded measurements after dilution was done in triplicate. Further information on cytometry methods can be found in Appendix III, section IV.

3.1.2.3 Spectrophotometry cell density assessment

For convenience, simultaneous measurements with a PowerWave XS spectrophotometer (BioTek, Winooski, VT) were carried out during the first stages of the treatment application and a combined measure with cultures with and without trypan blue stain. Samples were diluted by taking 250 µL of sample and mixing thoroughly with 750 µL of distilled water and then were placed on a 96-well microplate for immediate reading at 470; 517; 535; 562; 653; and 666 nm wavelengths. Results were later correlated to a calibration curve with known concentration of cells obtained by direct cytometer count using a Z1. This method of cell counting was used as the preferred method during the sampling of the Central Rotatable Non-Lethal (CRN) assay around Maximum Values as described below. A brief description of the overarching principle of spectrophotometry is presented in section V of Appendix III.

3.1.3 Treatments

3.1.3.1 Maximum level detection (MLD)

A modified medium with depleted silicon (CML_1 – Si) combined with each chemical species (i.e. Ag, Mo, V) for the individual treatments was microfiltered before inoculation.

As with the starter culture, all water was filtered and autoclaved before inoculation of the starter biomass. Media was cooled to 18°C before the addition of the diatom inoculum.

An initial inoculum was standardized to approximately 500,000 cells·mL⁻¹ (about 1 mg of dry biomass per flask) to further account for possible effects produced by the initial setting of the experiment or effects of cell abundance when the stressor was added. The three elemental treatments included the addition of silver, vanadium, or molybdenum at four levels of treatment concentrations as established: $2.5 \times 10^{-4} \text{ mol} \cdot \text{L}^{-1}$ (single treatment), 7.5 x 10⁻⁵ mol·L⁻¹ (two treatments equal concentration), 5.0 x 10⁻⁵ mol·L⁻¹ (three treatments equal concentration), and 1.0 x 10⁻⁴ mol·L⁻¹ - 2.5 x 10⁻⁵ mol·L⁻¹ (three treatments with intermediate concentrations), for each element. The four treatment levels for each element were $2.5 \times 10^{-5} \text{ mol} \cdot \text{L}^{-1}$ (2.658 x $10^{-3} \text{ g Ag} \cdot \text{L}^{-1}$, 1.274 x 10-3 g V·L⁻¹, and 2.399 x 10^{-3} g Mo·L⁻¹), 5.0 x 10^{-5} mol·L-1 (5.35 x 10^{-3} g Ag·L⁻¹, 2.547 x 10^{-3} g V·L⁻¹, and $4.798 \times 10^{-3} \text{ g Mo} \cdot \text{L}^{-1}$), $7.5 \times 10^{-5} \text{ mol} \cdot \text{L}^{-1}$ ($8.025 \times 10^{-3} \text{ g Ag} \cdot \text{L}^{-1}$, $3.82 \times 10^{-3} \text{ g V} \cdot \text{L}^{-1}$, and 7.196 $\times 10^{-3}$ g Mo·L⁻¹), 1.0 x 10⁻⁴ mol·L⁻¹ (1.07 x 10⁻³ g Ag·L⁻¹, 5.094 x 10⁻³ g V·L⁻¹, and 9.595 x 10⁻¹ 3 g Mo·L $^{-1}$) and 1.5 x 10 $^{-4}$ mol·L $^{-1}$ (1.605 x 10 $^{-2}$ g Ag·L $^{-1}$, 7.641 x 10 $^{-3}$ g V·L $^{-1}$, and 1.44 x 10 $^{-1}$ ² g Mo·L⁻¹). The proportions in each mixture were calculated to add up to 1.5 x 10⁻⁴ mol·L⁻¹ ¹ for the total media mixture levels for each treatment. One third of each treatment concentration was added every 24 hours starting on day 7 and was completed on day 9. The addition of the metals occurred at the 6th and 7th hour of the light period, to allow for cellular repair before and after the treatment. Other variables (e.g., temperature, pH, light, nutrients) were monitored. The experiment was conducted in triplicate. The CML₁-Si medium combined with each chemical solution for the individual treatments was always microfiltered before inoculation.

Liquid samples (1 mL) of algae cultures were collected by vacuum suction in a sampling chamber attached to the culture vessel two hours after treatment addition to account for acclimation processes and preserved in glutaraldehyde (0.5 mM) for further analysis. The experiment ended on the 11th day.

3.1.3.2 Central rotatable nonlLethal maximum values (CRN)

Based on the results of the MLD analysis, concentration levels for silver, vanadium, and molybdenum were introduced based on predicted non-lethal maximum concentrations of 1×10^{-4} M for silver $(1.079 \times 10^{-2} \text{ g Ag·L}^{-1})$, 1.5×10^{-4} M for vanadium $(7.64 \times 10^{-3} \text{ g Ag·L}^{-1})$, and 1×10^{-4} for molybdenum $(9.594 \times 10^{-3} \text{ g Mo·L}^{-1})$. The levels for silver (i.e. $0, 3.75 \times 10^{-5}, 9.24 \times 10^{-5}, 1.47 \times 10^{-4}, 1.85 \times 10^{-4})$, vanadium (i.e. $0, 5.97 \times 10^{-5}, 1.47 \times 10^{-4}, 2.35 \times 10^{-4}, 2.95 \times 10^{-4})$, and molybdenum (i.e. $0, 3.43 \times 10^{-5}, 8.45 \times 10^{-5}, 1.35 \times 10^{-4}, 1.69 \times 10^{-4})$, were randomly assigned to combinations of the three to generate a new central rotatable composite design (Myers, 1971). This secondary design was established to pinpoint the maximum acceptable concentration of treatments that *P. tricornutum* could sustain without a significant impact on the cell viability within the culture. Following the conditions of the previous assay, temperature, pH, light, and nutrients were monitored, and the experiment was conducted in triplicate. The CML₁–Si medium combined with each chemical solution for the individual treatments was microfiltered before inoculation.

The treatments were performed around the 6th and 7th hour of the light period, to allow cellular repair before and after the treatment. An initial inoculum was standardized to approximately 500,000 cells / mL (about 1 g of dry biomass per flask). For each one of the treatments (Ag, Mo, V) and treatment levels the combinations followed an Augmented Extreme Vertices Design, i.e. Mixture Experimental Design (JMP®, 2012; Cornell, 1990). One tenth of the total treatment was added every 30 minutes calculated to add up to the final concentration in the medium. The culture media used for the first four days was the modified CML₁+Si culture medium described before, which was prepared in artificial seawater (Instant Ocean, Blacksburg, VA, USA).

3.2 Sampling

To account for acclimation processes, 2.5 mL samples from each culture unit were collected before treatment addition and divided into two samples of 1 mL each on capped Eppendorf tubes. During the maximum level detection (MLD) assay, samples were taken via vacuum suction using a specially designed sampling port attached to the top of the flask for convenience (Figure 3.1) twelve hours after each fraction of the treatments was

added to the cultures. A sterile 10 mL syringe with a metal tip needle pierced full of filtered air collected through a 0.2 µm micropore syringe filter (NalgeneTM, Thermo Scientific, Waltham, MA). The rubber stopper of the sample port cap is pierced and suction in the syringe barrel creates a vacuum that moves the culture from the bottom of the culture chamber into the port glass container (Figure 3.1 – green rectangle with arrow). Air is forced from the barrel and into the culture chamber and then suction created to move a portion of culture mixture into the tubbing. Before sample collection, a series of 10 negative and positive movements on the y-axis of the plunger of the syringe were performed before filling the sampling port chambers and collecting the final 2 mL to guarantee homogeneous suspension of the cells from the culture vessel in the sample. For the CRN, samples were taken before the second, fifth, and tenth (last) addition of the metal pollutants and 24 hours after this last addition.

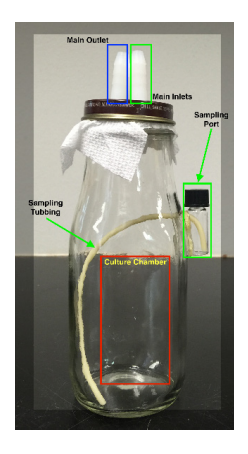


Figure 3.1. Culture vessel. A glass bottle with a round bottom was used for convenience. On the top of the cover, two access inlets and one outlet on the side (green rectangle with arrow), a sample port, connected via tubbing to the chamber of the culture (red rectangle with yellow labelling text).

Biomass samples from the treatments were split to two 1-mL Eppendorf tubes with lid (1 mL each) and labelled with the code for each sample and one letter (X, Y). The first tube (X) containing 1 mL of sample was concentrated by centrifugation (10,000 rpm for 5 minutes), the supernatant collected in an Eppendorf tube labeled (W) and the remaining pellet washed three (3) times with distilled water, the pellet collected, the tube labeled (XS), weighted, and freeze dried (i.e. lyophilized) for 24-hour period, target shelf

temperature was set to -20 °C at an approximate rate of 1 °C·min⁻¹ and a pressure of 0.37 mbar, until only powder remained (Gamma 1-16 LSC plus, Martin Christ Gefriertrocknungsanlagen GmbH, Osterode am Harz, Germany). Biomass of the tube was measured at 12 hours and then at 24 to confirm complete removal (sublimation) of the liquid phase. The second fraction (Y) was divided among three Eppendorf tubes with lids, the first (P) was diluted by adding 250 μ L of the fraction Y to 750 μ L distilled water and labeled for use with the PowerWave XS spectrophotometer measurement of biomass. The second fraction taken from Y was labeled T and diluted with 4% Trypan Blue and distilled water (250 μ L sample: 250 μ L Trypan Blue: 500 μ L distilled water) and after counting on hemocytometer, it was used for spectrophotometric analysis of dead cells. The third fraction was labeled Z and was created by dilution of 250 μ L of sample from Y in 750 μ L distilled water and used later for cell cytometry measurements. The final fraction (250 μ L) was preserved and freeze stored (-79 °C) at a ratio of 1:1 of sample: glutaraldehyde (0.5 mM) for further analysis. A detailed schematic diagram with the distribution and sequential dilutions of the samples can be seen in Figure 3.2.

3.2.1 Medium (supernatant)

Centrifugation was carried at 10,000 rpm for 5 minutes and the supernatant was separated from the pellet using a 1,000 μ L micropipette (Gilson Inc., Middleton, WI) set to 500 μ L, 250 μ L, and finally 100 μ L to measure an approximate volume of the sampled supernatant. The supernatant was then transferred to a 1-mL lidded Eppendorf tube labeled W and dilutions of the three fractions used for nitrate (N), pH (H), and ICP-MS (M) tests were prepared. The fraction used for nitrate determination was prepared by diluting 150 μ L with 850 μ L of distilled water to complete 1 mL. The fraction for pH was immediately tested and an aliquot of 100 μ L was deposited in a 96-well plate and processed as described of section 3.3.3 in this document. The remaining portion of the supernatant was kept at -79 °C for its use in the ICP-MS series of analysis.

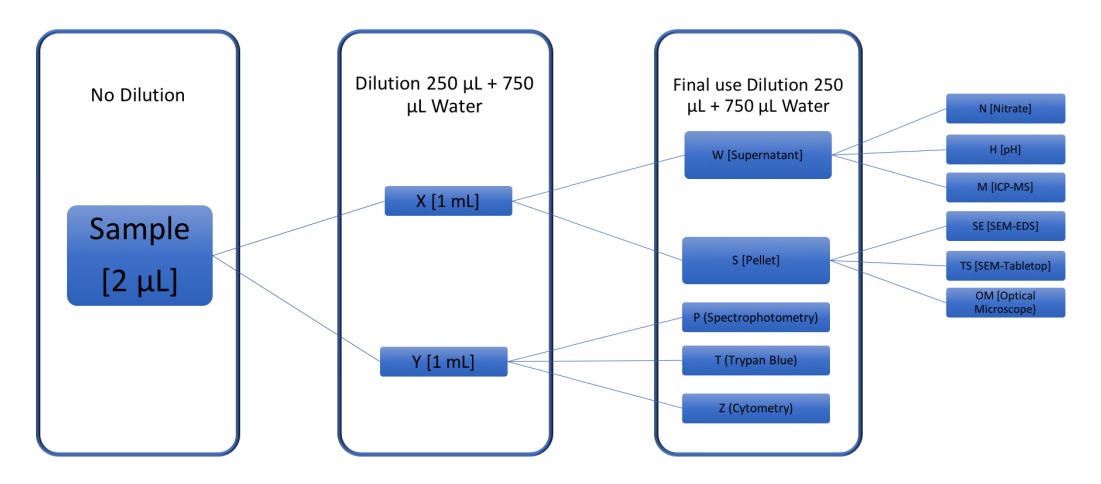


Figure 3.2. Experimental sample distribution. Schematic chart of the distribution of samples and dilutions.

3.2.2 Frustules (pellets)

After centrifugation (10,000 rpm for 5 minutes) and separation from the supernatant, the remaining pellet was washed three times using distilled water to eliminate salts that might have precipitated with the cells of *P. tricornutum*. Each wash was performed by adding 750 μ L of distilled water and suspending via vortex to separate via centrifugation (10,000 rpm for 5 minutes) and the new supernatant was discarded. After the second wash, the pellet is suspended in water to a volume of 250 μ L and a 50 μ L aliquot is taken to a lidded Eppendorf tube for optical microscopy visualization (labelled OM) and then additional 500 μ L of distilled water were added to the remaining fraction for the last wash. After the third and final wash was completed and the supernatant was discarded, the pellet was suspended in a matrix of 20 % ethanol (v/v) to a volume of 1 mL and divided into two lidded Eppendorf tubes (500 μ L each) and stored at -79 °C under labels SE and TS until required for SEM analysis and visualization.

3.3 Monitoring

3.3.1 Nitrogen monitoring

lonic nitrogen (i.e. nitrate) concentrations were determined by spectrophotometric analysis using a standard API Fishcare Nitrate Test Kit (API, Chalfont, PA) applied against a standard curve of known nitrate concentrations (i.e. 0; 5; 10; 25; 30; 35; 50; 100; and 200 mg NO_3 -L- 1 as $NaNO_3$) and absorbance was read with a PowerWave XS microplate

spectrophotometer (BioTek, Winooski, VT), at 535 nm wavelength. Liquid samples (1 mL) obtained after centrifugation of 2 mL of culture from each experimental unit were collected in a 1.5 mL lidded Eppendorf tube. Samples were diluted in a clean tube by mixing 150 μ L from the supernatant sample with 850 μ L of distilled water to reach concentrations below 50 mg/L for improved accuracy of the readings. For nitrate measurement, 150 μ L from the diluted tube labeled N, were added to a 96-well plate and mixed with 15 μ L of standard solution 1 (API Nitrate Test Kit) and mixed carefully pipetting back the liquid 10 times to guarantee thorough mixing of the two liquids. Subsequently, 15 μ L of standard solution 2 (API Nitrate Test Kit) were added and mixed using the method described for solution 1. After the mixing was completed, 5 minutes of incubation for color development were provided prior to measurement in the spectrophotometer. Absorbance values were plotted against the known concentration curve via extrapolation after which the equation for the linear regression was determined.

3.3.2 Temperature

Culture temperature was monitored throughout the life span of the culture in the morning, noon and evening. Measurements were made with a non-contact IR thermometer with laser target pointer (BENETECH®, Shenzhen, PRC) aimed at the center of each unit for approximately 15 s ±1 s or until the reading from the apparatus stabilized to one value. To calibrate possible differences between the actual temperature of the culture and the reading from the apparatus, a dummy culture (i.e. cells and culture medium not intended to use for treatments) was slowly heated in a plate, with temperature readings applied to the center using a regular mercury thermometer while the laser pointer of the non-contact IR thermometer was aimed at the bulb of the mercury thermometer used for measurement.

3.3.3 Irradiance

An initial irradiance measurement at every flask position without any flask present, with 10 nm resolution, using a LI-193 quantum sensor (LI-COR Biosciences, Lincoln, Nebraska, USA) calibrated to the location was performed. During the culture of the algae, a MQ-200 quantum meter (Apogee Technologies, Logan, UT) was used to confirm that light

irradiance was held constant around 75-100 μ mol m⁻²·s⁻¹ during light periods and nearly 0 μ mol m⁻²·s⁻¹ during the dark periods.

Difficulty in calculating the punctual irradiance at every point using the LI-193 when the flasks were present made this method of determination inefficient and the Apogee measurement was preferred over the LI-COR counterpart for the regular measurements. Measurements with individual flasks and boundary flasks (i.e. filled with water) showed that it was possible to assume that the irradiance was constant for all the culture units within the system, even when the outer cover of the system was removed and ambient light could enter, the effects on irradiance values due to external inputs was negligible.

3.3.4 pH

Every sample was tested to monitor changes in pH using a colorimetric API High-Range pH test kit specifically designed for pH ranges between 7.4 and 8.8 (API, Chalfont, PA) by pipetting 100 μ L of liquid sample (after centrifugation) to a 96-well plate 5 μ L of the API test solution mixing via pipetting. Ranges were assessed by comparing to a color-coded card provided with the kit and samples with measures outside the defined range of 7.8 and 8.2 were labelled for further analysis.

3.4 Optical microscopy

Samples from all the culture chambers were observed directly as the pre-concentrated samples of *P. tricornutum* cultured cells (Eppendorf tubes labelled OM) were placed via drip on glass slides as baseline samples, using a micropipette (10 µL), and examined under an optical Hund Wetzlar H600 Light Microscope (Helmut Hund GmbH Wetzlar, Germany). Selected samples were taken to the Department of Mechanical Engineering at École de Technologie Superieure (ETS, Montreal, QC) and visualized using a DSX 510 Digital Microscope (Olympus Corporation, Tokyo, Japan). A short recount on the history of optical microscopy is presented in section VI of Appendix III.

3.5 Scanning electron microscopy

3.5.1 Sample preparation

A small volume (50 µL) of each TS-labeled tube containing washed diatom frustules in a 20% ethanol suspension was transferred to aluminum stubs mounts for SEM (PELCO®, Ted Pella Inc., Redding, CA) for visualization with a Hitachi SEM TM3000 (Hitachi Corporation, Tokyo, Japan). The second fraction (SE) was washed three (3) additional times with distilled water to further eliminate attached particles and molecules from culture medium, freeze-dried, and kept refrigerated until ready for analysis. These samples were analyzed at the Laboratory for Material Engineering McGill University, using a Hitachi Cold FE SU-8000 SEM (Hitachi Corporation, Tokyo, Japan) equipped with backscattered and secondary electron detectors coupled with a silicon drift EDS detector (SDD EDS Xflash® 6, Bruker, Massachusetts, United States). The SEM-EDS offered detailed imaging information about the morphology, surface texture, and elemental composition of the samples.

3.5.2 Tabletop SEM preliminary exploration

The first set of aluminum stubs was mounted and visualized at 5 kV and 15 kV to account for surface detail and a maximum magnification of 12,000X on a Hitachi tabletop SEM TM3000 (Hitachi Corporation, Tokyo, Japan). All the samples were explored and scanned for abnormal structures and shapes, as well as for out of the ordinary formations or elements that might not be part of the algal cells or the culture in general. Quality control of the washing process was taken into consideration and samples that showed a great amount of crystal formation were labeled for additional washing prior to the use of the FE SU-8000 SEM (Hitachi Corporation, Tokyo, Japan). Imaging was captured using the standard software and capture application from the manufacturer. Linear measurements for analysis of size distribution were done with ImageJ an imaging software developed by the National Institutes of Health (Abramoff et al., 2004).

3.5.3 **SEM-EDS**

Samples were prepared after washing three additional times with distilled water and suspended in 100% ethanol, by placing a small volume (50 μ L) on an aluminum stub

specially manufactured for SEM use. SEM-EDS visualization was used to determine the general chemical composition of the individual particles and visible formations around the structures visible on the sample. Initially, samples were observed at different locations and with different voltages (3 kV, 5 kV, and 10 kV) and interesting or abnormal spots were recorded in the memory of the device via topographical references (coordinates) for later analysis using the EDS detectors (SDD EDS Xflash® 6, Bruker, Massachusetts, United States). Particle morphology, external surface structure and external elemental distribution of individual diatom frustules were assessed via exploratory analysis of the sample. Each sample was characterized by randomly selecting three to four fields of view and all particles were examined for structures that could be observed within the selected fields. The chemical composition and morphology were noted for each particle and compiled for each sample.

Elemental analysis was performed in a "spot mode" in which the beam is localized on a single area manually chosen within the field of view. The location is represented on the provided SEM images by a "+" or a small square. The EDS detector can differentiate elements with atomic number equal to or greater than six. The intensity of the peaks in the EDS is not a quantitative measure of elemental concentration, although relative quantities can be inferred from relative peak heights. Images were acquired after a scan through the entire sample and coordinate references were set. More information regarding the SEM-EDS principles can be found in Appendix III section VII.

3.6 ICP-MS analysis of the liquid phase

Samples labeled M from the fractions of the supernatant collected as described previously on numeral 3.2 were diluted using ultrapure 18 M Ohm deionized water taking 50 μ L of the sample supernatant and diluting to 10 mL of 1 % nitric acid. Concentrations of silver and vanadium in the liquid phase of the samples were calculated using a Varian ICP-820MS instrument (now Analytik-Jena Inc., Jena, Germany).

Standards were prepared accordingly using diluted acid and a multi element stock standard (SCP 14-110-012, SCP Science, Baie D'Urfé, QC, Canada). Quality control was maintained using water reference solutions from Environment Canada Proficiency

Testing Program Study 104 (Environment and Climate Change Canada, Brampton, ON, Canada) as control samples. Results of Ag, Cd, Co, Cr, Cu, Mn, Ni, Rb, Sr, V, and Zn were collected. Unavailability of Mo made it impossible to measure the concentration of the element and it was scrapped from the analysis; however, it is recorded and mentioned to keep in mind its presence in the samples. Recoveries on all metal measurements remained within 4% of the actual value. A brief description of the operational principles of ICP-MS analysis can be found in Appendix III section VIII.

3.7 Life cycle assessment (LCA)

3.7.1 Goal and scope of study

3.7.1.1 Goal definition

This study attempted to establish the differences between the traditional least environmentally damaging methods for silver nanoparticles production and an alternative biogenic process using *P. tricornutum* (Bohlin, 1897) as the manufacturing vector (i.e. organism). From the industrial production perspective, the boundaries are defined within the use of the chemicals, and the production of the nanoparticles. On the algal side of the analysis, the production goes from the manufacture of the chemicals required for the algal production (i.e. culture medium) and finish at the production of the silver nanoparticles.

3.7.1.2 Scope

The considered systems were limited to a cradle-to-gate analysis, where the production of nano silver in both the industrial and biogenic approaches, took into consideration the source of the initial raw material, and its evolution within the system. In the specific case of algae production, the source of the inoculum was the isolated culture at the lab facility, and not the original wild type of the algae. The origin of each used nutrient source was based on approximate calculations in the manufacturing of each compound, based on both Ecoinvent data (Frischknecht et al., 2005; Wernet et al., 2016) and the manufacturing requirements obtained from the literature. Approximate estimations based on literature data for homologous processes were used when both database and literature information was not available, and was described as such in the analysis of the

information. In these cases, the average values were assigned more conservative values using uncertainty to account for possible differences between actual and estimation values and normalization uncertainty was used to account for potential differences when calculating the impact effects of the process (Ciroth et al., 2004; Lo, et al., 2005; Hung & Ma, 2009). Packaging and other processes further down the value chain of the functional unit were not considered, as the system and material for package, as well as the transportation and other considerations were assumed to be the same for both approaches (Varun & Nautiyal, 2016). In the case of algae, the initial approach did not account for regular and traditional by products that can improve the overall environmental performance of the algae method (e.g. animal feed, biofuels) not to obscure the real performance of the method by means of other compensative aspects of algae culture.

3.7.1.3 Environmental impacts

Water resources, land use and location, carbon fertilization, fossil fuel inputs, eutrophication, genetically modified organisms (mutations), and toxicity are among the most significant and frequently mentioned concerns in the literature and among circles of stakeholders (European Commission Joint Research Centre, 2010). For this purpose, the information was provided by personal experience from the author, bibliographic research, and approximate values based on an average of the region. Values were pooled and averaged from available inventories such as the database v 3.3 from Ecoinvent centre (Frischkenecht et al., 2005; Wernet et al., 2016); the version 1.3 of the Agribalyse® from the French Environment and Energy Management Agency, ADEME, (Koch & Salou, 2016); the New Energy Externalities Development for Sustainability (NEEDS) project for future electricity supply systems (NEEDS, 2016); the version 3.2 (October 2015) from the European reference Life Cycle Database (ELCD) of the Joint Research Center; the bioenergy supply chain processes data from the German BioEnergieDat research project (Schebeck et al., 2013); the version 1.1 of the USDA crop data from the United States Department of Agriculture National Agricultural Statistics Service (USDA-NASS); and Economic Research Service (ERS) surveys available directly from the software openLCA nexus download page (GreenDelta, 2016, USDA-NASS, 2017).

3.7.1.4 Functional unit

The functional unit was defined as one (1) kilogram of colloidal nano-silver (20%) with a particle size of less than 100 nm placed at the gate from production facility, ready for packaging and distribution. As mentioned before the package units and processing was not considered, as the final form of the product would be handled in the same way for either process.

3.7.2 System description and boundaries

Figures 3.3 and 3.4 show the boundaries for each of the processes considered in this analysis. In Figure 3.3 it is possible to see the traditional industrial redox approach using hydroquinone from the production and entrance of chemicals to the facility (cradle) to the final dried powder at production site (gate). Figure 3.4 shows the alternative biogenic production including the conditioning of media (cradle) from production of chemicals, to the final dried powder at production site (gate). Water, chemicals, and energy are considered as inputs for both systems, the outputs for the boundaries defined is the same, and no additional consideration was given to the excess algal biomass produced by the alternative; nonetheless, it was not considered as waste to landfill and hence the final waste weight was not added to the system. In both cases water recirculation was assigned a value of 90 % after separation. Some energy optimization processes were considered within the biogenic method, and values were accounted when possible. However, since there was a small potential for energy feedback within the traditional system, it was considered negligible.

3.7.2.1 Regular silver nanoparticle production process

For the purposes of this research, a chemical reduction of silver cations was used as the reference process to obtain the nanoparticles. The reaction carried in solution yields a final product in colloidal form (i.e. no drying required) much like that from algae. The process, known as co-precipitation includes different phenomena; reduction, nucleation, growth, coarsening, and agglomeration (Cushing et al., 2004). The reducing agent chosen for the comparison was hydroquinone.

Oxidation with hydroquinone (HQ) comprises an electron transfer (2e) combined with a protonic loss (2H⁺) to reduce Ag⁺ and produce the AgNP (Hudnall, 2000). To produce particles of medium size and low polydispersion a medium concentration of HQ was considered to guarantee that the particles were within the range of 100 nm in diameter (Hudnall, 2000). Silver nitrate was assigned as the precursor of silver in solvated Ag⁺(Pérez et al., 2008). A three-step mechanism (Figure 3.5) starts with an exothermic nucleation (reduction) that produces clusters of roughly 2.6 nm followed by an endothermic growth phase that yields particles of roughly 4.1 nm in size. The last step is an additional exothermic process of aggregation that provides the final size, after an additional input of HQ (Patakfalvi & Dekany, 2005).

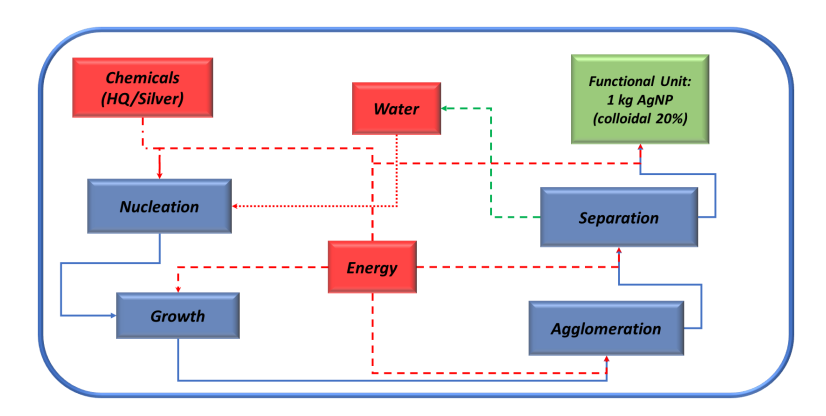


Figure 3.3. Production boundaries HQ-AgNP process. Boundaries for the traditional redox manufacturing of silver nanoparticles using hydroquinone as redox agent(i-AgNP) based on Pérez et al. (2008).

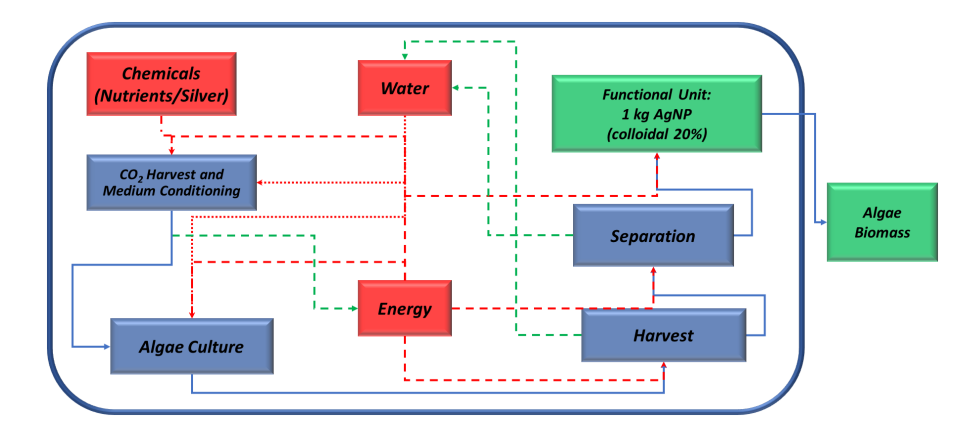


Figure 3.4. Production boundaries biogenic-AgNP process. Boundaries for the alternative redox manufacturing of silver nanoparticles using algae biomass(b-AgNP).

After the particles are agglomerated and stable, drying takes place. Powder was produced from the electrospray-drying of the colloidal silver (5%) at 200°C (Peltonen et al., 2010; EPA, 2012).



Figure 3.5. Schematic representation of the reduction process. Three step representation of the process for manufacture of silver nanoparticles (AgNP) Using Hydroquinone. Modified from Pérez et al. (2008).

3.7.2.2 Biogenic silver nanoparticle production process

For methodology purposes, the species selected for this analysis is *P. tricornutum* (Bohlin, 1897) a Bacillariophyta from the order Bacillariophyta and the family Phaeodactylaceae, which under the right conditions can produce silver nanoparticles (Galan et al., article in press). To produce the algae, a regular culture of *P. tricornutum* is used, based on the methodology described in a previous study (Galan et al., article in press).

Figure 3.6. shows an overall diagrammatic representation of a biorefinery facility, which for this document will be the basic set up of the facility that is proposed. The basic steps of one run of the process are (1) nutrient delivery, carbon capture, and medium conditioning; (2) algae culture; (3) harvesting and drying; (4) and nanoparticle separation. The boundaries for this analysis end on the chemical processing of the recovered biomass after extraction (i.e. extraction of nanoparticles). The culture system was defined as a PBR-based low volume to surface ratio (Surface / Volume = 0.2508 m⁻¹) container, henceforth known as HVLS-system, set within a modified biorefinery (Figure

3.6.) based on descriptions by Yang et al. (2013); Alba, (2013); Gao et al. (2013); and Sirin (2013).

In the proposed design, enriched water (i.e. culture medium) is piped to the culture vessels (Figure 3.7D). For this purpose, the vessels are mainly thermo-resistant stainless steel-glass composite (Figure 3.7E) cylindrical (d=3.8 m x h= 4.2 m, filled to 95% of the total volume = 45.2 m³). The water vessels and inlets are designed so that they can optimize flow and mixing is effected via water injection (low pressure jets). A two-stage culture system is used for practical purposes. To reduce energy costs, CO2 is predissolved in chamber and water mixing is achieved via hydrodynamic flow. Light is concentrated on the surface of the vessel and conducted through a Plexiglas piping system using non-imaging optics with periodical inclusions for light diffusion at 30 cm intervals. The tubes are distributed radially at 30 cm intervals along concentric radial circumferences from the central axis of the vessel. Each tube is placed as to have a small displacement from the radial projections, thus guaranteeing a high level of distribution within the vessel. To account for winter and low solar irradiance days, the system is coupled with LED light engines. The wavelengths in this case are to be specific for blue (470 nm) and red (625 nm) guaranteeing a minimum of 75 µmol photon m⁻²·s⁻¹ which was found to be the optimum for *P. tricornutum* for the normal growth phase.

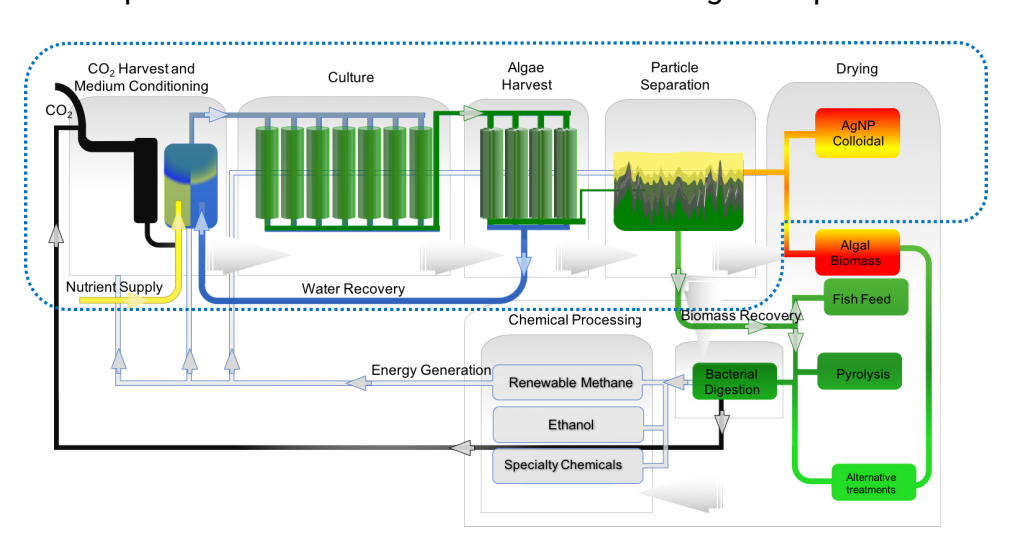


Figure 3.6. Schematic diagram of an integrated microalgae biorefinery. A facility for production of algal oil (biofuel) and other value-added products. Some microalgae are rich in carbohydrate and can be harvested and used as feedstock for fermentation to

produce ethanol and other chemicals [PUFA, polyunsaturated fatty acid] Adapted from (Alba, 2013; Gao et al., 2013; Sirin, 2013).

Water that is recovered from the harvesting and drying process is reincorporated into the system (Figure 3.7C), thus the reduced percentage of water losses (1%). UV radiation is recommended to eliminate potential cross-contamination with species associated with the wastewater and the consumption of an UVA-LED system is considered as part of the production process. Recirculating materials will not be double counted to provide better calculations.

The system includes a periodical harvest drainage (around 30 % volumetric – Figure 3.7F) through a battery of settling chambers and centrifugation columns designed to allow better clustering of cells during the process creating a highly concentrated, low moisture paste of algal biomass (Figure 3.7G). Extracted water residue is treated and piped back to the conditioning station (Figure 3.7H and 3.7C connecting pipe) thus water use is not considered as loss above 1% after harvesting.

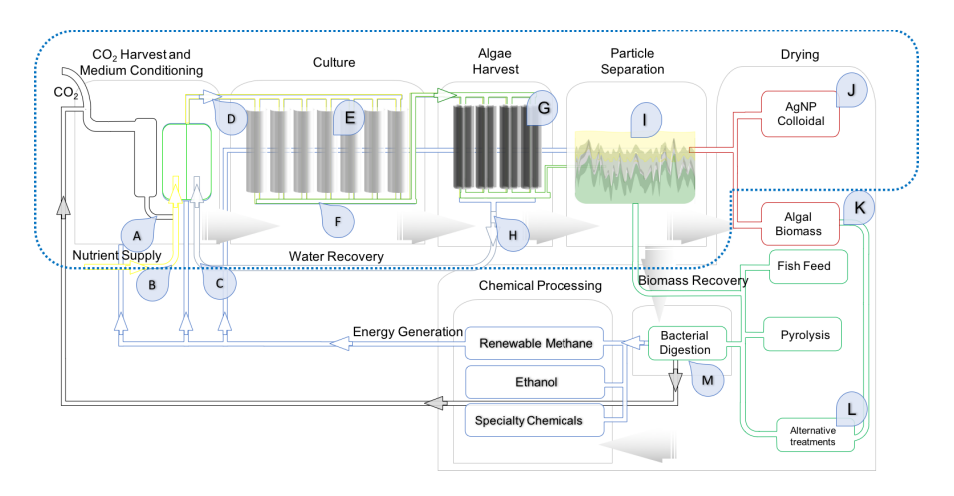


Figure 3.7. Simplified diagram of an integrated microalgae biorefinery. Intended for production of algal oil (biofuel) and other value-added products. Harvested CO2 enters the system (A), and combines with nutrients and recycled water (B and C) leaving via piping regulated by valve (D) for the culture chambers (E). Collectors (F) transfer to the harvesting system (G) where concentration and separation of liquid (H) and solid (I) phases of the culture, and further separation of the colloidal nano particles (J) and the remaining algal biomass (K) which is further processed for alternative uses (L) and

further bacterial digestion, returning energy to the system (M). Adapted from (Yang et al., 2013; Alba, 2013; Sirin, 2013).

The harvested biomass is then transported via pump to an extraction chamber where a primary nanoparticle separation process is performed (Figure 3.7I) followed by a drying of the particles (Figure 3.7J). The remaining extract can be used for specialty chemicals production, PUFAs supplementation or biodiesel (Figure 3.7K, L and M). For this analysis, no additional conversion of waste or residues was taken into consideration. All residues were considered as waste and were not included for recycling or as input to other systems or processes within this system, guaranteeing a more conservative set of values for the performance of the algae-based production of nano silver. At this point, the gate is reached and the functional unit is produced (i.e. kilogram of silver nanoparticles in colloidal in 20% suspension) ready to be delivered.

3.7.2.3 Special considerations and assumptions

Microalgae uses CO₂ and inorganic compounds to produce biomass and on average, one kilogram of dry biomass of algae requires 1.8 kg of CO₂ (Falkowski & Raven, 2007). The core nutrient of the process is CO₂, which is in turn transformed into carbohydrates and molecular oxygen in the presence of water (Falkowski and Raven, 2007).

$$2_nCO_2 + 2_nDH_2 + photons \rightarrow 2(CH_2O)_n + 2_nDO$$

Carbon dioxide + electron donor + light energy → carbohydrate + oxidized electron donor.

From the previous equation, we can deduce that for oxygenic photosynthesis the balance turns into:

$$2_n CO_2 + 2_n H_2 O + photons \rightarrow 2(CH_2)_n + 2_n O_2$$

CO₂ is not the only limiting factor when growing algae in controlled environments. A series of macro and micronutrients are indispensable to guarantee proper cultivating conditions. Nutrient solutions are prepared by mixing soluble molecules of different chemicals (usually as salts) and water (either regular or distilled). For the purposes of this document this nutrient solution will be referred to as growth media (GM) indistinct of the name of media specific for the kind of algae that is to be chosen. Besides carbon

(CO₂) the most important macronutrients nitrogen, phosphorus and silicon and major ionic forms of sodium, potassium, magnesium, calcium, chlorine, and sulfur (i.e., Na^+ , K^+ , Mg_2^+ , Ca_2^+ , Cl^- , and $SO_4^{2^-}$) will help regulate the growth rate of the culture. For the normal growth of the selected species (*P. tricornutum*) the growth medium used was a modified L_1 medium with a 25% surplus of silicon in (CML₁+Si) artificial seawater medium as described in 3.1.1. of this document. Each element was included in the bill of materials as input to the system and the manufacture process is included to account for impacts on the manufacture of the chemical. The preparation method was accounted for electricity use as part of the mixing and conditioning process.

It was assumed for this analysis that the proposed PBR system can increase the photosynthetic yield to 5% but it is understood that the ceiling is 10% due to physiological limitations (Stephens et al., 2010). Losses due to human error and equipment failure were established around a non-cumulative 5% with an uncertainty value of ±1%. Being a closed system, these values were determined by assuming function within ranges of industry, and no frequent losses due to human error. Outflows were considered as part of the maintenance of the equipment, and harvest of total biomass accounts for the drainage of the vessels.

The latent heat considered for evaporation of the culture medium was the same known for water vaporization, i.e. 2,548 kJ/kg; $1 \text{ kJ/kg} = 970.5 \text{ Btu/lb}_m = 541.7 \text{ kcal/kg}$ (Datt, 2011) so for a 30% harvest a day, each harvested vessel would require around 3.440×10^7 kJ for drying the harvest of one single vessel ($1.152 \times 10^8 \text{ kJ}$ for drying the whole vessel). Now, that was found to be quite expensive and altogether made the system inefficient even with high-value products. A separation engine (Evodos STP dynamic settler type 25, Evodos, Netherlands) to treat 4,000 L of harvested slurry per hour and returns an almost extracellular water free slurry easily processed in the downstream steps was recommended and included in the calculations. In this case, a content of water of less than 5% translates into 0.05 kg of water per kilogram of biomass harvested and a net energy expenditure of 112.85 kJ. At the same time, less than 1% of water per kilogram of nanoparticles (0.01 kg) translates into 22.57 kJ of total energy used for drying per kilogram of nanosilver so a factor of 6.561×10^{-7} was used in the final product of

nanosilver from algae. The manufacturing provided energetic consumption values, a recovery efficiency of 95% and a water recirculation of 90% was taken to the production stage of the biomass. Energy required for concentration was taken as 150 kJ kg⁻¹ of water as reported by the manufacturer of the concentrator (Evodos, 2013).

The life span of the system was defined as fifteen (15) years after construction for the tank and container components, pipes and lines were considered to last between 5 and 10 years according to the manufacturer, and their replacement was considered by multiplying the value by a factor of 3 (assumed at 5-year replacement for pipes and lines). According to the manufacturer of the separation equipment, the value for the equipment was assigned as a portion of the total volume that the equipment could handle in a lifespan of fifteen (15) years (Total volume for lifespan was established as $2.19 \times 10^7 \text{ m}^3$ factor 4.566×10^{-9}). The illumination system, including LED lights and non-imaging optics conductors were adjusted by a factor of 1.5 for LED bulbs, and 0.75 for the non-imaging system to account for the production during a total of fifteen (15) years. The total production of an algae unit during the lifespan of the system was considered on average as 16,450 kg dried biomass year⁻¹ for a total of 246,765 kg and the system factor of weight on one kilogram of algae was calculated accordingly (4.0524×10^{-6}) .

3.7.3 Inventory data collection

3.7.3.1 Regular silver nanoparticle data collection

Inventory data for the industrial silver nanoparticle production process were collected from a systematized analysis of material flow which was used as reference for the process mentioned before. Individual parameters for impact were extrapolated on the production of indium tin oxide powder in a suspension of hydroquinone in nanoscale production, via co-precipitation from a raw aqueous solution, like the one used to produce the silver nanoparticles, starting from silver nitrate (AgNO₃) based on Swiss standards, and accounting for geolocation differences (uncertainty). Approximation, extrapolation, and normalization of data were performed using the available Swiss standard values and modifying available data for Canada (Lautier et al., 2010; Roy et al., 2014).

3.7.3.2 Biogenic silver nanoparticle data collection

Inventory data for the biogenic silver nanoparticle process were collected during previous feasibility assays for the use of *P. tricornutum* for the bioremediation of silver pollution combined with regular culturing techniques for the same species. HVLS-system extrapolation data were calculated with assistance of modelling approaches available on an excel file but not included here. Values for productivity were assumed comparable to those in regular flat PBR systems and laboratory production (Spruijt et al., 2014). During the previous studies, data were collected at intervals and growth curves and average maximum productivity in optimal conditions were recorded, including growth data with silver treatments around the maximum non-lethal rotatable design (CRN).

3.7.3.3 Quality and consistency of data

Unfortunately, due to budgetary constraints, no actual emission data measurements were made for either system in a full scale, thus published and database values were used (Lardon et al., 2009; Clarens et al., 2010; Sander & Murthy, 2010; Stephenson et al., 2010; Brentner et al., 2011; Collet et al., 2011; Campbell et al., 2011; Singh & Olsen, 2011; Sills et al., 2013; Barlow et al., 2016; Gnansounou & Raman, 2016; Kern et al., 2017; Mu et al., 2017). Quality of some of the data cannot be verified and some emission measurements taken at laboratory scale cannot be consistently extrapolated to industrial scale production. Some data were based on European unit process data considered to vary little from the Canadian (Quebec) information, uncertainty for said cases were considered. Given these conditions, the study cannot contain a data quality rating assessment, as ratings for some data found in the databases were not known. Process data for different units were adapted to equal levels of detail to allow comparison among both systems. Availability of resources was assumed to be 100% and all elements were sourced locally, with less than 10 km transportation processes for the chemicals. Biogenic carbon was not included on the traditional industrial system, but was included in the algae production system. Differential values were considered and accounted for, given the differences in the two methods of production (Sills et al., 2013).

The factors used for characterization only refer to flows contained in the reference data of the openLCA software, including the databases mentioned before. Numerous flows were not included in the list of references as some of the elementary flows are not used by current available databases. The flows the highest characterization factors were selected when different values for the same element were found in different databases (Acero et al., 2017).

3.7.4 Life cycle impact assessment

The categories of environmental impact assessment comprised in the Green Delta openLCA methods uses a wider number of factors than those used by Ecoinvent. Additional factors come from the application of normalized and weighed ecoinvent factors as found in different methods. Table 3.2. contains a description of the most common impact categories that can be found in some of the recognized methods for impact assessment (Acero et al., 2017).

Table 3.2. Impact categories available per impact analysis method. Green blocks and red blocks represent the availability or unavailability of the category in the presented method. (Acero et al., 2017).

Category	Acidification	Climate Change	Resource depletion	Ecotoxicity	Energy Use	Eutrophication	Human Toxicity	Ionizing Radiation	Land Use	Odor	Ozone Layer Depletion	Particulate matter / Respiratory Inorganics	Photochemical Oxidation
Method	Ac	Cli	Re	B	핍	Ē	로	<u>o</u>	Fa	В	OZ	Pa Re	돈 S
CML (baseline)													
CML (non-baseline)													
Cumulative Energy demand													
Eco-indicator 99 (E)													
Eco-indicator 99 (H)													
Eco-indicator 99 (I)													
Eco-scarcity 2006													
ILCD 2011, midpoint													
ILCD 2011, endpoint													
ReCiPe Endpoint (E)													
ReCiPe Endpoint (H)													

ReCiPe Endpoint (I)							
ReCiPe Midpoint (E)							
ReCiPe Midpoint (H)							
ReCiPe Midpoint (I)							
TRACI 2.1							
USEtox							

For the LCIA of this document, two methodologies were taken into consideration for the analysis of environmental impacts, TRACI Version 2.1 (Bare et al., 2012) and ReCiPe Version 1.11 (Goedkoop et al., 2009) and a comparison of the performance of both systems under each of these methodologies was used to account for differences in geolocation. Table 3.2 shows a short description of each of the categories used for analysis with a definition, the description of the impact indicator, special considerations, the damage categories, and the unit used to normalize the contribution of each element in the LCI. Table 3.3 shows a comparison of the Impact categories included in each of the methods. It is noteworthy to mention that not any one method accounts for all categories established.

For these calculations, nine common environmental indicators were considered (i.e. acidification, ecotoxicity, eutrophication, climate change, human toxicity, ozone layer depletion, photochemical oxidation, particulate matter, and resource depletion). Given that TRACI 2.1 does not include a method for calculating ionizing radiation and land use (Table 3.3), these categories were not considered for comparison.

The LCIA was performed based on inventory data using OpenLCA software following the elements of the ISO 14044 (ISO, 2006). Midpoint and endpoint indicators were chosen based on their relevance to the functional unit in use and on the process of production. Results were presented on a normalized comparison form based on the ISO normalization category (ISO, 2006). Values based on world population were used. The potential impact on human health and environmental burden were evaluated using ReCiPe 1.08-2008 (Goedkoop et al., 2013). The three perspectives (i.e. individualist, hierarchic, and egalitarian) were chosen and compared (Goedkoop et al., 2008), and the 100-year horizon for climate change for comparison of sensitivity analysis.

Table 3.3. Comparison of Impact categories TRACI 2.1 vs. ReCiPe 1.11. Comparison of the Impact categories included in the analysis from TRACI 2.1 and ReCiPe 1.11 (Acero et al., 2017).

Impact Category Group	Name of Category in TRACI 2.1	Name of Category in ReCiPe 1.11								
		Midpoint			Endpoint					
		E	Н	1	E	Н	1			
		Terrestrial Acidificat	ion		Terrestrial Acidi	fication				
Acidification	Acidification	TAP500-E	TAP100-H	TAP20-I	TAPinf EQ-E	TAP100 EQ-H	TAP20 EQ-I			
		Freshwater Ecotoxic	ity		Freshwater Ecotoxicity					
		FETPinf-E	FETP100-H	FETP20-I	FETPinf EQ-E FETP100 EQ-H FETP20 EQ-I					
		Marine Ecotoxicolog	ıy		Marine Ecotoxic	eity				
Ecotoxicity	Ecotoxicity	METPinf-E	МЕТР100-Н	METP20-	METPinf EQ-E	METP100 EQ-H	METP20 EQ-I			
		Terrestrial Ecotoxico			Terrestrial Ecotoxicity					
		TETPinf-E	TETP100-H	TETP20-I	TETPinf EQ-E	TETP100 EQ-H	TETP20 EQ-I			
		Freshwater Eutrophi	C.		Freshwater					
Eutrophication	Eutrophication, total	FEPinf-E	FEP100-H	FEP20-I						
Latropriication		Marine Eutrophication			FEPinf EQ-E	FEP100 EQ-H	FEP20 EQ-I			
		MEPinf-E	MEP100-H	MEP20-I		. 2				
01:	Global Warming	Climate Change			Climate Change					
Climate Change		GWP500-E	GWP100-H	CWB20 I	GWPinf HH-E	GWP100 HH-H	GWP20 HH-I			
Change		GWF300-E		GWP20-I	GWPinf EQ-E	GWP100 EQ-H	GWP20 EQ-I			
Human toxicity	Human Health – air pollutants criteria Human Health –	Human Toxicity			Human Toxicity					
riaman toxiony	carcinogenics Human Health – non-carcinogenics	HTPinf-E	HTP100-H	HTP20-I	HTPinf HH-E	HTP100 HH-H	HTP20 HH-I			
	Ozone Depletion	Ozone Depletion			Ozone Depletion					
Ozone layer		ODPinf-E	ODP100-H	ODP20-I	00:	00100111111	000011111			
depletion		M2E-E	M2E-H	M2E-I	ODinf HH-E	OD100 HH-H	OD20 HH-I			
lonizing	N1/A	Ionizing Radiation	•	•	Ionizing Radiation	on				
Radiation	N/A	IRPinf-E	IRP100-H	IRP20-I	IRPinf HH-E	IRP100 HH-H	IRP20 HH-I			
Dhatashanisal	Smog Formation	Photochemical Oxid	ant Formation		Photochemical	Oxidant Formation	•			
Photochemical oxidation		POFPinf-E	POFP100-H	POFP20-	POFPinf HH-E	POFP100 HH-H	POFP20 HH-I			
	N/A	Agricultural Land Oc	cupation		Agricultural Lan	d Occupation				
		ALOPinf-E	ALOP100-H	ALOP20-	ALOPinf EQ-E ALOP10 EQ-H		ALOP20 EQ-I			
Land Use		LOP-H LOP-								
		Urban Land Occupat	tion	•	Urban Land Occupation					
		ULOP100-H UL		ULOP20-	ULOPinf EQ-E	ULOP100 EQ-H	ULOP20 EQ-I			
		Natural Land Occup	ation		Natural Land Occupation					
		LTPinf-E	LTP100-H	LTP20-I	I TDinf CO C	L TD100 FO LL	1 TD20 FO L			
		LTP-E	LTP-H	LTP-I	LTPinf EQ-E	LTP100 EQ-H	LTP20 EQ-I			
Particulate	N/A	Particulate Matter F	ormation		Particulate Matter Formation					
Matter		PMFPinf-E	PMFP100-H	PMFP20-	PMFPinf HH-E	PMFP100 HH-H	PMFP20 HH-			
Resource Depletion/ Depletion of Abiotic Resources	Resource Depletion – Fossil Fuels	Metal Depletion			Metal Depletion					
		MDPinf-E MDP100-H MDI			MDDinf DD C	MDD30 DD I				
		Fossil Depletion			MDPinf RD-E MDP100 RD-H MDP20 RD-I					
		FDPinf-E	FDP100-H	FDP20-I	Fossil Depletion					
		Water Depletion			FDPinf RD-E	FDP100 RD-H	FDP20 RD-I			
		WDPinf-E	WDP100-H	WDP20-I						

To compare region-specific methods ReCiPe, CML, and TRACI were used, based on the same parameters. Proximity with the US (TRACI) was considered for longitude comparison, and latitude was based on the similarities with Northern European countries. Sensitivity analysis with TRACI and ReCiPe were used to compare overall results.

3.8 Experimental design

A sequence of multiple mixtures and experiments were defined to describe and/or explain the variation of responses under heavy metal stress by silver, vanadium, and molybdenum (i.e. treatments). Based on the expected outcome, different levels for each treatment in a mixture design that accounted for less than 10 % of the concentration of silicon in the medium were prepared (Figure 3.8) to assess whether P. tricornutum was capable to sustain external concentrations of heavy metals. The conditions that were designed to be altered were ionic concentrations of metallic elements (i.e. silver, vanadium, and molybdenum) in order to obtain the desired reduction on cell count (dependent) and reduction on ionic concentrations in the culture medium (dependent) around a time interval (independent). In terms of validity (i.e. accurate correspondence to reality), reproducibility (i.e. duplicability), and reliability (i.e. trustworthiness in the results), the experiment was designed in triplicate and with different levels to determine how well the correlation of factors to responses were following a preliminary experiment. These three concerns were addressed via the selection of a good predictor (i.e. cell counts and density), the management of error (i.e. multiple measurements to account for human and statistical error), and detailed documentation. Factors that were irrelevant to the outcome and objectives (i.e. concentration of other ionic elements in the medium, light irradiance, temperature, light cycle, and pH) were controlled and monitored to account for and reject potential confounding effects of those factors that were considered outside of the scope and irrelevant to the objectives.

3.8.1 Statistical methods and analysis

Complementing the experimental design, results were analyzed with a specifically devised analysis of variance (ANOVA). Properly devised statistical analyses took into consideration the type of effects, the different assumptions of specific regression and

ANOVA models, and the inference space (SAS Institute, 2015). Changes in the response due to changes in factor levels were defined as effects. Experiments were used to determine whether significant differences in the responses across different levels of each given treatment (i.e. fixed effects, metal concentration) or if any interaction among treatment levels existed (Fang, 2005; Montgomery, 2009). These types of analyses were quite straightforward and anomalies such as outliers, missing data, homogeneous variances, and unbalanced sample sizes were easily managed (SAS Institute, 2015). The elements of the design (i.e. temperature, pH, light irradiance, nitrogen concentration) were assumed to have no interaction among them and elements of the treatment structure blocks (i.e. ionic compounds) and thus were treated as fixed effects.

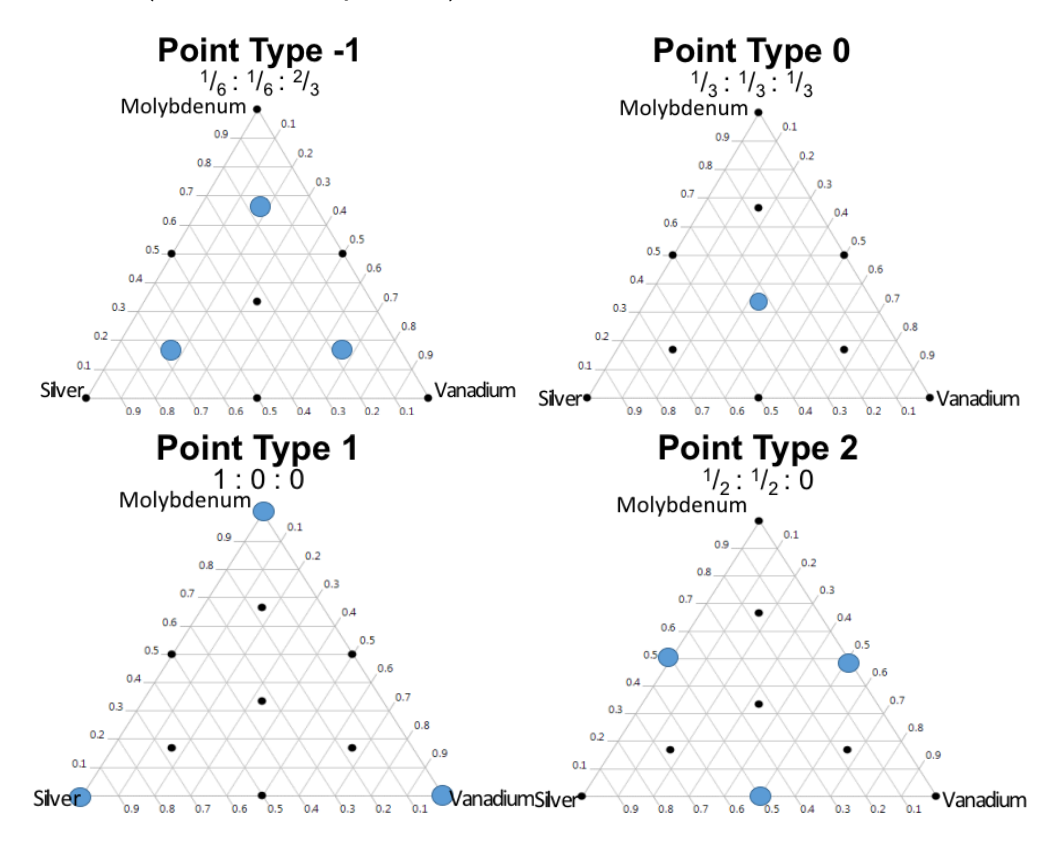


Figure 3.8. Experimental levels. Values for silver, vanadium, and molybdenum were defined around a three-element mixture design. Levels for each element were set at concentrations proportional to the total mixture (10 % of silicon content in the culture medium) at 0 (not added), ½ (half of the mixture belongs to the element and half to another as in point type 2), 1/3 (all elements added in proportional concentrations equally).

No error specific to the model was assumed, that is, the response corresponds to the dependent variable, that the independent variables influence the dependent variable and that the relationships between the dependent variable and the independent variables is linear, not nonlinear, in the parameters. Correspondingly, measurement error was assumed, i.e. the dependent variables were continuous and that the independent variables were measured correctly and accurately, which was confirmed using several correlations of measuring methods and multiple counting on the same samples. Low correlation between two independent variables (no collinearity) was also assumed, and finally, the error term and residuals were assumed to have a mean equal to zero, homoscedastic, did not show signs of autocorrelation or large correlation between independent variables, and were normal in distribution, which was confirmed via statistical testing.

Finally, the inference space was defined as the species *Phaeodactylum tricornutum* (CPCC 162), grown under the conditions described above and results obtained within the design of this specific experiment could not be extrapolated or transferred to a different species or strain unless proper test for this possibility was performed (Fang et al., 2005; Montgomery, 2009; SAS Institute, 2015).

3.9 Additional considerations

Once the methods and materials required for the experimental procedures were identified, the execution of the trials, the report, and analysis of results followed a specific format to present a more accurate image of the soundness of the experiments. Initially, information on the monitoring of the cultures is referenced as a preamble to introduce the lack of effects from other factors not included as treatments (e.g. temperature and nitrogen concentration). The following results show the culture and biomass modification for the first response variables after the treatments were introduced to the culture. Emphasis was given to growth under the treatments and the relation discovered via statistical analysis of the effects of each treatment (i.e. stressors) on the growth of the cultures, and potential associations among the three. Variation of biomass was quantified and the changes in the ionic content in the medium were measured. Additionally, the physical properties of the algae were determined via optical and electron

microscopy analysis. Next, an analysis of the elemental composition of the solid phase of the culture was presented to show how the production of silver nanoparticles was, in fact, a by-product of the remediation by algae and not a mere chemical response for the interaction between the medium ionic species. Finally, the results of the LCA are presented and analyzed.

CHAPTER IV RESULTS AND DISCUSSION

4.1 General monitoring

Temperature data yielded a linear relation between mercury measurements and IR readings with an R^2 of 0.99821 which demonstrated that the temperature read from the non-contact IR thermometer was closely related to the actual mercury-based measurement and thus the method was accepted to monitor the temperature of the culture (i.e. water). The relation of the two temperatures was determined by the equation $T_{Hg} = 0.5749 + 0.9401T_{IR}$, where T_{Hg} is the value measured by the mercury thermometer and T_{IR} is the value measured by the infra red sensor. Regular monitoring showed that the temperature along the culture units remained constant with a maximum at 20.3 °C and a minimum at 15.7 °C with no stratification along the culture units. Irradiance was maintained between 75 and 92 μ mol·s⁻¹·m⁻²

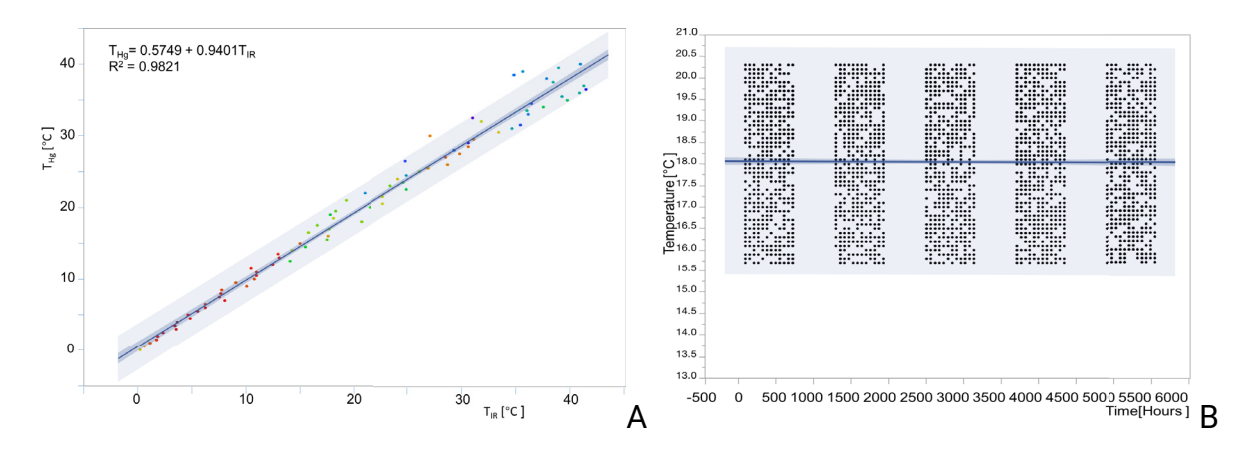


Figure 4.1. Temperature correlation mercury and IR measurements. A) Graph showing the correlation between the measurement of temperature using a mercury thermometer and an IR-laser sensor prediction shadows account for 95% of the measurements and. B) Temperature measurements clustered by irradiance levels. Ranges remained between 15.7 °C and 20.3 °C while irradiance ranged between 75 and 92 µmol s⁻¹·m⁻².

Nitrogen as nitrate curve (Figure 4.2) showed an inverse correlation between culture density and available nitrogen, although the available nitrogen never reached a concentration value lower than 5% of the original concentration of the medium at the time of inoculation $(6.572 \times 10^{-2} \text{ g NO}_3 \cdot \text{L}^{-1})$. It was therefore established that nitrogen limitation

was not a factor triggering the uptake of silver nitrate as a source of nitrogen because the concentration of this reagent was never above 0.001% that of available nitrogen.

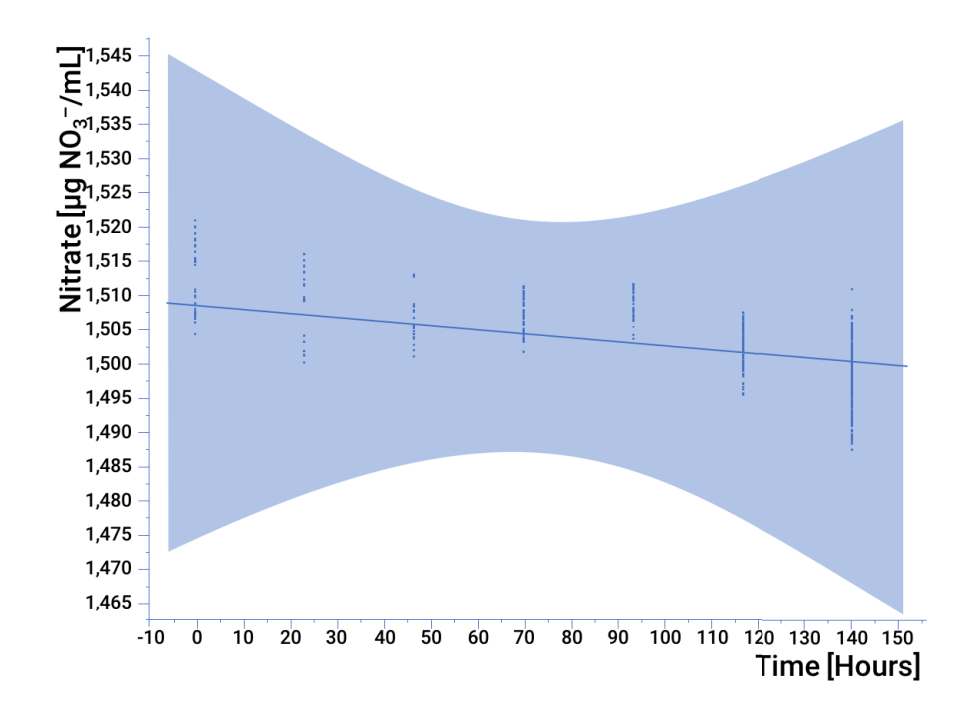


Figure 4.2.Nitrogen concentration curves. Measured as a total of nitrogen as nitrate, measured in μg NO₃-L⁻¹, each time the culture was sampled. The red lines label the difference between the maximum and minimum concentrations; the difference between initial concentrations and final at 150 hours does not account for 5 % of the initial concentration at any given time and point in any of the set of cultures.

4.2 Cell culture and biomass determination

Visual exploration revealed that there were no apparent changes in the appearance of the cultures during the first days after the introduction of the heavy metal treatments. It was only until after the seventh day after heavy metal treatments were administered that some of the cultures started to show apparent changes in physical appearance as signs of decay. The cultures with silver levels at 1.5 mM showed the highest degree of visual deterioration which was later confirmed by cell counts (Figure 4.4 silver level 1); however, these cultures returned to healthy visual appearances after the fourteenth day of culture.

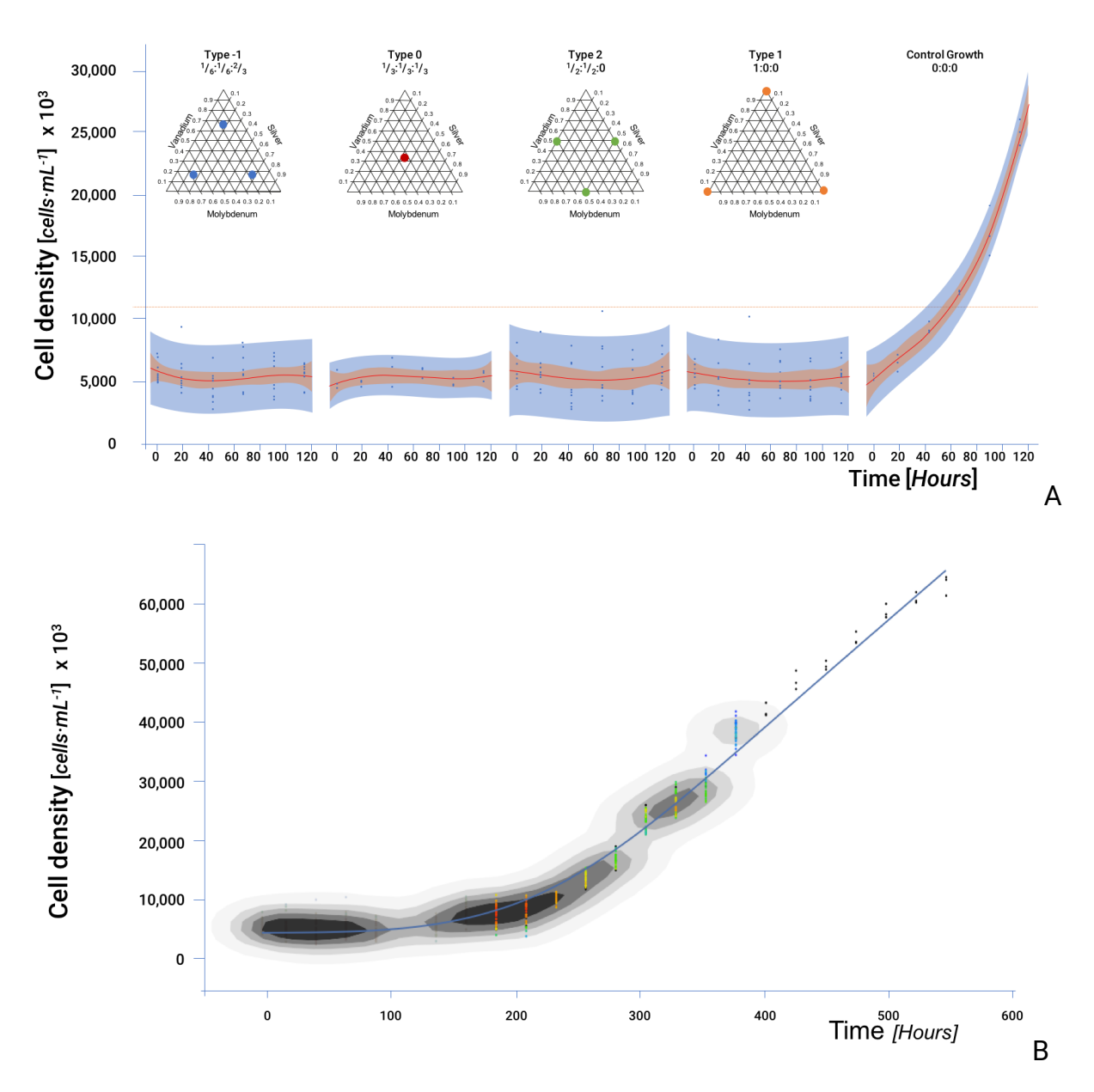


Figure 4.3. Cell density graphs. Comparison of cell density (cells × mL⁻¹) counts for heavy metal concentrations and regular growth (control on the far right). (A) The triangles on the top represent the different levels of concentrations for each treatment level (i.e. ionic concentrations) used during the experiment. The horizontal line represents the maximum level of growth after heavy metal insertion and is provided as reference to the control growth curve. (B) The graph shows a phased-out plot of the control cultures (i.e. treatments equal to zero), accounting for the stress induced by the addition of the treatments the highlighted color markers correspond to the period where the treated

cultures returned to normal growth (after 180 hours after treatment), shadows show the clustering of values around 90% similarity or correspondence in trend.

To confirm the apparent visual lack of effects due to heavy metal addition, growth curves were built based on the data for the measured values of cell density [cells·mL⁻¹]. These curves show an apparent halt in the growth of the cultures when compared to the control group during the first five days following the introduction of the treatments (Figure 4.3 B in shadowed region). It seems like the introduction of the metals hindered the ability of the cells to replicate or divide as sown by the behavior of the treatments compared to the control group in Figure 4.3 A. The presence of the metal treatments altered the growth response as perceived in the changes of slope in the graps of Figure 4.3 A. A decreased slope in the growth curves at different levels of silver (Figure 4.4) suggests that the reproduction of the cells was somehow affected by the presence of the different treatments. It is possible that the cause of this "lag" period is the increased sorption of the metals by the algae prior to a slow release back into the medium like what was reported by Skjak Brek et al. (1980) for cadmium and zinc.

The set of parameters came from estimates derived from preliminary results of a response surface analysis of the data. The analysis yielded the following equation, which plots into the graphs shown in Figure 4.5.

```
Cell Density = 12.59 + (79.06 \times Ag) + (-480.03 \times V) + (162.26 \times Mo) + (-86.14 \times Ag^2) + (385.21 \times V \times Ag) + (472.85 \times V^2) + (-256.65 \times Mo \times Ag) + (304.60 \times Mo \times V) + (-169.22 \times Mo^2). (Equation 4.1.)
```

From the equation above, the values of the term estimates of the different treatments (i.e., silver, vanadium, and molybdenum in concentrations of 0.025; 0.05; 0.1; 0.075; and 0.15 mM/L) were used as the parameters for the GLIMMIX (Theriot & Stoemer, 1984) analysis, which yielded the following pair of equations:

```
A = 1.4985 + (0.1876 \times Ag) + (0.1874 \times V) + (0.3084 \times Mo) + (-0.004 Ag \times V) + (-0.7585 \times Ag \times Mo) + (0.5037 \times V \times Mo) + (-0.9614 \times Ag \times V \times Mo)  (Equation 4.2.) 

B = 0.2492 + (-0.2477 \times Ag) + (-0.2348 \times V) + (-0.2760 \times Mo) + (-0.0736 \times Ag \times V) + (0.1104 \times Ag \times Mo) + (-0.0876 \times V \times Mo) + (0.5571 \times Ag \times V \times Mo)  (Equation 4.3.)
```

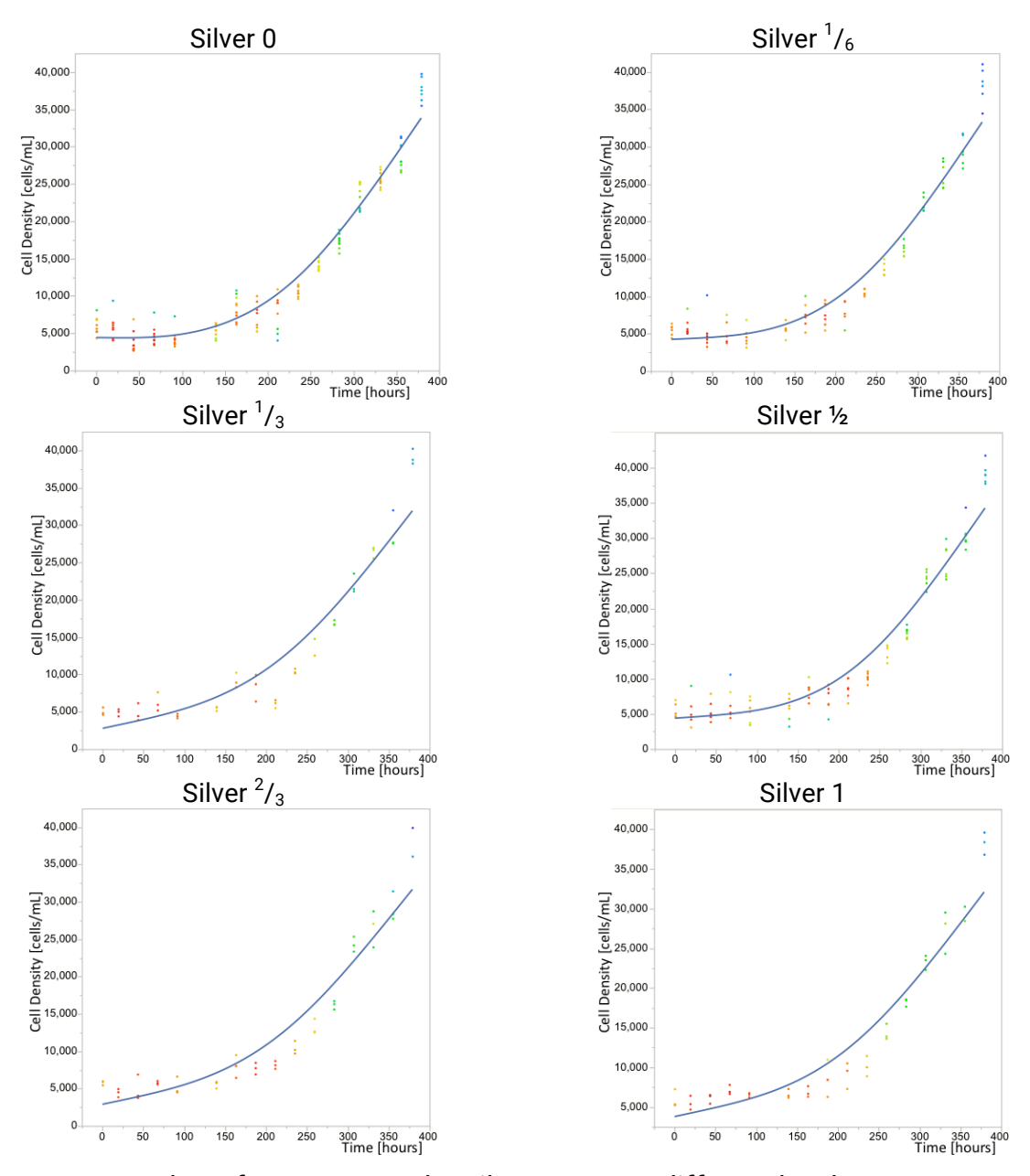


Figure 4.4. Growth performances under silver stress at different levels.

A shifted t distribution analysis showed a high level of correlation among the observed values for the constant parameters of the predicted model. From the analysis of variance for the model it is possible to observe that the test for each factor (Ag, V, and Mo) was highly significant, p < 0.0001. The mixture of signs, on the eigenvalues, indicates that there was no unique solution to the eigenvector equations. Therefore, there was no stationary minimum or maximum indicated by this data. The stationary point was a

saddle point. It was determined that to maximize the experimental measure further, a central rotatable composite design experiments should center on maximum predicted concentrations of 1×10^{-4} M for silver, 1.5×10^{-4} M for vanadium, and 1×10^{-4} for molybdenum based on the results of the ridge analysis.

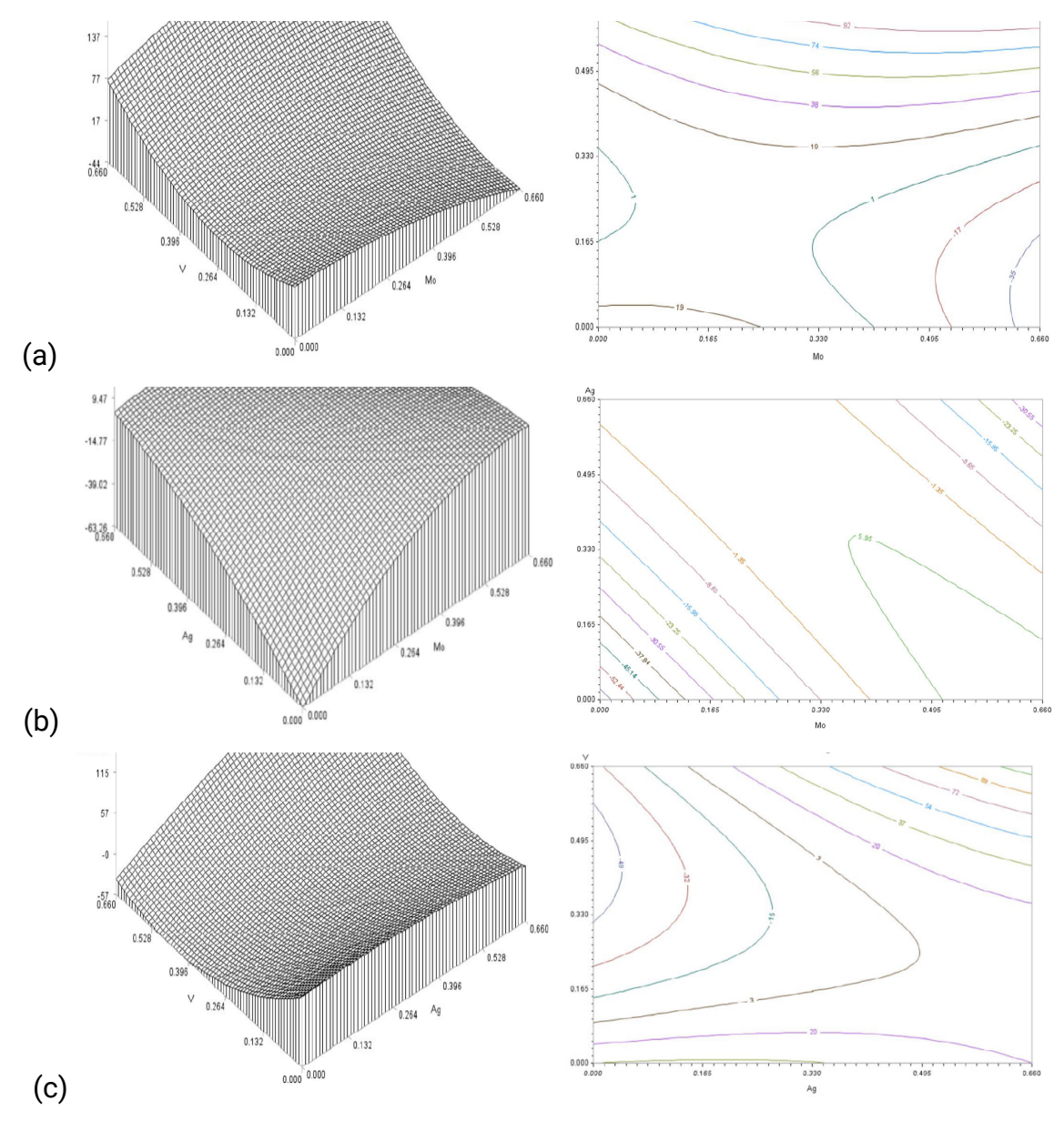


Figure 4.5. Surface plots for cell density. Set of surface plots derived from the equation for cell density of the surface response analysis, (a) molybdenum at a silver level of 0.6173, (b) silver at a molybdenum level of 0.1958, and (c) vanadium at a molybdenum level of 0.1875. The trend of these graphs shows an apparent saddle point outside the concentration values of reference (SAS, 2015).

For the second portion of the treatment assays, the increased concentration levels for each treatment (silver, vanadium, and molybdenum) introduced with the new design looked to determine the specific growth response of the algae to pollutant stressors (i.e. treatments), and an explanatory model analysis was selected. The goal was to determine the relationship among the parameters of the model (i.e. cell density, silver, vanadium, and molybdenum concentrations). A preliminary ANOVA using time as a predictor variable alone, showed significant evidence to reject the null hypothesis thus providing evidence of some relationship between time and cell density. However, when including the treatment levels as grouping factors, the R² increased by 10%, which suggested a better fit model based on the interaction of the treatments in time. The model explained to some extent the effects the stressors had on the growth of the culture (cell density). Further exploratory methods were used to determine how well a different non-linear model would have explained the data. A principal component analysis (PCA defined by Theriot & Stoemer, 1984) was performed on the responses of the variables which was started by using the value of one as prior commonality estimates for each component (Ray-Mukherjee et al., 2014). After using the principal axis method, followed by an orthogonal rotation (i.e. varimax), it was possible to extract the components (Kim & Mueller, 1978; Kline 1994). From this analysis, it was found that only three elements had eigenvalues greater than 1.00, and a scree test (D'Agostino & Russell, 2005) suggested that all three were meaningful (Figure 4.6). Therefore, these three components were retained for rotation. When combined, these components accounted for roughly 80% of the total variance (44%, 23%, and 13%, respectively).

While interpreting the rotated factor pattern, an item was recognized to load on a given component if the factor load was 0.40 or greater for that component and less than 0.40 for the other. Following these criteria, two variables were found to load on the first element, which was subsequently labeled "Ion Change" based on the characteristics of the variables involved. Two variables individually loaded on the second and third components labeled "Ion Read" and "Growth" respectively. The two ions that showed the strongest incidence in the response variable (cell density) were silver and vanadium.

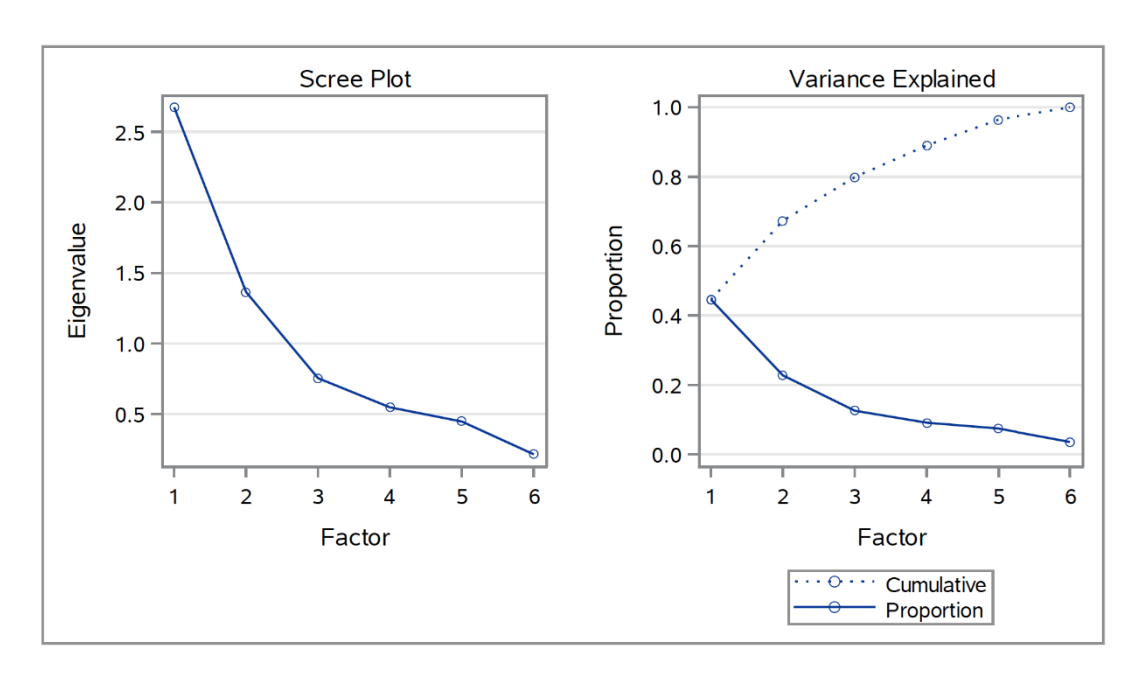


Figure 4.6. Scree and variance plots principal component analysis. Scree and variance plots from the Principal Component Analysis. The total accumulative variance of factors 1, 2, and 3 accounted for 80% of the total. These three factors were affected by the changes in Ionic concentrations (SAS, 2015).

Following the component analysis, the data were grouped (blocks) and increasing the R² for the model closer to 1 (0.999). When the change in silver concentration was compared to the different variables, the effects with significant evidence for the fit of the model were: 1)the change in cell density after stressor introduction (DeltaDensity); 2) time (Time); 3) their interaction (DeltaDensity×Time); 4) the level of silver introduced to the system (AgIn) and its interaction with both 5) the change in cell density (DeltaDensity×AgIn) and 6) time (Time×AgIn); 7) the level of vanadium introduced (VIn) and 8) its interaction with time (Time×VIn) and 9) silver (AgIn×VIn) were considered. When the analysis included the different levels of molybdenum as a stressor, there was no significant evidence to reject the null hypothesis (no effects) either for silver or vanadium, and thus, molybdenum was not included in further analysis. From the previous results and statistical analysis, it is possible to see some level of relation between the concentration of the two stressors (vanadium and silver) and the cell density. The grouping of the data provided some evidence of interaction between the cell density and the availability of ions in the medium. The changes in ionic concentrations over time and

their relationship to cell densities suggest that in some way the cells were responsible for this variations and further analysis is required to determine the degree of interaction and variation caused by changes in ionic deliver and cell densities. All the data analysis for this paper was generated using SAS software, Version 9.4 of the SAS System for Windows (SAS, 2015).

4.2.1 Ion removal from the water column

Upon the addition of ionic treatments (i.e. silver, vanadium, molybdenum), measurements with ICP analysis accounted for silver and vanadium with reduction in ionic concentration in the liquid medium equivalent in percentage from 90 to 98% of the original silver concentration (Figure 4.7 in blue) for all levels of silver, and between 70 and 90% in vanadium (Figure 4.7 in red). Upon observation, the concentration of molybdenum that generated a more consistent performance in the reduction of ionic concentrations in the medium was 1.35 x 10⁻⁴ g Mo·L⁻¹ which accounted for a more elevated and collected removal in all concentrations of silver and vanadium (Figure 4.7). When no molybdenum was added to the mixture, it was clear that the removal ratio was not enhanced in any way and concentrations of both silver and vanadium were the influential factor. Once molybdenum was added, the overall performance of the culture in the removal of the ionic species was enhanced and higher concentrations reduced the differences in removal for all levels and concentrations of silver and vanadium. However, excessive molybdenum (i.e. concentrations above 1.35 x 10⁻⁴ g Mo·L⁻¹) returned the performance to a less consistent reduction of ionic concentrations in the medium.

As mentioned before, molybdenum is an essential trace element in the metabolism of carbon, nitrogen and sulfur species inside the algae, and indirectly influences the formation of metallothionein proteins being part of the major facilitator superfamily of proteins (Tejada-Jiménez et al., 2011) and low concentrations of the ion, could correspond with a limited activity of the proteins. Equally, excessive concentrations of molybdenum in the surrounding medium can account for interference in the metallic defense mechanisms, as higher concentrations can compete for the intake of vanadium (Pannesi et al., 2013). This can be inferred by the fact that after molybdenum concentrations surpassed the ideal value (i.e. 1.35 x 10⁻⁴ g Mo·L⁻¹) the consistency of the

performance was affected and the predictor interval widened as seen in Figure 4.7 for level at 1.69×10^{-4} g Mo·L⁻¹, where only the vanadium removal is affected by excess molybdenum (red).

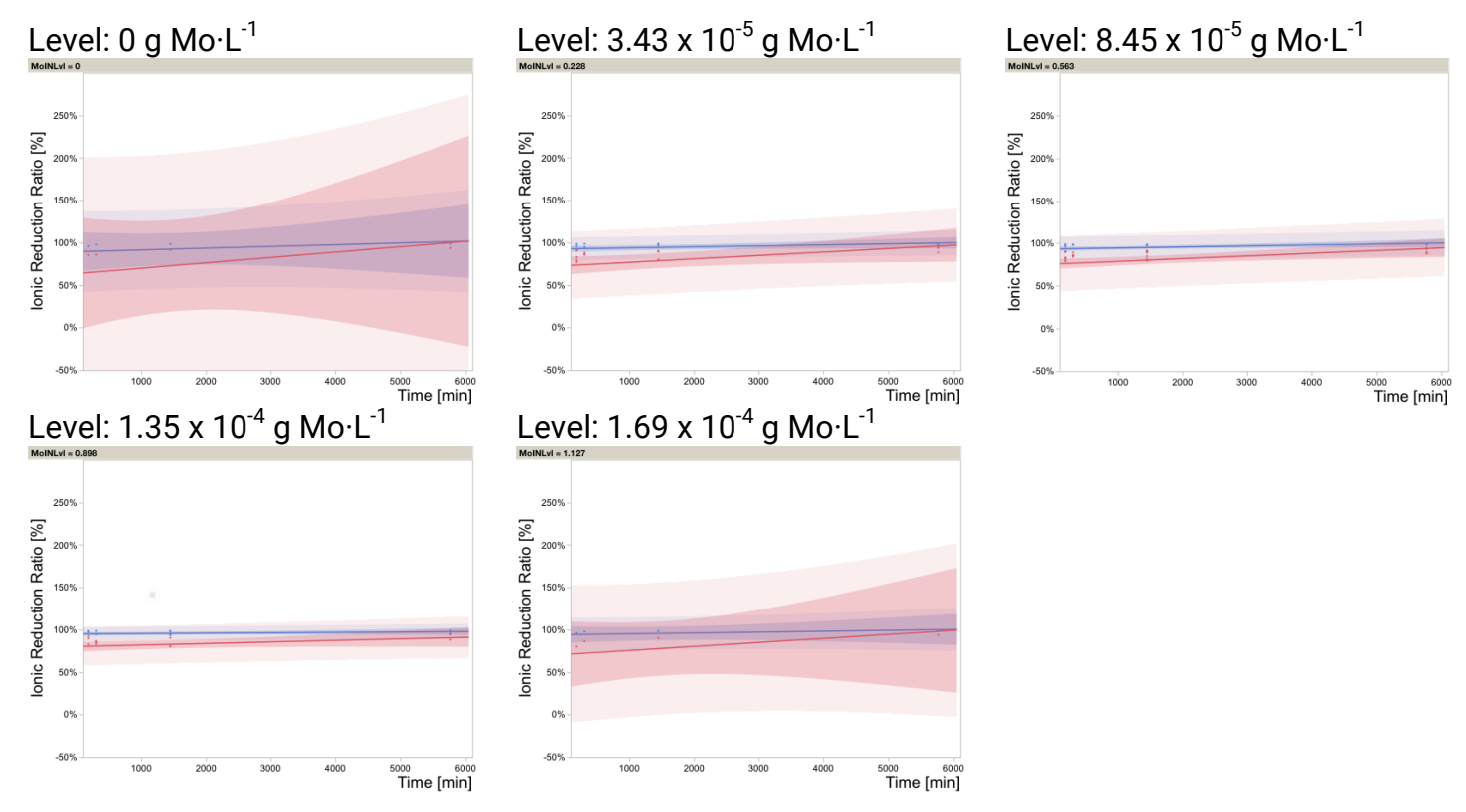


Figure 4.7. Silver and vanadium removal ratios agglomerated by molybdenum level. Ionic removal ratios of silver (blue) and vanadium (red) classified by molybdenum treatment level. Darker shadows represent the confidence interval (90 %) of removal for each time of measurement (in minutes), and lighter shadows represent the predicted variability in removal in time.

4.2.2 Physical appearance

For convenience during the SEM observations, five (5) type of structures were identified and analyzed within the scope of this research. The first type of structure was labeled as a damaged cell/frustule with extracellular contents (DMG-EC) and was identified as structures with a significant amount of frustule constituents (i.e. Si, Mg, O) or flat-shaped features with a strong proximity of organic contents (i.e. C) from the cell as it can be seen in Figure 4.9 (point 1 the frustule structural elements and point 2 the exuded organic, mostly carbon based) and Figure 4.10 (point 4). The second type of structure was a

regular spherically-shaped particle, labeled extra-cellular particle (ECP) that appeared structurally detached and concentrated near the frustules (cellular bodies) with a diameter of less than 100 nm (Figure 4.10, point 3), these particles were visible near clusters of frustules or DMG-ECs, therefore, special attention was given to clusters or abundant occurrences of these formations. These formations were principally made of elemental silver, carbon (probably background organic matter from the cell), and oxygen (point 3). The third type of structure was labeled as a surface particle secretion (SPS) and consisted of clear formations, of amorphous shape, coming from the frustule surface slightly attached to the frustule structure (Figures 4.11 and 4.12; points 5, 6, and 8). Some surface secretions sometimes appeared as a formation altering the shape of the surface of the frustule body, in this case they were labeled as the fourth type of structure listed or surface grown body (SGB) as seen in Figures 4.12 (except point 8) and 4.13. The fifth type of structure was the background (BKG) and was sampled to account for interferences caused by the elemental composition of the stub (Figure 4.14). A full classification with the chemical analysis of each point presented on the figures of this document is listed in Table 4.1. The sizes of the particles (i.e. diatom frustules) observed in this study ranged from 5-20 µm. Under regular growth conditions, most of the frustules ranged in size from approximately 10 – 20 µm and were generally fusiform, i.e. spindlelike shaped, tapering at both ends, and wide in the middle (Figure. 4.8). After the heavy metal stress described in the Section 3.1 in materials and methods was applied, the shapes mostly retained the traditional fusiform shape of P. tricornutum (Figure 4.8), but with a reduction in the size distribution and range (5 to 10 μ m).

The images of the diatoms frequently showed damaged frustules with agglomerated magnesium and silicon oxides spilled around the general shape of the frustule (detail visible in Figure 4.9, points 1 and 2). Minerals and mineral aggregates (Figures 4.10, 4.11, 4.12, and 4.13) often appeared as amorphous surface secretions from the cell. Special attention focused on agglomerated and regularly shaped particles of less than 200 nm in diameter (usually > 100 nm) that appeared near the surface of destroyed frustules in the treatment with a silver concentration of 1.47 x 10^{-4} g L⁻¹ (Figure 4.10, point 3). This concentration of silver was found to be the maximum that the organism could sustain as

measured in the previous assessment to the capacity of P. tricornutum to whistand heavy-silver polluted waters. Further analysis with the EDS detector showed these particles measured high concentrations of silver, aluminum, carbon and oxygen. Smaller sized frustules showed the appearance of being irregularly shaped around the apical ends of the silicon structures (Figure 4.13) which were found in the lower end of the size distribution in frustules (around 5 μ m in size).

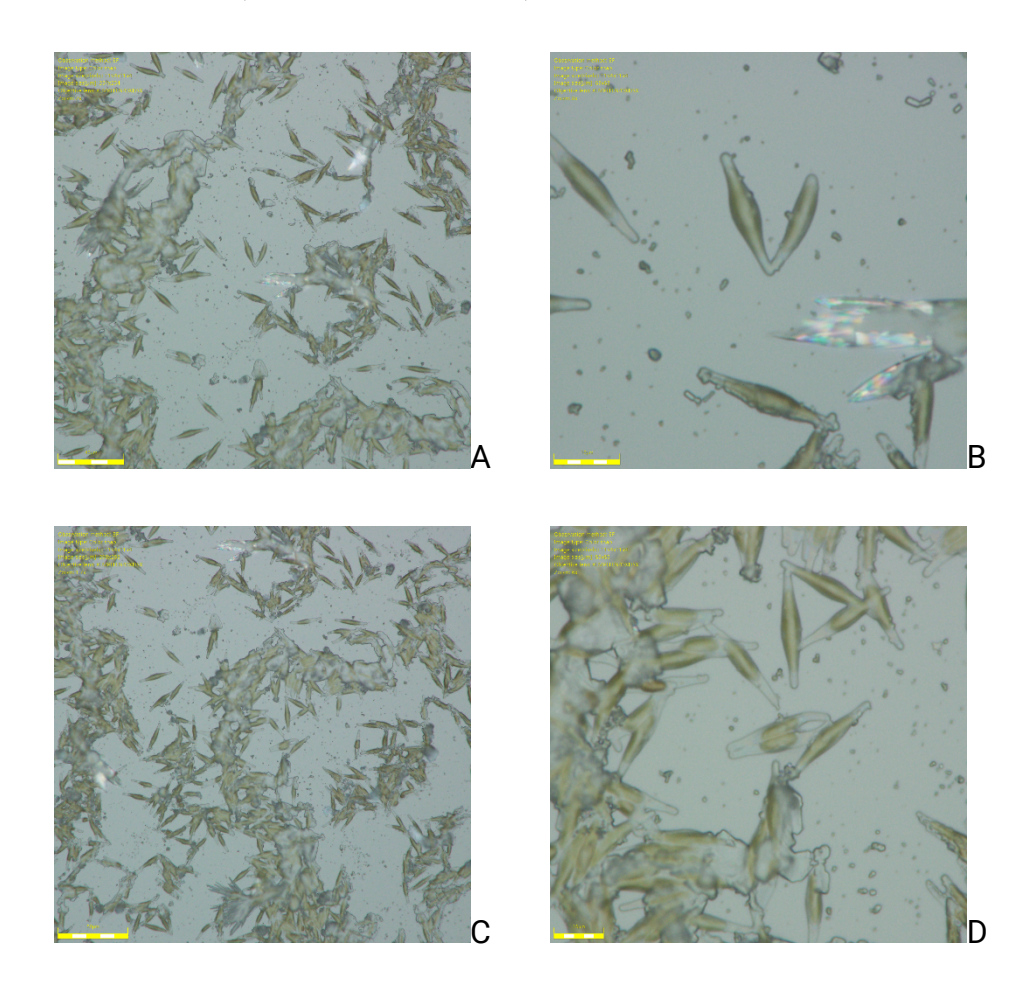


Figure 4.8. *P. tricornutum* under optical microscope. Optical microscopy images of regular shaped cultures of *P. tricornutum*. A) and C) normal appearance of a culture of *P. tricornutum* under normal growth; B) close visualization of cells, D) the fusiform shape of the average cell and some reproductive cells joined along the valvar axis (Measure bar = $10 \mu m$).

4.2.3 Elemental composition

As determined by EDS, the elements considered of interest in the samples were aluminum (all points), silicon (except points 2, 14, and 15), magnesium (except points 14 and 15), carbon (except points 14 and 15), silver (point 3 and a considerably low concentration on point 9), sodium (points 7- 12), nitrogen (except points 14 and 15), calcium (point 6), molybdenum (low concentration on all points and absent on 1, 14, and 15) and oxygen (all points). Lower amounts of potassium (points 7, 8, and 9) and sulfur were observed in some areas of the samples.

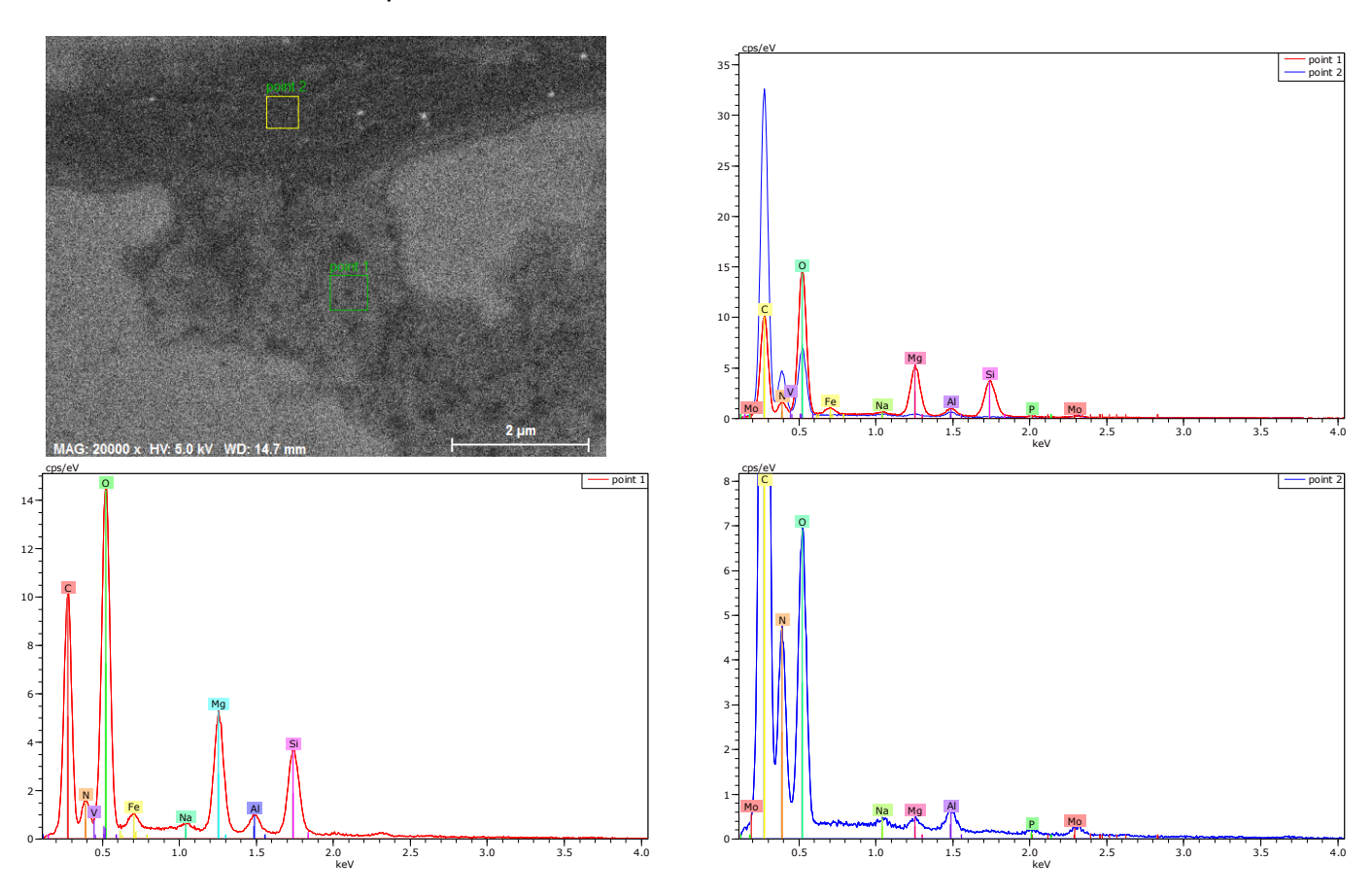


Figure 4.9. Typical *P. tricornutum* frustule damage after heavy metal treatment. Backscattered electron (BSE) images of frustule damage (DMG) tied with EDS analysis of focal points. Magnesium and silicon exhuded as amorphous growths (point 1) to the outside of the frustule (near point 2) from typical *P. tricornutum* frustules grown under silver stress (Measure bar = $2 \mu m$). Axes correspond to kilo-electron volt (i.e. keV) for the independent axis and counts per second per electron-volt (i.e. cps/eV) for the dependent.

From a purely chemical constituent perspective, high peaks of oxygen, and carbon were common in most measurements (points 1, 2, 4-13), usually peaking outside the range of other elemental compositions, except for oxygen on point 3 (Figure 4.10). Additionally, the EDS analysis of constituents of the mineral aggregates showed a proportionally considerable content of aluminum (points 1-15), magnesium and silicon (points 1, 5, and 7-13), sodium (points 7-13), and iron (points 1, 5, 7, 10-13, and 15). A higher intensity measure (Figure 4.13) showed the presence of some peaks that could be overlapping with other elemental concentrations (i.e. molybdenum, calcium, potassium, vanadium, and phosphorus) that appear at the lower threshold of confidence of the equipment and thus were not considered in the analysis of the particles.

Table 4.1. Classification and composition of structures. Classification and general composition of the points and structures identified for analysis from the treatments. Analysis made using SEM-EDS.

Point	Type	Si	Mg	Ag	Al	Мо	С	0	N	Fe	Cu	Р	Ca	Na	Figure
1	DMG-EC	3.8	5.3	-	1.0	-	>10. 0	>10. 0	1.5	1.0	-	-	-	0.7	2
2	DMG-EC	-	0.5	-	0.6	<0.5	>10. 0	6.9	4.8	-	-	<0.5	-	0.5	2
3	ECP	0.5	1.0	2.4	6.4	<0.4	3.8	1.4	<0.5	-	-	-	-	0.5	3
4	ECP	<0.5	0.4	-	<0.5	<0.5	>10. 0	4.0	3.7	-	-	-	-	0.4	3
5	SPS	2.5	4.0	-	1.1	<0.5	>10. 0	>10. 0	2.5	0.8	-	-	-	0.5	4
6	SPS	<0.5	<0.5	-	1.1	<0.5	>10. 0	5.2	2.0	-	-	-	<0.5	0.3	4
7	SGB	1.3	1.6	-	2.9	<0.5	>10. 0	9.0	2.6	0.5	-	-	-	1.1	5
8	SPS	1.4	1.4	-	2.9	<0.5	>10. 0	9.0	2.3	-	0.9	<0.5	-	1.2	5
9	SGB	<0.5	<0.5	0.1	0.7	<0.4	>10. 0	6.0	2.3	-	0.9	<0.5	-	0.9	5
10	SGB	2.5	5.0	-	9.0	<0.5	6.6	8.6	1.2	0.8	1.2	-	-	0.8	6
11	SGB	2.9	3.5	-	2.7	<0.5	>10. 0	>10. 0	1.7	0.9	0.7	-	-	0.9	6
12	SGB	3.3	4.5	-	1.9	<0.5	>10. 0	>10. 0	1.6	1.0	0.7	-	-	1.2	6
13	SGB	2.5	3.0	-	>10. 0	<0.5	5.6	8.0	1.0	0.8	1.4	-	-	0.7	6
14	BKG	-	-	-	33.0	-	-	1.0	-	-	2.0	-	-	-	7
15	BKG	-	-	-	24.8	-	-	1.8	-	2.0	6.5	-	-	-	7

Definition of Point Types:

- DMG-EC Damaged cell, exuded contents
- ECP Extra-Cellular Particle
- SPS Surface Particle Secretion
- SGB Surface Grown Body
- BKG Background

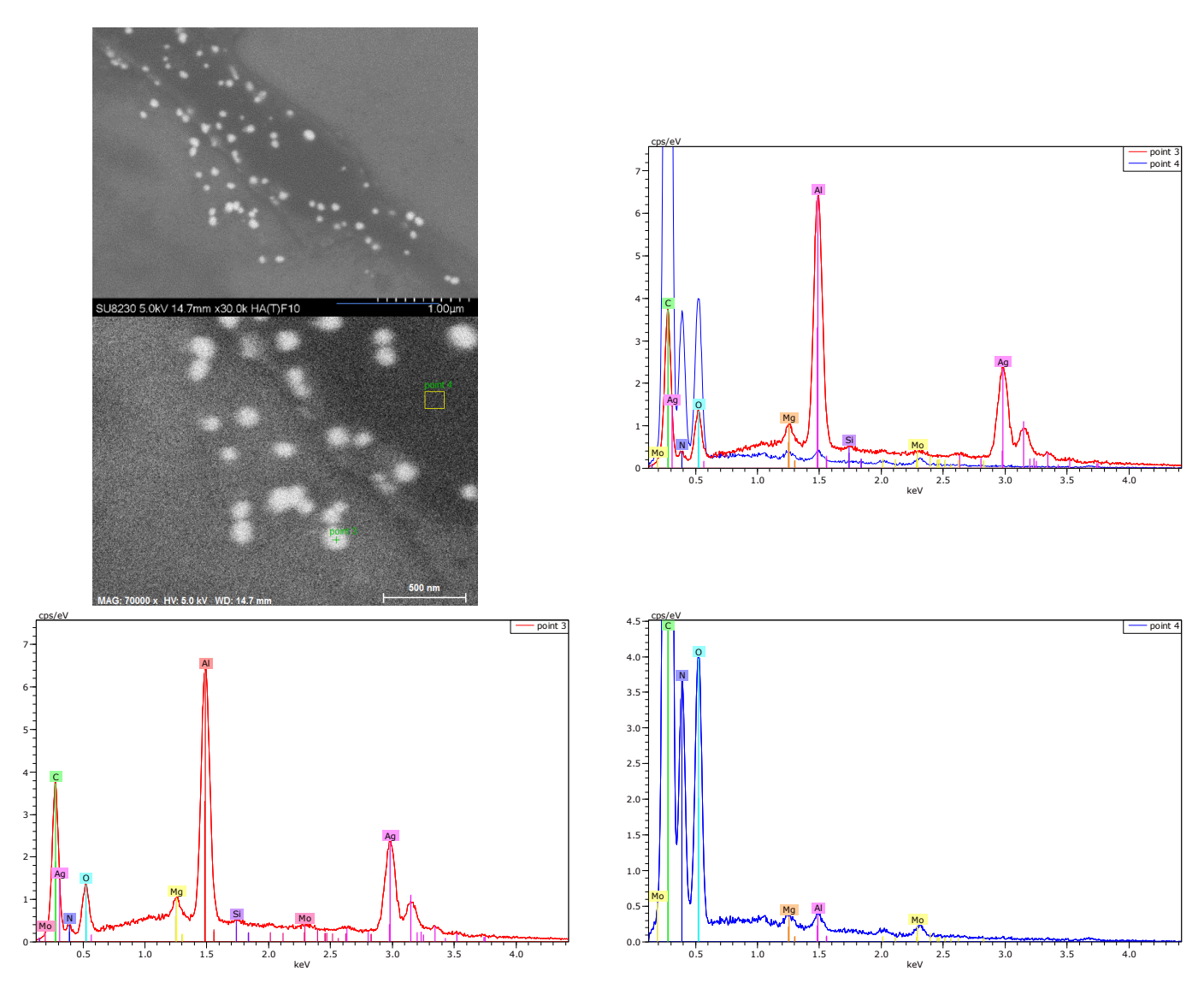


Figure 4.10. Typical extracellular particles under silver stress in *P. tricornutum*. Backscattered electron (BSE) images of silver extracellular particles (ECP) produced by a typical *P. tricornutum* cell under heavy metal treatment with silver. Concentration level is 1.47 x 10⁻⁴ g L⁻¹ of silver treatment culture. Notice the mostly spherical shape and dimension of the particles (<100 nm). Axes correspond to kilo-electron volt (i.e. keV) for the independent axis and counts per second per electron-volt (i.e. cps/eV) for the dependent.

Noteworthy is the high presence of aluminum, sodium, magnesium, and silicon, on most sampling sites, and all points in Figure 4.12 (points 7, 8, and 9), with a small appearance of silver on point 9. The relative scale shows a higher concentration of ions on point 8

when compared to 7 and 9. The lowest concentration of elements appears at point 9. The fact that silicon appears in varied concentrations combined with magnesium throughout the structure of the frustule in most of the samples, this agrees with the understanding that this algae species uses facultative silicon deposition (Johansen, 1991; Tesson et al., 2008; Martin-Jézéquel & Tesson, 2013).

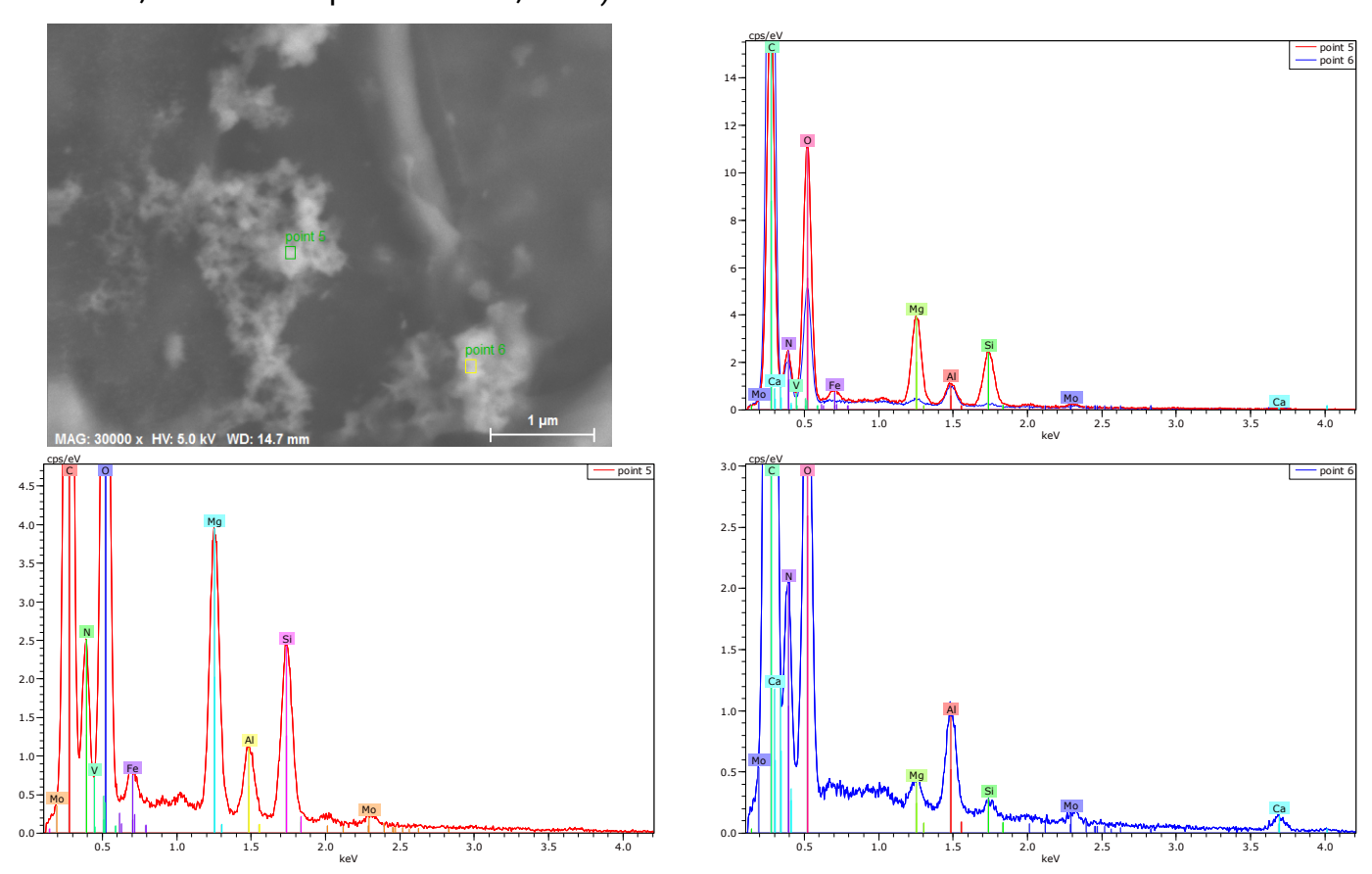


Figure 4.11. Surface frustule secretion on *P. tricornutum* under heavy metal treatment. Backscattered electron (BSE) images of a surface secretion (SPS) from typical *P. tricornutum* frustules grown under heavy metal treatment conditions. A heavy deposition of magnesium and silicon present on point 5 as compared to point 6. Axes correspond to kilo-electron volt (i.e. keV) for the independent axis and counts per second per electron-volt (i.e. cps/eV) for the dependent.

The combination of the silicon-magnesium-sodium spots present in most points of analysis, brought forth the question of whether the sodium ions were part of the magnesium-silicon matrix or depositions of sodium salts from the surrounding medium. The concentration of chlorine or other elemental associates for the salt theory in the

samples suggested that the counts of elemental sodium are not in any way an isolated precipitation of sodium salts as solubility rules would not account for said phenomenon in the culture medium (Soustelle, 2016). Furthermore, other alternatives for accounting the presence of insoluble sodium coming as compounds (e.g. sodium octamolybdate, sodium aluminate, sodium thiosulfate) could be disregarded, because, except for aluminum, other elements present in these compounds (i.e. molybdenum, aluminum, and sulfur) were not present in sufficient stoichiometric counts. Prudence dictates that the assumption of sodium aluminate formation was not supported by the concentration of aluminum in the culture medium and that the presence of aluminum counts most probably were the result of measurements from the elements in the background (Figure 4.14).

Given that the culture conditions were carefully monitored during the duration of the experimental phase of the research, it is safe to assume that the chemical properties and composition of the diatom particles could only be related to the original composition of minerals in the culture medium and the growth conditions, since there was no contamination or addition of other chemical substances. During the culture process, owing to the chemistry of water, the concentration of ions caused these inorganic minerals to become available or to react with other ions within the environment or the inner space of the cell (Brzezinsk et al., 1990). It is well known that organisms, including unicellular species, attempt to, and to a certain extent can, maintain the concentration of specific substances in a specific range. This ability to maintain this balance, no matter the concentration of the substance in the surrounding environment is known as homeostasis (Cannon, 1932). During the frustule formation process, amorphous silicon structures are built by the protein machinery and excessive presence of some ionic species can be mixed either by mistake (i.e. chemical affinity to silicon ions) or by design (i.e. specific proteomic response to pollutants) with the silicon matrix producing a secreted accumulation, or restructuring the final frustule composition to have the metal held in position (Cumming & Gregory, 1990; Conner & Schimid, 2003; Bowler et al., 2010). It is well known that the production of antioxidants is one of the mechanisms available to unicellular algae to fend the potential damage of reactive oxygen species (Krinsky, 1989; Woodall et al., 1997; Pinto et al., 2003). Algae has been reported to respond to heavy metal via the action of enzymes (e.g. superoxide dismutase, glutathione peroxidase, ascorbate peroxidase, catalase) to directly prevent the formation of highly reactive oxygen species as consequence of heavy metal presence in the environment or in the cytoplasm (Pinto et al., 2003). It is well known that the ability of algae to accumulate heavy metals can be increased with the availability of nutrients (Wang & Dei, 2001; Pinto et al., 2003).

Not accounting for carbon or oxygen counts, the morphology and elemental data indicated that frustule samples in different locations of the frustule were composed of over 50% amorphous silicon and magnesium oxides and a lower count of ionic clusters. The relative distribution of components in each sample is listed in Table 4.1 and presented to discriminate in graphics by sampling location. Based on the chemical composition of the culture medium, the relative amounts of aluminum, iron, and copper were determined to be the result of background emissions from the stub (Figure 4.14, points 14 and 15), and thus these ions were not considered in the analysis as part of the sample because the medium contained only trace elements of aluminum from the artificial seawater, and iron and copper from both the seawater and the trace element solution (i.e. L₁ medium). The relative concentration of silicon and magnesium varied from location to location although presenting more magnesium than silicon, except for point 8 where they were almost identical (1:1), and points 14 and 15 (background measurements) where both silicon and magnesium were absent. These results might be indicative of a variation dependent on location interfering with the manufacturing process of the silicon-magnesium frustule in P. tricornutum (Sivakumar et al., 2012). The exopolymers excreted by a cell of P. tricornutum provide sites for the nucleation of magnesium ions and crystal growth (Tesson et al., 2008). This reaction probably comes from the interaction between magnesium and organic matter (i.e. polysaccharides and membrane proteins) on the cell surface (Tesson et al., 2009).

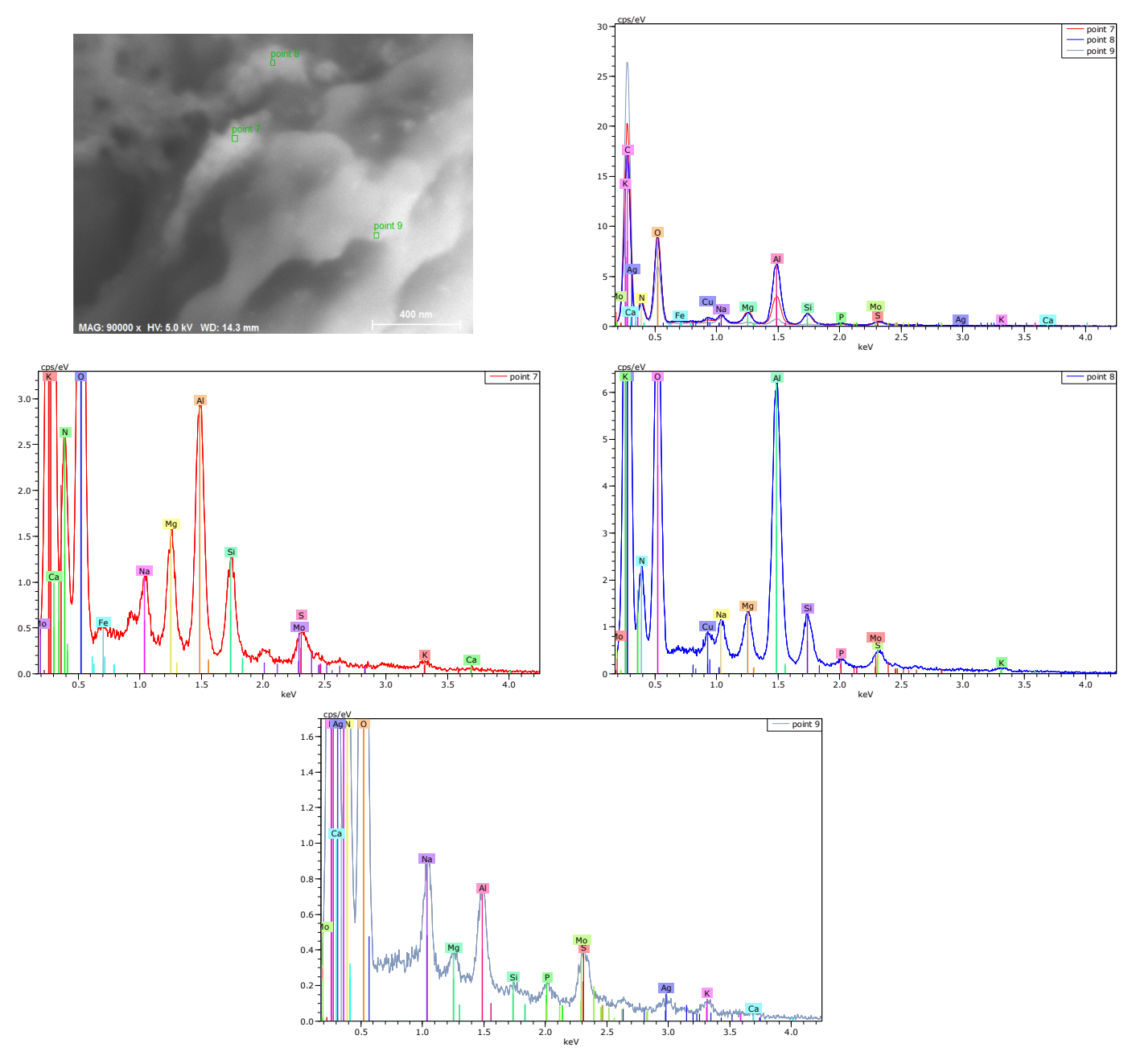


Figure 4.12. Abnormal surface growth in *P. tricornutum* under heavy metal treatment. Backscattered electron (BSE) image of surface deformation or grown bodies (SGB) produced by a typical *P. tricornutum* cell under silver stress conditions. The growth bodies were located around the surface of the middle of the frustule, near the center of the trans apical axis. High presence of Na, Mg, and Si (points 7, 8, and 9), a small concentration of Ag (point 9) can be seen. Axes correspond to kilo-electron volt (i.e. keV) for the independent axis and counts per second per electron-volt (i.e. cps/eV) for the dependent.

Nevertheless, the low silicon content is not concomitant with the previous analysis from Tesson et al. (2008, 2009) for the frustule composition of *P. tricornutum* in fusiform shape, as they reported higher ratio of silicon to magnesium. The amount of silicon and magnesium seemed to vary in the samples with a remarkable consistency. In those spots where silicon was concentrated, magnesium was present in higher concentrations which is consistent with the results found by Borowitzka and Volcani (1978), Johansen (1991), Martin-Jézéquel and Tesson (2013), who determined that the fusiform shape of *P. tricornutum* had a magnesium-heavy frustule within a polypeptide and silicon matrix which is different from the silicon-heavy frustule of the oval form. From the appearance of the structures observed in this study and from three dimensional images of similar samples in the literature (Francius et al., 2008), whether the presence of other ionic species is just due to medium precipitation or intermixing processes during shell formation with the magnesium-silicate matrix could not be well established.

Spectra taken from the material indicate that it is composed of aluminum, iron and copper and was compared to spectra of the darker amorphous silicate (Figure 4.14). The concentrations of the ions in the culture medium suggest that readings of aluminum are probably the result of the backscatter of electrons from the surface of the stub used to place the samples where the thickness of the particle or the substance is not enough to prevent noise from the background.

The SEM data indicated the presence of additional ionic species combined with the silicon and magnesium matrix, and a specific alteration of the composition of the frustule under varied growth conditions. Nonetheless, the relatively weak signal intensities for potassium, calcium, and iron (accounting for the background iron that could be present as well) indicate much lower concentrations of these elements in the samples. Vanadium overlaps with oxygen and molybdenum with sulfur, making it difficult to determine counts of these elements at comparatively low concentrations (Allan, 1995; Lefebvre & Edwards, 2009).

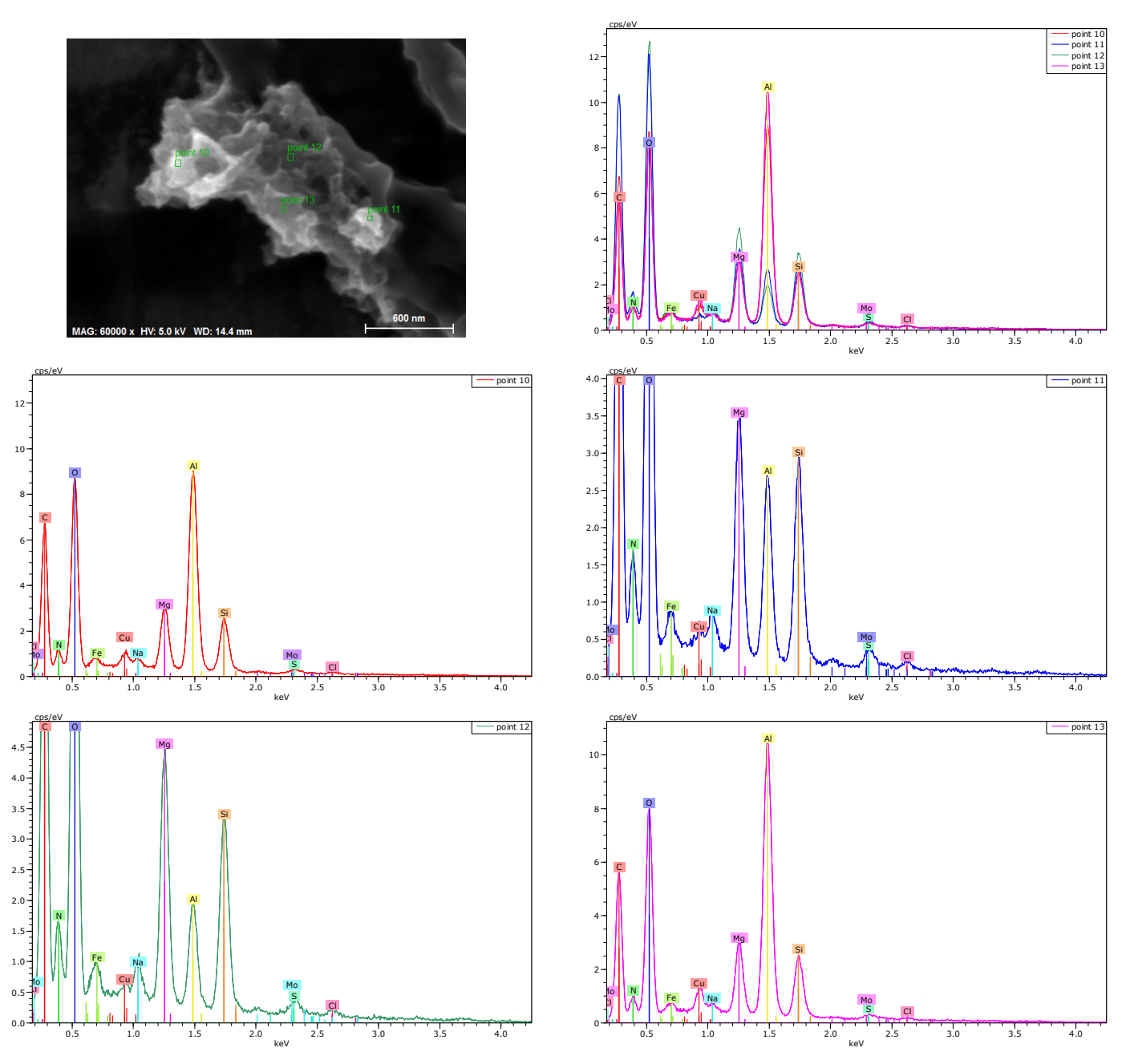


Figure 4.13. Abnormal apical formations in *P. tricornutum* under heavy metal treatments. Backscattered electron (BSE) image of the surface deformation or grown bodies (SGB) produced by a typical *P. tricornutum* cell under silver stress conditions. These growths were located around the apical end of the frustule. Axes correspond to kilo-electron volt (i.e. keV) for the independent axis and counts per second per electron-volt (i.e. cps/eV) for the dependent.

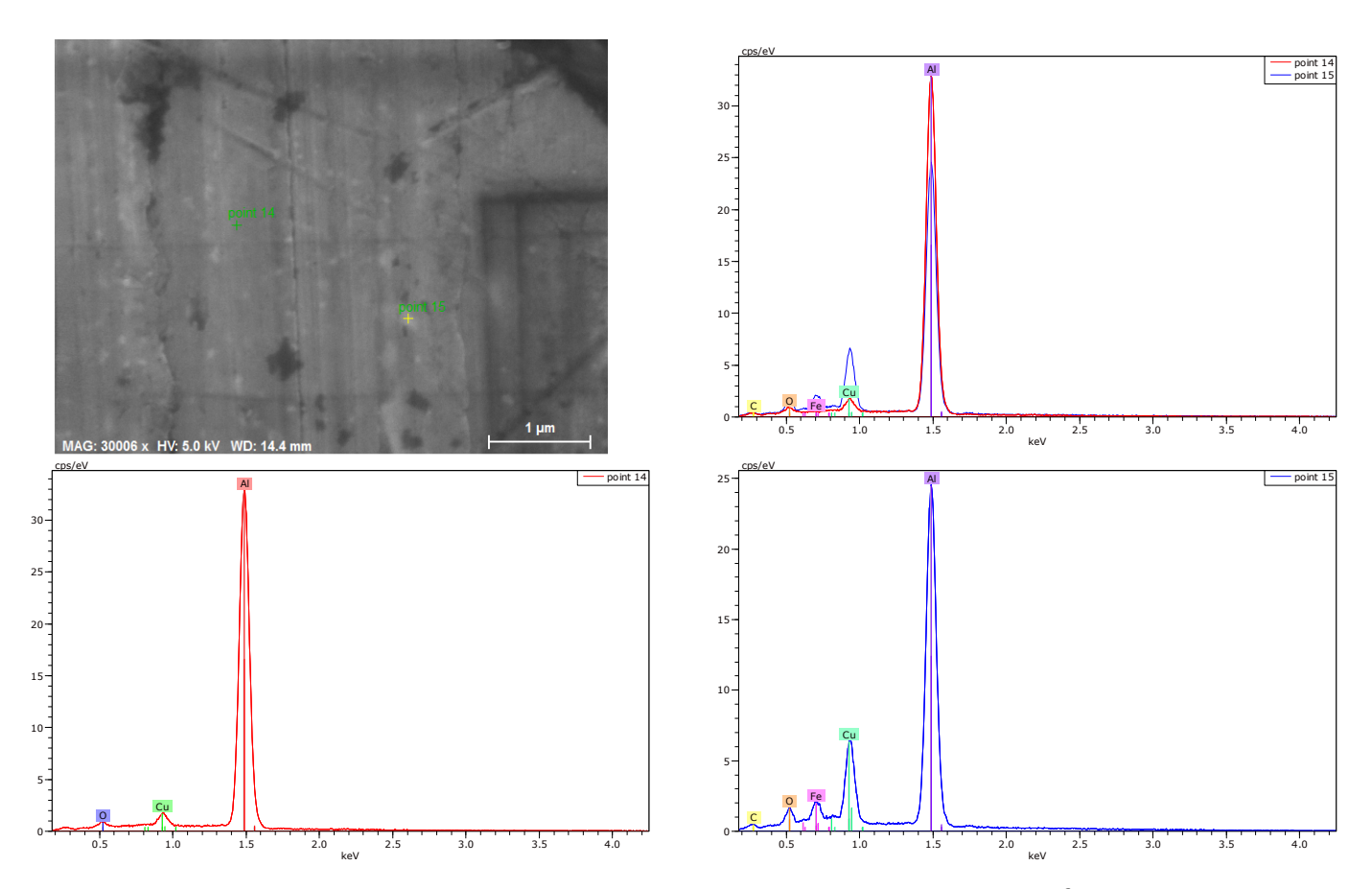


Figure 4.14. Substrate analysis and imaging. Backscattered electron of the aluminum stub substrate used for chemical analysis determination of surface composition of frustules of *P. tricornutum* grown under chemical stress. The values for carbon, oxygen, and nitrogen usually present on other samples are not considerable on this, and a strong presence of aluminum and copper, with a small presence of iron on point 15, show the general constituents of the stub. Axes correspond to kilo-electron volt (i.e. keV) for the independent axis and counts per second per electron-volt (i.e. cps/eV) for the dependent.

The heavy oxygen presence throughout the samples is consistent with the nature of the frustules of *P. tricornutum frustules* made of silicon and magnesium oxides (Borowitzka & Volcani 1978; Francius et al., 2008). The presence of sodium can be a response of the cell to availability of silicon as most silicon transfer proteins are co-factored by sodium. Small concentrations of molybdenum combined with the magnesium silicon matrix seem to be present in some of the sampled locations; however, further analysis must be carried out to confirm this result because sulfur can trigger a response in the readings. The

difference in textures on the surface (Figures 4.11, 4.12, 4.13) of these locations suggest a diverse process to keep these dopants in check.

The particle in Figure 4.13 (points 10, 12 and 13) exhibits a "spiked" texture while point 11 shows a smoother rounded process with a variety of textures. The images in Figure 4.11, 4.12 and 4.13 show mixed shapes and general frustule deformations especially irregular near the apical end of the frustules (Figure 4.13). While Figure 4.12 and 4.13 are composed almost entirely of the silicon-magnesium matrix, there were other formations that showed lower counts of silicon or magnesium. Further separation processes and more accurate EDS analysis should be performed to better differentiate the source of peaks in points (5 to 9) where low responses of overlapping elements can be found. The nitrogen/vanadium phases observed need further differentiation and an alternative method for calculation. Amorphous particles fundamentally contain magnesium-silicon aggregates and additional elemental ions. Chemical analysis of the water matrix where the medium was collected via centrifugation showed reduction of silver ions in the surrounding environment.

The elemental spectra of the bright white spots (Figure 4.10 point 4) is similar in composition to those observed frequently in the surrounding vicinity (Figure 4.9). In the case of these silver-based (Figure 4.10) sphere-like phenomena, it seems apparent that these formations were not a random chemical result of water chemistry, but the possible result of internal biochemical action by the machinery of organism, because no heavy redox species (e.g. hydroquinone, citrate), stabilization polymers (e.g. polyvinylpyrrolidone - PVP), or any other chemicals that could be responsible for the formation of AgNPs were present in the medium by preparation. To date, several studies have tried to determine the actual mechanisms of biogenic silver nanoparticle production (Naik et al., 2002; Durán et al., 2005; Durán et al., 2009; Rai et al., 2009) but the actual mechanisms behind these phenomena are still not fully understood. It was established that alkalinity in the environment did not increase the potential for precipitation of silver salts as chloride, as values were not high enough to reduce solubility. Some researchers have found that peptides of amino acid (e.g. arginine, cysteine, lysine, methionine, and tyrosine) functional groups mediated reduction at high pH (i.e. 9~10) via NADH electronic

transfer (Selvakannan et al., 2004; Ray et al., 2010) and some have found that diatom silicon deposition vacuoles reduce pH to acidic levels (i.e. 5) increasing the solubility and availability of ions inside the cytoplasms (Vrieling et al., 1999b).

From the literature, the presence of silver can produce membrane alterations increasing porosity and disrupting the transport of ions into the cytoplasm (Castro-Bugallo et al., 2014). Ionic silver produces oxygen species (ROS) when it interacts with organisms and in the presence of other factors, e.g. UV radiation (Miao et al., 2010). To protect themselves from heavy metal pollution (e.g. silver, zinc, cadmium, gold, lead) diatoms species initially produce higher amounts of polysaccharides, and phytochelatins, intracellularly and later the surface of the cell as the concentration of the heavy metal increases and surpasses the threshold of the algae becoming toxic intracellularly (Torres et al., 1998; Schmitta et al., 2001; Lebeau & Robert, 2003).

Different mechanisms for defense from these cytotoxic characteristics of metal ions have been proposed (Grill et al., 1985; Grill et al., 1989; Cobbett & Goldsborough, 2002; Perales-Vela et al., 2006). Some algae can produce vacuole-partitioned organometallic complexes of heavy metal binding peptides. These peptides, known as metallothioneins, are grouped in two categories: short chain polypeptides (i.e. phytochelatins) and geneencoded proteins. From the information provided by the results, it is possible that molecules from the first category (i.e. class III metallothioneins or phytochelatins), found in certain fungi, algae, and higher plants, (Grill et al., 1985; Gaur & Rai, 2001; Cobbett & Goldsborough, 2002) are responsible for the defense of P. tricornutum against heavy metal stressors. Grill et al., (1989) found that the γ -glutamylcysteine dipeptidyl transpeptidase (E.C. 2.3.2.15; Vatamaniuk et al., 2004) named phytochelatin synthase (PCS) was the enzyme responsible for producing MtIII. It is known that genes responsible for the synthesis of phytochelatin synthase (i.e. transcript IDs: 9478 - Chr_1, 48175 -Chr_16, and 50006 Chr_26) can be found in P. tricornutum as reported in the genome portal of the Department of Energy Joint Genome Institute (JGI) database (Grigoriev et al., 2012; Nordberg et al., 2014). Similarly, Grill et al. (1987) proved that several metal salts (e.g. Cd⁺², Pb⁺², Zn⁺², Cu⁺²) as well as some metalloids (e.g. As and Se) can enhance the synthesis of MtIII, while other oxidative stressors or other type of stressors (e.g. heat,

cold, UV radiation, hormonal activity, anoxia) do not trigger MtIII synthesis (Steffens, 1990). This suggests that heavy metal defenses in P. tricornutum can be driven by concentrations and the presence of glutathione, which is heavy metal dependent (Loeffler et al., 1989; Vatamaniuk et al., 2004), might prove that MtIII are responsible for the mechanisms, as glutathione is regulated by the synthesis of γ -glutamylcysteine synthetase and glutathione synthetase (Zhu et al., 1999; Xiang et al., 2001). Therefore, glutathione can be considered the primary peptide responsible for binding heavy metals (Howe & Merchant, 1992; Vatamaniuk et al., 2004) and the synthesis of MtIII in unicellular organisms (Grill et al., 1989). Similarly, the JGI has genes reported to be involved in the glutathione metabolic process coding the protein identified as 35819 (Chr_8). Torres et al. (1998) argued that the action of long-chain class III metallothioneins in the formation of PC-coated crystallites was one of the defense mechanisms of P. tricornutum in the presence of high concentrations of cadmium, which leads to believe that it is the same in the case of silver.

The elemental spectra of the bright white spots (Figure 4.10 – point 4) and the absence of chlorine suggested that they result mostly from the interaction of the cells with the ionic concentration of silver. This explanation was considered as the only alternative because the concentration of the redox agents capable to reduce the energy level of silver to Ag⁰ in the culture, and the possibility of precipitation of silver cations by association with chlorine ions in the medium (i.e. AgCl) as the latter was not reflected in the counts from the EDS analysis; hence it does not suggest otherwise. This leads to understanding that the extracellular bodies were produced by a secretion processes of the cell, as there are no recorded temperature or pressure shifts that might account for the reactions that had to have occurred to isolate the ions into clusters by mere energy input from physical factors, i.e. evaporation of silver and condensation or light ablation (Iravani et al., 2014). These results are simultaneous with reported silver nanoparticle production by *P. tricornutum* by Wishkerman (2016) as presented in poster during the 24th International Diatom Symposium (Quebec City, 2016, Canada).

Available silver cations in water solution might precipitate in the presence of chlorine ions or other anionic species in the surrounding medium, however, the analysis of the particles

did not suggest or account for chlorine species and it is safe to assume that these are not made of silver chloride. Similarly, the counts as consequence of nitrogen presence in the sample are low to be a precipitate of silver nitrate; moreover, as silver nitrate is soluble in water and confirm that these formations are not made of silver nitrate or any other silver salt. The lack of additional analysis of the cell response and chemical composition and characteristics of the particles makes it difficult to determine the responsible mechanisms for their production. It has been suggested for similar oxidative stress that glutathione and associated phytochelatins (PCs, glutathione-related peptides) are highly related in concentration to the level of response of the organism (*P. tricornutum*) to highly oxidative species present in the medium (Morelli et al., 2015; Wang et al., 2016).

To date, and to the understanding of this author, there are no reported works that deal with the production of silver nanoparticles using normal cultures of P. tricornutum as biogenic trigger for the process. Even though there was a group in Israel that reported the use of P. tricornutum to produce silver nanoparticles (Wishkerman & Arad, 2017), other than the fact that they mention the species, there was no evidence that suggested that either the method or the algae species was the same. The production of nanoparticles, even as it seems plausible from the concentrations used in the article cannot confirm the presence of silver in the structures shown because, unlike this experiment, the use of any elemental tracing mechanism is not suggested by the presenters. Furthermore, communication with the lead author was not possible. Upon observation of the SEM images (provided from the poster in an appendix at the end of this document) the species does not seem to be the same, as none of the morphotypes of *P. tricornutum* shares the same characteristics as the ones showed on the images from the poster both shape and size are not in agreement with those reported for *P. tricornutum* in the previous literature (See section 2.1.5 of this document). This research is believed to be the first of its kind dealing with silver remediation and nanoparticle production via biogenic manufacture using P. tricornutum.

4.3 Life cycle assessment

The absence of a clear baseline study for environmental impact assessments usually misrepresents the actual cost of design and operation of any algal biomass production

facility. Presumably, proper management and accounting of carbon dioxide, nutrients, and water can reduce the cost of production by over 50% (Barlow et al., 2016); however, this kind of approach could limit the number of possible production sites (Kern et al., 2017). To date, traditional infrastructure required for algae production has a high land requirement but not as high as that of traditional land crops (Clarens at al., 2010).

A detailed fluid dynamics analysis could aid and provide enough information to determine how much energy is invested in mixing and culture homogenation, once the system is established. The absence of this analysis limited the accuracy of this document, although an approximation was taken, and additional uncertainty steps were calculated to account for the differences (Sills et al., 2013). One additional restriction and limitation of an LCA is the lack of standardized boundaries and functional units for the reviewed data found, as well as the different assumptions coming from individual criteria and individual analysis. These constraints come into play when comparing different LCA findings, and therefore, it is necessary to standardize and normalize units and processes to develop a consistent system boundary to encompass the cultivation, harvesting, and extraction of products (e.g., nanoparticles, oil, pigments).

Once the underlying biochemical pathways used by enzymatic transformation of elemental compounds into the structures that are of interest, is fully understood, it might be possible to enlist the reproductive capabilities of diatoms to generate considerable amounts (i.e. 10^{12} - 10^{14} cells m⁻³) of said structures in a matter of weeks, and even days depending on the species (Castro et al., 2013; Aziz et al., 2015; Sinha et al., 2015). Some species replicate up to eight times a day, and the attraction lies in their capacity to create complex structures on a small scale which could serve as the foundation of a powerful technology to the industrial evolution of new materials (Schröfel et al., 2011). To derive further, it is necessary to study the molecular mechanisms that underlie shell formation and those associated with heavy metal management within the cell, but that is not the scope of this research.

4.3.1 Comparison of characterized results between both production methods

Normalized results for each impact category are compared for both processes and presented in Table 4.2 and 4.3 as well as the visual characterization in Figures 4.15 and 4.16. Figure 4.15 and Table 4.3 shows the relative results for all the categories for the TRACI 2.1 analysis, including in clusters the environmental, human health, and resource related categories of the analysis. In each method, results for each category are presented in relative normalized values from 0 to 100 being 100 the equivalent to the maximum between both results. Figure 4.16, in junction with Table 4.3, show the endpoint categories for the ReCiPe 1.11 method (egalitarian perspective), again grouping in environmental, human health, and resource related categories of the analysis. The graphs in Figures 4.17 and 4.18 along with Table 4.3, show the results of these same categories and analysis method from a hierarchist and individualist perspective. Except for land use, the biogenic alternative performs better in all the impact categories. Specific factors within categories can be found in the graphics of the Appendix IV.

Table 4.2. Impact values from the TRACI 2.1 LCIA method. Analysis for a hydroquinone-based (HQ-Industrial) and an algae-based (PT-Biogenic) production of silver nanoparticles (AgNP).

Impact category [Units]	Calculated va	lues PT-Biogenic	Percentage comparison HQ-Industrial PT-Biogenic		
Acidification [kg SO ₂ eq.] Ecotoxicity [CTUe]	14.78 624,311.00	1.90 3,485.92	100.00 % 100.00 %	12.89 % 0.56%	
Eutrophication [kg N eq.]	149.73	3.03	100.00 %	2.03 %	
Global Warming [kg CO ₂ eq.] Human Health – carcinogenics [CTUh]	821,120.00 7.72 x 10 ⁻⁰³	385.81 1.98 x 10 ⁻⁰⁴	100.00 % 100.00 %	0.05 % 2.56 %	
Human Health - non-carcinogenics [CTUh]	3.29 x 10 ⁻⁰²	8.42 x 10 ⁻⁰⁵	100.00 %	0.26 %	
Ozone Depletion [kg CFC-11 eq.]	6.61 x 10 ⁻⁰⁴	3.58 x 10 ⁻⁰⁵	100.00 %	5.42 %	
Photochemical ozone formation [kg O_3 eq.]	222.01	18.84	100.00 %	8.48 %	
Resource depletion - fossil fuels [MJ surplus]	1,687.74	792.89	100.00 %	46.98 %	
Respiratory effects [kg PM2.5 eq.]	3.66	0.19	100.00 %	5.13 %	

4.3.2 Ecosystem categories

In total, the ecosystem impact potential from the algal alternative only accounts for 0.11% in the endpoint egalitarian and individualist perspectives of the ReCiPe LCIA and 0.12%

in the hierarchist perspective of that from the hydroquinone manufacture (E = 1.57×10^{-2} ; H = 5.52×10^{-3} ; I = 6.52×10^{-3} species yr.). The highest contribution from the hydroquinone process comes from the production of carbon dioxide from fossil origins (97.61%) followed by the production of chemicals and pollution from mining processes. The biogenic alternative had a total ecosystem impact potential divided among the production of the culture media (83.96%), the production of the LED bulbs used for illumination purposes (13.63%), and a small percentage (2.41%) from the maintenance and operation of the culture (Clarens et al., 2010; Brentner et al., 2011).

Table 4.3. Normalized midpoint results and ratio of difference. Values from the ReCiPe 1.11 LCIA method analysis for a hydroquinone-based (HQ-Industrial) and an algae-based (PT-Biogenic) production of silver nanoparticles (AgNP), taking each perspective into consideration. (E – egalitarian, H – hierarchist, I – Individualist).

Impact category [Unit]	HQ-Industrial	PT-	Difference	HQ-	PT-
ReCiPe Midpoint (E) 2000 [person/year]		Biogenic		Industrial	Biogenic
Agricultural land occupation [m ² ·a]	46.41	126.97	80.56	36.55 %	100.00 %
Climate Change [kg CO ₂ eg.]	820.888.00	320.94	820,567.06	100.00 %	0.04 %
Fossil depletion [kg oil eq.]	344.57	156.53	188.04	100.00 %	45.43 %
Freshwater ecotoxicity [kg 1,4-DB eq.]	678.54	5.49	673.05	100.00 %	0.81 %
Freshwater eutrophication [kg P eq.]	20.11	0.21	19.90	100.00 %	1.05 %
Human toxicity [kg 1,4-DB eq.]	1778,810.00	5927.70	1772,882.30	100.00 %	0.33 %
Ionizing radiation [kg U ²³⁵ eq.]	4,583.85	67.59	4516.26	100.00 %	1.47 %
Marine ecotoxicity [kg 1,4-DB eq.]	854,838.00	5263.59	849,574.41	100.00 %	0.62 %
Marine eutrophication [kg N eg.]	4.16	0.75	3.41	100.00 %	18.07 %
Metal depletion [kg Fe eq.]	4,856.82	142.45	4,714.37	100.00 %	2.93 %
Natural land transformation [m ²]	1.19	1.55	0.36	76.85 %	100.00 %
Ozone depletion [kg CFC-11 eq.]	5.98 x 10 ⁻⁴	2.97 x 10 ⁻⁵	5.68 x 10 ⁻⁴	100.00 %	4.97 %
Particulate matter formation [kg PM ₁₀ eq.]	7.27	0.59	6.68	100.00 %	8.07 %
Photochemical oxidant formation [kg	11.31	0.92	10.39	100.00 %	8.10 %
NMVOC]					
Terrestrial acidification [kg SO ₂ eq.]	14.96	2.00	12.96	100.00 %	13.35 %
Terrestrial ecotoxicity [kg 1,4-DB eq.]	72.23	0.52	71.71	100.00 %	0.72 %
Urban land occupation [m ² ·a]	68.42	17.66	50.77	100.00 %	25.80 %
Water depletion [m³]	40,682.80	6424.60	34,258.20	100.00 %	15.79 %
ReCiPe Midpoint (H) 2000 [person/year]					
Agricultural land occupation [m ² ·a]	46.41	126.97	80.56	36.55 %	100.00 %
Climate Change [kg CO ₂ eq.]	820,979.00	373.06	820,605.94	100.00 %	0.05 %
Fossil depletion [kg oil eq.]	344.57	156.53	188.04	100.00 %	45.43 %
Freshwater ecotoxicity [kg 1,4-DB eq.]	677.28	5.44	671.84	100.00 %	0.80 %
Freshwater eutrophication [kg P eq.]	20.11	0.21	19.90	100.00 %	1.05 %
Human toxicity [kg 1,4-DB eq.]	60,328.80	145.41	60,183.39	100.00 %	0.24 %
lonizing radiation [kg U ²³⁵ eq.]	4,583.85	67.59	4,516.26	100.00 %	1.47 %
Marine ecotoxicity [kg 1,4-DB eq.]	643.62	5.00	638.61	100.00 %	0.78 %
Marine eutrophication [kg N eq.]	4.16	0.75	3.41	100.00 %	18.07 %
Metal depletion [kg Fe eq.]	4,856.82	142.45	4,714.37	100.00 %	2.93 %
Natural land transformation [m ²]	1.19	1.55	0.36	76.85 %	100.00 %
Ozone depletion [kg CFC-11 eq.]	5.98 x 10 ⁻⁴	2.97 x 10 ⁻⁵	5.68 x 10 ⁻⁴	100.00 %	4.97 %

Impact category [Unit]	HQ-Industrial	PT-	Difference	HQ-	PT-
		Biogenic		Industrial	Biogenic
Particulate matter formation [kg PM ₁₀ eq.]	7.27	0.59	6.68	100.00 %	8.07 %
Photochemical oxidant formation [kg NMVOC]	11.31	0.92	10.39	100.00 %	8.10 %
Terrestrial acidification [kg SO ₂ eq.]	13.51	1.84	11.67	100.00 %	13.60 %
Terrestrial ecotoxicity [kg 1,4-DB eq.]	6.47	0.23	6.24	100.00 %	3.54 %
Urban land occupation [m²·a]	68.42	17.66	50.77	100.00 %	25.80 %
Water depletion [m³]	40,682.80	6,424.60	34,258.20	100.00 %	15.79 %
ReCiPe Midpoint (I) 2000 [person/year]					
Agricultural land occupation [m ² ·a]	46.41	126.97	80.56	36.55 %	100.00 %
Climate Change [kg CO ₂ eq.]	821,138.00	399.01	820,738.99	100.00 %	0.05 %
Fossil depletion [kg oil eq.]	344.57	156.53	188.04	100.00 %	45.43 %
Freshwater ecotoxicity [kg 1,4-DB eq.]	677.24	5.23	672.01	100.00 %	0.77 %
Freshwater eutrophication [kg P eq.]	20.11	0.21	19.90	100.00 %	1.05 %
Human toxicity [kg 1,4-DB eq.]	25,673.20	12.22	25,660.98	100.00 %	0.05 %
Ionizing radiation [kg U ²³⁵ eq.]	4,494.28	46.40	4,447.88	100.00 %	1.03 %
Marine ecotoxicity [kg 1,4-DB eq.]	344.90	3.26	341.63	100.00 %	0.95 %
Marine eutrophication [kg N eq.]	4.16	0.75	3.41	100.00 %	18.07 %
Metal depletion [kg Fe eq.]	4,856.82	142.45	4,714.37	100.00 %	2.93 %
Natural land transformation [m ²]	1.19	1.55	0.36	76.85 %	100.00 %
Ozone depletion [kg CFC-11 eq.]	5.98 x 10 ⁻⁴	2.97 x 10 ⁻⁵	5.68 x 10 ⁻⁴	100.00 %	4.97 %
Particulate matter formation [kg PM ₁₀ eq.]	7.27	0.59	6.68	100.00 %	8.07 %
Photochemical oxidant formation [kg		0.92	10.39	100.00 %	8.10 %
NMVOC]		0.72			01.0
Terrestrial acidification [kg SO ₂ eq.]	12.78	1.73	11.04	100.00 %	13.58 %
Terrestrial ecotoxicity [kg 1,4-DB eq.]	6.43	0.04	6.39	100.00 %	0.60 %
Urban land occupation [m ² ·a]	68.42	17.66	50.77	100.00 %	25.80 %
Water depletion [m ³]	40,682.80	6,424.60	34,258.20	100.00 %	15.79 %
	. 5,5525	0,120	0 .,000	100.00 10	1017 2 10
isotory Effects 5.13%					
Doenllatory					
Resource Depletion – Fossil Fuel		46.98%			
Photochemical Ozone Formation 8.48%					
Photochemical Ozone Formas 8.48%					
Ozone Depletion 5.42%					
inggenics					
Human Health – non-carcinogenics 0.26%					
Human 118 - carcinogenics 2.56%					
Human Health 9					
Global Warming 0.05%					
Eutrophication 2.03%					
Ecotoxicity 0.56%					
and the second s					
ar - ation	0/				
Acidification 12.89		್ಗು enic = HQ-Indu	60 10	<i>Oo O</i>	700

Figure 4.15. TRACI 2.1 impact categories. Graphic comparison of the relative TRACI 2.1 impact categories of the production of silver nanoparticles (AgNP) via a biogenic alternative using *P. tricornutum* (orange) and a traditional redox reaction using hydroquinone (HQ) as reduction agent (blue).

In the other perspective analysis from the ReCiPe 1.11 method (i.e. hierarchist and individualist), the performance of the biogenic method failed behind that of the hydroguinone redox in aspects of transformation of natural land. In this category, the hydroquinone method outperformed the algal based method (H = 3.15×10^{-6} ; I = 4.31×10^{-6}) 10-7 species·yr) with an impact potential of 84.38% for the hierarchist and 83.90% on the individualist perspective of that total for the biogenic process (H = 3.15×10^{-6} ; I = 2.69×10^{-6}) 10⁻⁶ species·yr). The highest percentage of natural land transformation comes from the manufacture of chemicals (89.24%) and the production of the LED bulbs (7.30%) with a 3.40% because of the culture itself (location and water vessels) and a small percentage for the maintenance and operation activities of the culture (Clarens et al., 2010). In the case of the urban land occupation, the hydroquinone method accounted for a higher potential (E and H = 1.42×10^{-6} ; I = 1.20×10^{-6} species·yr) than that of algae (E, H, I 25.80%). The highest percentage of urban land occupation for the algal method was associated with the production of chemicals and the actual culture of the algae (97.92%) and the manufacture of the LED bulbs (2.08%) used for the illumination system, while for the hydroquinone method it was due to the mining and storage of silver (99.13%).

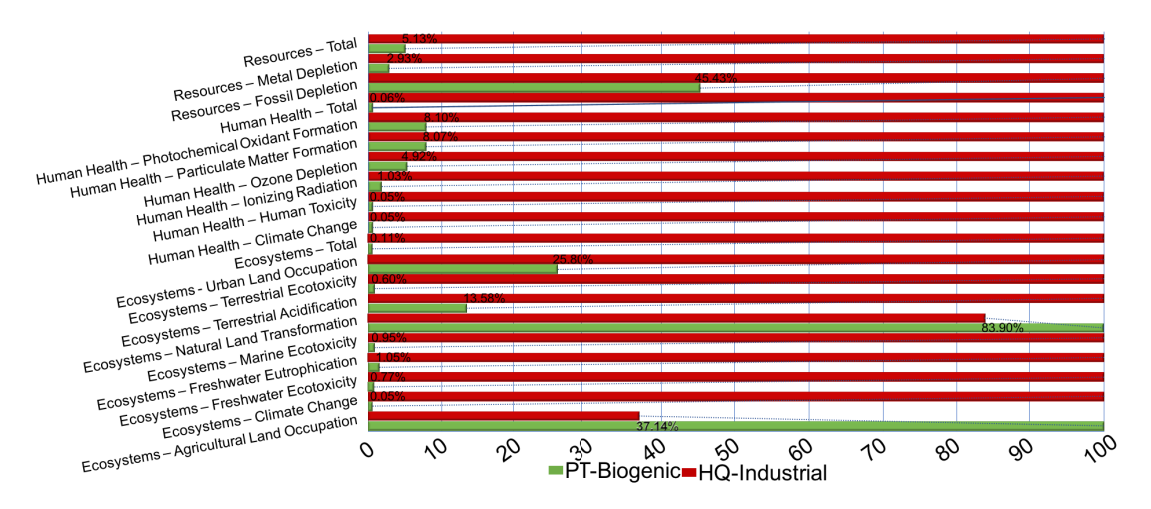


Figure 4.16. ReCiPe 1.11 egalitarian relative endpoint comparison. The figure shows the relative values comparing the environmental impact results of the relative endpoint egalitarian perspective analysis (E) ReCiPe 1.11 impact categories of the production of silver nanoparticles (AgNP) via a biogenic alternative using *P. tricornutum* (orange) and a traditional redox reaction using hydroquinone (HQ) as redox agent (blue).

4.3.3 Climate change

The analysis from the application of the ReCiPe 1.11 methodology showed that the climate change impact potential for the biogenic method is considerably less (E = 0.04%; H and I = 0.05%) than that of the traditional redox counterpart (E = 1.54×10^{-2} ; H and I = 6.51×10^{-3} species·yr). It was expected and a fair assumption, as it is necessary to consume close to 2 times the mass of dry biomass in CO_2 to produce algae. The amount of culture required to produce 1 kg of AgNP (7,426.2 kg of algae biomass) accounts for the high reduction in GHG from CO_2 . Additionally, the biomass generated was considered as captured carbon in biogenic form, so there was no release to the environment up to the process boundary. Additional consideration to the biomass transformation processes can be useful to determine how the global warming potential can change once other algae by products are considered (Stephenson et al., 2010).

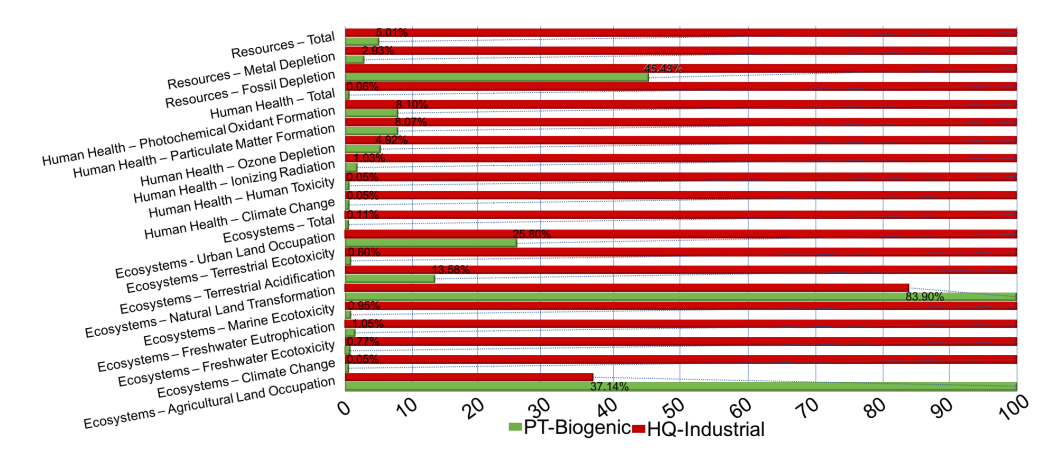


Figure 4.17. ReCiPe 1.11 hierarchist relative endpoint comparison. The figure shows the relative values comparing the environmental impact results of the relative endpoint hierarchist perspective analysis (H) ReCiPe 1.11 impact categories of the production of silver nanoparticles (AgNP) via a biogenic alternative using *P. tricornutum* (orange) and a traditional redox reaction using hydroquinone (HQ) as reduction agent (blue).

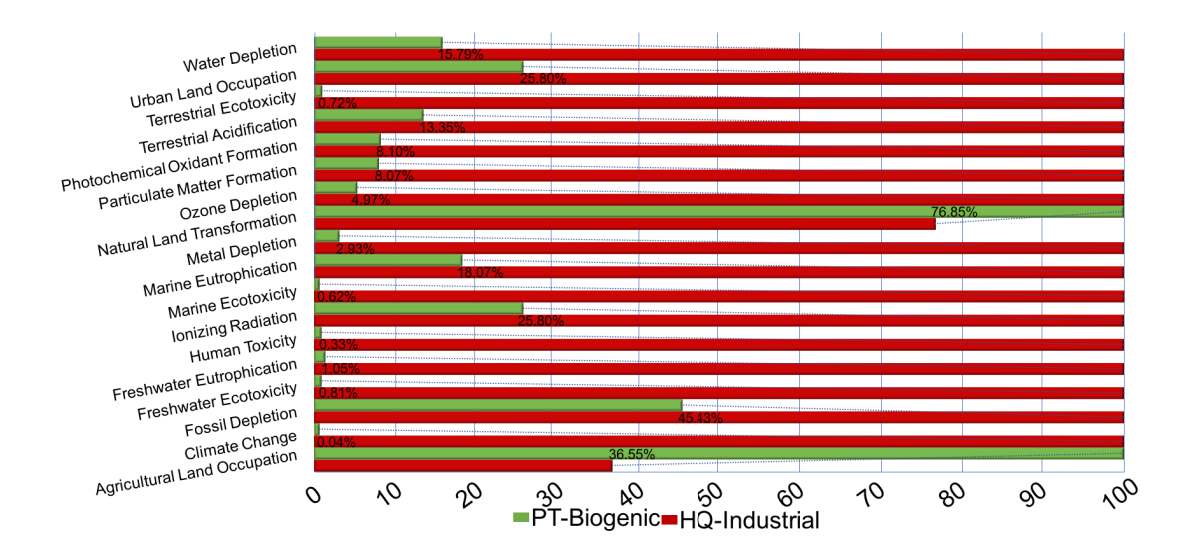


Figure 4.18. ReCiPe 1.11 individualist relative endpoint comparison. The figure shows the relative values comparing the environmental impact results of the relative endpoint individualist perspective analysis (I) ReCiPe 1.11 impact categories of the production of silver nanoparticles (AgNP) via a biogenic alternative using *P. tricornutum* (orange) and a traditional redox reaction using hydroquinone (HQ) as reduction agent (blue).

In general terms, and taking the results of the midpoint analysis from the ReCiPe 1.11 methodology, for each kilogram of AgNP produced, algae will produce roughly 0.05% of the global warming impact on the ecosystem compared to the industrial hydroquinone-based method (E = 820,888; H = 820,979; I = 821,138 kg CO_2 eq.). In the case of the redox process, almost 100% of the GHG equivalents were generated during the production of nanosilver, probably associated with the emission of gases on a low population density area (Gnansounou & Raman, 2016; Mu et al., 2017). Even though small, the contribution of the production of the algae and the culture medium (50.67%) and the manufacture of the LED bulbs used to compensate darkness periods in the system, accounted for 74.06% of the total impact potential, and the remaining 25.94% was divided among the operative energy costs of the maintenance and care of the culture (Brentner et al., 2011).

4.3.4 Ecotoxicity

The biogenic process performed better on the tests for freshwater and marine water ecotoxicity; using the endpoint analysis and an egalitarian perspective, it accounted for 0.80% of the total potential from the redox process (5.82 x 10⁻⁷ species·yr), mostly spread

about the manufacture of sodium nitrate and phosphate salts (58.72%) and the manufacture of the LED bulbs (22.46%), while the remaining chemicals needed for the culture media and other maintenance activities within the culture accounted for the remaining 18.82%. Similarly, from the hierarchist and individualist perspectives, the biogenic method accounted for less than 0.80% of that potential from the hydroquinone method (H = 5.82×10^{-7} ; I = 5.83×10^{-7} species·yr).

Accounting for the redox production, the mining and refining of the silver used to produce the nanoparticles accounted for 93.22% of the total contribution of the process. Here it is important to clarify that most ionic species that can account for the potential of water ecotoxicity are used by the algae in their regular growth processes, and thus accumulated within the biomass. Even though almost all the impacts caused by the production of the redox AgNP comparably lower as net input to those of the algae counterpart, the later does compensate with the assimilation of most of them during the life-cycle of a cell, and thus reduce the output in the long run. The massive quantity of algal biomass required to produce the same amount of AgNP, did in fact indirectly act as a remediation alternative (Lardon et al., 2009; Campbell et al., 2011; Mu et al., 2017). The analysis at midpoint from the three perspectives showed similar results for freshwater ecotoxicology potentials with 0.81%, 0.80%, and 0.77% of the hydroquinone method for the egalitarian (678.54 kg 1,4 DB eq.), hierarchist (677.28 kg 1,4 DB eq.), and individualist (677.24 kg 1,4 DB eq.) perspectives, respectively.

The case of marine water ecotoxicity fared slightly better, as the algae-based process only accounted for 0.62% of the potential impacts from the redox hydroquinone-based manufacture (E = $1.51 \times 10^{-4} \text{ kg}$ 1,4 DB eq.; H = $1.13 \times 10^{-7} \text{ kg}$ 1,4 DB eq.; I = $6.08 \times 10^{-8} \text{ kg}$ 1,4 DB eq.). Similarly, the concentration of ionic species used by the algae reduced the overall potential and as in the case of the freshwater ecotoxicity analysis, the production of the mined silver accounts for a high percentage of the total potential for impacts (87.70%). The remaining 12.30% was accounted for by the actual AgNP production and the use of reagents and energy, as well as the concentration stages.

The alternative biogenic production performed better on the terrestrial ecotoxicity (E = 0.72%; H = 3.54%; I = 0.60%, of the potential from the hydroquinone process E = 1.09×10^{-1}

 5 ; H = 9.75 x 10^{-7} ; I = 9.69 x 10^{-7} species·yr). More dispersed contributions come from the production of nitrates and other culture media ingredients (83.99%) and the remaining divided among other maintenance activities (1.86%) and the production of the LED bulbs used for dark-cycle illumination (14.15%). The core potential for terrestrial ecotoxicity comes from mercury produced as a by-product of the mining process (63.65%), and silver dispersed in air accounting for 17.20%. The remaining 80.85% comes from other ionic species associated with mining activities. The percentage values for algae from the midpoint analysis for each perspective were the same and the hydroquinone contributions were 72.23; 6.47; and 6.43 kg 1,4 DB eq. for the egalitarian, hierarchist, and individualist perspectives respectively.

4.3.5 Freshwater eutrophication

Only 1.05% of the total freshwater eutrophication potential (endpoint egalitarian analysis) of the hydroquinone production method (E, H, and I = 8.96×10^{-7} species·yr = 20.11 kg P eq.) was accounted for the biogenic alternative. Again, the bulk of the production of species with eutrophication potential came from the mining of the silver in the case of the hydroquinone redox method (94.10%) with the highest percentage contribution coming from phosphates in water and ground water.

In contrast, the biogenic alternative had the highest contribution to its eutrophication potential coming from the production of the LED bulbs (33.02%) and third of the total percentage was due to maintenance and operations, with the maximum contribution from the ultra-purification of water for the initial separation of the inoculum (30.29%). The remaining percentage (36.20%) was produced by the processes involved in the manufacture of the chemicals used for the culture media.

4.3.6 Acidification potential

Similarly, the acidification potential generated by the biogenic alternative would only generate 13.35%, 13.60%, and 13.58% from the egalitarian, hierarchist, and individualist perspectives, respectively, versus total acidification potential produced by the chemical redox method (E = 2.13×10^{-7} ; H = 7.84×10^{-8} ; I = 1.94×10^{-8} species·yr or 14.96, 13.51, and 12.78 kg SO₂ eq. for the midpoint analysis respectively). It is necessary to determine

the actual value when the biomass is transformed to other high-end products. The concentration of SO_2 and NO_x emissions are mitigated by the consumption of these species by the biomass of the algae, and thus it is bio-accumulated in the resulting paste (Falkowski & Raven, 2007).

The core of the emissions come from the mining of silver at the regional state which accounts for 57.49% of the total contribution and the process of production of the nano powder (26.96%) most probably associated with the silver nitrate used as precursor of the reaction. The remaining percentage is introduced by the manufacture and storage of silver (15%). For this analysis, cut off was defined at 2%. The acidification species released by the redox process was determined equivalent to 52.92% of sulfur dioxide, 42.18% of nitrogen oxides, and 4.78% of ammonia.

4.3.7 Resource depletion categories

The total resource depletion potential for the biogenic AgNP alternative production accounted for only 8.93% from the egalitarian and hierarchist and 5.01% from the individualist perspectives of the total potential of the hydroquinone process (\$404.28 and \$365.08, respectively). The greatest differences were seen in metal depletion, which showed a 2.93% of the biogenic process compared to the hydroquinone process (\$347.26) from all three perspectives. The differences between the fossil fuel were less considerable and the algal process accounted for 45.43% of the total from the hydroquinone process (\$57.01 from the egalitarian and hierarchist, and \$17.82 for the individualist perspectives). From the midpoint analysis, the potential from the hydroquinone accounted for 344.57 kg oil eq. for the fossil depletion and 4,856.82 kg Fe eq. for the metal depletion, while the algal alternative had a potential of 45.43% and of 2.93 of the first and the second potential impacts, respectively.

4.3.8 Human health categories

The ReCiPe 1.11 method for impact potential determination considers the potential for climate change in both the ecosystem and the human health group of categories. In the later, the index is based on the DALY unit, as defined before in this document (DALY = YLD+YLL). In this category, the algal alternative production method outperformed the

hydroquinone as the former only produces 0.04% from the egalitarian and 0.05% from the hierarchist and individualist perspectives, of the overall potential for human health climate change from the later (E = 2.88; H = 1.15; I = 0.977 DALY). The highest contribution to this potential impact came from the carbon dioxide production from the manufacture of the AgNP, whereas the algal counterpart owes its contributions to the manufacture of chemicals (75.95%) and the assembly of the LED bulbs used for the illumination (23.39%).

In the case of human toxicity (HTP), analysis of impact performed with the ReCiPe 1.11 modelling system showed a considerable percentage difference between the algal-based alternative manufacturing process and the hydroquinone-based methodology, with the former producing only 0.33%, 0.24, and 0.05 from the egalitarian, hierarchist, and individualist perspectives respectively, of the total impact produced by the later (E = 1.25; H = 4.22×10^{-2} ; I = 1.80×10^{-2} DALY or 1,778,810.00; 60,328.80; and 25,673.20 kg 1,4 DB eq., respectively). The major contributors from the algal manufacturing process coming from the LED production (37.33%) process and the chemical manufacture (61.24%).

Similarly, the percentage of ionizing radiation (IRP) from the algal manufacture only accounts for 1.47% for the egalitarian and hierarchist perspective, and 1.03% for the individualist, of the potential from the hydroquinone manufacture (E, H = 7.50×10^{-5} ; I = 7.25×10^{-5} DALY or 4,583.85; and 4,494.28 kg U²³⁵ eq. respectively). Again, the main parameter influencing the impacts on the category for the former came from the production of the LED bulbs used in the illumination system (69.19%) and the chemical manufacture (29.44%). The hydroquinone production process itself accounted for 95.41% of the total ionizing potential in the alternative method.

The ozone depletion potential (ODP) percentage, measured to determine relative destruction of a compound on the ozone layer, accounted by the algal process was only 4.98% (E and H), and 4.92 (I), compared to that of the hydroquinone counterpart (E and H = 1.59×10^{-6} and I = 3.87×10^{-7} DALY) and 4.97% of the potential of the hydroquinone method (5.98×10^{-4} kg CFC-11 eq.). The results were the same for the three perspectives in the midpoint analysis. In this case, the highest weight of impact for the algae production came from the manufacture of chemicals (80.90%) and then the LED manufacture (16.91%).

Similarly, the particulate matter formation potential (PMFP) from the biogenic AgNP was only 8.07% of that of the HQ-AgNP (1.89×10^{-3} DALY). The first process owed the core of its potential impact on the manufacturing of chemicals (79.45%) and the production of LED bulbs (19.46%). For the hydroquinone counterpart, the heaviest weight of impact potential was associated with the mining of silver process (46.84%) and the production of the AgNP (43.55%).

In the case of photochemical oxidant formation potential (POFP), the two systems performed differently and the biogenic produced only 8.10% of that of the equivalent in the hydroquinone process (4.41 x 10⁻⁷ DALY or 11.31 kg NMVOC) from all three perspectives (i.e. E, H, I perspectives for ReciPe 1.11) and both mid and endpoint analysis., accounted by the chemical production (77.37%) and the LED manufacturing (21.70%) with other accounting for the small remaining (097%) in the biogenic production. For the hydroquinone method, the silver mining, storage, and hydroquinone production accounted for 84.19% of the total photochemical ozone formation, and the actual redox production 15.63% with a small 0.18 % coming from other components within the process.

4.3.9 Process contribution analysis

For convenience, only results from the TRACI 2.1 methodology were used for the analysis of process contributions. In the case of the hydroquinone production the main contributors to the potential impacts were the mining process and storage, the manufacturing of hydroquinone, the heat production for the process and the nanoparticle manufacturing process itself. In the biogenic counterpart, the core processes, within the boundaries, responsible for the highest percentage of impact potential were the manufacturing of chemicals for the medium (e.g. sodium nitrate, sodium phosphate, sodium dichromate, and sodium silicate), the mining and storage of silver, the production or manufacture of the LED bulbs used for the illumination in times of darkness, the production of ultrapure water, and the culture process itself.

CHAPTER V CONCLUSIONS

The primary objective of this research was to assess the potential use of P. tricornutum in the remediation of heavy metal pollution. The results show a considerable reduction in ionic concentration in the samples at different levels. It also was possible to assess that the organism is, in fact, an appropriate alternative for the remediation of heavy metal species in a water sample, and mainly silver (Ag) and vanadium (V) in maximum concentrations of 1.9×10^{-4} g Ag·L⁻¹ and 3.0×10^{-4} g V·L⁻¹, respectively.

Additionally, the presence of silver nanoparticles, even though there were no chemicals in the medium that would spontaneously induce a protonation process, suggests that the organism was, in fact, the vector responsible for the synthesis of the nanoparticles. The analysis also yielded sufficient evidence to accept the premise that *P. tricornutum* is a potential candidate for further research in nanotechnological applications and biomimetic synthesis of nanoparticles of different elements.

Furthermore, it was determined that the optimum mixture concentration of silver and molybdenum for both the reduction of ionic species and the synthesis of nanoparticles was $1.47 \times 10^{-4} \text{ g Ag} \cdot \text{L}^{-1}$ and $1.35 \times 10^{-4} \text{ g Mo} \cdot \text{L}^{-1}$. Similarly, the best combination of vanadium and molybdenum was $2.35 \times 10^{-4} \text{ g V} \cdot \text{L}^{-1}$ with $1.35 \times 10^{-4} \text{ g Mo} \cdot \text{L}^{-1}$.

The synthesis of silver nanoparticles via regulated culture of *P. tricornutum* was possible and enhanced when the addition of the treatment allowed for a small acclimation period for the algae (i.e. sequential every 1 hour for 5 hours). Subsequent additions of ions were also taken by the organism and the optimal concentrations of silver and molybdenum were established at 1.47 and 1.35 mg ion·L⁻¹, respectively, with light and temperature kept constant around $75 \,\mu$ mol m⁻²·s⁻¹, and $18 \,^{\circ}$ C, with constant mixing via bubbling as the most adequate protocol for the synthesis of these particles.

The results of the ICP analysis and the positive relation found through the statistical analysis suggest that to an extent, *P. tricornutum* cells were responsible for the reduction in silver and vanadium levels in the surrounding medium. It is safe to assume that *P. tricornutum* is a viable species to treat relatively high concentrations of silver and

vanadium pollution in water. To further determine the interaction between these two ions and the cell biology, it is recommended to perform additional trials using surface exploratory methods and molecular assays to determine how the proteome is affected.

P. tricornutum frustules were characterized after culture conditions were altered to introduce a heavy metal stressor (i.e. silver). The carefully monitored culture conditions make it possible to conclude that the formation of any compound on the surface or outer vicinity of the cells was a consequence of the biochemistry of the cells and not accidental contamination from external sources. It was possible to see silver-based nanoparticles around surrounding some cell and cell structures. The characteristics of the particles and the nature of the culture medium for the algae suggest that it is probable that these particles were the result of the algae's heavy-metal response and thus manufactured by the diatom. The nitrogen concentrations never fell below levels that would trigger intake of nitrate ions from the silver and protonation on the silver by chemical interactions. These preliminary findings open a door for further analysis of the interaction between P. tricornutum cells and heavy metal loaded environments.

The low concentration of iron, copper, and aluminum in the culture medium rendered these values as consequence of background noise coming from the stub. It is noteworthy that if these ions are to be analyzed, a different type of substrate should be used. Additionally, the only trace elements identified were vanadium and molybdenum; and they were observed in only a few of the samples, typically overlapping with sulfur and oxygen peaks making it difficult to differentiate or conclude that they were at all present in the samples. The high concentration of oxygen made it difficult to analyze molybdenum evolution in the samples. Thus, it is not advisable to use SEM-EDS techniques to identify or trace the metal in organic samples unless oxygen can be removed from the sample. The closeness of the energy required for emission from the elemental sulfur and vanadium made it impossible to draw any conclusion or analysis based on these counts.

The composition of most locations around the frustule formations suggests the interchangeable nature of the magnesium and silicon ions in the formation of the hardened structure of the outer mineralized wall (i.e. frustule) of *P. tricornutum*. The association of sodium in concentrations that were higher than the ones that most

probably would be related to the presence of sodium-mediated enzymes acting on the cell wall (i.e. frustule) formation process, suggests an active deposition, and further analysis is recommended. If this is confirmed, the potential for the use of *P. tricornutum* as a green synthetic biorefinery of silicate clays (sodium-magnesium-silicate) for bulking purposes might surpass in attractiveness the currently accepted processes in the cosmetic industry.

From the comparative life cycle analysis carried out in this study, it is possible to establish that the overall performance of the biogenic algae-based method (*P. tricornutum*) has considerably lower impacts when compared to the industrially available hydroquinone redox method. The only category where the hydroquinone method performs better from an environmental perspective is the land use (agricultural and natural transformation). After further understanding on how the diatom species transforms available silver into nanoparticles, and the biochemical pathways underlying the process, the challenges would lie in learning how to take advantage of the silicon pathways of diatoms to manufacture biomedical, telecommunications, energy storage, and sensing devices.

CHAPTER VI CONTRIBUTIONS TO KNOWLEDGE, FUTURE RESEARCH RECOMMENDATIONS, AND SCALE-UP POTENTIAL

6.1 Contributions to knowledge

Upon analysis and review of this document, it was clear that this research helped determine that *P. tricornutum* has an incredible potential to both mitigate heavy metal contamination in water bodies, and in manufacturing silver nanoparticles.

The sequence in which the development of the thesis was done, and the use of mixtures in the experimental design, allowed for a faster determination of the potential of algal species in the treatment of metallic contamination in water bodies, reducing both the use of time and resources for that purpose and providing a faster method to test similar combinations in the future.

This work is also the first to use *P. tricornutum* with specific silver and molybdenum combination to optimize the response in the manufacture of nanoparticles biogenically, and with a specific protocol for the addition of the ionic species in the regulation of the size and concentration of the particles in the final product. This work differs from the mentioned development in Israel in that the strain of the species used here is a certified strain of *P. tricornutum* obtained from the Canadian Phycological Culture Centre for Algae, cyanobacteria, and Lemna at the University of Waterloo (Waterloo, ON, Canada) while the report presented by the group in Israel fails to clarify which organism is the one used for the study, visual exploration of the SEM images provided, does not aid in the identification of the species. Nonetheless, the main differences lay on the confirmation via EDs analysis of the constitution of the particles discovered; the concentrations found to be optimal in our analysis, which are 50 % higher due to the presence and optimization character of molybdenum in the process; and the method presented here for the addition of the ionic silver and the overall synthesis of silver nanoparticles, which was more specific, different in temperature, medium conditions, and instrumental analysis.

To the knowledge of the author, to date this is the first approach in comparing biogenic and traditional redox-based silver nanoparticles processes in their environmental impacts. Even though, the analysis of some of the data came from bibliographic

considerations, it was also a first and interesting approach to open a door for further analysis and more specifically, to start considering the use of microorganisms in a larger scale for the development of biogenic approaches in industrial manufacturing of metallic nanoparticles.

6.2 Future research recommendations

For those wanting to choose biomineralization as a research topic, the areas of research derived from the varied assortment of organisms, structures and processes, components, and intermediate substances open a full spectrum of possibilities. Nonetheless, the most promising pathways are associated with the potential to mimic the already available processes of nature for human applications. Industrial development has taken notice of the incredible potential of applying biomineralization strategies as a reference for manufacturing processes and recent trends in manufacturing technologies focus on the fact that industrial production is mostly a top-down process that could be replaced by working on a bottom-up approach.

From all the classes and groups of organisms capable of biomineralization of substances, diatoms are of interest. They can develop highly intricate and replicable structures, with a degree of efficiency and safety (low temperature and pressure) that is particularly desirable for industrial manufacturing processes. This remarkable evolutionary trait can be a stepping-stone for further and more advanced biotechnological applications. Doping diatoms can yield a unique array of materials with applications in photovoltaics, photocatalysis, LED manufacture, and almost any field that uses semiconducting materials. Additionally, it is possible to use doping techniques to enhance drug delivery properties of diatom shells for a more target-specific, low-release delivery mechanism. Even from a molding perspective, diatoms offer an impressive array of shapes and sizes that can work as scaffolding surfaces for novel nanoscopic patterned structures.

It is theorized, that glutathione production can be an appropriate measure of the response of the organism, as this nanoparticle production might be the result of a physiological response to oxidative stress. Reported literature confirms that these levels might provide a better understanding of the stress response by *P. tricornutum* cells. Additionally, as it was found in literature, class II and class III metallothioneins (MtII and MtIII) are frequently synthesized in response to metal exposure and their presence is a specific signal of metal ion uptake and thus, an additional determination of concentration of these proteins throughout the phases of the culture and exposure to the metal stressor, can address for the actual bioavailability of ionic silver. It is recommended to perform a proteomic and transcriptomic analysis with algae collected after the second day of exposure to the silver stress, and compare those to the responses of control cells grown under optimal conditions. If the proteins involved in the production of nanoparticles are readily available and easy to use, these algae can be an interesting alternative for physicochemical processes of synthesis of metal nanoparticles. For this purpose, several proteins and encoding sequences can be researched from the JGI database. It is recommended to do some acclimation assays where the proteomic and genomic responses of algae with and without a silver exposure period would increase or not the production of the molecules produced during the stress period of the culture.

Even though the future of diatom biotechnology is promising, further research is required to elucidate the vast array of molecules and interactions between inorganic and organic molecules that take place during frustule formation in diatoms.

6.3 Scale-up potential

Further analysis and research would help hone down to a more specific process, the amount of silver and the actual time intervals for the addition of the ionic treatments to optimize both shape and size of the particles.

Further fluid dynamics and light distribution simulations would help determine the best scaling up settings for a more efficient production vessel, which in turn will reduce the contributions to land impact and increase the potential of the process to be scaled up and optimized for industrial purposes.

REFERENCES

Abraham, M. A. and N. Nguyen, 2003. Green Engineering: Defining the Principles—Results from the Sandestin Conference. Environmental Progress, 22(4): 233-236.

Abramoff, M. D., Magalhaes, P. J., and S. J. Ram, 2004. Image Processing with ImageJ. Biophotonics International, 11(7): 36-42.

Acero, A. P., Rodríguez, C., and A. Ciroth, 2017. LCIA methods. Impact assessment methods in Life Cycle Assessment and their Impact categories – Version 1.5.6. Green Delta GmbH. Berlin, Germany. 23 pp.

Adachi, S., 2009. Properties of Semiconductor Alloys. Wiley Series in Materials for Electronic & Optoelectronic Applications, ed. P. Capper, S. Kasap, and A. Willoughby. Wiley.

Alba, L.G., 2013. Algae Biorefinery: An experimental study on liquid fuels production and nutrients recycling, in Chemical Engineering, University of Twente: Enschede, The Netherlands.

Allan R. J, 1995. Impact of mining activities on the terrestrial and aquatic environment with emphasis on mitigation and remedial measures. In: Förstner, U., Salomons, W., and P. Mader (eds.). Heavy Metals: Problems and Solutions. Part of the series Environmental Science. 119-140

Amores, D. R. and L. A. Warren, Metabolic patterning of biosilicification. Chemical Geology, 2009. 268(1–2): 81-88.

Anastas, P. T., and J. B. Zimmerman, 2003. Design Through the 12 Principles of Green Engineering. Environmental Science & Technology, 37(5): 94A-101A.

Anastas, P. T., and J. C. Warner, 2000. Green chemistry: theory and practice. Oxford university press.

Andersen, R. A., 2005. Algal Culturing Techniques. Elsevier Inc. Burlington, MA. United States.

Anderson, H. C., Narsuzawa, T. Sajdera, S. W. and S. Y. Ali, 1970. Membranous particles in calcifying cartilage matrix. Transactions of the New York Academy of Sciences, 32(5): 619-630.

André, R., Natalio, F., Nawaz Tahir, M., Berger, BR., and W. Tremel, 2013. Self-cleaning antimicrobial surfaces by bio-enabled growth of SnO₂ coatings on glass. Nanoscale. 5(8): 3447-3456.

André, R., Tahir, M. N., Natalio, F., W. Tremel, 2012. Bioinspired synthesis of multifunctional inorganic and bio-organic hybrid materials. FEBS Journal. 279(10): 1737-1749.

Annenkov, V. V., Patwardhan, S. V., Belton, D., Danilovtseva, E. N., and C. C. Perry, 2006. A new stepwise synthesis of a family of propylamines derived from diatom silaffins and their activity in silicification. Chemical Communications (Cambridge). 2006(14): 1521-1523.

Antonides, L. E., 1998. Diatomite: U. S. Geological Survey Mineral Commodity Summaries. p. 56-57.

Arcos, D. and M. Vallet-Regí, 2010. Sol-gel silica-based biomaterials and bone tissue regeneration. Acta Biomaterialia. 6(8): 2874-2888.

Arcos, D., López-Noriega, A., Ruiz-Hernández, E., Terasaki, O., and M. Vallet-Regí, 2009. Ordered Mesoporous Microspheres for Bone Grafting and Drug Delivery. Chemistry of Materials. 21(6): 1000-1009.

Arcos, D., Peña, J., and M. Vallet-Regí, 2003. Influence of a SiO₂-CaO-P₂O₅ Sol-Gel Glass on the Bioactivity and Controlled Release of Ceramic/Polymer/Antibiotic Mixed Materials. Chemistry of Materials, 15(21): 4132-4138.

Arcos, D., Ragel, C. V., and M. Vallet-Regí, 2001. Bioactivity in glass/PMMA composites used as drug delivery system. Biomaterials. 22(7): 701-708.

Armbrust, E. V., 2009. The life of diatoms in the world's oceans. Nature. 459(7244): 185-192.

Ashman, R. B., Cowin, S. C., Van Buskirk, W. C., and J. C. Rice, 1984. A continuous wave technique for the measurement of the elastic properties of cortical bone. Journal of Biomechanics. 17(5): 349-361.

ASTM E2456 – 06 (2012). Standard Terminology Relating to Nanotechnology

Aw, M. S., Bariana, M., Yu, Y., Addai-Mensah, J., and D. Losic, 2013. Surface-functionalized diatom microcapsules for drug delivery of water-insoluble drugs. Journal of Biomaterials Applications. 28(2): 163-174.

Aw, M. S., Simovic, S., Yu, Y., Addai-Mensah, J., and D. Losic, 2012. Porous silica microshells from diatoms as biocarrier for drug delivery applications. Powder Technology. 223: 52-58.

Aziz, N., Faraz, M., Pandey, R., Shakir, M., Fatma, T., Varma, A., Barman, I., and R. Prasad, 2015. Facile Algae-Derived Route to Biogenic Silver Nanoparticles: Synthesis, Antibacterial, and Photocatalytic Properties." Langmuir 31(42): 11605-11612.

Bacciagaluppi, G. and A. Valentini, 2009. Quantum Theory at the Crossroads: Reconsidering the 1927 Solvay Conference (Cambridge University Press, 2009)

Bae, C. H., Nam, S. H., and S. M. Park, 2002. Formation of silver nanoparticles by laser ablation of a silver target in NaCl solution. Applied Surface Science. 197–198, 628–634.

Bare, J., Young, D., and M. Hopton, 2012. Tool for the Reduction and Assessment of Chemical and Other Environmental Impacts (TRACI) User's Manual. Software Name and Version Number: TRACI version 2.1. Office of Research and Development. United States Environmental Protection Agency (EPA) EPA/600/R-12/554 | July 2012. Cincinnati, OH., United States. 24 pp.

Bariana, M., Aw, M. S., and D. Losic, 2013. Tailoring morphological and interfacial properties of diatom silica microparticles for drug delivery applications. Advanced Powder Technology. 24(4): 757-763.

Barlow, J., Sims, R. C., and J. C. Quinn, 2016. Techno-economic and life-cycle assessment of an attached growth algal biorefinery, Bioresource Technology, 220: 360-368.

Basharina, T. N., Danilovtseva, E. N., Zelinskiy, S. N., Klimenkov, I. V., Likhoshway, Y. V., and V. V. Annenkov, 2012. The effect of titanium, zirconium and tin on the growth of diatom *Synedra acus* and Morphology of Its silica valves. Silicon. 4(4): 239-249.

Bäuerlein, E., 2003. Biomineralization of unicellular organisms: An unusual membrane biochemistry for the production of inorganic nano- and microstructures. Angewandte Chemie - International Edition. 42(6): 614-641.

Baurain, D., Brinkmann, H., Petersen, J., Rodríguez-Ezpeleta, N., Stechmann, A., Demoulin, V., Roger, A. J., Burger, G., Lang, B. F., and H. Philippe, 2010. Phylogenomic evidence for separate acquisition of plastids in cryptophytes, haptophytes, and stramenopiles. Molecular Biology and Evolution. 27(7): 1698-1709.

Ben Fadhel, M., Zouaghi, T., Amri, A., and M. Ben Youssef, 2014. Radiolarian and planktic foraminifera biostratigraphy of the early Albian organic rich beds of Fahdene Formation, Northern Tunisia. Journal of Earth Science. 25(1): 45-63.

Beniash, E., Aizenberg, J., Addadi, L., and S. Weiner, 1997. Amorphous calcium carbonate transforms into calcite during sea urchin larval spicule growth. Proceedings of the Royal Society B: Biological Sciences. 264(1380): 461-465.

Beniash, E., L. Addadi, and S. Weiner, 1999. Cellular control over spicule formation in sea urchin embryos: A structural approach. Journal of Structural Biology. 125(1): 50-62.

Benning, L. G., Phoenix, V. R., Yee, N., and K. O. Konhauser, 2004. The dynamics of cyanobacterial silicification: an infrared micro-spectroscopic investigation. Geochimica et Cosmochimica Acta. 68(4): 743-757.

Bhushan, B., Luo, B., Schricker, D., Sigmund, S. R., and W. Zauscher, 2014. Handbook of nanomaterials properties.

Binnig, G. and H. Rohrer, 1983. Scanning tunneling microscopy. Surface Science. 126: 236-244.

Binnig, G. and H. Rohrer, 1984. Scanning tunneling microscopy. Physica B+C. 127(1-3): 37-45.

Binnig, G. and H. Rohrer, 1986. Scanning tunneling microscopy. IBM Journal of Research and Development. 30(4): 355.

Binnig, G. and H. Rohrer, 1987. Scanning tunneling microscopy—from birth to adolescence. reviews of modern physics, 59(3): 615-625.

Binnig, G., Quate, C. F., and C. Gerber, 1986. Atomic force microscope. Physical Review Letters, 56(9): 930-933.

Bohlin, K. 1897. Zur Morphologie und biologie einzelliger algen. Öfversigt af Kongliga Vetenskaps-Akademiens Förhandlingar. Stockholm. 9: 507–529.

Bohr, N., 1961. The Solvay meetings and the development of quantum mechanics. Niels Bohr at the occasion of the 12th Solvay Conference in Physics, 9-14 October 1961. Retrieved online: http://www.solvayinstitutes.be/pdf/Niels_Bohr.pdf

Borowitzka M. A. and B. E. Volcani, 1978. The polymorphic diatom *Phaeodactylum tricornutum*: ultrastructure of its morphotypes. Journal of Phycology 14: 10–21.

Borowitzka, M. A. and A. W. D. Larkum, 1974. Chloroplast development in the caulerpalean alga *Halimeda*. Protoplasma. 81(2-3): 131-144.

Borowitzka, M. A. and A. W. D. Larkum, 1976. Calcification in the green alga *Halimeda*: III. The sources of inorganic carbon for photosynthesis and calcification and a model of the mechanism of calcification. Journal of Experimental Botany, 27(5): 879-893.

Borowitzka, M. A., 1981. Photosynthesis and calcification in the articulated coralline red algae *Amphiroa* anceps and *A. foliacea*. Marine Biology, 62(1): 17-23.

Borowitzka, M. A., 1982. Morphological and cytological aspects of algal calcification. International Review of Cytology. 74: 127-162.

Bouvier N. M. and P. Palese, 2008. The biology of influenza viruses. Vaccine. 26(Suppl. 4): D49-D53.

Bowler C., Allen, A. E., Badger, J. H., Grimwood, J., Jabbari, K., Kuo, A., Maheswari, U., Martens, C., Maumus, F., Otillar, R. P., Rayko, E., Salamov, A., Vandepoele, K., Beszteri, B., Gruber, A., Heijde, M., Katinka, M., Mock, T., Valentin, K., Verret, F., Berges, J. A., Brownlee, C., Cadoret, J-P., Chiovitti, A., Choi, C. J., Coesel, S., De Martino, A., Detter, J. C., Durkin, C., Falciatore, A., Fournet, J., Haruta, M., Huysman, M. J. J., Jenkins, B. D., Jiroutova, K., Jorgensen, R. E., Joubert, Y., Kaplan, A., Kröger, N., Kroth, P. G., La Roche, J., Lindquist, E., Lommer, M., Martin–Jézéquel, V., Lopez, P. J., Lucas, S., Mangogna, M., McGinnis, K., Medlin, L. K., Montsant, A., Oudot–Le Secq, M-P., Napoli, C., Obornik, M., Schnitzler Parker, M., Petit, J.-L., Porcel, B. M., Poulsen, N., Robison, M., Rychlewski, L., Rynearson, T. A., Schmutz, J., Shapiro, H., Siaut, M., Stanley, M., Sussman, M. R., Taylor, A. R., Vardi, A., von Dassow, P., Vyverman, W., Willis, A., Wyrwicz, L. S., Rokhsar, D. S., Weissenbach, J., Armbrust, E. V., Green, B. R., Van de Peer, Y., and I. V. Grigoriev, 2008. The *Phaeodactylum* genome reveals the evolutionary history of diatom genomes. Nature 456: 239–244.

Bowler C., De Martino A., and A. Falciatore, 2010. Diatom cell division in and environmental context. Plant Biology 13: 1-8

Bozarth, A., Maier, U. G., and S. Zauner, 2009. Diatoms in biotechnology: Modern tools and applications. Applied Microbiology and Biotechnology. 82(2): 195-201.

Braek G. S., Malnes D., and A. Jensen, 1980. Heavy metal tolerance of marine phytoplankton. IV. Combined effect of zinc and cadmium on growth and uptake in some marine diatoms. Journal of Experimental Marine Biology and Ecology. 42 (1): 39-54

Brentner, L. B., Eckelman, M. J., and J. B. Zimmerman, 2011. Combinatorial life cycle assessment to Inform process design of industrial production of algal biodiesel. Environmental Science & Technology. 45 (16): 7060-7067.

Briggs, J. A. G., Wilk, T., Welker, R., Kräusslich, H.-G., and S. D. Fuller, 2003. Structural organization of authentic, mature HIV-1 virions and cores. The EMBO Journal, 22(7): 1707–1715.

Brummer, G. J. A., Hemleben, C., and M. Spindler, 1987. Ontogeny of extant spinose planktonic foraminifera (Globigerinidae): A concept exemplified by *Globigerinoides sacculifer* (Brady) and G. Ruber (d'Orbigny). Marine Micropaleontology. 12(C): 357-381.

Brunner, E., Gröger, C., Lutz, K., Richthammer, P., Spinde, K., and M. Sumper, 2009. Analytical studies of silica biomineralization: towards an understanding of silica processing by diatoms. Applied Microbiology and Biotechnology. 84(4): 607-616.

Brzezinski M. A., Olson R. J., and S. W. Chisholm, 1990. Silicon availability and cell-cycle progression in marine diatoms. Marine Ecology Progress series 67: 83–96.

Butler, C.S., 2012. Metals, non-metals and minerals: The complexity of bacterial selenate respiration. Biochemist. 34(5): 23-27.

Campbell, P. K., Beer, T., and D. Batten, 2011. Life cycle assessment of biodiesel production from microalgae in ponds, Bioresource Technology, Volume 102, Issue 1, January 2011, Pages 50-56.

Cannon, W. B., 1929. Organization for Physiological Homeostasis. Physiological Reviews, IX (3): 399-431.

Cao, S., Wang, J., and D. Chen, 2013. Settlement and cell division of diatom *Navicula* can be influenced by light of various qualities and intensities. Journal of Basic Microbiology. 53(11): 884-894.

Caramujo, M. J., Boschker, H. T. S., and W. Admiraal, 2008. Fatty acid profiles of algae mark the development and composition of harpacticoid copepods. Freshwater Biology. 53(1): 77-90.

Cardozo, K. H. M., Oliveira, M. A. L., Tavares, M. F. M., Colepicolo, P. And E. Pinto, 2002. Daily oscillation of fatty acids and malondialdehyde in the dinoflagellate Lingulodinium polyedrum. Biol. Rhythm Res. 33:371–81.

Cassella, J. P., Stamp, T. C. B., and S. Y. Ali, A 1996. morphological and ultrastructural study of bone in osteogenesis imperfecta. Calcified Tissue International. 58(3): 155-165.

Castro-Bugallo, A., González-Fernández, Á., Guisande, C., and A. Barreiro, 2014. Comparative Responses to Metal Oxide Nanoparticles in Marine Phytoplankton. Archives of Environmental Contamination and Toxicology, 67(4): 483-493.

Castro, L., Blázquez, M. L., Muñoz, J. A., González, F., and A. Ballester, 2013. Biological synthesis of metallic nanoparticles using algae. IET Nanobiotechnology. 2012: 1-8.

Caswell, K. K., Bender, C. M., and C. J. Murphy, 2003. Seedless, surfactantless wet chemical synthesis of silver nanowires. Nano Lett. 3(5): 667–669.

Charistides, C. A., Georgiou, P., Koklioti, M. A., Trompeta, A-F., and V. Markakis, 2014. Manufacturing nanomaterials: from research to industry. Manufacturing Rev.2014, 1, 11.

Chauton, M. S., Skolem, L. M. B., Olsen, L. M., Vullum, P. E., Walmsley, J., and O. Vadstein, 2015. Titanium uptake and incorporation into silica nanostructures by the diatom *Pinnularia* sp. (Bacillariophyceae). Journal of Applied Phycology. 27(2): 777-786.

Chen, D., Wang, R., Arachchige, I., Mao, G., and S. L. Brock, 2004. Particle-rod hybrids: Growth of arachidic acid molecular rods from capped cadmium selenide nanoparticles. Journal of the American Chemical Society. 126(50): 16290-16291.

Chen, L., Shen, Y., Xie, A., Huang, B., Jia, R., Guo, R., and Tang, W., 2009. Bacteria-Mediated Synthesis of Metal Carbonate Minerals with Unusual Morphologies and Structures. Crystal Growth & Design, 9(2): 743-754

Chepurnov, V. A., Chaerle, P., Vanhoutte, K., and D. G. Mann, 2012. How to Breed Diatoms: Examination of Two Species with Contrasting Reproductive Biology. In: R. Gordon and J. Seckbach (Eds.), The Science of Algal Fuels: Phycology, Geology, Biophotonics, Genomics and Nanotechnology (pp. 323-340). Dordrecht: Springer Netherlands.

Choi, S. U. S. and J. A. Eastman, 1995. Enhancing thermal conductivity of fluids with nanoparticles. American Society of Mechanical Engineers, Fluids Engineering Division (Publication) FED. pp. 99-105.

Ciroth, A., Fleischer, G. & Steinbach, 2004. Uncertainty calculation in life cycle assessments. The International Journal of Life Cycle Assessment. 9: 216.

Clarens, A. F., Resurreccion, E. P., White, M. A., and L. M. Colosi, 2010. Environmental Life Cycle Comparison of Algae to Other Bioenergy Feedstocks. Environmental Science & Technology 44 (5): 1813-1819.

Cobbett, C. and P. Goldsbrough, 2002. Phytochelatins and metallothioneins: Roles in heavy metal detoxification and homeostasis. Annual Review of Plant Biology, 53: 159-182

Collet, P., Hélias, A., Lardon, L., Ras, M., Goy, R-A., and J-P. Steyer, 2011. Life-cycle assessment of microalgae culture coupled to biogas production, Bioresource Technology, Volume 102(1): 207-214.

Compton, R. G., Eklund, J. C., and F. Marken, 1997. Sonoelectrochemical processes: a review. Electroanalysis. 9(7): 509–522.

Congestri, R. and P. Albertano, 2011. Bentic diatoms in biofilm culture, in the diatom world, J. Seckbach, Editor. Springer.

Conner, S. D. and Schimid, S. L. 2003. Regulated portals of entry into the cell. Nature 422:37 – 44.

Conner, S. F. and S. L. Schimid, 2006. Regulated portals of entry into the cell. Nature. 422: 37-44.

Cotté-Krief, M-H., Thomas, A. J., and J-M. Martin, 2002. Trace metal (Cd, Cu, Ni and Pb) cycling in the upper water column near the shelf edge of the European continental margin (Celtic Sea). Marine Chemistry, 779 (1): 1-26

Cox, E. J., 1999. Variation in patterns of valve morphogenesis between representatives of six biraphid diatom genera (Bacillariophyceae). Journal of Phycology. 35(6): 1297-1312.

Cox, E. J., 2011. Morphology, Cell Wall, Cytology, Ultrastructure and Morphogenetic Studies: Overview and Specific Observations, in The Diatom World, J. Seckbach and J.P. Kociolek, Editors.

Cox, E. J., 2012. Diatoms and forensic science, in forensic ecology handbook: From crime scene to court. John Wiley and Sons. 141-151.

Craggs R. J., McAuley, P. J., and V. J. Smith, 1997. Wastewater nutrient removal by marine microalgae grown on a corrugated raceway. Water Research, 31 (7): 1701-1707

Craggs R. J., Smith V. J., and P. J. McAuley, 1995. Wastewater nutrient removal by marine microalgae cultured under ambient conditions in mini-ponds. Water Science & Technology. 31 (12): 151-160.

Crick, R. E., 1989. Origin, evolution, and modern aspects of biomineralization in plants and animals.

Croteau, M. N., Dybowska, A. D., Luoma, S. N., and E. Valsami-Jones, 2011. A novel approach reveals that zinc oxide nanoparticles are bioavailable and toxic after dietary exposures. Nanotoxicology. 5(1): 79-90.

Csögör Z., Melgar D., Schmidt K., and C. Posten, 1999. Production and particle characterization of the frustules of *Cyclotella cryptica* in comparison with siliceous earth, Journal of Biotechnology, Volume 70, Issues 1–3, 30, Pages 71-75.

Cuberes, M. T., Schlittler, R. R., and J. K. Gimzewski (1996). Room-temperature repositioning of individual C60 molecules at Cu steps: Operation of a molecular counting device. Applied Physics Letters 69(20): 3016-3018.

Cumming, J. R. and J. T. Gregory, 1990. Mechanisms of metal tolerance in plants: physiological adaptions for exclusion of metal ions from the cytoplasm. In Alscher, R. G. and J. R. Cumming, (Eds.) Stress Responses in Plants: Adaptation and Acclimation Mechanisms. Wiley-Liss, New York, pp. 338–55.

Cupp, E. E., 1943. Marine Plankton Diatoms of the West Coast of North America. Bulletin of the Scripps Institute of Oceanography of the University of California La Jolla. 5: 1-238.

Curnow, P., Senior, L., Knight, M. J., Thamatrakoln, K., Hildebrand, M., P. J. Booth, 2012. Expression, Purification, and Reconstitution of a Diatom Silicon Transporter. Biochemistry. 51(18): 3776-3785.

Cushing, B. L., Kolesnichenko, V. L., and C. J. Oconnor, 2004. Recent advances in the liquid-phase syntheses of inorganic nanoparticles. Chem. Rev. 104, 3893–3946.

D'agostino R. B. and H. K. Russell, 2005. Scree Test. In: Encyclopedia of Biostatistics 7. Wiley Online.

Dahiya, A., 2012. Integrated Approach to Algae Production for Biofuel Utilizing Robust Algal Species. 25: 83-100.

Dahl, C. and C. G. Friedrich, 2008. Microbial sulfur metabolism. Springer e-books. Berlin. Springer.

Dalton, J., 1808. On the Constitution of Bodies and On Chemical Synthesis. Originally published in "A new system of Chemical Phylosophy", Manchester, 1808 pp.: 141-143. In: Foundations of the Atomic Theory: Comprising Papers and Extracts by John Dalton, William Hyde Wollaston, M. D., and Thomas Thomson, M. D. (1802-1808). Issue 2 of Alembic Club Reprints. W. F. Clay (Eds.) Harvard University. 1893. pp: 27-34.

Daniel, M. C. and D. Astruc, 2004. Gold Nanoparticles: Assembly, Supramolecular Chemistry, Quantum-Size-Related Properties, and Applications Toward Biology, Catalysis, and Nanotechnology. Chemical Reviews, 104(1): 293-346.

Datt, P., 2011. Latent Heat of Vaporization/Condensation. Encyclopedia of Snow, Ice and Glaciers. V. P. Singh, P. Singh and U. K. Haritashya. Dordrecht, Springer Netherlands: 703-703.

Davis, S. C., Sheppard, V. C., Begum, G., Cai, Y., Fang, Y., Berrigan, J. D., Kröger, N., and K. H. Sandhage, 2013. Rapid flow-through biocatalysis with high surface area, enzyme-loaded carbon and gold-bearing diatom frustule replicas. Advanced Functional Materials. 23(36): 4611-4620.

De Martino A., Bartual A., Willis A., Melchenin A., Vilazan B., Maheswari U., and C. Bower, 2011. Physiological and molecular evidence that environmental changes elicit morphological interconversion in the model diatom *Phaeodactylum tricornutum*. Protist 162: 462-481

de Nooijer, L. J., Spero, H. J., Erez, J., Bijma, J., and G. J. Reichart, 2014. Biomineralization in perforate foraminifera. Earth-Science Reviews. 135: 48-58.

De Stefano, L., Rea., I., Rendina, I., De Stefano, M., and L. Moretti, 2007. Lensless light focusing with the centric marine diatom *Coscinodiscus walesii*. Optics Express. 15(26): 18082-18086.

De Stefano, M. and L. De Stefano, 2005. Nanostructures in diatom frustules: Functional morphology of valvocopulae in cocconeidacean monoraphid taxa. Journal of Nanoscience and Nanotechnology. 5(1): 15-34.

De Tommasi, E., Rea, I., Mocella, V., Moretti, L., De Stefano, M., Rendina, I., and L. De Stefano, 2010. Light confinement in marine centric diatoms: main characteristics and wavelength dependence. Proceedings SPIE 7782, The Nature of Light: Light in Nature III, 778203

Desbois, A. P., Mearns-Spragg, A., and V. J. Smith, 2009. A fatty acid from the diatom *Phaeodactylum tricornutum* is antibacterial against diverse bacteria including multi-resistant *Staphylococcus aureus* (MRSA). Marine Biotechnology. 11(1): 45-52.

Dixit, S. S. and J. P. Smol, 1994. Diatoms as indicators in the Environmental Monitoring and Assessment Program-Surface Waters (EMAP-SW). Environmental Monitoring and Assessment. 31(3): 275-307.

Dixit, S. S., Smol, J. P., Kingston, J. C., and D. F. Charles, 1992. Diatoms: powerful indicators of environmental change. Environmental Science & Technology. 26(1): 22-33.

Dobrestov, N., Kolchanov, N., Rozanov, A., and G. Zavarzin, (Eds.), 2008. Biosphere origin and evolution. Springer.

Doo, S. S., Fujita, K., Byrne, M., and S. Uthicke, 2014. Fate of calcifying tropical symbiont-bearing large benthic foraminifera: Living sands in a changing ocean. The Biological Bulletin. 226(3): 169-186.

Drexler, K. E. 1981. Molecular engineering: An approach to the development of general capabilities for molecular manipulation. Proceedings of the National Academy of Sciences, 78(9): 5275-5278.

Drum, R. W. and R. Gordon, 2003. Star Trek replicators and diatom nanotechnology. Trends in Biotechnology. 21(8): 325-328.

Dunstan, G. A., Baillie, H. J., Barrett, S. M., and J. K. Volkman, 1996. Effect of diet on the lipid composition of wild and cultured abalone. Aquaculture. 140(1-2): 115-127.

Durán N., Marcato P. D., Alves O. L., De Souza G. I. H., and E. Esposito, 2005. Mechanistic aspects of biosynthesis of silver nanoparticles by several *Fusarium oxysporum* strains. Journal of biomaterials and Nanobiotechnology 3:8.

Durán N., Marcato P. D., Ingle A., Gade A., and M. Rai, 2009. Fungi mediated synthesis of silver nanoparticles: characterization processes and applications. In: M. Rai, G. Kövics (eds.) Progress in mycology: biosynthesis of nanoparticles by microbes and plants. Scientific, Rajasthan, pp 425–449. Springer Netherlands. ISBN: 978-90-481-3712-1.

Durkin, C. A., Koester, J. A., Bender, S. J., and E. V. Armbrust, 2016. The evolution of silicon transporters in diatoms. Journal of Phycology 52(5): 716-731.

Dybowska, A. D., Croteau, M.-N., Misra, S. K., Berhanu, D., Luoma, S. N., Christian, P., O'Brien, P., and E. Valsami-Jones, 2011. Synthesis of isotopically modified ZnO nanoparticles and their potential as nanotoxicity tracers. Environmental Pollution. 159(1): 266-273

Ehrlich, H., 2010. Chitin and collagen as universal and alternative templates in biomineralization. International Geology Review, 52(7-8): 661-699.

Eigler, D. M. and E. K. Schweizer, 1990. Positioning single atoms with a scanning tunnelling microscope. Nature 344(6266): 524-526.

Elkhooly, T. A. A., 2014, Coating of surfaces of composite materials with enzimatically formed biosilica. Johannes Gutenberg-Universität. 147.

Ellis, B. F. M. A. R. A. M. o. N. H., Catalogue of Foraminifera. 1940, New York: The American Museum of Natural History.

Esser, B. K. and A. Volpe, 2002. At-sea high-resolution trace element mapping: San Diego Bay and its plume in the adjacent coastal ocean. Environmental Science & Technology, 36 (13): 2826-2832.

Estes A. and R. R. Dute, 1994. Valve abnormalities in diatom clones maintained in long-term culture. Diatom Research. 9: 249-258

European Commission Joint Centre Institute for Environment and Sustainability, 2010. ILCD Handbook: Analysing of existing Environmental Impact Assessment methodologies for use in Life Cycle Assessment. First Edition. Ispra (VA) Italy. 115 pp.

Evans-Freeman, J. H. and A. R. Peaker, 2001. Chapter 7 - Erbium in silicon and silicon-germanium, in silicon-based material and devices, H. S. Nalwa, Editor. Academic Press: Burlington. 247-274.

Evodos Type 25, in Evodos Separation Excellence, E. NL, Editor 2013: Raamsdonksveer.

Fairbrother, L., Etschmann, B., Brugger, J., Shapter, J., Southam, G., and F. Reith, 2013. Biomineralization of gold in biofilms of *Cupriavidus metallidurans*. Environmental Science & Technology. 47(6): 2628-2635.

Falasco, E., Bona F., Ginepro M., Hlúbiková D., Hoffmann L., and L. Ector, 2009. Morphological abnormalities of diatom silica walls in relation to heavy metal. contamination and artificial growth conditions. South African Water Research Commission. Retrieved online on Dec. 23, 2015.

Falciatore, A. and C. Bowler, 2002. Revealing the molecular secrets of marine diatoms, In: Annual Review of Plant Biology. 109-130.

Falkowski, P. G., and J. A. Raven, 2007. Aquatic Photosynthesis: (Second Edition). Princeton University Press.

Fang, K., Fan, J., and G. Li, 2005. Contemporary multivariate analysis and design of experiments. New Jersey. World Scientific.

Farrant, P. A., Borowitzka, M. A., Hinde, R., and R. J. King, 1987. Nutrition of the temperate Australian soft coral Capnella gaboensis - I. Photosynthesis and carbon fixation. Marine Biology. 95(4): 565-574.

Fattakhova-Rohlfing, D., Zaleska, A., and T. Bein, 2014. Three-Dimensional Titanium Dioxide Nanomaterials. Chemical Reviews. 114(19): 9487-9558.

Feynman, R. P., 1959. In: Feynman, R. P., 1992. There's plenty of room at the bottom. Journal of Microelectromechanical Systems. 1(1): 60-66.

Fields, M. W., Hise, A., Lohman, E. J., Bell, T., Gardner, R. D., Corredor, L., Moll, K., Peyton, B. M., Characklis, G. W., and R. Gerlach, 2014. Sources and resources: Importance of nutrients, resource allocation, and ecology in microalgal cultivation for lipid accumulation. Applied Microbiology and Biotechnology. 98(11): 4805-4816.

Finkel, Z. V. and B. Kotrc, 2010. Silica use through time: Macroevolutionary change in the morphology of the diatom fustule. Geomicrobiology Journal. 27(6-7): 596-608.

Fitzpatrick, R., 2006. The atomic theory of matter. UTexas. Access Online: http://farside.ph.utexas.edu/teaching/sm1/lectures/node5.html

Fon Sing, S., Isdepsky, A., Borowitzka, M. A., and N. R. Moheimani, 2013. Production of biofuels from microalgae. Mitigation and Adaptation Strategies for Global Change, 18(1): 47-72.

Fourest, E., and B. Volesky, 1997. Alginate properties and heavy metal biosorption by marine algae. Applied Biochemistry and Biotechnology, 67(3): 215-226.

Francius, G., B. Tesson, E. Dague, V. Martin-Jézéquel and Y.F. Dufrêne. 2008. Nanostructure and nanomechanics of live *Phaeodactylum tricornutum* morphotypes. Environmental Microbiology 10: 1344–1356.

Freundlich, M. M., 1963. Origin of the Electron Microscope. Science 142(3589): 185-188.

Frischknecht R., Jungbluth N., Althaus H.-J., Doka G., Dones R., Heck T., Hellweg S., Hischier R., Nemecek T., Rebitzer G. and Spielmann M., 2005, The ecoinvent database: Overview and methodological framework, International Journal of Life Cycle Assessment 1, 3–9.

Fuhrmann, T., Landwehr, S., El Rharbi-Kucki, M., and M. Sumper, 2004. Diatoms as living photonic crystals. Applied Physics B, 78(3): 257-260.

Furey, P.C. and A. Liess, 2013. Substratum-associated microbiota. Water Environment Research. 85(10): 1786-1827.

Gale, D. K., Jeffryes, C., Gutu, T., Jiao, J., Chang, C., and G. L. Rorrer, 2011. Thermal annealing activates amplified photoluminescence of germanium metabolically doped in diatom biosilica. Journal of Materials Chemistry. 21(29): 10658-10665.

Gao, X., Y. Yu, and H. Wu, 2013. Life Cycle Energy and carbon footprints of microalgal biodiesel production in Western Australia: A comparison of by products utilization strategies. ACS Sustainable Chemistry & Engineering, 1(11): 1371-1380.

Garrels, R. M., 1989. Some factors influencing biomineralization in Earth history, in: Origin, evolution, and modern aspects of biomineralization in plants and animals, R.E. Crick, Editor. Springer.

Gaur, J. P. and C. Rai, 2001. Heavy metal tolerance in algae. In: Rai L.C., Gaur J.P. (eds) Algal adaptation to environmental stresses: 363-388. Springer, Berlin, Heidelberg.

Gautier, C., Livage, J., Coradin, T., and P. J. López, 2006. Sol-gel encapsulation extends diatom viability and reveals their silica dissolution capability. Chemical Communications (Cambridge), 2006(44): 4611-4613.

Gazit E., and A. Mitraki, 2013. Plenty of room for biology at the bottom: An introduction to bionanotechnology. 2nd Edition. Imperial College Press. London, U. K.

Gnansounou, E., and J. K. Raman, 2016. Life cycle assessment of algae biodiesel and its co-products, Applied Energy, 161(1):300-308.

Godhe, A., Asplund, M. E., Härnström, K., Saravanan, V., Tyagi, A., and I. Karunasagar, 2008. Quantification of diatom and dinoflagellate biomasses in coastal marine seawater samples by real-time PCR. Applied and Environmental Microbiology. 74(23): 7174-7182.

Goedkoop M. J., Heijungs R., Huijbregts M., De Schryver A., Struijs J., Van Zelm R, ReCiPe 2008, A life cycle impact assessment method which comprises harmonised category indicators at the midpoint and the endpoint level; First edition Report I: Characterization; 6 January 2009. Available online: http://www.lcia-recipe.net [Downloaded via link on June 27, 2016: https://sites.google.com/site/lciarecipe/file-cabinet/ReCiPe_main_report_REVISED_13-07-2012.pdf?attredirects=0]

Goedkoop, M., Heijungs, R., Huijbregts., M., De Schryver., A., Struijs., J., and R. van Zelm, 2013. ReCiPe 2008: A life cycle impact assessment method which comprises harmonized category indicators at the midpoint and the endpoint level. First edition (version 1.08) Report I: Characterization. May, 2013. Available online: https://sites.google.com/site/lciarecipe/file-cabinet/ReCiPe_main_report_MAY_2013.pdf?attredirects=0

Goho, A., 2004. Diatom menagerie: Engineering microscopic algae to produce designer materials. Science News, 166(3): 42-52.

González-Muñoz, M. T., Omar, N. B., Martínez-Cañamero, M., Rodríguez-Gallego, M., López A., and J. M. Arias, 1996. Struvite and calcite crystallization induced by cellular membranes of Myxococcus xanthus. Journal of Crystal Growth. 163(4): 434-439.

Google Scholar, 2017. Access online: https://scholar.google.com

Gordon, R., Losic D., Tiffany M. A., Nagy S. S., and F. A. Sterrenburg, 2009. The Glass Menagerie: diatoms for novel applications in nanotechnology. Trends in Biotechnology, 27(2): 116-127.

Gordon, R., Sterrenburg, F. A. S., and K. H. Sandhage, 2005. A special issue on diatom nanotechnology. Journal of Nanoscience and Nanotechnology. 5(1): 1-4.

Green, D. W., Lai, W. F., and H. S. Jung, 2014. Evolving marine biomimetics for regenerative dentistry. Marine Drugs. 12(5): 2877-2912.

Gribbin, J. and M. Gribbin (1997). Richard Feynman: a life in science. New York, Dutton. p. 170.

Griesshaber, E., Schmahl W. W., Neuser, R., Pettke, T., Blüm, M., Mutterlose, J., and U. Brand, 2007.Crystallographic texture and microstructure of terebratulide brachiopod shell calcite: An optimized materials design with hierarchical architecture. American Mineralogist. 92(5-6): 722-734.

Grigoriev I. V., Nordberg H., Shabalov I., Aerts A., Cantor M., Goodstein D., Kuo A., Minovitsky S., Nikitin R., Ohm R. A., Otillar R., Poliakov A., Ratnere I., Riley R., Smirnova T., Rokhsar D., and I. Dubchak, 2012. The Genome Portal of the Department of Energy Joint Genome Institute. Nucleic Acids Research. 40 (Database issue): D26-32.

Grill, E., Löffler, S., Winnacker, E.-L., and M. H. Zenk, 1989. Phytochelatins, the heavy-metal-binding peptides of plants, are synthesized from glutathione by a specific γ-glutamylcysteine dipeptidyl transpeptidase (phytochelatin synthase). Proceedings of the National Academy of Sciences of the United States of America, 86(18): 6838-6842.

Grill, E., Winnacker, E.-L., & Zenk, M. H. (1985). Phytochelatins: The principal heavy-metal complexing peptides of higher plants. Science, 230(4726), 674.

Group, V. Berkefel History. 2014 [cited 2014 September 2014]; Available from: http://www.berkefeld.com/en/company/history/.

Guillard, R. R. L., and P. E. Hargraves, 1993. *Stichochrysis immobilis* is a diatom, not a chrysophyte. Phycologia 32:234–6.

Guinee, J.B., 2002. Handbook on life cycle assessment operational guide to the ISO standards. Int J LCA. 7: 311.

Gutu, T., Gale, D. K., Jeffryes, C., Wang, W., Chang, C., Rorrer, G. L., and J. Jiao, 2009. Electron microscopy and optical characterization of cadmium sulphide nanocrystals deposited on the patterned surface of diatom biosilica. Journal of Nanomaterials. Article ID 860536. 1-7.

Hada, H., Yonezawa, Y., Yoshida, A., and A. Kurakake, 1976. Photoreduction of silver ion in aqueous and alcoholic solutions. The Journal of Physical Chemistry 80(25): 2728-2731.

Hamm, C. E., Merkel, R., Springer, O., Jurkojc, P., Maier, C., Prechtel, K., and V. Smetacek, 2003. Architecture and material properties of diatom shells provide effective mechanical protection. Nature. 421(6925): 841-843.

Hazelaar, S., Van Der Strate, H. J., Gieskes, W. W. C., and E. G. Vrieling, 2005. Monitoring rapid valve formation in the pennate diatom *Navicula salinarum* (Bacillariophyceae). Journal of Phycology. 41(2): 354-358.

He, J., Chen, D., Li, Y., Shao, J., Xie, J., Sun, Y., Yan, Z., and J. Wang, 2013. Diatom-templated TiO₂ with enhanced photocatalytic activity: biomimetics of photonic crystals. Applied Physics A. 113(2): 327-332.

Hecky, R. E., Mopper, K., Kilham, and P. E. T. Degens, 1973. The amino acid and sugar composition of diatom cell-walls. Marine Biology. 19: 323.

Heredia, A., Figueira, E., Rodrigues, C. T., Rodriguez-Galvan, A., Basiuk, V. A., Vrieling, E. G., and S. F. P. Almeida, 2012. Micromolar Cd²⁺ affects the growth, hierarchical structure and peptide composition of the biosilica of the freshwater diatom Nitzschia palea (Kutzing) W. Smith. Phycological research. 60(3): 229-240.

Hewakuruppu, Y. L., Dombrovsky, L. A., Chen, C., Timchenko, V., Jiang, X., Baek, S., and R. A. Taylor, 2013. Plasmonic "pump-probe" method to study semi-transparent nanofluids. Applied Optics. 52 (24): 6041–6050.

Hlúbiková, D., Luís, A. T., Vaché, V., Ector, L., Hoffmann, L., and P. Choquet, 2012. Optimization of the replica molding process of PDMS using pennate diatoms. Journal of Micromechanics and Microengineering. 22(11): 115019.

Hojer, M., Ahlroth, S., Dreborg, K.-H., Ekvall, T., Finnveden, G., Hjelm, O., Hochschorner, E., Nilsson, M., Palm, V., 2008. Scenarios in selected tools for environmental systems analysis. Journal of Clean Production, 16 (18): 1958e1970.

Holba, A. G., Dzou, L. I. P., Masterson, W. D., Hughes, W. B., Huizinga, B. J., Singletary, M. S., Moldowan, J. M., Mello, M. R., and E. Tegelaar, 1998. Application of 24-norcholestanes for constraining source age of petroleum. Organic Geochemistry. 29(5–7): 1269-1283.

Hornyak, G. L., Tibbals, H. F., Dutta, J., and J. J. Moore, 2008. Introduction to nanoscience and nanotechnology. CRC Press. Taylor & Francis Group. Boca Raton.

Hovland, E. K., Hancke, K., Alver, M. O., Drinkwater, K., Høkedal, J., Johnsen, G., Moline, M. and E. Sakshaug, 2014. Optical impact of an *Emiliania huxleyi* bloom in the frontal region of the Barents Sea. Journal of Marine Systems. 130: 228-240.

Howe, G., and S. Merchant, 1992. Heavy metal-activated synthesis of peptides in *Chlamydomonas* reinhardtii. Plant Physiology, 98(1): 127-136.

Hsu, S.-H., Paoletti, C., Torres, M., Ritchie, R. J., Larkum, A. W. D., and C. Grillet, 2012. Light transmission of the marine diatom *Coscinodiscus wailesii*. Proceedings SPIE 8339, Bioinspiration, Biomimetics, and Bioreplication 2012, 83390F.

Huang, P., Yang, D.-P., Zhang, C., Lin, J., He, M., Bao, L., and D. Cui, 2011. Protein-directed one-pot synthesis of Ag microspheres with good biocompatibility and enhancement of radiation effects on gastric cancer cells. Nanoscale. 3(9): 3623-3626.

Hübler, A. W. and O. Osuagwu, 2010. Digital quantum batteries: Energy and information storage in nanovacuum tube arrays. Complexity, 15: 48–55.

Hudnall, P.M., 2000. Hydroquinone. In: Ullmann's Encyclopedia of Industrial Chemistry. WileyVCH Verlag GmbH & Co, KGaA.

Hulkoti, N. I. and T. C. Taranath, 2014. Biosynthesis of nanoparticles using microbes—A review. Colloids and Surfaces B: Biointerfaces 121: 474–483

Hung, M. L. and H. W. Ma, 2009. Quantifying system uncertainty of life cycle assessment based on Monte Carlo simulation. International Journal of Life Cycle Assessment. 14:19-27.

Huntley, M. E. and D. G. Redalje, 2006. CO₂ Mitigation and Renewable Oil from Photosynthetic Microbes: A New Appraisal. Mitigation and Adaptation Strategies for Global Change. 12(4): 573-608.

Huysman, M. J. J., Vyverman, W., and L. De Veylder, 2014. Molecular regulation of the diatom cell cycle. Journal of Experimental Botany, 65(10): 2573-2584.

Ijima, S., 1991. Helical microtubules of graphitic carbon. Nature, 354(6348): 56-58.

Ingalls A. E., Whitehea K., and M. C. Bridoux, 2010. Tinted windows: The presence of the UV absorbing compounds called mycosporine-like amino acids embedded in the frustules of marine diatoms. Geochimica et Cosmochimica Acta. 74: 104–115.

International Standard Organization (ISO), 2006. Life cycle assessment. Principles and framework. ISO 14040. In: Environmental Management. International Organization for Standardization, Geneva.

Iravani, S. 2014. Bacteria in Nanoparticle Synthesis: Current status and future prospects. International Scholarly Research Notices. Article ID 359316, 18 pages

ISO. Nanotechnologies – Vocabulary part 1: Core terms. 2010. International Organization for Standardization (2010). ISO/TS 80004-1:2010. Retrieved from: https://www.iso.org/. Accessed: January 10, 2017.

Iwahori, K., Watanabe, J., Tani, Y., Seyama, H., and N. Miyata, 2014. Removal of heavy metal cations by biogenic magnetite nanoparticles produced in Fe(III)-reducing microbial enrichment cultures. Journal of Bioscience and Bioengineering. 117(3): 333-335.

Jain, P. K., Lee, K. S., El-Sayed, I. H., and M. A. El-Sayed, 2006. Calculated absorption and scattering properties of gold nanoparticles of different size, shape, and composition: Applications in biological imaging and biomedicine. Journal of Physical Chemistry B, 110(14): 7238-7248.

Jaroch, D., McLamore, E., Zhang, W., Shi, J., Garland, J., Banks, M. K., Porterfield, D. M., and J. L. Rickus, 2011. Cell-mediated deposition of porous silica on bacterial biofilms. Biotechnology and Bioengineering, 108(10): 2249-2260.

Jeffryes, C. S., 2009. Biological insertion of nanostructured germanium and titanium oxides into diatom biosilica, in chemical engineering. Oregon State University.

Jeffryes, C., Campbell, J., Li, H., Jiao, J., and G. L. Rorrer, 2011. The potential of diatom nanobiotechnology for applications in solar cells, batteries, and electroluminescent devices. Energy and Environmental Science. 4(10): 3930-3941.

Jeffryes, C., Gutu, T., Jiao, J., and G. L. Rorrer, 2008a. Metabolic insertion of nanostructured TiO₂ into the patterned biosilica of the diatom *Pinnularia* sp. by a two-stage bioreactor cultivation process. ACS Nano. 2(10): 2103-2112.

Jeffryes, C., Gutu, T., Jiao, J., and G. L. Rorrer, 2008b.Two-stage photobioreactor process for the metabolic insertion of nanostructured germanium into the silica microstructure of the diatom *Pinnularia* sp. Materials Science and Engineering C. 28(1): 107-118.

Jeffryes, C., Rosenberger, J., and G. L. Rorrer, 2013. Fed-batch cultivation and bioprocess modeling of *Cyclotella* sp. for enhanced fatty acid production by controlled silicon limitation. Algal Research. 2(1): 16-27.

Jiang, L., Wang, A., Zhao, Y., Zhang, J. and J. Zhu, 2004. A novel route for the preparation of monodisperse silver nanoparticles via a pulsed sonoelectrochemical technique. Inorganic Chemistry Communications 7(4): 506-509.

Johansen, J. R., 1991. Morphological variability and cell wall composition of *Phaeodactylum tricornutum* (Bacillarophyceae). Great Basin Naturalist 51(4): 310-315

Jones, V., 2007. Diatom Introduction. In Encyclopedia of Quaternary Science. 474-484.

Juzenas, P., Chen, W., Sun, Y.-P., Coelho, M. A. N., Generalov, R., Generalova, N., and I. L. Christensen, 2008. Quantum dots and nanoparticles for photodynamic and radiation therapies of cancer. Advanced drug delivery reviews. 60(15): 1600-1614.

Kalloniatis, M. and C. Luu, 2007. Visual Acuity. Webvision: The Organization of the Retina and Visual System. Available online: http://webvision.med.utah.edu/book/part-viii-gabac-receptors/visual-acuity [Retrieved: December 2016]

Kaplan, D., 2013. Absorption and adsorption of heavy metals by microalgae. In: Handbook of Microalgal culture. Richmond, A. (Ed.). Wiliey & Sons, Ltd. 602-661.

Kasama, T., Pósfai M., Chong, R. K. K., Finlayson, A. P., Buseck, P. R., Frankel, R. B., and R. E. Dunin-Borkowski, 2006. Magnetic properties, microstructure, composition, and morphology of greigite nanocrystals in magnetotactic bacteria from electron holography and tomography. American Mineralogist. 91(8-9): 1216-1229.

Kathiraven, T., Sundaramanickam, A., Shanmugam N., and T. Balasubramanian, 2015. Green synthesis of silver nanoparticles using marine algae *Caulerpa racemosa* and their antibacterial activity against some human pathogens. Applied Nanoscience 5(4): 499-504.

Kempe, S., J. ZKazmierczak, and E. T. Degens, 1989. The Soda Ocean concept and its bearing on biotic evolution, in: Origin, evolution, and modern aspects of biomineralization in plants and animals, R.E. Crick, Editor, Springer.

Kennish, T., 1996. Trace metal-sediment dynamics in estuaries: Pollution assessment. In: Reviews of environmental contamination and toxicology. Reviews of Environmental Contamination and Toxicology, 155: 69-110.

Kern, J. D., Hise, A. M., Characklis, G. W., Viamajala, R. G. S., and R. D. Gardner, 2017. Using life cycle assessment and techno-economic analysis in a real options framework to inform the design of algal biofuel production facilities, Bioresource Technology, 225: 418-428.

Kesarcodi-Watson, A., Kaspar, H., Lategan, M. J., and L. Gibson, 2008. Probiotics in aquaculture: The need, principles and mechanisms of action and screening processes. Aquaculture. 274(1): 1-14.

Kieu, K., Li, C., Fang, Y., Cohoon, G., Herrera, O. D., Hildebrand, M., Sandhage, K. H., and R. A. Norwood, 2014. Structure-based optical filtering by the silica microshell of the centric marine diatom *Coscinodiscus wailesii*. Optics Express. 22(13): 15992-15999

Kilham, S. S., Kreeger, D. A., Lynn, S. G., Goulden, C. E., and L., 1998. COMBO: A defined freshwater Kim, J. O. and C. W. Mueller, 1978. Introduction to factor analysis: What it is and how to do it. Beverly

Hills, CA: Sage.

Kim, S. D., Zhang, W. L., and H. J. Choi, 2014. Pickering emulsion-fabricated polystyrene-graphene oxide microspheres and their electrorheology. Journal of Materials Chemistry C. 2(36): 7541-7546.

Kim, S., Kim, D., Kim, H. J., Lee, Y. J., Hwang, S. S., and Baek, K. Y., 2012. Hybrid nanocomposite of CdSe quantum dots and a P3HT-b-PDMAEMA block copolymer for photovoltaic applications. In Materials Science Forum. 700: 120-124

Kim, W. J., Chun, W. Y., Park, J. S., and C. J. Lee, 2011. Characterization of Mortar Using Calcified Cell-CaCO₃ by Microbial Biomineralization. Structures Congress.

Kirschvink, J. L., Jones, D. S., and B. J. McFadden, 1996. Magnetite biomineralization and magnetoreception in organisms: A New Biomagnetism. 5.

Kleypas, J. A. and K. K. Yates, 2009. Coral reefs and ocean acidification. Oceanography, 22(SPL.ISS. 4): 108-117.

Kline, P., 1994. An easy guide to factor analysis. New York, NY: Routledge.

Knoll, A. H., 2003. The geological consequences of evolution. Geobiology, 1(1): 3-14.

Koch, P. and T. Salou, 2016. AGRIBALYSE®: Rapport Méthodologique – Version 1.3. November 2016. Ed. ADEME, Angers, France. 343 pp.

Kolinko, S., Richter, M., Glöckner, F.-O., Brachmann, A., and D. Schüler, 2016. Single-cell genomics of uncultivated deep-branching magnetotactic bacteria reveals a conserved set of magnetosome genes. Environmental Microbiology 18(1): 21-37.

Korbekandi, H., Iravani, S., and S. Abbasi, 2009. Production of nanoparticles using organisms Production of nanoparticles using organisms. Critical Reviews in Biotechnology, 29(4): 279-306.

Koumandou, V. L., Nisbet, R. E. R., Barbrook, A. C., and C. J. Howe, 2004. Dinoflagellate chloroplasts-where have all the genes gone? Trends in Genetics. 20(5): 261-7.

Krinsky, N. I., 1989. Antioxidant functions of carotenoids. Free Radic Biol Med, 7(6): 617-635.

Krishnaswamy, K. 2015. Green nanotechnology approach for synthesis and encapsulation of gold nanoparticles from agricultural waste. Doctoral Thesis. McGill University, Faculty of environmental and Agricultural Studies. Department of Bioresource Engineering.

Kröger, N. and N. Poulsen, 2005. Biosilica nanofabrication in diatoms: The structures and properties of regulatory silaffins. in 2005 MRS Spring Meeting. San Francisco, CA.

Kröger, N. and N. Poulsen, 2008a. Biochemistry and menetics of silica biomineralization in diatoms, in handbook of biomineralization: Biological aspects and structure formation. Wiley-VCH Verlag GmbH & Co. KGaA. 43-58.

Kröger, N. and N. Poulsen, 2008b. Diatoms-from cell wall biogenesis to nanotechnology. Annual Review of Genetics. 42: 83-107.

Kröger, N., 2007. Prescribing diatom morphology: toward genetic engineering of biological nanomaterials. Current Opinion in Chemical Biology, 11(6): 662-669.

Kroto, H. W., Heath, J. R., O'Brien, S. C., Curl, R. F., and R. E. Smalley, 1985. C 60: buckminsterfullerene. Nature, 318(6042): 162-163.

Lang, C. and D. Schüler, 2008. Expression of green fluorescent protein fused to magnetosome proteins in microaerophilic magnetotactic bacteria. Applied and Environmental Microbiology. 74(15): 4944-4953.

Lang, Y., Monte, F. d., Rodriguez, B. J., Dockery, P., Finn, D. P., and A. Pandit, 2013. Integration of TiO₂ into the diatom *Thalassiosira weissflogii* during frustule synthesis. Scientific Reports. 3: 3205.

Lardon L., Hélias, A., Sialve, B., Steyer, J-P., and O. Bernard, 2009. Life-Cycle Assessment of biodiesel production from microalgae. Environmental Science & Technology 43 (17): 6475-6481.

Lautier, A., R. K. Rosenbaum, M. Margni, J. Bare, P.-O. Roy and L. Deschênes, 2010. Development of normalization factors for Canada and the United States and comparison with European factors. Science of The Total Environment 409(1): 33-42.

Lavens, P. and P. Sorgeloos, Ed. 1996. Manual on the production and use of live food for aquaculture. FAO Fisheries Technical Paper.

Lebeau, T. and J. M. Robert, 2003. Diatom cultivation and biotechnologically relevant products. Part II: Current and putative products. Applied Microbiology and Biotechnology. 60(6): 624-632.

Lee, D., Wang, W., Gutu, T., Jeffryes, C., Rorrer, G. L., Jiao, J., and C. Chang, 2008. Biogenic silica based $Zn_2SiO_4:Mn^{2+}$ and $Y_2SiO_5:Eu^{3+}$ phosphor layers patterned by inkjet printing process. Journal of Materials Chemistry. 18(31): 3633.

Lee, M., 2014. Remarkable Natural Material Surfaces and Their Engineering Potential.

Lefebvre D. D. and C. Edwards, 2009. Decontaminating heavy metals from water using photosynthetic microbes. In: Shah, V. (Ed.) Emerging Environmental Technologies, Volume II. Springer London. 57-73

Lenz, M., Kolvenback, B., Gygax, B., Moes, S., and P. F. X. Corvini, 2011. Shedding light on selenium biomineralization: Proteins associated with bionanominerals. Applied and Environmental Microbiology. 77(13): 4676-4680.

Leonardi, P. I., Popovich, C. A., and M. C. Damiani, 2011. Feedstocks for second-generation biodiesel: Microalgae's biology and oil composition, in economic effects of biofuel production, M.A.D.S. Bernardes, Editor. InTech: Rijeka, Croatia. 452.

Lewin, J. C, 1958. The taxonomic position of *Phaeodactylum tricornutum*. Journal of Geneneral Microbiology 18: 427–432.

Lewin, J., 1966. Silicon Metabolism in Diatoms. V. Germanium Dioxide, a Specific Inhibitor of Diatom Growth. Phycologia. 6(1): 1-12.

Li, J., Benzerara, K., Bernanrd, S., and O. Beyssac, 2013. The link between biomineralization and fossilization of bacteria: Insights from field and experimental studies. Chemical Geology, 359(0): 49-69.

Li, J., Pan, Liu, Y., Yu-Zhang, Q., Menguy, K., Che, N., Qin, R., Lin, H., Wu, W., Petersen, W., N., and X. Yang, 2010. Biomineralization, crystallography and magnetic properties of bullet-shaped magnetite magnetosomes in giant rod magnetotactic bacteria. Earth and Planetary Science Letters. 293(3-4): 368-376.

Li, S. S. and H. J. Tsai, 2009. Transgenic microalgae as a non-antibiotic bactericide producer to defend against bacterial pathogen infection in the fish digestive tract. Fish and Shellfish Immunology. 26(2): 316-325.

Liang Zhu, Y., Pilon-Smits, E. A. H., Jouanin, L., and N. Terry, 1999. Overexpression of glutathione synthetase in Indian mustard enhances cadmium accumulation and tolerance. Plant Physiology, 119: 73-80.

Liang, A., Paulo, C., Zhu, Y., & Dittrich, M., 2013. CaCO₃ biomineralization on cyanobacterial surfaces: Insights from experiments with three *Synechococcus* strains. Colloids and Surfaces B: Biointerfaces, 111: 600-608.

Likhoshway, Y. V., Sorokovikova, E. G., Belykh, O. I., Kaluzhnaya, O. L. V., Belikov, S. I., Bedoshvili, Y. D., Kaluzhnaya, O. K. V., Masyukova J. A., and T. A. Sherbakova, 2008. Visualization of the silicon biomineralization in cyanobacteria, sponges and diatoms. In: Biosphere origin and evolution. N. Dobretsov, N. Kolchanov, A. Rozanov and G. Zavarzin. (Eds.) Boston, MA, Springer US: 219-230.

Liu, H. and C. J. Wu, 2016. Effect of silica content of diatom prey on the production, decomposition and sinking of fecal pellets of the copepod *Calanus sinicus*. Biogeosciences. 13: 4767-4775.

Liu, J. and M. Antonietti, 2013. Bio-inspired NADH regeneration by carbon nitride photocatalysis using diatom templates. Energy & Environmental Science. 6(5): 1486.

Liu, J., Cazelles, R., Chen, Z. P., Zhou, H., Galarneau, A., and M. Antonietti, 2014. The bioinspired construction of an ordered carbon nitride array for photocatalytic mediated enzymatic reduction. Physical Chemistry Chemical Physics. 16(28): 14699-14705.

Liu, S., 2005, Characterization of silicon-germanium nanocomposites fabricated by the marine diatom *Nizschia frustulum*. Oregon State University.

Livingston, B. T., Killian, C. E., Wilt, F., Cameron, A., Landrum, M. J., Ermolaeva, O., Sapojnikov, V., Maglott, D. R., Buchanan, A. M., and C. A. Ettensohn, 2006. A genome-wide analysis of biomineralization-related proteins in the sea urchin *Strongylocentrotus purpuratus*. Developmental Biology. 300(1): 335-348.

Lloyd, J.R., Pearce, C. I., Coker, V. S. van der Laan, G., Cutting, R., Vaughan, D. J., Paterson-Beedle, M., Mikheenko, I. P., Yong, P., and L. E. Macaskie, 2008. Biomineralization: Linking the fossil record to the production of high value functional materials. Geobiology. 6(3): 285-297.

Lo, S. C., Ma, H. W., and S. L. Lo, 2005. Quantifying and reducing uncertainty in life cycle assessment using the Bayesian Monte Carlo method, Science of The Total Environment, 340 (1–3): 23-33.

Lockwood, D. J. and L. Pavesi, 2004. Silicon fundamentals for photonics applications, in silicon photonics, Topics, L. Pavesi and D. J. Lockwood, Editors. Springer: Berlin.

Loeffler, S., Hochberger, A., Grill, E., Winnacker, E. L., and M. H. Zenk, 1989. Termination of the phytochelatin synthase reaction through sequestration of heavy metals by the reaction product, FEBS Letters, Volume 258(1): Pages 42-46

López P. J., Descles J., Allen A.E., and C. Bowler, 2005. Prospects in diatom research. Current Opinion in Biotechnology 16: 180–186.

Losic D., Rosengarten G., Mitchell J. G., and N. H. Voelcker, 2006a. Pore architecture of diatom frustules: Potential nanostructured membranes for molecular and particle separations. Journal of Nanoscience and Nanotechnology 6: 982–989.

Losic, D., Mitchell, J. G., and N. H. Voelcker, 2005. Complex gold nanostructures derived by templating from diatom frustules. Chemical Communications (Cambridge) (39): 4905-7.

Losic, D., Mitchell, J. G., and N. H. Voelcker, 2006b. Fabrication of gold nanostructures by templating from porous diatom frustules. New Journal of Chemistry. 30(6): 908.

Losic, D., Mitchell, J. G., Lal, R., and N. H. Voelcker, 2007a. Rapid Fabrication of Micro- and Nanoscale Patterns by Replica Molding from Diatom Biosilica. Advanced Functional Materials. 17(14): 2439-2446.

Losic, D., Rosengarten, G., Mitchell, J. G., and N. H. Voelcker, 2006c. Pore architecture of diatom frustules: Potential nanostructured membranes for molecular and particle separations. Journal of Nanoscience and Nanotechnology. 6(4): 982-989.

Losic, D., Short, K., Mitchell, J. G., Lal, R., N. H. Voelcker, 2007b. AFM nanoindentations of diatom biosilica surfaces. Langmuir, 23(9): 5014-5021.

Losic, D., Triani, G., Evans, P. J., Atanacio, A., Mitchell, J. G., and N. H. Voelcker, 2006d Controlled pore structure modification of diatoms by atomic layer deposition of TiO₂. Journal of Materials Chemistry. 16(41): 4029-4034.

Lowenstam, H. A., 1981. Minerals formed by organisms. Science. 211(4487): 1126-1131.

Luef, B., Fakra, S. C., Csencsits, R., Wrighton, K. C., Williams, K. H., Wilkins, M. J., Downing, K. H., Long, P. E., Comolli, L. R., and J. F. Banfield, 2013. Iron-reducing bacteria accumulate ferric oxyhydroxide nanoparticle aggregates that may support planktonic growth. ISME Journal. 7(2): 338-350.

Lutz, K., Gröger, C., Sumper, M., and E. Brunner, 2005. Biomimetic silica formation: analysis of the phosphate-induced self-assembly of polyamines. Physical Chemistry Chemical Physics. 7(14): 2812-2815.

Lyshevski, S. E., 2005. Nano- and micro-electromechanical systems: Fundamentals of nano- and microengineering, Second Edition, CRC Press. pp.: 23.

Mafuné, F., Kohno, J.-Y., Takeda, Y., Kondow, T., and H. Sawabe, 2000. Structure and Stability of Silver Nanoparticles in Aqueous Solution Produced by Laser Ablation. The Journal of Physical Chemistry B 104(35): 8333-8337.

Makarov, V. V., Love, A. J., Sinitsyna, O. V., Makarova, S. S., Yaminsky, I. V., Taliansky, M. E., and N. O. Kalinina, 2014. "Green" Nanotechnologies: Synthesis of Metal Nanoparticles Using Plants. Acta Naturae 6(1): 35-44.

Malhotra, A., Dolma, K., Kaur, N., Rathore, Y. S., Ashish, Mayilraj, S., and A. R. Choudhury, 2013. Biosynthesis of gold and silver nanoparticles using a novel marine strain of Stenotrophomonas. Bioresource Technology. 142: 727-731.

Malpas, J., "Donald Davidson", The Stanford Encyclopedia of Philosophy (Winter 2012 Edition), Edward N. Zalta (Ed.), [Accessed online: December 2016] URL: https://plato.stanford.edu/archives/win2012/entries/davidson/

Mandal D., Bolander M. E., Mukhopadhyay D., Sarkar G., and P. Mukherjee, 2006. The use of microorganisms for the formation of metal nanoparticles and their application. Applied Microbiology and Biotechnology. 69: 485–492

Mann, D.G. Life cycle of a centric diatom. II: The sexual phase. 2007. [cited: September 28, 2013]; Available from: http://rbg-web2.rbge.org.uk/algae/auxospores/lifecycle_sexual.html.

Mao, L., Liu, J., Zhu, S., Zhang, D., Chen, Z., and C. Chen, 2014. Sonochemical fabrication of mesoporous TiO₂ inside diatom frustules for photocatalyst. Ultrasonics Sonochemistry. 21(2): 527-34.

Marcinko, C. L. J., Painter, S. C., Martin, A. P., and J. T. Allen, 2013. A review of the measurement and modelling of dinoflagellate bioluminescence. Progress in Oceanography, 109, 117-129.

Martin-Jézéquel, V., and P. J. López, 2003. Silicon - a central metabolite for diatom growth and morphogenesis. In: Muller WEG, ed. Silicon biomineralization: Biology, Biochemistry, Molecular Biology, Biotechnology. Heidelberg: Springer Verlag, 99–124.

Martin, C. P., Blunt, M. O., Vaujour, E., Fahmi, A., D'Aléo, A., De Cola, L., Vögtle, F., and P. Moriarty, 2008. Chapter 1. Self-organised nanoparticle assemblies: A panoply of patterns, in studies in multidisciplinarity, N. Krasnogor, et al., Editors. 5: 1-20.

Martin, R.E., 1996. Biomineralization and endosymbiosis in foraminifera in response to ocean chemistry. Paleontological Journal. 30(6): 662-668.

Masmoudi, S., Nguyen-Deroche, N., Caruso, A., Ayadi, H., Morant-Manceau, A., Tremblin, G., Bertrand, M., and B. Schoefs, 2013. Cadmium, copper, sodium and zinc effects on diatoms: from heaven to hell — a review. Cryptogamie, Algologie 34 (2): 185-225

Mather, L., Ehrman, J. M., and I. Kaczmarska, 2014. Silicification of auxospores in the araphid diatom *Tabularia fasciculata* (Bacillariophyta). European Journal of Protistology. 50(1): 1-10.

Matsunaga, T., Suzuki, T., Tanaka, M. and A. Arakaki, 2007. Molecular analysis of magnetotactic bacteria and development of functional bacterial magnetic particles for nano-biotechnology. Trends in Biotechnology. 25(4): 182-188.

Mazumder, N., Gogoi, A., Buragohain, A. K., Ahmed, G. A., & Choudhury, A. (2014). Structural and optical characterization of fresh water diatoms (*Cyclotella* sp.): nature's nanoporous silica manufacturing plant. Proceedings SPIE 8996, Quantum Dots and Nanostructures: Synthesis, Characterization, and Modeling XI, 89960Y

McConville, M. J., Wetherbee R., and A. Bacic, 1999. Subcellular location and composition of the wall and secreted extracellular sulphated polysaccharides/proteoglycans of the diatom *Stauroneis amphioxys* Gregory. Protoplasma 206: 188–200.

McFarlane, G. R. and M. D. Burchett, 2000. Cellular distribution of copper, lead and zinc in the grey mangrove, *Avicennia marina* (Forks.) Vierh. Aquatic Botany, 68 (1): 45-59.

McGinnis, K. M., Dempster, T. A., and M. R. Sommerfeld, 1997. Characterization of the growth and lipid content of the diatom *Chaetoceros muelleri*. Journal of Applied Phycology. 9(1): 19-24.

McGinty, E. S., Pieczonka, J., and L.D. Mydlarz, 2012. Variations in reactive oxygen release and antioxidant activity in multiple *Symbiodinium* types in response to elevated temperature. Microb Ecol, 64(4): 1000-7.

Medlin, L. K., 2009. The use of the terms centric and pennate. Diatom Research. 24(2): 499-501.

Medlin, L. K., Williams, D. M. and P. A. Sims, 1993. The evolution of the diatoms (Bacillariophyta). I. Origin of the group and assessment of the monophyly of its major divisions. European Journal of Phycology. 28(4): 261-275.

Metzler, R. A., Kim, I. W., Evans, J. S., Zhou, D., Beniash, E., Wilt., F., Abrecth, M., Chiou, J. W., Guo, J., Coopersmith, S. N., and P. U. Gilbert, 2008. Probing the organic-mineral interface at the molecular level in model biominerals. Langmuir. 24(6): 2680-2687.

Miao, A. J., Luo, Z., Chen, C. S., Chin, W.-C., Santschi, P. H., and A. Quigg, 2010. Intracellular uptake: A possible mechanism for silver engineered nanoparticle toxicity to a freshwater alga *Ochromonas danica*. PLOS ONE, 5(12): e15196.

Mock, T. and L. K. Medlin, 2012. Genomics and genetics of diatoms, in Advances in Botanical Research. 245-284.

Mohan, S.V. and A. Pandey, 2013. Biohydrogen Production: 1-24.

Moheimani, N. R., Isdepsky, A., Lisec, J., Raes, E., and A. Borowitzka, 2011. Coccolithophorid algae culture in closed photobioreactors. Biotechnology and Bioengineering. 108(9): 2078-2087.

Moheimani, N. R., Webb, J.P., and M. A. Borowitzka, 2012. Bioremediation and other potential applications of coccolithophorid algae: A review. Algal Research. 1(2): 120-133.

Moisescu, C., Ardelean, I. I., and L. G. Benning, 2014. The effect and role of environmental conditions on magnetosome synthesis. Frontiers in Microbiology. 5(FEB).

Montgomery, D. C. 2009. Design and analysis of experiments (7th edition) Hoboken. John Wiley & Sons.

Montsant A., Maheswari U., Bowler C., P. J. López, 2005. Diatomics: toward diatom functional genomics. Journal of Nanoscience and Nanotechnology 5: 5–14.

Moore, G. E., 1965. Cramming more components onto integrated circuits. Electronics. 38(8): 114 ff.

Morelli, E., Salvadori, E., Basso, B., Tognotti, D., Cioni, P., and E. Gabellieri, 2015. The response of *Phaeodactylum tricornutum* to quantum dot exposure: Acclimation and changes in protein expression. Marine Environmental Research, 111: 149-157

Mu, D., Ruan, R., Addy, M., Mack, S., Chen, P., and Y. Zhou, 2017. Life cycle assessment and nutrient analysis of various processing pathways in algal biofuel production, Bioresource Technology, 230: 33-42.

Müller, E. W., 1936. Die Abhängigkeit der Feldelektronenemission von der ustrittsarbeit. Zeitschrift für Physik. 102(11): 734-761.

Müller, E. W., 1951. Das Feldionenmikroskop. Zeitschrift für Physik. 131(1):136-142

Müller, W. E. G. (Ed.), 2011. Molecular Biomineralization: Aquatic Organisms Forming Extraordinary Materials. Springer Berlag. 52.

Mulvaney, P. 1996. Surface plasmon spectroscopy of nanosized metal particles. Langmuir, 12(3): 788-800.

Muse, J. O., Stripeikis, J.D., Fernández, F.M., d'Huicque, L., Tudino, M.B, Carducci, C.N., and O.E. Troccoli, 1999. Seaweeds in the assessment of heavy metal pollution in the Gulf San Jorge, Argentina. Environmental Pollution, 104 (2): 315-322.

Myers, R. H., 1971. Response surface methodology. Boston: Allyn and Bacon, Inc.

Naik, R. R., Stringer, S. J., Agarwal, G., Jones, S. E., and M. O. Stone, 2002. Biomimetic synthesis and patterning of silver nanoparticles. Nat Mater, 1(3): 169-172.

Naja, G. and B. Volesky, 2011. The mechanism of metal cation and anion biosorption. In: Microbial Biosorption of Metals (eds P. Kotrba, M. Mackova & T. Macek), Springer, Dordrecht. pp. 19–58.

Naka, K., 2007. Biomineralization I: Crystallization and Self-Organization Process. 270.

Nakatsu, T., Ravi, B. N., and D. J. Faulkner, 1981. Antimicrobial constituents of *Udotea flabellum*. Journal of Organic Chemistry. 46(12): 2435-2438.

Nam, D., Lee, B., Eom, I., Kim, P., and M. Yeo, 2014. Uptake and bioaccumulation of titanium- and silver-nanoparticles in aquatic ecosystems. Molecular & Cellular Toxicology. 10(1): 9-17.

Narayanan, K. B. and N. Sakthivel, 2010. Biological synthesis of metal nanoparticles by microbes. Advances in Colloidal and Interface Science.156: 1-13

National Nanotechnology Initiative, 2016. Official website of the United States National Nanotechnology Initiative (NNI). Accessed online [December 15]: https://www.nano.gov/about-nni/what

Nature Nano. Editorial. 2014. Bringing solar cell efficiencies into the light. Nature Nano. 9(9): 657-657.

Nelson, D. M., Tréguer, P., Brzezinski, M. A., Leynaert, A., and B. Quéguiner, 1995. Production and dissolution of biogenic silica in the ocean: Revised global estimates, comparison with regional data and relationship to biogenic sedimentation. Global Biogeochemical Cycles. 9(3): 359-372.

Ni, W., J. Chen, and Q. Xu, 2008. Synthesis and characterization of hierarchically porous silica with poplar tissue as template with assistance of supercritical CO₂. BioResources. 3(2): 461-476.

Niemi, G. J. and M. E. McDonald, 2004. Application of ecological indicators, in Annual Review of Ecology, Evolution, and Systematics. 89-111.

Nishikawa, H. Editor., 2001. Chapter 3 - Structures and properties of amorphous silicon dioxide—Issues on the reliability and novel applications, in silicon-based material and devices, H. S. Nalwa, Academic Press: Burlington. 93-122.

Nobel Media, 2017. The Official Web Site of the Nobel Prize: http://www.nobelprize.org

Nordberg H., Cantor M., Dusheyko S., Hua S., Poliakov A., Shabalov I., Smirnova T., Grigoriev I. V., and I. Dubchak, 2014. The genome portal of the Department of Energy Joint Genome Institute: 2014 updates. Nucleic Acids Research. 42(1): D26-31.

Norris, D. J., 2007. Materials science: Silicon life forms. Nature, 446(7132): 146-147.

Norton, T. A., Melkonian, M., and R. A. Andersen, 1996. Algal biodiversity. Phycologia, 35 (4): 308-326

Not, F., et al., 2012. Diversity and Ecology of Eukaryotic Marine Phytoplankton, in Advances in Botanical Research. p. 1-53.

Nowack, B., Krug, H. F., and M. Height, 2011. 120 Years of nanosilver history: Implications for policy makers. Environmental Science & Technology 45(4): 1177-1183.

Okuda, M., Suzumoto, Y., Iwahori, K., Kang, S., Uchida, M., Douglas, T., and I. Yamashita, 2010. Biotemplated CdSe nanoparticle synthesis in a cage shaped protein, Listeria-Dps, and their two-dimensional ordered array self-assembly. Chemical Communications. 46(46): 8797-8799.

Olguín, E. J. and G. Sánchez-Galván, 2012. Heavy metal removal in phytofiltration and phycoremediation: The need to differentiate between bioadsorption and bioaccumulation. New Biotechnology. 30(1): 3-8.

Pacioni, N. L., Borsarelli, C. D., Rey, V., and A. V. Veglia, 2015. Synthetic routes for the preparation of silver nanoparticles: A mechanistic perspective. In: Alarcon, E. I., Griffith, M., and K. I. Udekwu (Eds.), 2015. Silver Nanparticle Applications, Engineering Materials, Springer International Publishing Switzerland. pp: 13-46.

Paciotti, G. F., Myer, L., Weinreich, D., Goia, D., Pavel, N., McLaughlin, and R. E., Tamarkin, L. 2004. Colloidal gold: A novel nanoparticle vector for tumor directed drug delivery. Drug Delivery: Journal of Delivery and Targeting of Therapeutic Agents, 11(3): 169-183.

Pan, Y., Stevenson, R. J., Hill, B. H., Herlihy, A. T., and G. B. Collins, 1996. Using diatoms as indicators of ecological conditions in lotic systems: A regional assessment. Journal of the North American Benthological Society. 15(4): 481-495.

Parker, A. R. and H. E. Townley, 2007. Biomimetics of photonic nanostructures. Nature Nanotechnology, 2: 347-353.

Parker, A. R., 2012. Natural photonic structures: An overview, in optical biomimetics: Materials and applications. Elsevier Inc. 1-19.

Parkinson J. and R. Gordon, 1999. Beyond micromachining: the potential of diatoms, Trends in Biotechnology, Volume 17, (5): Pages 190-196

Pastoriza-Santos, I. and L. M Liz-Marzán, 1999. Formation and stabilization of silver nanoparticles through reduction by N, N-dimethylformamide. Langmuir 15, 948–951.

Pastoriza-Santos, I. and L. M. Liz-Marzán, 2002. Synthesis of silver nanoprisms in DMF. Nano Letters. 2(8): 903–905.

Patakfalvi, R. and I. Dekany, 2005. Nucleation and growth of silver nanoparticles monitored by titration microcalorimetry. Journal of Thermal Analysis and Calorimetry 79(3): 587-594.

Patel, A., Barrington, S., and M. Lefsrud, 2012. Microalgae for phosphorus removal and biomass production: a six-species screen for dual-purpose organisms. GCB Bioenergy. 4(5): 485-495.

Patil, V., Källqvist, T., Olsen, E., Vogt, G. and H. R. Gislerød, 2007. Fatty acid composition of 12 microalgae for possible use in aquaculture feed. Aquaculture International. 15(1): 1-9.

Patwardhan, S. V., Clarson, S. J., and C. C. Perry, 2005. On the role(s) of additives in bioinspired silicification. Chemical Communications (Cambridge) (9): 1113-21.

Paul, S. and A. Chugh, 2011. Assessing the role of Ayurvedic 'Bhasms' as ethno-nanomedicine in the metal based nanomedicine patent regime. Journal of Intellectual Property Rights, 16, 509-515.

Peng, G., Tisch, U., Adams, O., Hakim, M., Shehada, N., Broza, Y.Y., Billan, S., Abdah-Bortnyak, R., Kuten, A., Haick, H. 2009. Diagnosing lung cancer in exhaled breath using gold nanoparticles. Nature Nanotechnology, 4(10): 669-673.

Pennesi, C., Totti, C., and F. Beolchini, 2013. Removal of vanadium(III) and molybdenum(V) from wastewater using *Posidonia oceanica* (Tracheophyta) biomass. PLoS One. 8(13): e76870.

Perales-Vela H. V., Peña Castro J. M., and R. O. Cañizares-Villanueva, 2006. Heavy metal detoxification in eukaryotic microalgae. Chemosphere 64:1-10

Pérez, M. A., Moiraghi, R., Coronado, E. A., and V. A. Macagno, 2008. Hydroquinone synthesis of silver nanoparticles: A simple model reaction to understand the factors that determine their nucleation and growth. Crystal Growth & Design 8(4): 1377-1383.

Perkins, D., 2002. Mineralogy. Upper Saddle River, N. J. Prentice Hall.

Perry, C. C., 2003. Silicification: The processes by which organisms capture and mineralize silica. Reviews in Mineralogy and geochemistry 54 (1): 291-327

Pickett-Heaps, J. D., Wetherbee, R., and D. R. A. Hill, 1988. Cell division and morphogenesis of the labiate process in the centric diatom *Ditylum brightwellii*. Protoplasma. 143(2-3): 139-149.

Pietak, A., Sayer, M., and M. J. Stott, 2004. Crystallization kinetics of Si-TCP bioceramic films. Journal of Materials Science, 39(7): 2443-2449.

Pillai, Z. S. and P. V. Kamat, 2004. What factors control the size and shape of silver nanoparticles in the citrate ion reduction method? The Journal of Physical Chemistry B 108, 945–951.

Pinto, E., Sigaud-kutner, T. C. S., Leitão, M. A. S., Okamoto, O. K., Morse, D., and P. Colepicolo, 2003. Heavy metal-induced oxidative stress in algae. Journal of Phycology, 39(6): 1008-1018.

Pistocchi R., Mormile M. A., Guerrini F., Isani G., and L. Boni, 2000. Increased production of extra- and intracellular metal-ligands in phytoplankton exposed to copper and cadmium. Journal of Applied Phycology. 12 (3): 469–477

Pokrovsky, O. S., Pokrovski, G. S., Gélabert, A., Schott, J., and A. Boudou, 2005. Speciation of Zn associated with diatoms using X-ray absorption spectroscopy. Environmental Science & Technology. 39(12): 4490-4498.

Pollock, F. M. and J. D. Pickett-Heaps, 2005. Spatial determinants in morphogenesis: Recovery from plasmolysis in the diatom *Ditylum*. Cell Motility and the Cytoskeleton. 60(2): 71-82.

Polte, J., Tuaev, X., Wuithschick, M., Fischer, A., Thuenemann, A. F., Rademann, K., Kraehnert, R., and F. Emmerling, 2012. Formation mechanism of colloidal silver nanoparticles: analogies and differences to the growth of gold nanoparticles. ACS Nano 6(7): 5791–5802.

Pouget, E., Dujardin, E., Cavalier, A., Moreac, A., Valery, C., Marchi-Artzner, V., Weiss, T., Renault, A., Paternostre, M., and F. Artzner, 2007. Hierarchical architectures by synergy between dynamical template self-assembly and biomineralization. Nature Materials. 6(6): 434-439.

Poulsen, N. and N. Kroger, 2004. Silica morphogenesis by alternative processing of silaffins in the diatom *Thalassiosira pseudonana*. Journal of Biological Chemistry. 279(41): 42993-9.

Poulsen, N., Scheffel. A., Sheppard, V. C., Chesley, P. M., and N. Kröger, 2013. Pentalysine clusters mediate silica targeting of silaffins in *Thalassiosira pseudonana*. Journal of Biological Chemistry. 288(28): 20100-20109.

Prozorov, T., Bazylinski, D. A., Mallapragada, S. K., and R. Prozorov, 2013. Novel magnetic nanomaterials inspired by magnetotactic bacteria: Topical review. Materials Science and Engineering: R: Reports, 74(5): 133-172.

Prozorov, T., Palo, P., Wang, L., Nilsen-Hamilton, M., Jones, D., Orr, D., Mallapragada, S. K., Narasimhan, B., Canfield, P. C., and R. Prozorov, 2007. Cobalt ferrite nanocrystals: Out-performing magnetotactic bacteria. ACS Nano. 1(3): 228-233.

Rabalais, N.N., Turner, R., Justić, D., Dortch, Q., Wiseman, W., and B. K. Sen Gupta, 1996. Nutrient changes in the Mississippi river and system responses on the adjacent continental shelf. Estuaries. 19(2 B): 386-407.

Ragueneau, O., Schultes, S., Bidle, K., Claquin, P., and B. Moriceau, 2006. Si and C interactions in the world ocean: Importance of ecological processes and implications for the role of diatoms in the biological pump. Global Biogeochemical Cycles. 20(4).

Rai M., Yadav A., and A. Gade, 2009. Silver nanoparticles as a new generation of antimicrobials. Biotechnology Advances 27:76–83

Rai, P. K., 2009. Heavy metal phytoremediation from aquatic ecosystems with special reference to macrophytes. Critical Reviews in Environmental Science and Technology. 39(9): 697-753.

Ramachandra, T. V., Mahapatra, D. M., and B. Karthick, 2009. Milking diatoms for sustainable energy: Biochemical engineering versus gasoline-secreting diatom solar panels. Industrial and Engineering Chemistry Research. 48(19): 8769-8788.

Ray-Mukherjee, J., Nimon, K., Mukherjee, S., Morris, D. W., Slotow, R., and M. Hamer, 2014. Using commonality analysis in multiple regressions: a tool to decompose regression effects in the face of multicollinearity. Methods in Ecology and Evolution. 5: 320-328.

Ray, C. P., Yu, H., and P. P. Fu, 2010. Toxicity and environmental risks of nanomaterials: Challenges and future needs. Journal of Environmental Science and Health, Part C. Environmental Carcinogenesis and Ecotoxicology Reviews. 2009. 27(1): 1-35.

Redmond, F., 2014. Demonax, Hellenic Library. Access Online: http://www.demonax.info/doku.php

Reece, S. Y., Hamel, J. A., Sung, K., Jarvi, T. D., Esswein, A. J., Pijpers, J. J. H., and D. G. Nocera, 2011. Wireless solar water splitting using silicon-based semiconductors and earth-abundant catalysts. Science, 334(6056): 645-648.

Reid, B. T. and S. M. Reed, 2016. Improved methods for evaluating the environmental impact of nanoparticle synthesis. Green Chemistry. 18, 4263-4269.

Reisse, J., Francois, H., Vandercammen, J., Fabre, O., Kirsch-de Mesmaeker, A., Maerschalk, C., and J. L. Delplancke, 1994. Sonoelectrochemistry in aqueous electrolyte: A new type of sonoelectroreactor. Electrochimica Acta 39(1): 37-39.

Ren, F., Camppbell, J., Wang, X., Rorrer, G. L., and A. X. Wang, 2013. Enhancing surface plasmon resonances of metallic nanoparticles by diatom biosilica. Optics Express. 21(13): 15308-15313.

Rentsch, C., Rentsch, B., Heinemann, S., Bernhardt, R., Bischoff, B., Förster, Y., Scharnweber, D., and S. Rammelt, 2014. ECM inspired coating of embroidered 3D scaffolds enhances *Calvaria* bone regeneration. BioMed Research International, (2014) Article ID 217078.

Richards, R. G. and B. J. Mullins, 2013. Using microalgae for combined lipid production and heavy metal removal from leachate. Ecological Modelling, 249: 59-67.

Richmond, A. (Ed.), 2004. Handbook of Microalgal Culture: Biotechnology and Applied Phycology.

Roberts, S. and J. W. Murray, 1995. Characterization of cement mineralogy in agglutinated foraminifera (Protista) by Raman spectroscopy. Journal - Geological Society (London). 152(1): 7-9.

Rodríguez-Gattorno, G., Díaz, D., Rendón, L., and G. O. Hernández-Segura, 2002. Metallic nanoparticles from spontaneous reduction of silver(I) in DMSO. Interaction between nitric oxide and silver nanoparticles. The Journal of Physical Chemistry B 106(10): 2482-2487.

Rodríguez, J. A. and M. Fernández-García, 2007. Synthesis, properties, and applications of oxide nanomaterials, Wiley.

Rose, D. T. and E. J. Cox, 2013. Some diatom species do not show a gradual decrease in cell size as they reproduce. Fundamental and Applied Limnology. 182(2): 117-122.

Rosen, B. 1996. Bacterial resistance to heavy metals and metalloids. JBIC Journal of Biological Inorganic Chemistry. 1: 273–7.

Rosengarten, G., 2009. Can we learn from nature to design membranes? The intricate pore structure of the diatom. in 7th International Conference on Nanochannels, Microchannels, and Minichannels, ICNMM. Pohang.

Round, F. E., Crawford, R. M., and D.G. Mann, 1990. The diatoms. Biology and morphology of the genera. Cambridge: Cambridge University Press.

Roy, P.-O., L. Deschênes and M. Margni, 2014. Uncertainty and spatial variability in characterization factors for aquatic acidification at the global scale. The International Journal of Life Cycle Assessment 19(4): 882-890.

Ruska, E., 1979. Die frühe Entwicklung der Elektronenlinsen und der Elektronenmikroskopie. Acta Hist. Leopoldina 12, 7–136.

Ruska, E., 1987. The Development of the electron microscope and of electron microscopy (Nobel Lecture). Angewandte Chemie International Edition in English 26(7): 595-605.

Rycenga, M., Cobley, C. M., Zeng, J., Li, W., Moran, C. H., Zhang, Q., Qin D., and Y. Xia, 2011. Controlling the synthesis and assembly of silver nanostructures for plasmonic applications. Chemical Reviews 111(6): 3669-3712.

Sáez, V. and T. Mason, 2009. Sonoelectrochemical synthesis of nanoparticles. Molecules. 14(10): 4284–4299.

Sajid, M., Ilyas, M., Basheer, C., Tariq, M., Daud, M., Baig, N., and Shehzad, 2015 Impacts of nanoparticles on human and environment: review of toxicity factors, exposures, control strategies, and future prospects. Environmental Science and Pollution research. (22) 6: 4122-4143.

Sakamoto, M., Fujistuka, M., and T. Majima, 2009. Light as a construction tool of metal nanoparticles: synthesis and mechanism. Journal of Photochemistry and Photobiology C: Photochemistry Reviews. 10(1): 33–56.

Sander, K. and G. S. Murthy, 2010. Life Cycle analysis of algae biodiesel. The International Journal of Life Cycle Assessment. 15: 704.

Sandhage, K. H., Dickerson, M. B., Huseman, P. M., Caranna, M. A., Clifton, J. D., Bull, T. A., Heibel, T. J., Overton, W. R., and M. E. A. Schoenwaelder, 2002. Novel, bioclastic route to self-assembled, 3D, chemically tailored meso/nanostructures: Shape-preserving reactive conversion of biosilica (diatom) microshells. Advanced Materials. 14(6): 429-433.

Saravanamuthu, R., 2010. Industrial exploitation of microorganisms: I.K. International Publishing House Pvt. Limited.

SAS Institute, 2015. JMP: Version 12. Design of experiments guide.

SAS Software for Windows. Copyright © 2015, SAS Institute Inc. SAS and all other SAS Institute Inc. product or service names are registered trademarks or trademarks of SAS Institute Inc., Cary, NC, USA.

Sato, S., Tamotsu, N., and D. G. Mann, 2013. Morphology and life history of *Amphora commutata* (Bacillariophyta) I: The vegetative cell and phylogenetic position. Phycologia. 52(3): 225-238.

Sau, T. K. and A. L. Rogach, 2012. Colloidal synthesis of noble metal nanoparticles of complex morphologies. in: Complex-shaped metal nanoparticles, Wiley-VCH Verlag GmbH & Co. KGaA, pp. 7-90.

Sawada, K. and Y. Shiraiwa, 2004. Alkenone and alkenoic acid compositions of the membrane fractions of Emiliania huxleyi. Phytochemistry. 65(9): 1299-307.

Sbihi, K., Cherifi, O., Bertrand, M., and A. El Gharmali, 2014. Biosorption of metals (Cd, Cu and Zn) by the freshwater diatom *Planothidium lanceolatum*: a laboratory study. Diatom Research. 29(1): 55-63.

Scaiano, J. C., Billone, P., Gonzalez, C. M., Maretti, L., Marin, M. L., McGilvray, K. L., and N. Yuan, 2009. Photochemical routes to silver and gold nanoparticles. Pure and Applied Chemistry. 81(4): 635–647.

Scala S. and C. Bowler, 2001. Molecular insights into the novel aspects of diatom biology. Cell Molecular and Life Sciences. 58: 1666–1673

Schebeck, L., Cikovani, Y., Biemann, K, Baluch, W., Poganietz, W-R., Düpmeier, C., Kusche, O., Simon, S., Ciroth, A., Srocka, M., Röwer, V., Salomo, B., Zschunke, T., Lohmann, J., Rosner, V., Wagner, H-J., Eltrop, L., Henßler, M., Arnold, K., and T. Targiel, 2013. Schlussbericht Vorhaben BioEnergieDat. Version 1.0. http://www.bioenergiedat.de/dokumente.html [Accessed online: October 14, 2016]

Schmitta D., Müllera A., Csögör Z, Frimmela F. H., and C. Posten, 2001. The adsorption kinetics of metal ions onto different microalgae and siliceous earth. Water Research. 35 (3): 779-785.

Schröder, H. C., Wang, X., Tremel, W., Ushijima, H., and W. E. G. Müller, 2008. Biofabrication of biosilicaglass by living organisms. Natural Product Reports. 25(3): 455-474.

Schrödinger, E., 1926. An undulatory theory of mechanics of atoms and molecules. The physical review. Second Series. 28(6): 1049-1070.

Schröfel, A., Kratošová, G., Bohunická, M., Dobročka E., and I. Vávra, 2011. Biosynthesis of gold nanoparticles using diatoms—silica-gold and EPS-gold bionanocomposite formation. Journal of Nanoparticle Research 13(8): 3207-3216.

Scopus, 2017. Access online: https://www.scopus.com

Seckbach, J. (Ed.), 2011. The diatom world. Cellular origin, life in extreme habitats and astrobiology, Vol. 19: Springer.

Selvakannan P. R., Swami A., Srisathiyanarayanan D., Shirude P. S., Pasricha R., Mandale A. B., and M. Sastry, 2004. Synthesis of aqueous Au core—Ag shell nanoparticles using tyrosine as a pH-dependent reducing agent and assembling phase-transferred silver nanoparticles at the air—water interface. Langmuir 20:7825–7836.

Sewell, S. L. and D. W. Wright, 2006. Biomimetic synthesis of titanium dioxide utilizing the R5 peptide derived From *Cylindrotheca fusiformis*. Chemistry of Materials. 18(13): 3108-3113.

Sewell, S. L., Rutledge, R. D., and D. W. Wright, 2008. Versatile biomimetic dendrimer templates used in the formation of TiO₂ and GeO₂. Dalton Transactions. (29): 3857-3865.

Sharma, K. K., Schuhmann, H., and P. M. Schenk, 2012. High lipid Induction in microalgae for biodiesel production. Energies, 5(12): 1532-1553.

Sheehan, J., Dunahay, T., Benemann, J., and P. Roessler, 1998. A look back at the U.S. Department of Energy's Aquatic Species Program: Biodiesel from algae. US Department of Energy's Office of Fuels Development.

Shim, H.-W., Jin, Y.-H., Seo, S.-D., Lee, S.-H., and D. W. Kim, 2011. Highly reversible lithium storage in *Bacillus subtilis* - Directed porous Co₃O₄ nanostructures. ACS Nano, 5(1): 443-449.

Shockley, W. and H. J. Queisser, 1961. Detailed balance limit of efficiency of p-n junction solar cells. Journal of Applied Physics. 32(3): 510-519.

Sills, D. L., Paramita, V., Franke, M. J., Johnson, M. C., Akabas, T. M., Greene, C. H., and J. W. Tester, 2013. Quantitative uncertainty analysis of Life Cycle Assessment for algal biofuel production. Environmental Science & Technology, 47 (2): 687-694.

Simkiss, K. and K. M. Wilbur, 1989, The origins of biomineralization—microbial systems. In: Biomineralization, K. Simkiss and K.M. Wilbur, Editors. Academic Press: San Diego. p. 21-31.

Simkiss, K. and M. G. Taylor, 2001. Trace element speciation at cell membranes: Aqueous, solid and lipid phase effects. Journal of Environmental Monitoring, 3(1): 15-21.

Simkiss, K., 1984. The karyotic mineralization window (KMW). Integrative and Comparative Biology. 24(4): 847-856.

Singh, A., and S. I. Olsen, 2011. A critical review of biochemical conversion, sustainability and life cycle assessment of algal biofuels, Applied Energy, 88(10): 3548-3555.

Singh, R., Gautam, N., Mishra, A., and R. Gupta, 2011. Heavy metals and living systems: An overview. Indian Journal of Pharmacology 43(3):246-253.

Sinha, S. N., Paul, D., Halder, N., Sengupta D., and S. K. Patra, 2015. Green synthesis of silver nanoparticles using fresh water green alga *Pithophora oedogonia* (Mont.) Wittrock and evaluation of their antibacterial activity. Applied Nanoscience 5(6): 703-709.

Sirin, S., 2013. Pre-concentration strategies for microalgae harvesting as biorefinery process chain, in Escola Tecnica Superior d'Enginyeria Quimica - Department of Chemical Engineering, Universitat Rovira i Virgili: Tarragona. p. 172.

Sivakumar G., Xu J. F., Thompson R. W., Yang Y., Randol-Smith, P., P. J. Weathers, 2012. Integrated green algal technology for bioremediation and biofuel. Bioresource Technology, 107: 1-9.

Skinner, H. C. W. and A. H. Jahren, 2007, Biomineralization, in: Treatise on Geochemistry, H. D. Holland and K. K. Turekian, Editors. Pergamon: Oxford. p. 1-69.

Skinner, H. C. W. and H. Ehrlich, 2014. Biomineralization, in: Treatise on Geochemistry (Second Edition), H.D. Holland and K.K. Turekian, Editors. Elsevier: Oxford. p. 105-162.

Skjak Brek, G., Malnes, D., and A. Jensen, 1980. Heavy metal tolerance of marine phytoplankton. IV. Combined effect of zinc and cadmium on growth and uptake in some marine diatoms. Journal of Experimental Marine Biology and Ecology, 42 (1): 39-54.

Smestad, G. P., 1998. Education and solar conversion: Demostrating electron transfer. Solar Energy Materials and Solar Cells, 55: 157-178.

Smith, V. H., 2003. Eutrophication of freshwater and coastal marine ecosystems: A global problem. Environmental Science and Pollution Research. 10(2): 126-139.

Soustelle, M., 2016. Precipitation reactions and equilibria ionic and electrochemical equilibria (pp. 135-162): John Wiley & Sons, Inc.

Spruijt, J., Schipperus, R., Kootstra, M., Viser, C. L. M. de, and B. Parker, 2014. AlgaEconomics: bio-economic production models of micro-algae and downstream processing to produce bio energy

carriers, Public Output report of the EnAlgae project, Swansea, June 2015, 67 pp. Available online at: www.enalagae.eu

Stamplecoskie, K., and J. Scaiano, 2012. Silver as an example of the applications of photochemistry to the synthesis and uses of nanomaterials. Photochemistry and Photobiology. 88(4): 762–768.

Steffens, J. C., 1990. The Heavy Metal-Binding Peptides of Plants. Annual Review of Plant Physiology and Plant Molecular Biology. Vol. 41:553-575

Steinigeweg, D. and S. Schlücker, 2012. Monodispersity and size control in the synthesis of 20–100 nm quasi-spherical silver nanoparticles by citrate and ascorbic acid reduction in glycerol–water mixtures. Chemical Communications. 48(69): 8682–8684.

Stephens, E., Ross, I. L., Mussgnug, J. H., Wagner, L. D., Borowitzka, M. A., Posten, C., Kruse, O., and B. Hankamer, 2010. Future prospects of microalgal biofuel production systems. Trends in Plant Science. 15(10): 554-564.

Stephenson, A. L., Kazamia, E., Dennis, J. S., Howe, C. J., Scott, S. A., and A. G. Smith, 2010. Life-Cycle Assessment of potential algal biodiesel production in the United Kingdom: A comparison of raceways and air-lift tubular bioreactors. Energy & Fuels. 24 (7): 4062-4077.

Sumper, M., E. Brunner, and G. Lehmann, 2005. Biomineralization in diatoms: characterization of novel polyamines associated with silica. FEBS Lett, 579(17): 3765-9.

Sun, Y., 2013. Controlled synthesis of colloidal silver nanoparticles in organic solutions: empirical rules for nucleation engineering. Chemical Society Reviews. 42, 2497–2511.

Suzuki, N. and Y. Aita, 2011. Radiolaria: Achievements and unresolved issues: Taxonomy and cytology. Plankton and Benthos Research. 6(2): 69-91.

Tabatabaei, M., Tohidfar, M., Jouzani, G. S., Safarnejad, M., and M.& Pazouki, 2011. Biodiesel production from genetically engineered microalgae: Future of bioenergy in Iran. Renewable and Sustainable Energy Reviews. 15(4): 1918-1927.

Taghavi, S. M., Momenpour, M., Azarian, M., Ahmadian, M., Souri, F., Taghavi, S. A., Sadeghain, M., and M., Karchani, 2013. Effects of nanoparticles on the environment and outdoor workplaces. Electronic physician. 2013 (5) 4: 706-712.

Taniguchi, N., 1974. On the basic concept of 'Nano-Technology'. Proceedings of the International Conference on Production Engineering. Tokyo Part II, Japan Society of Precision Engineering. 5-10.10

Taylor, R., Coulombe, S., Otanicar, T., Phelan, P., Gunawan, A., Lv, W., Rosengarten, G., Prasher, R., and H. Tyagi, 2013. Small particles, big impacts: A review of the diverse applications of nanofluids. Journal of Applied Physics. 113: 011301

Tazaki, K., 2013. Chapter 12 - Clays, Micro-organisms and Biomineralization, in Developments in Clay Science, B. Faïza and L. Gerhard, Editors. Elsevier. p. 613-653.

Teich, R., Zauner, S., Baurain, D., Brinkmann, H., and J. Petersen, 2007. Origin and distribution of Calvin Cycle fructose and sedoheptulose bisphosphatases in plantae and complex algae: A single secondary origin of complex red plastids and subsequent propagation via tertiary endosymbioses. Protist. 158(3): 263-276.

Tejada-Jiménez, M., Galván, A., and E. Fernández. 2011. Algae and humans share a molybdate transporter. PNAS 108(16): 6420-6425.

Tesson, B. and M. Hildebrand, 2013. Characterization and localization of insoluble organic matrices associated with diatom cell walls: Insight into their roles during cell wall formation. PLoS ONE. 8(4).

Tesson, B., Gaillard, C., and V. Martin-Jézéquel, 2008. Brucite formation mediated by the diatom *Phaeodactylum tricornutum*. Marine Chemistry, 109(1–2), 60-76.

Tesson, B., Gaillard, C., and V. Martin-Jézéquel, 2009. Insights into the polymorphism of the diatom *Phaeodactylum tricornutum* Bohlin Botanica Marina (52): 104.

Thamatrakoln, K. and M. Hildebrand, 2008. Silicon uptake in diatoms revisited: a model for saturable and nonsaturable uptake kinetics and the role of silicon transporters. Plant Physiology, 146(3): 1397-407.

Theriot E, Stoemer EF. 1984. Principal component analysis of character variation in *Stephanodiscus niagarae* Ehrenb.: morphological variation related to lake trophic status. In: Mann DG, (Ed.) Proceedings of the seventh international diatom symposium. Koenigstein, Germany: Otto Koeltz Science Publishers, 97–111.

Theriot, E. C., 2001. Diatoms, In: L. S. John Wiley & Sons, Ltd.

Thomson F. R. S., J. J., 1904. XXIV. On the structure of the atom: an investigation on the stability and periods of oscillation of a number of corpuscles arranged at equal intervals around the circumference of a circle; with application of the results to the theory of atomic structure, Philosophical Magazine Series 6. 7: 237-265.

Tiffany, M. A., 2005. Diatom auxospore scales and early stages in diatom frustule morphogenesis: Their potential for use in nanotechnology. Journal of Nanoscience and Nanotechnology. 5(1): 131-139.

Todd, T., Zhen, Z., Tang, W., Chen, H., Wang, G., Chuang, Y. J., Deaton, K., Pan, Z., and J. Xie, 2014. Iron oxide nanoparticle encapsulated diatoms for magnetic delivery of small molecules to tumors. Nanoscale. 6(4): 2073-2076.

Tomozawa, M., 2001. Chapter 3 - Amorphous silica, in Silicon-Based Material and Devices, H.S. Nalwa, Editor, Academic Press: Burlington. 127-154.

Tong, Z., Jiang, Y., Yang, D., Shi, J., Zhang, S., Liu, C., and Z. Jiang, 2014. Biomimetic and bioinspired synthesis of titania and titania-based materials. RSC Advances. 4(24): 12388-12403.

Torres, E., Cid A., Herrero C, and J. Abalde, 1998. Removal of cadmium ions by the marine diatom *Phaeodactylum tricornutum* Bohlin accumulation and long-term kinetics of uptake Bioresource Technology, 63 (3): 213-220.

Toskas, G., Cherif, C., Hund, R.-D., Laourine, E., Mahltig, B., Fahmi, A., Heinemann, C., and T. Hanke, 2013. Chitosan(PEO)/silica hybrid nanofibers as a potential biomaterial for bone regeneration. Carbohydrate Polymers. 94(2): 713-722.

Toster, J., Iyer, K. S., Xiang, W., Rosei, F., Spiccia, L., and C. L. Raston, 2013a. Diatom frustules as light traps enhance DSSC efficiency. Nanoscale. 5(3): 873-876.

Toster, J., Kusumawardani, I., Eroglu, E., Iyer, K. S., Rosei, F., and C. L. Raston, 2014. Superparamagnetic imposed diatom frustules for the effective removal of phosphates. Green Chemistry. 16(1): 82-85.

Toster, J., Zhou, Q. L., Smith, N. M., Iyer, K. S., Rosei, F., and C. L. Raston, 2013b. In situ coating of diatom frustules with silver nanoparticles. Green Chemistry. 15(8): 2060.

Townley, H. E., 2011. Diatom Frustules: Physical, Optical, and Biotechnological Applications, in The Diatom World, J. Seckbach and P. Kociolek, Editors. Springer Netherlands. 273-289.

Townley, H. E., Parker, A. R., and H. White-Cooper, 2008. Exploitation of Diatom Frustules for Nanotechnology: Tethering Active Biomolecules. Advanced Functional Materials. 18(2): 369-374.

Townley, H. E., Woon, K. L., Payne, F. P., White-Cooper, H., Parker, A. R., 2007. Modification of the physical and optical properties of the frustule of the diatom Coscinodiscus wailesii by nickel sulfate. Nanotechnology, 18(29): 295101.

Treves, K., Traub, W., Weiner, S., and L. Addadi, 2003. Aragonite formation in the chiton (Mollusca) girdle. Helvetica Chimica Acta. 86(4): 1101-1112.

Tsiourvasa, D., Tsetsekou, A., Papavasiliou, A., Arkas, M., and N. Boukos, 2013. A novel hybrid sol-gel method for the synthesis of highly porous silica employing hyperbranched poly(ethyleneimine) as a reactive template. Microporous and Mesoporous Materials, 175: 59-66.

Tsuji, T., Okazaki, Y., and M. Tsuji, 2008. Photo-induced morphological conversions of silver nanoparticles prepared using laser ablation in water—Enhanced morphological conversions using halogen etching. Journal of Photochemistry and Photobiology A: Chemistry. 194(2–3): 247–253.

Turkevich, J., Stevenson, P.C., and J. Hillier, 1951. A study of the nucleation and growth processes in the synthesis of colloidal gold. Discussions of the Faraday Society, 11, 55-75.

Umemura, K., Gao, Y., Nishikawa, T., and R. Kuroda, 2009. Scanning electron microscopy and atomic force microscopy of Coscinodiscus granii frustules treated by the liquid phase deposition. in 2nd International Conference on Smart Materials and Nanotechnology in Engineering. Weihai. Proceedings SPIE 7493, Second International Conference on Smart Materials and Nanotechnology in Engineering, 74932P

United States Environmental Protection Agency (EPA), 2016. Module 3: Characteristics of Particles - Particle Size Categories.

http://web.archive.org/web/20101203205130/http://www.epa.gov/apti/bces/module3/category/category.htm

United States Environmental Protection Agency (EPA), National Center for Environmental Assessment Office of Research and Development, 2012. Nanomaterial Case study: Nanoscale Silver in Disinfectant Spray. EPA/600/R-10/081F. Research Triangle Park, NC. United States.

Unocic, R. R., Zalar, F. M., Sarosi, P. M., Cai, Y., and K. H. Sandhage, 2004. Anatase assemblies from algae: coupling biological self-assembly of 3-D nanoparticle structures with synthetic reaction chemistry. Chem Commun (Camb), 2004(7): 796-797.

Valiadi, M., Iglesias-Rodriguez, M. D., and A. Amorim, 2012. Distribution and genetic diversity of the luciferase gene within marine dinoflagellates. Journal of Phycology. 48(3): 826-836.

van Dam, A. A., Beveridge, M. C. M., Ekram Azim, M., and M. C. J. Verdegem, 2002. The potential of fish production based on periphyton. Reviews in Fish Biology and Fisheries. 12(1): 1-31.

van den Hoek, C., Mann, D. G., and H. M. Jahns, 1995. Algae: An Introduction to Phycology, Cambridge: Cambridge University Press.

Van Eynde, E., Tygat, T., Smits, M., Verbruggen, S. W., Hauchecorne, B., and S. Lenaerts, 2013. Biotemplated diatom silica-titania materials for air purification. Photochemical Photobiological Sciences. 12(4): 690-695.

Vanysek, P., 2004. Electrochemical series. In: Lide, D. R. (Ed.) CRC Handbook of Chemistry and Physics, p. 8.21–8.31. CRC Press, LLC (2003–2004)

Varun, A. S. and H. Nautiyal, 2016. Environmental impacts of packaging materials. In: Environmental footprints of Packaging. Subramanian Senthilkannan Muthu Ed. Springer.

Vasconcelos, M. T. S. D., López-Ruiz, J. L., García, A., Leal, M. F. C., and A. Fachini, 2004. Effect of zeolites on cultures of the marine micro-algae *Emiliania huxleyi*. Aquacultural Engineering. 31(3-4): 205-219.

Vatamaniuk, O. K., Mari, S., Lang, A., Chalasani, S., Demkiv, L. O., and P. A. Rea, 2004. Phytochelatin synthase, a dipeptidyltransferase that undergoes multisite acylation with y-glutamylcysteine during

catalysis: stoichiometric and site-directed mutagenic analysis of *Arabidopsis thaliana* pcs1-catalyzed phytochelatin synthesis. Journal of Biological Chemistry, 279(21): 22449-22460.

Venugopal, V., 2016. Marine polysaccharides: Food applications, CRC Press.

Vinegoni, C., Cazzanelli, M., and L. Pavesi, 2001. Chapter 4 - Porous silicon microcavities. In: Silicon-based material and devices, H. S. Nalwa, Editor. Academic Press: Burlington. 123-192.

von Stosch, H. A., 1950. Oogamy in a centric diatom. Nature. 165(4196): 531-532.

von Stosch, H. A., 1951. Entwicklungsgeschichtliche Untersuchungen an zentrischen Diatomeen I - Die Auxosporenbildung von *Melosira varians*. Archiv für Mikrobiologie. 16(1-4): 101-135.

von Stosch, H. A., 1956. Entwicklungsgeschichtliche Untersuchungen an zentrischen Diatomeen. - II. Geschlechtszellenreifung, Befruchtung und Auxosporenbildung einiger grundbewohnender Biddulphiaceen der Nordsee. Archiv für Mikrobiologie. 23(4): 327-365.

von Stosch, H. A., 1958. Entwicklungsgeschichtliche Untersuchungen an zentrischen Diatomeen - III. Die Spermatogenese von *Melosira moniliformis* Agardh. Archiv für Mikrobiologie, 31(1): 274-282.

Vrieling E. G., Poort L., Beelen T. P. M., and W. W. C. Gieskes, 1999a. Growth and silica content of the diatoms *Thalassiosira weissflogii* and *Navicula salinarum* at different salinities and enrichments with aluminium. European Journal of Phycology 34: 307–316.

Vrieling E. G., Sun Q., Tian M., Kooyman P. J., Gieskes W. W., van Santen R. A., and N. A. Sommerdijk, 2007. Salinity-dependent diatom biosilicification implies an important role of external ionic strength. Proceedings of the National Academy of Sciences, USA 104: 10441–10446.

Vrieling, E. G., Gieskes, W. W. C., and T. P. M. Beelen, 1999b. Silicon deposition in diatoms: Control by the pH inside silicon deposition vesicle. Journal of Phycology. 35: 548-559.

Wang X., Lu, G., Heinz, C. Schröder, H. C., and W. E. G. Müller, 2013. Paradigm shift in bioinorganic chemistry: enzymatic polycondensation reaction of silica in siliceous sponges. Progress in Chemistry. 25(4): 435-445.

Wang, L. and M. Nilsen-Hamilton, 2013. Biomineralization proteins: From vertebrates to bacteria. Frontiers in Biology. 8(2): 234-246.

Wang, W. X. and R. C. Dei, 2001. Metal uptake in a coastal diatom influenced by major nutrients (N, P, and Si). Water Research, 35(1): 315-321.

Wang, X. and W. E. G. Müller, 2009. Marine biominerals: perspectives and challenges for polymetallic nodules and crusts. Trends in Biotechnology. 27(6): 375-383.

Wang, X. H., Gan, L., and W. E. G. Müller, 2009, Contribution of biomineralization during growth of polymetallic nodules and ferromanganese crusts from the Pacific Ocean. Frontiers of Materials Science in China. 3(2): 109-123.

Wang, X., Schloßmacher, U., Wiens, M., Batel, R., Schröder, H. C., and W. E. G. Müller, 2012. Silicateins, silicatein interactors and cellular interplay in sponge skeletogenesis: formation of glass fiber-like spicules. FEBS Journal. 279(10): 1721-1736.

Wang, Y., Zhu, X., Lao, Y., Lv, X., Tao, Y., Huang, B., Wang, J., Zhou, J., and Z. Cai, 2016. TiO₂ nanoparticles in the marine environment: Physical effects responsible for the toxicity on algae *Phaeodactylum tricornutum*. Science of The Total Environment, 565: 818-826.

Wassmann, P., Reigstad, M., Haug, T., Rudels, B., Carroll, M. L., Hop, H., Gabrielsen, G. W., Falk-Petersen, S., Denisenko, S. G., Arashkevich, E., Slagstad, D., and O. Pavlova, 2006. Food webs and carbon flux in the Barents Sea. Progress in Oceanography. 71(2–4): 232-287.

Weatherspoon, M. R., Allan, S. M., Hunt, E., Cai, Y., and K. H. Sandhage, 2005. Sol-gel synthesis on self-replicating single-cell scaffolds: applying complex chemistries to nature's 3-D nanostructured templates. Chemical Communications (Cambridge), 2005(5): 651-3.

Weaver, J. C., Pietrasanta, L. I., Hedin, N., Chmelka, B. F., Hansma P. K., and D. E. Morse, 2003. Nanostructural features of demosponge biosilica. Journal of Structural Biology. 144(3): 271-281.

Web of Science, 2017. Access online: https://www.webofknowledge.com

Weber, M. X. and M. Medina, 2012. The role of microalgal symbionts (*Symbiodinium*) in holobiont physiology. 64: 119-140.

Wei, H., Ma, N., Shi, F., Wang, Z., and X. Zhang, 2007. Artificial nacre by alternating preparation of layer-by-layer polymer films and CaCO₃ strata. Chemistry of Materials. 19(8): 1974-1978.

Weiner, S. and P. Dove, 2003. An overview of biomineralization processes and the problem of the vital effect. Reviews in Mineralogy and Geochemistry, 54(1): 1-29.

Wernet, G., Bauer, C., Steubing, B., Reinhard, J., Moreno-Ruiz, E., and Weidema, B., 2016. The ecoinvent database version 3 (part I): overview and methodology. The International Journal of Life Cycle Assessment, 21(9):1218–1230.

White, R. J., Luque, R., Budarin, V. L., Clark, J. H., and D. J. Macquarrie, 2009. Supported metal nanoparticles on porous materials. Methods and applications. Chemical Society Reviews, 38(2): 481-494.

Wieneke, R., Bernecker, A., Riedel, R., Sumper, M., Steinem, C., and A. Geyer, 2011. Silica precipitation with synthetic silaffin peptides. Organic & Biomolecular Chemistry. 9(15): 5482-5486.

Wiens, M., Bausen, M., Natalio, F., Link, T., Shlossmacher, U., and W. E. G. Müller, 2009. The role of the silicatein-α interactor silintaphin-1 in biomimetic biomineralization. Biomaterials. 30(8): 1648-1656.

Wiens, M., Elkhooly, T. A., Schröder, H. C., Mohamed, T. H. A., and W. E. G. Müller, 2014. Characterization and osteogenic activity of a silicatein/biosilica-coated chitosan-graft-polycaprolactone. Acta Biomaterialia. 10(10) 4456-4464.

Wiens, M., Wang, X. H., Schlossmacher, U., Lieberwirth, I., Glasser, G., Ushijima, H., Schröder, H. C., and W. E. G. Müller, 2010. Osteogenic potential of biosilica on human osteoblast-like (SaOS-2) Cells. Calcified Tissue International. 87(6): 513-524.

Wikfors, G. and R. Ukeles, 1982. Growth and adaptations of estuarine unicellular algae in media with excess copper, cadmium or zinc, and effect of metal-contaminated algal food in *Crassostrea virginica* larve. Marine Ecology – Progress Series, 7: 192-206.

Wilbur, K. M. and K. Simkiss, 1979. Carbonate turnover and deposition by metazoa. Studies in Environmental Science. 3(C): 69-106.

Wiley, B., Herricks, T., Sun, Y., and Y. Xia, 2004. Polyol synthesis of silver nanoparticles: Use of chloride and oxygen to promote the formation of single-crystal, truncated cubes and tetrahedrons. Nano Letters 4(9): 1733-1739.

Wiley, B., Y. Sun, B. Mayers and Y. Xia, 2005. Shape-controlled synthesis of metal nanostructures: The case of silver. Chemistry – A European Journal 11(2): 454-463.

Willems, G., Lambrechts, P., Braem, M., Celis, J. P., and G. Vanherle, 1992. A classification of dental composites according to their morphological and mechanical characteristics. Dental Materials. 8(5): 310-319.

Wilt, F. H., 2002. Biomineralization of the spicules of sea urchin embryos. Zoological Science. 19(3): 253-261.

Wilt, F. H., 2005. Developmental biology meets materials science: Morphogenesis of biomineralized structures. Developmental Biology, 280(1): 15-25.

Wishkerman, A., Coehn, B., Itzhaky, E., Oren, A., Shahar, B., and S. Arad, 2016. Biosynthesis of silver nanoparticles by *Phaeodactylum tricornutum*. Conference paper. IDS 2016 – 24th International Diatom Symposium, Quebec City, Quebec, Canada.

Wolff, A., Frese, K., Wißbrock, M., Eckstädt, K., Ennen, I., Hetaba, W., Loeffler, S., Regtmeier, A.-K., Thomas, P., Sewald, N., Schattschneider, P., and A. Hütten, 2012. Influence of the synthetic polypeptide c25-mms6 on cobalt ferrite nanoparticle formation. Journal of Nanoparticle Research. 14(10).

Woodall, A. A., Britton, G., and M. J. Jackson, 1997. Carotenoids and protection of phospholipids in solution or in liposomes against oxidation by peroxyl radicals: relationship between carotenoid structure and protective ability. Biochim Biophys Acta, 1336(3): 575-586.

Wu, J. and Z. M. Wang, 2014. Quantum dot solar cells. Springer-Berlag. 15.

Wuithschick, M., Paul, B., Bienert, R., Sarfraz, A., Vainio, U., Sztucki, M., Kraehnert, R., Strasser, P., Rademann, K., Emmerling, F., and J. Polte, 2013. Size-controlled synthesis of colloidal silver nanoparticles based on mechanistic understanding. Chemistry of Materials 25(23): 4679-4689.

Xiang, C., Werner, B. L., E'Lise, M. C., and D. J. Oliver, 2001. The biological functions of glutathione revisited in *Arabidopsis* transgenic plants with altered glutathione levels." Plant Physiology 126.2: 564-574.

Xu, G., Qiao, X., Qiu, X., and J. Chen, 2008. Preparation and characterization of stable monodisperse silver nanoparticles via photoreduction. Colloids and Surfaces A: Physicochemical and Engineering Aspects 320(1–3): 222-226.

Xu, M., Gratson, G. M., Duoss, E. B., Shepherd, R. F., and J. A. Lewis, 2006. Biomimetic silicification of 3D polyamine-rich scaffolds assembled by direct ink writing. Soft Matter. 2(3): 205-209.

Yan, D., Yin, G., Huang, Z., Yang, M., Liao, X., Kang, Y., Yao, Y., Hao, B., and D. Han, 2009a. Characterization and bacterial response of zinc oxide particles prepared by a biomineralization process. The Journal of Physical Chemistry B, 113(17): 6047-6053.

Yang, L. and C. Zhong, 2013. Advanced engineering and biomimetic materials for bone repair and regeneration. Frontiers of Materials Science. 7(4): 313-334.

Yang, S. H., Park, J. H., Cho, W. K., Lee, H. S., and I. S. Choi, 2009. Counteranion-directed, biomimetic control of silica nanostructures on surfaces inspired by biosilicification found in diatoms. Small. 5(17): 1947-1951.

Yang, S., Kang, H., K., and I. S. Choi, 2008. Biomimetic approach to the formation of titanium dioxide thin films by using poly(2-(dimethylamino)ethyl methacrylate). Chemistry - An Asian Journal. 3(12): 2097-2104.

Yang, W., Lopez, P. J., and G. Rosengarten, 2011.Diatoms: self-assembled silica nanostructures, and templates for bio/chemical sensors and biomimetic membranes. Analyst. 136(1): 42-53.

Yoosaf, K., Ipe, B. I., Suresh, C. H., and K. G. Thomas, 2007. In situ synthesis of metal nanoparticles and selective naked-eye detection of lead ions from aqueous media. The Journal of Physical Chemistry C 111(34): 12839-12847.

Yu, M., Yuan, P., Zhang, J., Wang, H., Zhang, Y., Hu, Y., Wang, Y., and C. Yu, 2010. A bioinspired route to various siliceous vesicular structures. Journal of Nanoscience and Nanotechnology, 10(1): 612-615.

Zane, A. C., Michelet, C., Roehrich, A., Emani, P. S., and G. P. Drobny, 2014. Silica morphogenesis by lysine-leucine peptides with hydrophobic periodicity. Langmuir. 30(24): 7152-7161.

Zhang, D., Wang, Y., Cai, J., Pan, J. F., Jiang, X. G., and Y. G. Jiang, 2012. Bio-manufacturing technology based on diatom micro- and nanostructure. Chinese Science Bulletin. 57(30): 3836-3849.

Zhu, J., Liu, S., Palchik, O., Koltypin, Y., and A. Gedanken, 2000. Shape-controlled synthesis of silver nanoparticles by pulse sonoelectrochemical methods. Langmuir 16(16): 6396-6399.

Zimmermann, J., Jahn, R., and B. Gemeinholzer, 2011. Barcoding diatoms: evaluation of the V4 subregion on the 18S rRNA gene, including new primers and protocols. Organisms Diversity & Evolution. 11(3): 173-192.

APPENDICES

APPENDIX I NANOTHECHNOLOGY TERMINOLOGY

The American Society for Testing and Materials developed a set of standards for the nanotechnology industry (ASTM E 2456-06). In 2010, the International Organization for Standardization (ISO) developed a list of terminologies related to nanotechnologies as notated in the ISO/TS 80004-1:2010. The table below shows a list of relevant terms and definitions taken from the Technical Standard prepared by the ISO (ISO/TS 80004-1:2010).

Term	Definition
Nanoscale	Size range from approximately 1 nm to 100 nm. The introduction of the lower limit is used to avoid single and small atoms or molecules from being presented as nano-objects, in the event of absence of a lower limit.
Nanoscience	Study, discovery, and understanding of matter in the nanoscale. Size- and structure-dependent properties and phenomena are distinct from those associated with individual atoms or molecules and bulk materials.
Nanotechnology	Application of scientific knowledge to manipulate and control matter, including material synthesis, in the nanoscale to make use of size- and structure-dependent properties and phenomena, as different from those of individual atoms or molecules and bulk materials.
Nanomaterial	Material with external dimension in the nanoscale or having internal structure or surface structure in the nanoscale. Inclusive of nano-objects and nanostructured materials.
Nano-object	Material with one, two or three external dimensions in the nanoscale. Generic term for discrete objects on the nanoscale.
Nanostructure	Composition of inter-related constituent parts, one or more of which are in the nanoscale. Regions are defined as boundary-represented breaks in continuity of properties.
Nanostructured material	Material with internal or surface nanostructure. Not exclusive. If the external dimensions are on the nanoscale is better to refer to the material as nano-object.
Engineered nanomaterial	Nanomaterial designed for a specific purpose or function.
Manufactured nanomaterial	Nanomaterial intentionally produced for commercial purposes with a specific set of properties and or composition.
Incidental nanomaterial	Nanomaterial generated as an unintentional by product of a process, which include manufacturing, bio-technological or other processes.
Nanomanufacturing	Intentional synthesis, generation or control of nanomaterials, or fabrication steps in the nanoscale, for commercial purposes.
Nanomanufacturing process	Ensemble of activities to intentionally synthesize, generate or control nanomaterials, or fabrication steps in the nanoscale, for commercial purposes.
Nanoscale phenomenon	Effect attributable to nano-objects or nanoscale regions.
Nanoscale properties	Characteristics of nano-objects or nanoscale regions.

APPENDIX II LIST OF CHEMICALS AND SDS SHEETS

Chemical ^{1, 2}	CAS Number ²	PubChem Substance ID ³	EC Number ²	SDS File ⁴
Acetone	67-64-1	24850797	200-662-2	67-64-1.pdf
Acetonitrile	75-05-8	24856425	200-835-2	75-05-8.pdf
Benzyl alcohol	100-51-6	24858412	202-859-9	100-51-6.pdf
Carbon monoxide	630-08-0	24857760	211-128-3	630-08-0.pdf
Cyclohexane	110-82-7	24853606	203-806-2	110-82-7.pdf
Dichloromethane	75-09-2	24856423	200-838-9	75-09-2.pdf
Diethyl ether	60-29-7	N/A	N/A	60-29-7.pdf
Dimethyl ether	115-10-6	24857771	204-065-8	115-10-6.pdf
Ethyl acetate	141-78-6	24849485	205-500-4	141-78-6.pdf
Ethylene glycol	107-21-1	24859450	203-473-3	107-21-1.pdf
Glycerol	56-81-5	24895360	200-289-5	56-81-5.pdf
Hexadecyltrimethylammonium bromide	57-09-0	24895846	200-311-3	57-09-0.pdf
Hydrazine	302-01-2	24852873	206-114-9	302-01-2.pdf
Hydrogen peroxide	7722-84-1	24895421	N/A	7722-84-1.pdf
Hydroquinone	123-31-9	24278475	204-617-8	123-31-9.pdf
Hydroxylamine hydrochloride	5470-11-1	N/A	226-798-2	5470-11-1.pdf
N, N-Dimethylformamide	68-12-2	24893883	200-679-5	68-12-2.pdf
Phosporus	7723-14-0	24861136	231-768-7	7723-14-0.pdf
Polyvinylpyrrolidone	9003-39-8	24899318	N/A	9003-39-8.pdf
Silicon	7440-21-3	24871099	231-130-8	7440-21-3.pdf
Silver nanospheres	N/A	N/A	N/A	7440-22-4-20nm.pdf 7440-22-4-30nm.pdf 7440-22-4-40nm.pdf 7440-22-4-50nm.pdf 7440-22-4- 100nm.pdf 7440-22-4- 200nm.pdf
Silver nitrate	7761-88-8	24852543	231-853-9	7761-88-8.pdf
Sodium borohydride	16940-66-2	24868683	241-004-4	16940-66-2.pdf
Sodium chloride	7647-14-5	24899861	231-598-3	7647-14-5.pdf
Sodium Citrate	6132-04-3	N/A	200-675-3	6132-04-3.pdf
Sodium dodecylbenzenesulfonate	25155-30-0	24857418	246-680-4	25155-30-0.pdf
Sodium hydroxide	1310-73-2	24853242	215-185-5	1310-73-2.pdf
Tetrabutylammonium acetate	10534-59-5	24860355	234-101-8	10534-59-5.pdf
Tetrabutylammonium bromide	1643-19-2	24866693	216-699-2	1643-19-2.pdf
Tetraoctylammonium bromide	14866-33-2	24857704	238-936-9	14866-33-2.pdf
Trypan Blue	72-57-1	57654704	200-786-7	72-57-1.pdf

- 1. All compounds have a link to a web source. Some were not used but mentioned in this document
- 2. Source: Sigma Aldrich. Formula and molecular structure can be seen on the file or the website for each compound.
- 3. Source: PubChem Open Chemistry Database
- 4. Files attached electronically as annex or linked via archive.

APPENDIX III METHODOLOGIES, TECHNIQUES, AND EQUIPMENT

III.I Axenic algal culture

Algae can be produced in a controlled environment and in completely axenic cultures, when bacterial symbiotic by products, such as vitamins, are added to the culture medium (Wettstein, 1921; Hunter et al., 1950; Andersen, 2005). Additionally, the availability of chemically purified salts has made possible to culture algae in completely axenic environments, reducing the confounding activity of other organisms in the analysis of biochemical processes involving algae (Provasoli, 1958; Pinter, 1960).

III.II Batch culture

The first advances in the mass cultivation of microalgae came when Allen and Nelson (1910) developed the first new method for production with other purposes in mind. Later, Warburg (1919) managed to grow dense cultures of *Chlorella* sp. in laboratory conditions, and Ketchum and Redfield (1938) managed to produce a continuous culture of diatoms by periodical harvesting of a fixed portion of the original culture allowing the remaining cells to continue reproducing and guaranteeing a steady supply of cells for analysis. In general terms, a batch culture of microalgae has a limited supply of nutrients that after depleted will produce a reduction in the growth values of the culture. The goal is to monitor conditions and evaluate intakes of elements by the algae without masking these depletions by constant addition of nutrients or treatments. The main difference with continuous culture stands in the way the nutrients and harvest are performed as continuous cultures introduce nutrients at the same rate of harvest (Andersen, 2005).

III.III Use of a hemocytometer

Created in 1881 by Thoma, manufactured by Carl Zeiss and Company, and later improved by Hawksley, the Thoma-Zeiss hemocytometer was designated by Campbell Todd in 1912 as the most widely and satisfactory used instrument for counting cells (Verso, 1971; Davis, 1995). It evolved to the design by Büker between 1905 and 1913 (Davis, 1995). A simple but elegant design that holds a known volume in a grid carved on a glass slide allowing for the knowledge of areas and sizes of the cells under a light microscope (Figure 2.)

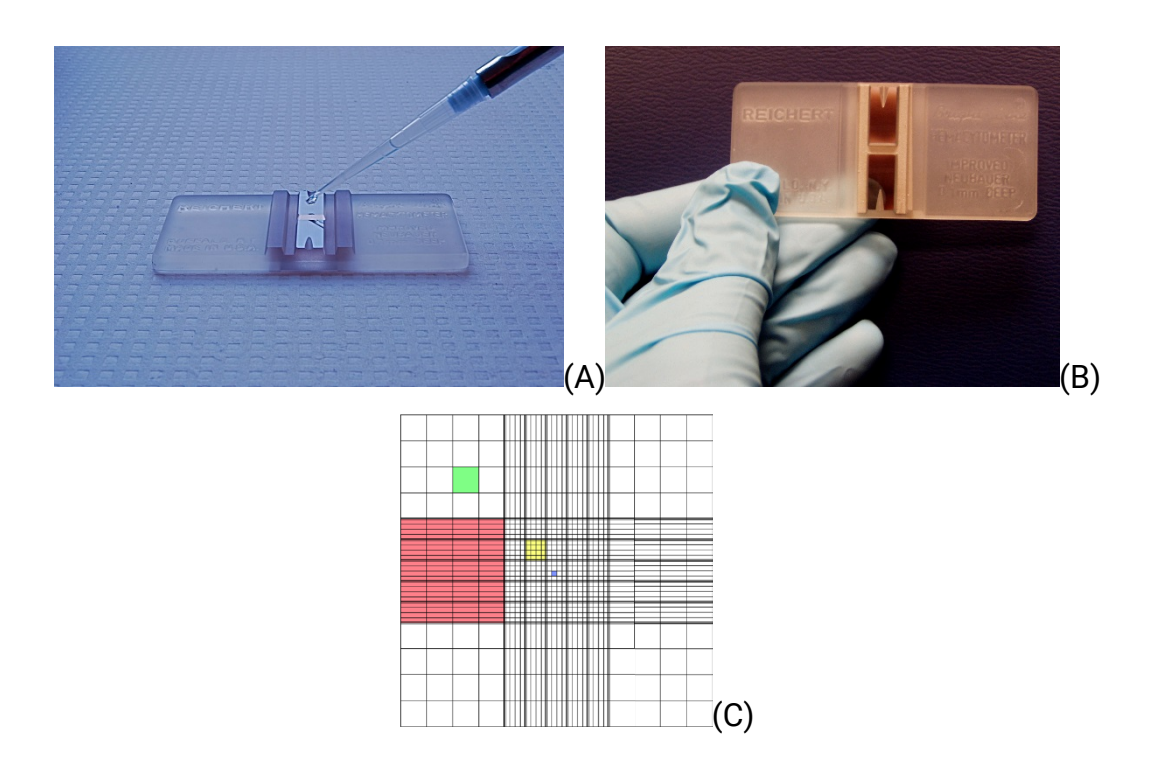


Figure 1. Hemocytometer. Commonly used hemocytometer: (A) Use of the load chamber. Image taken by Todd - originally posted to Flickr as 0356, CC BY-SA 2.0, available online: https://commons.wikimedia.org/w/index.php?curid=5193859. (B) Semi-reflective rectangles of the counting chambers. Image taken by Todd - originally posted to Flickr as 0356, CC BY-SA 2.0, available online (retrieved from file on 2017/07/26): https://commons.wikimedia.org/w/index.php?curid=5193859. (C) Grid. Squares in Red (100 nL), green (6.25 nL), white (i.e. inside the gridded cross equivalent to 1/20 of the of the red square ~ 5 nL), yellow (4 nL), and blue (0.25 nL) represent a known volume of liquid. Image taken by Zephyris at the English language Wikipedia, CC BY-SA 3.0, available online: https://commons.wikimedia.org/w/index.php?curid=10553213

The mechanism for counting cells in the cytometer is quite straight forward. A slightly protruded side of the counting chambers, covered by a glass slide, creates a space of exactly 0.1 mm of depth that can be calculated via a known surface of the gridded chamber (see Figure 2.10.C). The count is made in randomly selected squares across the region of the counting chamber, either in a defined pattern or by assigning coordinates to each square, as defined before the introduction of the culture medium with cells in the chamber (Figure 2.10.A). The total counted area of the sample, determined by the

addition of all the individual completely counted squares inside the chamber by using the following equation:

$$\textit{Cells Concentration } [\textit{cell} \cdot \textit{mL}^{-1}] = \left(\frac{\textit{Cells}_{\textit{count}}}{(\textit{Proportion}_{\textit{counted}}) \times (\textit{Volume Squares}_{\textit{counted}})}\right) \times \left(\frac{\textit{V}_d}{(\textit{V}_i)}\right) \qquad \text{Equation VI.1}$$

In Equation 2.1. $Cells_{count}$ is the total number of cell counted during the sample optical measurement, $Proportion_{chamber}$ multiplied by the volume of each square counted (Volume squares counted) yields the total counted volume and by dividing the total number of cells per unit of volume, we obtain a concentration in $cell \cdot mL^{-1}$. V_d represents the volume of the diluted sample, and V_i is the volume of the original culture in the sample. The ratio of this two values represents the dilution factor, and is needed to restore the concentration to the original concentration in the culture medium, based on the formula of equality of equivalent dilutions (Equation 2.2.):

$$C_1V_1 = C_2V_2$$
 Equation VI.2.

Where, C_1 is the total concentration of cells in the original sample (i.e. *Cell* concentration), V_1 corresponds to the volume of cells in the original sample (i.e. V_i), C2 is the concentration of cells in the sample or diluted subset (i.e. $Cells_{count} \cdot Proportion_{counted}^{-1} \cdot Volume$ $Squares_{counted}^{-1}$), and V_2 is the Volume of the diluted sample (i.e. V_d). Solving for C_1 , we obtain equation 2.1.

Among the considerations when working with a hemocytometer, the multiplicative nature of the calculations increases the probability of standard error due to manipulation, measurement, operator differences, and other factors that might interfere with the result. And the error is accumulative, as dilutions and factors, proportions of a total will increase the number of cells that would be missed during counting. It is known that some errors in hemocytometer counts can reach values of uncertainty of close to 43% (confidence of 95%) and 36% (confidence 90%) (Willén, 1976). Looking to reduce the magnitude of the error term in the count of cells a scientific could engage in good practices. First, taking care not to overload the chamber by using exactly the volume of medium that can be stored in the chamber, for that a micropipette can be a good alternative, if it is well calibrated. Additionally, a small increase of temperature of the cover-glass can add a

multicolor effect that would show where the solution is poorly distributed. And as mentioned before, using only volumetric measuring equipment with a small error or good calibration (Willén, 1976; Celeromics, 2017). Another source of error comes from the approximations to the population size (i.e. statistical) and it can be prevented by randomization of the areas to be counted, regardless the number of cells in the areas, and the application of probability theory (i.e. increasing the sample size and repeating sampling for different counts) and analysis methods however, the error associated with this processes accounts for 20 to 30% of the total error term in a reported datum and can grow as high as 43% if the number of samples is small (Willén, 1976). In some cases, laboratory technicians would count a determined number of cells and associate that number to a volume and not the other way around, even if it means preparing numerous counting chambers when concentrations are low (Canosa, 1999).

III.IV Cytometry

When a particle suspended in an electrolyte crosses a microchannel generated by two electric poles, the resistance generated by each particle will alter the response of a sensor attached to the channel. Size and shape would affect the time and magnitude of the resistance reading, thus allowing the sensor to discern among different particles types and sizes. Similarly, when a highly coherent light is beamed to a receptor, and suspended particles interfere with the path of the light, the time of delay, and the frequency the delay is recorded can be sufficient to determine a set of particles and sizes. In recent years, new automatic, laser- or impedance- based mechanisms have been developed to assist cell biologist with the counting, sorting, and assessing of cells in culture systems. The basic operational principle of these systems consists on suspending the cells disaggregated in a fluid and pass them through a sieving mechanism, or an electronic detection apparatus. It provides the possibility to perform multiparametric analysis of the basic physical characteristics of the culture, such as size, size distribution, in some cases shapes, and even some chemical characteristics via the use of tracers with speeds that surpass the thousands of particles per second. Some devices even take advantages of fluid dynamics to separate or sort the cells of interest given a set of parameters (e.g. size, shape, density, or presence of tracers) separating them from the flow through the sensing apparatus, be it laser- or impedance- based. Modern flow cytometers can identify and sort thousands of particles per second.

An extremely oversimplified of a flow cytometry system can be presented in a sequence of steps as follow: A liquid stream (i.e. flow cell) carries and aligns cells so they can pass in a single arrangement through the sensing beam or field which is attached to a measuring system emitter which produces the signal that is going to be detected and measured for changes of the unit and property (e.g. conductivity, impedance, photonic intensity, light incidence) either impedance or optical systems (e.g. mercury, xenon lamps, lasers, diode lasers). The change in the signal can be detected an analog-to-digital Conversion (ADC) system which translates or converts the signal from the physical system into a digital binary signal. The weak nature of the signal requires the use of an amplification system that increases the strength and quality of the signal to further transmit it to a computer where the different analyses of the signals are compiled into usable formats.

Automatic counting and sorting systems aid in the analysis of culture cells and reduce considerably the error produced by human manipulation of samples by providing a faster performance with reduced bias due to human error.

III.V Spectrophotometry

Further developments of digital technologies, particularly of photometers, to measure small variations of different wavelengths not easily discernible by the human eye (i.e. near ultraviolet and infrared), combined with monochromatic isolation techniques, allowed the use of reflection and transmission technologies to determine properties of materials by measuring light intensities in function of wavelengths resulting from the interaction between the material and an incident light source (Simoni et al., 2003; Allen et al., 2010; Trumbo, 2013). These properties can be the result of direct interactions or light with the material, or measurements light interaction with tracing agents that enhance the contrast of the incident wavelengths (i.e. indicators).

In general terms, and in an oversimplified manner, the principle of function of a spectrophotometer is described as follows: A light source produces a beam of a specific

light with known parameters (i.e. intensity, wavelength) that is passed then through a monochromator or filter with a diffraction grating system that eliminates wavelengths that are not of interest and structurally separates further the signal of the wavelengths of interest (Figure 2.11). The monochromatic light is then focused by an adjustable aperture which concentrates the beam before it can circulate through the sample. The sample is then exposed to the source in a cuvette placed between the light source and the measuring mechanism or sensor (i.e. photoresistor, photodiode or photomultipliers) that measures the characteristics of the light signal and transduces into a digital signal which in turn gets amplified to improve the quality of the digital source to finally transfer this enhanced signal to a display or user interface (UI) that allows for visualization in usable format.

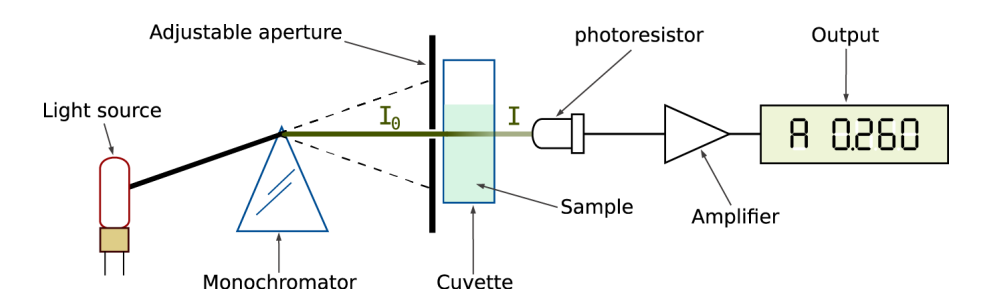


Figure 2. Single beam spectrophotometer.

General schematic representation of the structure of single beam spectrophotometers. Image available online: https://commons.wikimedia.org/wiki/File:Spetrophotometer-en.svg en.svg#/media/File:Spetrophotometer-en.svg

The method for count and measurement of light varies from equipment to equipment, but the operating principles remain the same, and the only variation is the unit of measurement (e.g. photons ·m⁻², photons·m⁻²·sr⁻¹, W·m⁻², W·m⁻²·sr⁻¹). Given that the sensor that measures the incidence of photons count individual photons, these instruments cannot function properly with high irradiances (Thomas & Burgess, 2007; Saakov et al., 2015).

III.VI Optical microscopy

The use of lenses to increase the capacity of humans to see objects and characteristics beyond eye resolution (6 to 29 μ m) dates to the 13th century (INO-CNR, 2017) and the first

compound devices started to show in records circa the early 17th century (Rosenthal, 1996; Van Helden et al., 2010; Seeger, 2016; MOI, 2017). The term microscope, from the Greek μικρον, mikrón, was coined by Giovanni Faber when he named the "occiolino" (i.e. "little eye"), a compound microscope that Galileo Galilei submitted to the Accademia dei Lincei in 1624 (Gould, 2000), and became popular when Antoine van Leeuwenhoek made the device a tool for biologist (van Leeuwenhoek & Hoole, 1800). Nevertheless, optics and technology were not sufficient for the advancement of the field until in the late 1800s a more homogeneous method for sample illumination developed by August Köhler (1893), became available. Later developments of phase contrast by Zernike (Tolansky, 1967) and differential interference contrast (DIC) by Normanski (Lang, 1968) allowed the visualization of transparent objects such as animal cells and cellular structures (Murphy, 2001).

III.VII SEM-EDS

III.VII.I Scanning electron microscopy (SEM)

Whereas an optical microscope produces an augmented image of an object using a beam of light, its limitations come from the size and coherence of the beam. Even when using a highly focused and coherent beam (i.e. laser) these beams are limited by the wavelength of the beam. A higher augmentation can be achieved when the beam has a smaller distance between particles thus differentiating smaller structures by contrast (i.e. resolution) and the smallest elementary particle that can be completely controlled and measured to a high level of certainty and precision in present times is the electron (Lyman, 1990; Schatten & Pawley, 2008). When the electrons of a beam interact with the atoms of a sample, several signals arise. These signals contain information on topography and composition, as each atom on the surface of the sample will interact in a different manner with the colliding electrons. The angle of incidence and the return signal (i.e. secondary electrons, back-scattered electrons, photons, x-rays, light, absorbed current, and transmitted electrons) provide enough information for an image with defined characteristics to be created, thus when a beam is scanned in a rectangular pattern (i.e. geolocation via raster scanning - from Latin rastrum and radere meaning rake and to scrape), the reading of the signals for each individual location on the surface of the

rectangle can be decoded into a pixel with specific values and an image is formed like the one created by a computer printer (Lyman, 1990). The resolution for these images can be around 1 nm to 20 nm, depending on several factors such as the wavelength of the electrons combined with the electron-optical system that generates the beam which defines the size of the electron spot, the size of the interaction volume, the volume of the specimen. To date, the highest resolution achieved by a SEM is 0.4 nm from an accelerating voltage of 30 kV and 1.2 nm at an acceleration of 1 kV without beam deceleration and 0.8 with beam deceleration technology (Hitachi SU9000, Hitachi Corporation, Tokyo) (Sunaoshi et al., 2016; Hitachi, 2017).

III.VII.II Energy-dispersive x-ray spectroscopy (EDS)

Energy-dispersive x-ray spectroscopy (EDS) is an analytical technique used for the elemental chemical characterization of a sample (i.e. elemental composition). The fundamental principle behind EDS analysis is that each element in the periodic table has a unique atomic structure that generates a unique signature-like signal and peaks of an electromagnetic emission spectrum (Russ, 1984; Kaur, 2009). When a high-energy beam of electrons or protons collides on the surface of a sample would excite the electrons of those atoms in the surface which unless otherwise treated, would be in a ground state (unexcited) and bound to the nucleus (Goldstein et al., 2003). As the incident beam hits the electrons on the surface atoms, their energy may excite those in an inner shell ejecting and creating holes which in turn are filled by electrons in the outer shells emitting an xray. The count of x-rays, as well as their energy, can be measured with an energydispersive spectrometer and thus the elemental composition of the sample can be measured as each element will generate a different spectrum (Newbury & Ritchie, 2013). In general terms, an EDS system would have an excitation source (electron or x-ray beam), a detector, a pulse processor and an analyzer software that provides the user interface (Goldstein et al., 2003).

III.VIII Inductively coupled plasma mass spectrometry (ICP-MS)

Inductively Coupled Plasma Mass Spectrometry (ICP-MS) is an analytical technique that combines the principles of mass spectrometry (MS) and the atomic absorption using plasma atomization of samples for identification (Holland & Tanner, 2003). Samples

enter an ionized inert gas plasma (e.g. argon) in droplets (aerosolized) and the components of the liquid phase are dried, molecules are dissociated, and one electron from each atom of the sample is removed by the plasma. These singly-charged ions are directed to a mass filter (MS) which in turn scans the mass range and separates based on molecular mass-to-charge ratios (McCloskey, 1990; Holland & Tanner, 2003). After the separation is completed, ions would hit a dynode (i.e. impact second emission electron multiplier) that works as a detector. This cascade of electrons is then amplified until the turn into a measurable pulse and recorded in the user interface (i.e. software) which is used to compare the intensity of the measured pulse with that of a standard calibration curve to determine the concentration of each element in the sample (Taylor, 2001; Holland & Tanner, 2003).

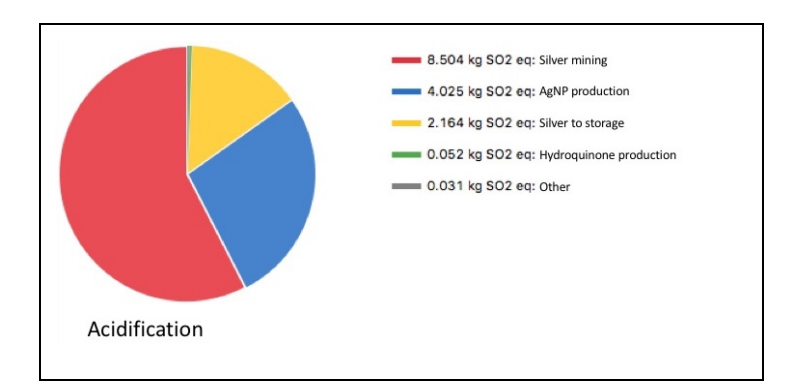
APPENDIX IV LIFE CYCLE ASSESSMENT COMPLEMENTARY DATA

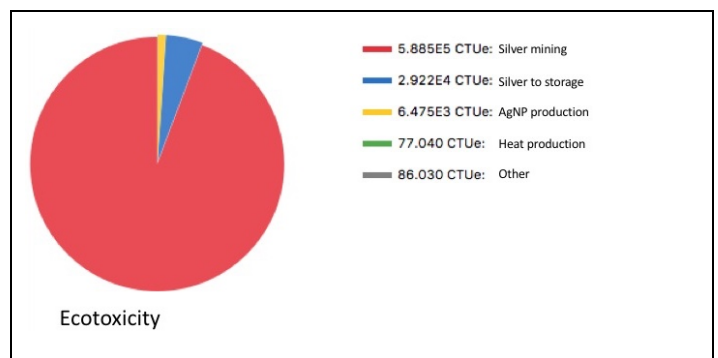
Outline of Impact categories. The outline of impact categories defined for the LCA in this document. (Acero et al., 2017)

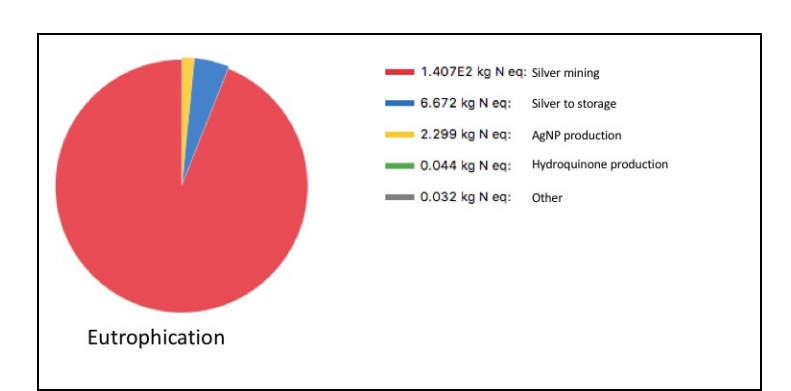
Impact Category		Ex	planatory remarks
Acidification	Definition		Reduction of pH. Acidifying effects of
			anthropogenic emissions
	Impact Indicator		Increase of acidity water and soil
	Damage	Categories	Damage to ecosystem quality. Decrease in
	(endpoint)		biodiversity
	Considerations		Acidifying potential of nitrogen and sulfur oxides
	Unit		kg SO ₂ equivalent
Climate Change	Definition		Alteration of global temperature due to
			greenhouse gases
	Impact Indicator		Disturbances in global temperature. Climatic
			phenomenon
	Damage	Categories	Decrease in biodiversity (e.g. forests, coral reefs,
	(endpoint)		crops)
			Temperature disturbances
			Climatic phenomenon abnormality (e.g.
	0		strongest cyclones, torrential storms)
	Considerations		Greenhouse gases (GHG) with global warming
	Unit		potential (e.g. methane, sulfur, carbon dioxide) kg CO ₂ equivalent
Danistian of Abiatia	Definition		į ,
Depletion of Abiotic	Definition		Decrease on non-biological resource availability
Resources	Impact Indicator		(non- and renewable) due to unsustainable use Decrease of resources
		Cotomorios	
	Damage (endpoint)	Categories	Damage to natural resources and potential
			ecosystem collapse
	Considerations		Distinctions between renewable and non- renewable resources
	Unit		Model dependent:
			 kg antimony equivalent
			o kg of minerals
			 MJ of fossil fuels
			o m ³ water consumption
Ecotoxicity	Definition		Toxic effects of chemicals in an ecosystem
	Impact Indicator		Biodiversity loss and or species extinction
	Damage	Categories	Damage to ecosystem quality and species
	(endpoint)		extinction
	Considerations		Toxicology and responses of different species.
			Nature of the chemical entering the ecosystem
			and in the ecosystem.
	Unit		Model dependent:
			o kg 1,4-Dichloro Benzene (1,4-DB)
			equivalent
			 PDF (Potentially Disappeared Fraction of Species)
			 PAF (Potentially Affected Fraction of
			Species)
			opeoico)

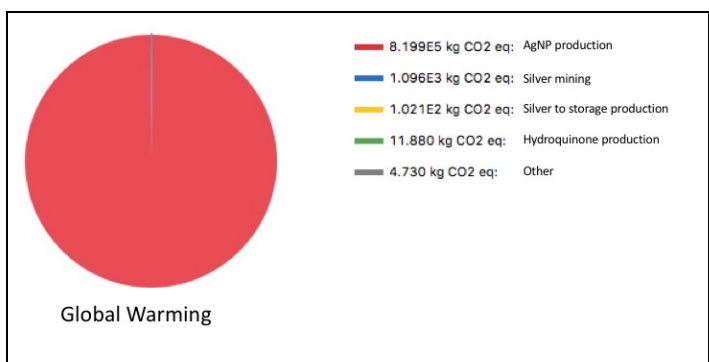
Impact Category		Ex	planatory remarks
Eutrophication	Definition		Accumulation of nutrients in an aquatic ecosystem
	Impact Indicator		Increase in nitrogen and phosphorus
			concentration. Biomass formation (e.g. algae,
			aquatic plants)
	Damage	Categories	Damage to ecosystem quality
	(endpoint)		
	Considerations		Nutrient transportation (i.e. air, water, land wash-off)
	Unit		Model dependent:
			○ kg PO ₄ ⁻³ equivalent
			 kg N equivalent
Human Toxicity	Definition		Toxic effect of chemicals on humans
	Impact Indicator		Cancer, respiratory diseases, non-carcinogenic
			effects, effects to ionizing radiation
	Damage	Categories	Human health
	(endpoint)		
	Considerations		Human toxicology and responses. Nature of the
	11 **		chemical when entering the human body.
	Unit		Model dependent:
			kg 1,4 DB equivalentDisability-adjusted life year (DALY)
			DALY = Years lived with disability (YLD) + years of life lost (YLL)
Ionizing Radiation	Definition		Radiation composed of particles with enough
3			energy to liberate an electron from an atom or
			molecule
	Impact Indicator		Effects of radiation (e.g. health decline, cancer, illness)
	Damage	Categories	Human health and ecosystem quality
	(endpoint) Considerations		Radiation from substances and toxicological
	Considerations		response of human and other species.
	Unit		Model dependent:
	O.I.I.		o kg U ²³⁵ equivalent
			o DALY
Land Use	Definition		Impact of anthropogenic activities (e.g.
			agriculture, human settlement, resource
			extraction) on the land
	Impact Indicator		Loss of species, loss of soil and soil quality,
			organic matter dry content
	Damage	Categories	Natural resource depletion (non- and renewable)
	(endpoint)		
	Considerations		Analysis of area of land to be altered, and
			observations on biodiversity that could be
	Unit		affected Model dependent:
	Offic		o PDF m ⁻²
			o m ² x a
Ozone Layer	Definition		Reduction of stratospheric ozone layer caused
Depletion Layer	Deminion		by anthropogenic emissions (i.e. ozone
Depiction			depleting substances)

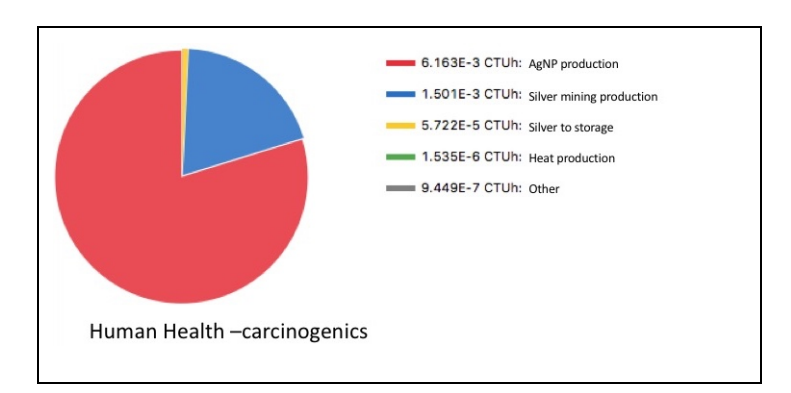
Impact Category	Explanatory remarks			
	Impact Indicator		UV-B radiation increase and number of cases of skin diseases/illnesses	
	Damage (endpoint)	Categories	Human health and ecosystem quality	
	Considerations		Atmospheric residence time of the depleting substance, and equivalent effective stratospheric chlorine (EESC)	
	Unit		kg CFC-11 equivalent	
Particulate Matter	Definition		Small particles of reduced size suspended on air with anthropogenic activity (e.g. combustion, resource extraction)	
	Impact Indicator		Increase on suspended particles on air (e.g. PM10, PM2.5, PM0.1)	
	Damage (endpoint)	Categories	Human health	
	Considerations		Interactions of the particles and behavior in the environment	
	Unit		kg particulate matter	
Photochemical Oxidation	Definition		Smog created from sunlight effects, heat, non- methane volatile organic compounds (NMVOC) and nitrogen oxides (NOx)	
	Impact Indicator		Increase in summer smog	
	Damage (endpoint)	Categories	Human health and ecosystem quality	
	Considerations		Meteorology of the area, chemical composition of the atmosphere and pollutants entering the air	
	Unit		Model dependent: o kg ethylene equivalent o kg NMVOC o kg formed ozone	

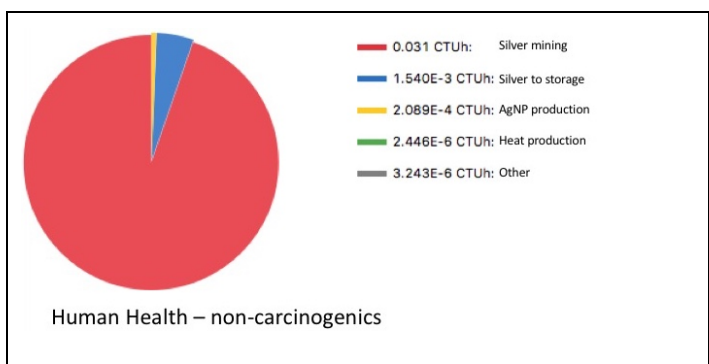


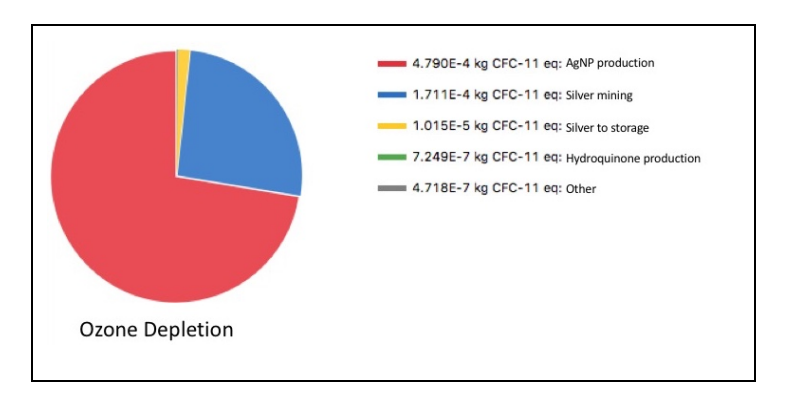


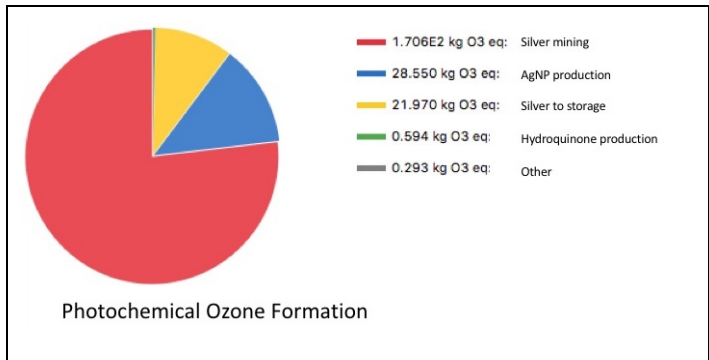


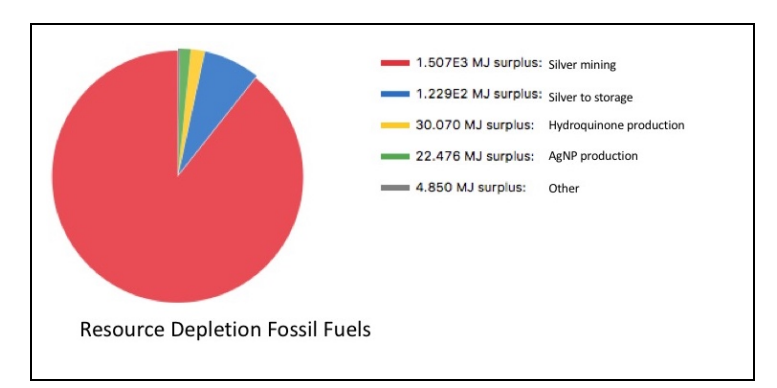












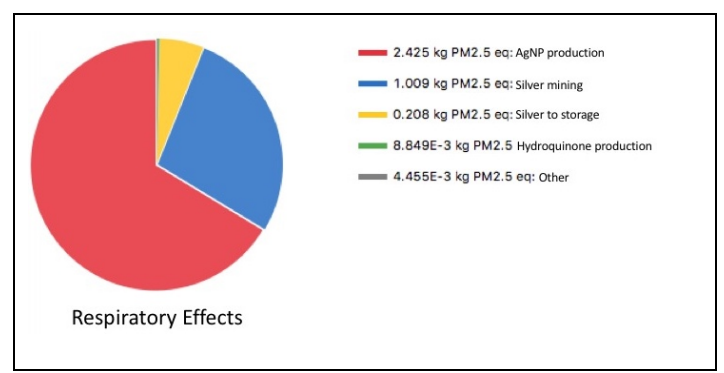
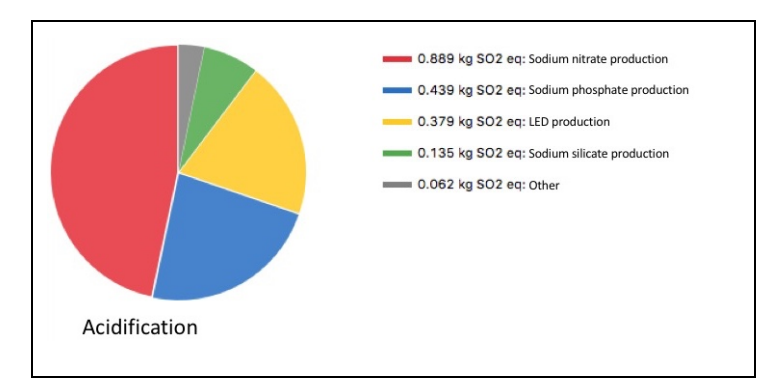
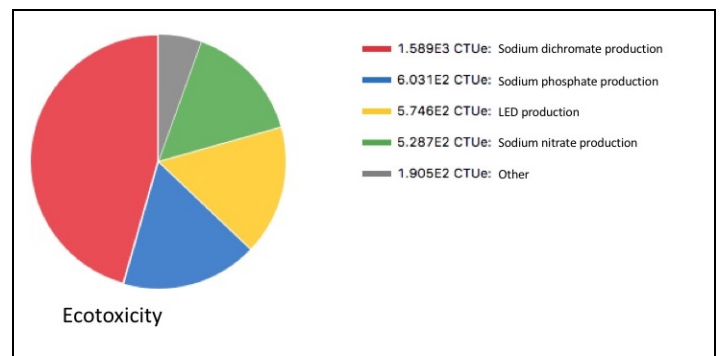
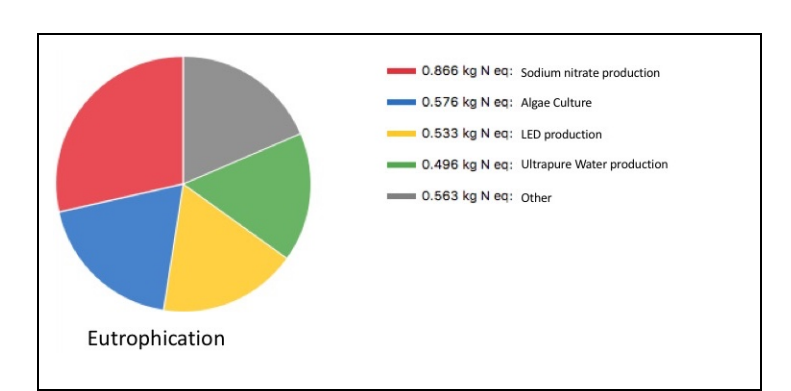
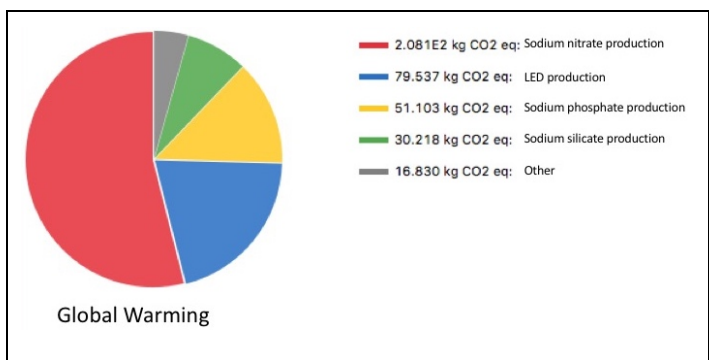


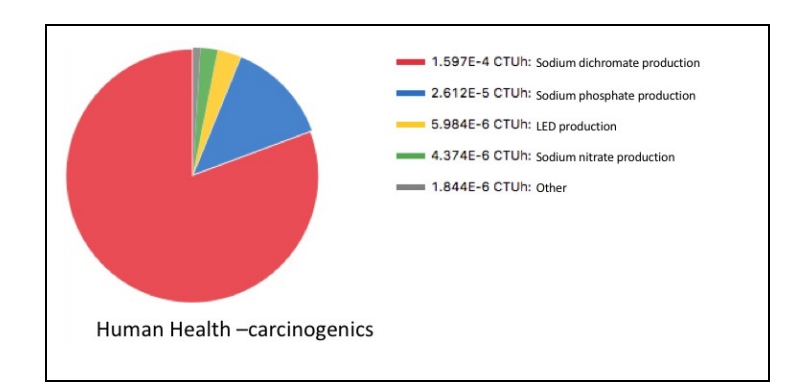
Figure 3. Overall contributions of hydroquinone-AgNP production TRACI 2.1. Overall contribution from each process to their corresponding categories for the industrial hydroquinone production process. From top to bottom left to right, acidification, ecotoxicity, eutrophication, global warming, human health – carcinogenics, human health – non-carcinogenics, ozone depletion, photochemical ozone formation, respiratory effects, and resource depletion – fossil fuels. Methodology TRACI 2.1.

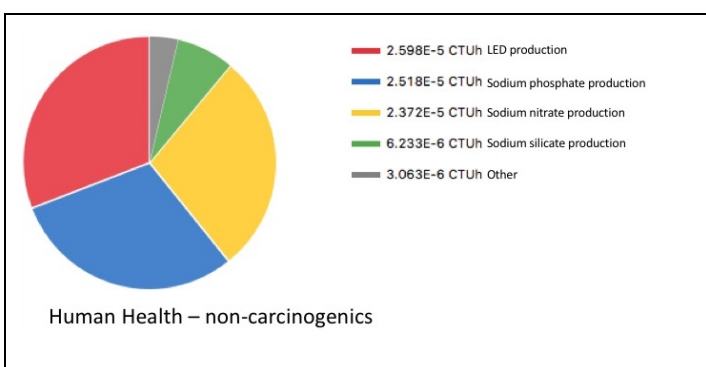


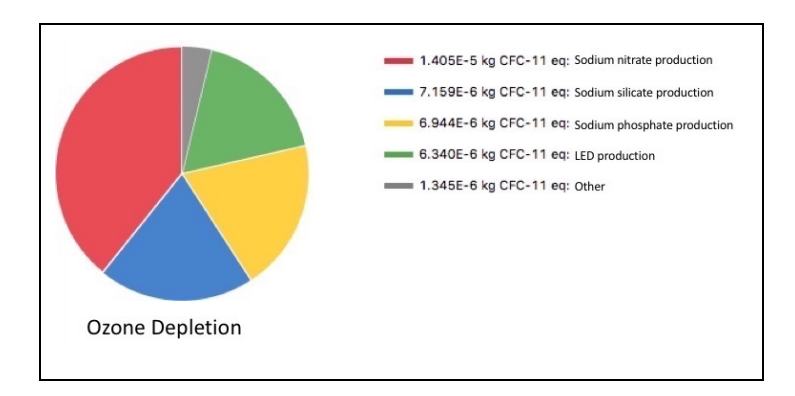


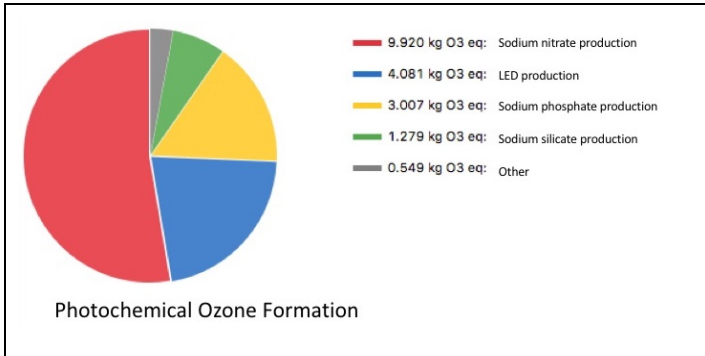


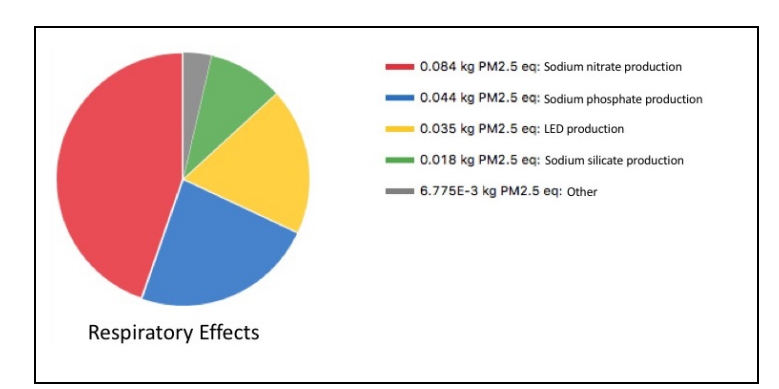












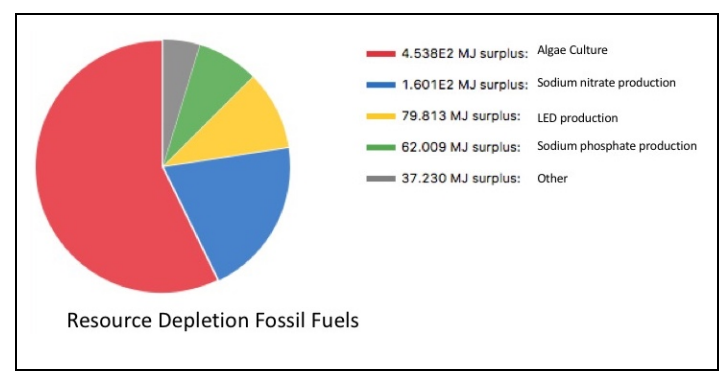


Figure 4. Overall contributions of biogenic-AgNP production TRACI 2.1. Overall contributions from each process to their corresponding categories for the biogenic production process. From top to bottom left to right, acidification, ecotoxicity, eutrophication, global warming, human health – carcinogenics, human health – non-carcinogenics, ozone depletion, photochemical ozone formation, respiratory effects, and resource depletion – fossil fuels. Methodology TRACI 2.1.